Multi-scale tectonic controls on fluvial terrace formation in a glacioeustatically-dominated river system: inferences from the lower Miño terrace record

Willem Viveen

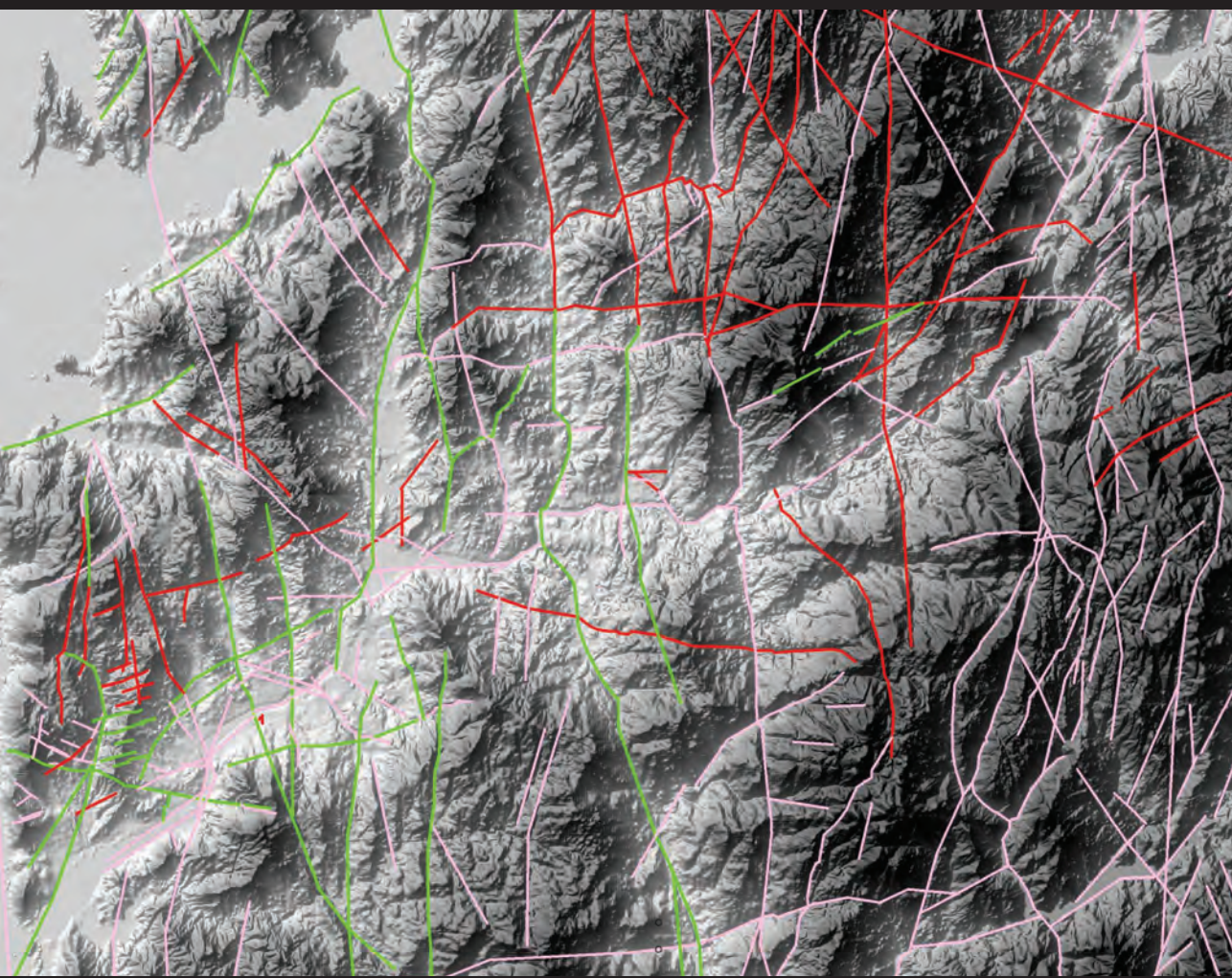

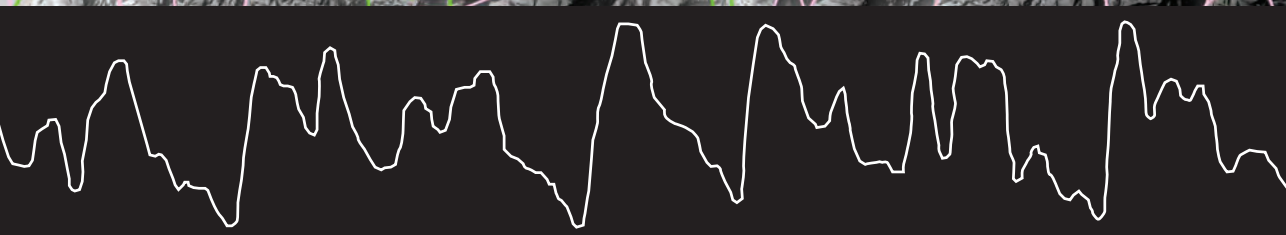

Multi-scale tectonic controls on fluvial terrace formation in a glacioeustatically-dominated river system: inferences from the lower Miño terrace record

Willem Viveen

Thesis committee

Thesis promotor
Prof. Dr. A. Veldkamp
Professor of Land Dynamics
Wageningen University

Thesis co-promotors
Prof. Dr. R.T. van Balen
Professor at the Faculty of Earth and Life Sciences
VU University Amsterdam

Prof. Dr. J.R. Vidal Romani
Professor at the Instituto Universitario de Geologia
University of A Coruña, Spain

Dr. J.M. Schoorl
Assistant professor, Soil Geography and Landscape Group
Wageningen University

Other members
Prof. Dr. D.R. Bridgland, Durham University, United Kingdom
Prof. Dr. S.A.P.L. Cloetingh, Utrecht University
Prof. Dr. C.J. Ritsema, Wageningen University
Prof. Dr. J. Vandenberghe, VU University Amsterdam

This research was conducted under the auspices of the C.T. De Wit Graduate School for Production Ecology and Resource Conservation (PE&RC).

Multi-scale tectonic controls on fluvial terrace formation in a glacioeustatically-dominated river system: inferences from the lower Miño terrace record

Willem Viveen

Thesis

Submitted in fulfilment of the requirements for the degree of doctor
at Wageningen University
by the authority of the Rector Magnificus
Prof. dr. M.J. Kropff,
in the presence of the
Thesis Committee appointed by the Academic Board
to be defended in public
on Wednesday 2 October 2013
at 1:30 p.m. in the Aula.

W. Viveen
Quaternary tectonics and glacioeustatic changes in a passive margin river system: inferences from the lower Miño fluvial terrace record
222 pages.

PhD thesis Wageningen University, Wageningen, NL (2013)
With references, with summaries in English and Dutch

ISBN 978-94-6173-728-1

A word of thanks

A great number of people have attributed to this thesis and without them this thesis would not have been possible. First of all, I would like to thank my promotor Tom Veldkamp. Tom, zonder jou zou deze thesis nooit van de grond zijn gekomen, want je hebt me de mogelijkheid gegeven om mijn MSc-thesis uit te bouwen naar een PhD-project en dat geheel op mijn eigen voorwaarden. Ik dank je voor het vertrouwen dat je me hebt geschonken, ondanks dat ik een hele matige BSc-student was. Ik dank je dat je me de mogelijkheid hebt gegeven om het hele project in A Coruña uit te voeren. Om goed te kunnen functioneren moet ik me geïnspireerd voelen, en dat lukte in Coruña door de mooie omgeving, de nabijheid van de zee en de Zuid-Europese levensstijl. In Nederland was ik nooit zover gekomen. De nabijheid van mijn veldwerkgebied zorgde er ook voor dat ik vaak even op en neer kon rijden en zo doende heel veel veldwerk kon doen, een aspect dat zeer belangrijk is gebleken voor deze thesis. Ik dank je ook voor je meer tastbare aanvullingen, zoals de vele wetenschappelijke discussies die we gehad hebben, je aanvullingen op de papers, je modelleerinput en de keren dat je naar Galicië bent gekomen voor veldwerk.

De tweede persoon die ik wil bedanken is mijn dagelijkse begeleider Jeroen Schoorl. Jeroen, je hebt me altijd bijgestaan in geval van twijfel over inhoud van de papers, bij het opzetten van de verschillende computermodellen en bij de honderden kleine praktische dingen die ik niet kon regelen omdat ik niet in Wageningen zat. Ik dank je ook voor het luisterend oor dat ik af en toe nodig had als ik weer vol frustratie zat over bepaalde zaken.

Mijn andere begeleider Ronald van Balen wil ik ook graag bedanken. Ronald, je bent belangrijk geweest voor de tektonische invulling van deze thesis en ook voor het beter begrijpen van de rivierdynamiek. Onze eerste paper over de tektoniek heb ik grotendeels met jou geschreven. Het was voor ons beiden een lastig proces, omdat het mijn eerste paper was en omdat we geen goed idee hadden over hoe we de paper invulling moesten geven. Toch mag het uiteindelijke resultaat er zijn, en daar ben ik trots op. Ik weet dat je in het begin wat moeite had met mijn recht-door-zee karakter, maar ik denk dat we uiteindelijk toch een goed team zijn geworden.

Tom, Jeroen en Ronald, voor jullie alledrie geldt dat jullie van onschatbare waarde zijn geweest. Door ons vele overleg zijn er een aantal goede ideeën geboren die we afzonderlijk niet bedacht zouden hebben. In die zin is deze PhD-thesis meer het product van ons als team dan van mij alleen. Dank jullie wel!

Jakob Wallinga wil ik graag bedanken voor de OSL-dateringen. Jakob, ik kan mij nog herinneren dat, toen we in 2009 samen de Eerbeek kernen aan het bemonsteren waren in Delft, ik aan je vroeg of je geen professor wilde worden. Zie hoe het leven een wending neemt! Nu ben je de nieuwe professor van mijn onderzoeksgroep!

Mijn drie afstudeervakkers/stagelopers Kees Lommertzen, Peter Kuijten en Jurriaan ten Broek wil ik ook graag bedanken. Kees, je was mijn eerste AV-student. We hebben samen

zes weken veldwerk gedaan terwijl we een huisje hadden gehuurd in La Guardia. Ik vond het erg gezellig met je en een deel van de kartering die je in O Rosal gedaan hebt, is goed van pas gekomen voor de FLUVER 2 modelleer paper. Ik hoop dat we de mariene terrassenkartering die je uitgevoerd hebt, nog eens kunnen publiceren! Peter, jou wil ik bedanken voor de tijd die je in Bordeaux hebt doorgebracht om aan de mariene diepzeekernen te werken! Jurriaan, ons veldwerk was een groot avontuur onder andere doordat we mijn bus moesten uitgraven en doordat we bijna gearresteerd werden door de Portugese geheime politie. De verweringsanalyses die je gedaan hebt zijn goed van pas gekomen om de Miño terrassen ruimtelijk te correleren.
In het rijtje van Nederlanders wil ik ook graag Henny van den Berg bedanken. Henny, je hebt me vaak geholpen met vele kleine praktische zaken zoals de financiële kant van mijn onderzoek en mijn leven is daardoor een stuk gemakkelijker geworden!
Tenslotte wil ik mijn familie nog bedanken. Mijn ouders zijn een aantal keer op vakantie gekomen met de caravan, waardoor ik deze als uitvalsbasis kon gebruiken voor mijn veldwerk campagnes. Hun aanwezigheid zorgde er ook voor dat ik me niet eenzaam voelde tijdens de eerste jaren van mijn MSc- en PhD-onderzoek, want al wildkamperend in mijn bus twee maanden in mijn eentje veldwerk doen was toch iets te veel van het goede! Ik wil mijn zusjes Anieke en Corina bedanken dat ze er altijd voor me zijn. Jullie vonden het wel leuk in Galicië!
Mijn lieve Sonya wil ik bedanken voor de vele jaren dat ze met me mee op veldwerk is geweest, en voor de duizenden kiezels die ze mee uit wanden heeft gehakt en mee heeft gedetermineerd. Naast je expertise als neurobiologe ben je nu ook volleerd kwartsietexpert!

Con respeto a los españoles, quiero agradecer primero a Juan Ramon Vidal Romani. Moncho, muchisimas gracias por dejarme trabajar en el Instituto de Geologia. Me has ayudado mucho a lo largo de los años, primero en facilitarme con bibliografia local, y luego con tus aportaciones cientificas, nuestros viajes por el campo, y la financiacion de las dataciones de OSL, y los analises del XRD y XRF. No creo que hubiera avanzado tanto sin tus aportaciones. Echaré de menos a nuestras discusiones sobre la geologia de Galicia! Y estoy seguro de que me vas a echar de menos a mi tambien, como ahora ya no quede nadie con quien puedes ir a comer en el indio.....
Mi compañero de despacho Jorge Sanjurjo Sanchez tambien quiero mencionar. Jorge, gracias por tu presencia y por tus aportaciones al respeto de las dataciones de OSL. Siempre has sido muy amable conmigo, aunque te veo bastante timido y en el principio te costó un poco abrirte. Sin embargo, creo que tenemos en comun nuestra dedicacion a la ciencia y la curiosidad en general.
Aurora, tu tambien muchas gracias por tu compañia todos estos años. Muchas veces me has dado sabios consejos sobre el manejo de Illustrator y eso de verdad me ha ayudado mucho. Es un programa de mierda, pero gracias ti acabé no rompiendo por frustracion el ordenador!

Por ultimo me gustaria agradecer a Maria Fernanda Sanchez Goñi. Maria, valoro mucho nuestras discuciones sobre la paleoclimatologia del NW de Iberia todos estos años. Me facilitaste con muchos datos climatologicos que al final han sido muy importantes para la modelizacion de la evolucion de la cuenca del Miño. No creo que mundialmente exista una modelizacion geomorfologica con un registro de datos climatologicos tan detallado como hemos hecho nosotros.

Then there is a significant number of non-Dutch and non-Spanish people who have helped me throughout the years. Maria da Assunção Araujo provided me with Portuguese geological maps and aerial photographs when I started working in the Miño in 2007. Assunção, I thank you very much for your help and your kindness. You let me stay in your house in Porto although we hadn't met before. I really appreciated that you know. I hope you and your cats are doing well ;)

An important cornerstone of this thesis is the set of ^{10}Be datings carried out by people from CEREGE in France. This thesis would therefore not have been the same without the help of Regis Braucher and Didier Bourlès. Regis spent a lot of time doing the chemical treatment of the samples and maybe even more time trying to figure out what the terrace ages could be. Regis, we had a really good time doing the sampling in the Miño! Do you remember that day when we had to dig out the car? Unfortunately we also had some communication problems when we were trying to calculate the sample ages, and I am aware that I pushed you a bit for the final results. Still, I think we wrote a really good paper together and I am grateful for all the help and time you invested. In my opinion CRE dating has the most potential in NW Iberia, even though the technique has its own inherent problems. In this light I would also like to thank Didier for the time he spent with us sampling in the Miño, and for our discussions afterwards. Didier, I hope you are doing well.

I would like to thank Stephanie Desprat for her attributions to the FLUVER 2 modelling paper. Stephanie, your palaeoclimatological knowledge has been very important for this work. I still hope that one day we will meet, because we have always communicated through email without even knowing each other.

Martin Stokes, J. Carcaillet, and David Bridgland are acknowledged for their thorough reviews of some of the published papers presented in this thesis. Especially Martin gave me a hard time with the ^{10}Be paper, but it resulted in a much improved paper.

Then there are a number of people who have shared their data or provided measurements that proved invaluable to this thesis: Richard Bintanja and Teresa Rodgigues for sea level and SST data, F. Chauvet for his help during sampling and samples physical-chemical preparation, M. Arnold, G. Aumaître and K. Keddadouche for their help during AMS measurements and to C.A. Johns for OSL sample preparations.

Table of contents

Chapter 1

General introduction

1.1 Background

Rivers are the main arteries of the world. They transport water and sediment within river catchments to the ocean. Worldwide, rivers transport an estimated 85-95% of the global sediment budget to the oceans (Syvitski et al., 2003). The way in which sediment is transported is not straightforward. A sediment particle for instance, may be taken up by a small tributary somewhere in the headwaters of a catchment. When it starts its journey towards the ocean, it will come to rest on the river bed, or on a floodplain, many times. To get the particle in motion again, erosion of the floodplains (De Moor et al., 2008), high river discharges (Stange et al., 2013), or even natural disasters such as earthquakes, cyclones, forest fires, or volcanic eruptions are needed (Veldkamp et al., 2012; Claessens et al., 2009). Such disturbances affect not only whether a sediment particle is transported, they also affect the physical properties, the layout, of the rivers themselves. The changes wrought upon them may be gradual or abrupt, but rivers are never stationary entities in time. They are transient features in an ever changing landscape (Schumm, 1977). The factors that are responsible for the transient state of a river are divided into internal and external factors (Bull, 1991). Internal factors are related to adjustments by the river itself. A river can for example adjust its channel depth, gradient, or sinuosity in response to internal, local changes in the ratio discharge: sediment load, resulting in meander displacement (Schumm, 1977). External factors on the other hand, are not inherent to a catchment itself, but result from regional or even global changes, and as such, affect a river system from the outside. Climate change, sea level variations caused by waxing and waning of the global ice caps (glacioeustacy), and tectonics are considered the main external factors that control the development of fluvial systems (Bull, 1991).

Numerous examples exist of how those three external factors change river systems: fluvial incision and deposition for instance, can be caused by climate-induced variations in sediment load and discharge (Bogaart and Van Balen, 2000). The disappearance of vegetation during a cold period, in combination with the development of a permafrost layer, could cause overland flow, resulting in surface erosion and increasing the sediment load in a river (Brocard et al., 2003; Bogaart et al., 2003; Gibbard and Lewin, 2009; Stokes et al., 2012a). At the same time, glacial melt during cold-warm period transitions causes peak discharges, which may lead to severe erosion in the upstream parts of a fluvial system, whereas the transported sediments may again be deposited along reaches where fluvial stream power decreases, for instances in broad river valleys (Maddy et al., 2001; Starkel, 2003; Vandenberghe, 2008; Stange et al., 2013).
Glacioeustatic motions have a profound effect on river valley development in the downstream reaches of a river, especially when during sea level fall at the onset of a glacial period, the river is forced to incise into its own alluvium (Tebbens et al., 2000; Törnqvist et al., 2006). During a rise in sea level on the other hand, the incised valley is filled up with

alluvium again (Blum and Törnqvist, 2000). Glacioeustatic motions may lead to an enlargement of the fluvial system by hundreds of kms where the continental shelf is wide and sub horizontal (Antoine et al., 2007; Tebbens et al., 2000), or hardly at all where the continental shelf is short (Blum and Aslan, 2006; Törnqvist et al., 2006). In the former case, all erosion and deposition processes that took place close to the high stand shore line, will migrate several hundreds of kms downstream to the new shoreline, whereas in the latter case, an incised valley will form (Meijer, 2002; Martin et al., 2011). The influence of glacioeustacy propagates upstream along a fluvial system, thereby causing the formation of knick points, but those knick points do not renew the entire fluvial profile. They are usually confined to the lowermost 100-150 km (Merritts et al., 1994; Blum and Törnqvist, 2000).

Tectonic processes also strongly influence the development of fluvial systems. Regional tectonic uplift may cause river incision, initiating the formation of river gorges and fluvial terraces (Maddy, 1997). Localised block movements may cause the formation of knick points in a river profile as well as hanging river valleys (D'Alessandro et al., 2008; Maroukian et al., 2008), or asymmetrically-developed catchments (Cox, 1994). Sometimes these movements cause unpaired fluvial terraces (Veldkamp and Van den Berg, 1993) or fragmentation of former floodplains (Cunha et al., 2008). Tectonic processes may also interact with climate processes. Long-term upland erosion and downstream deposition for instance, may cause uplift due to crustal rebound, which in turn forces a river to attain a new state of equilibrium (Bull, 1991). At the same time, climate and vegetation-induced changes in discharge and sediment supply interfere by changing the pattern of erosion and deposition within the system (Schumm, 1977; Gibbard and Lewin, 2009).

Another complication is that some processes operate on different timescales as others. Upstream migration of incision-induced knick points may take up several thousands to tens of thousands of years (Tebbens et al., 2000), which makes it difficult to assess whether this was caused by a former glacioeustatic or tectonic event. During this same period, several small climate fluctuations may have occurred, that also caused river incision along various parts of the river profile. This makes it even more difficult to find the cause of the incision event, and when it happened. This leads to a very complex fluvial response pattern, that depends on the timescales investigated as well as the position along a river profile.

Fluvial systems register all these changes in their morphology and sedimentology, which are partly preserved in fluvial terrace staircases, making them suitable to study the driving factors on these changes (Bridgland and Westaway, 2008a; Westaway et al., 2009; Stokes et al., 2012b). Fluvial terraces however, have their own intrinsic short-comings, because they only represent fragments of fluvial activity in time and space. On-going erosion of their surfaces means that they hardly ever preserve a full record of former fluvial activity. Under favourable circumstances, the timing of sediment deposition can be more or less

constrained, but the timing of terrace incision or lateral erosion is difficult to constrain. Correlating terraces along larger river reaches may also be problematic, especially in the absence of chronostratigraphical markers (Briant et al., 2012).
To complement such studies on river terrace records, which often are based on field and Digital Elevation Model (DEM) interpretations, other methods may be necessary that are able to make up for the lack of information in the fluvial terrace record. In such cases, numerical modelling of fluvial behaviour may give additional information that was not preserved in the fluvial terrace record (Veldkamp, 1992). In this way, large fluvial systems on longer timescales are investigated in a holistic way (Vandenberghe and Vanacker, 2008), and at the same time modelling contributes to a better understanding of the relative importance of climate change, glacioeustacy and tectonics on fluvial system development (e.g. Garcia-Castellanos et al., 2003). Numerical modelling simulations can be performed to isolate and study the effect of potential driving forces on fluvial behaviour and modelling outcomes can be tested against the geological record (e.g. Gargani et al., 2006; Kettner and Syvitski, 2009). This thesis will therefore include a combination of field studies, DEM interpretations, and numerical modelling experiments.

1.2 Aim and objectives

The aim of this thesis is to determine the long-term, separate effects of climate change, glacioeustacy, and tectonic movements on the development of a river system.
In order to do so, the lower Miño River in NW Iberia was chosen as a study site. Here, the main external factors that influence fluvial behaviour over longer timescales (glacioeustacy, climate change and tectonics; Bull, 1991) appear to be all present in the region. The Miño River is located near a very short, steep continental margin, that likely causes profound changes in the river gradient with varying sea level over several hundreds of ky, because the river cannot adjust its gradient much by channel lengthening (Blum and Törnqvist, 2000). Detailed palaeoclimatic reconstructions based on an offshore marine record indicate that climate in the lower Miño region has been highly variable (Desprat et al., 2005, 2006, 2007, 2009, Desprat, unpublished data; Sanchez-Goñi et al., 2005, 2008; Naughton et al., 2009), always with sufficient water availability to ensure constant erosion and sedimentation in the river valley. Investigations on tectonic activity in NW Iberia suggest the presence of multiple deformation phases that have left a landscape with a complex tectonic imprint, where tectonic activity during the Cenozoic still persists (De Vicente and Vegas, 2009). Birot and Solé-Sabaris (1954) even stated that "NW Iberia is a landscape of uplifted and subsided blocks, reminiscent of a piano keyboard". These characteristics make the Miño River a prime candidate for the aims and objectives of this thesis.

The following objectives have been formulated to be able to assess how glacioeustacy, climate change, and tectonics have affected the development of the lower Miño River system:

1. Create a detailed, regional map of fluvial terraces that covers both sides of the lower Miño River. Such a map is lacking and sorely needed;
2. Determine the regional tectonic framework and perform field studies to see if signs of recent tectonic activity in the fluvial terrace record can be found;
3. Date the fluvial terrace record in order to quantify incision rates caused by glacioeustacy and/or vertical tectonic deformation;
4. Assess how the fluvial terraces can be correlated over the entire lower Miño River reach as there is disagreement in the literature on how this should be;
5. By means of numerical modelling experiments determine what the relative influence is of glacioeustacy, climate change and tectonics on the development of the Miño River profile;
6. By means of numerical modelling assess what the relative influence is of local tectonic block movements in relation to terrace formation by glacioeustacy and climate change.
7. Integrate the results of the foregoing objectives to create a better understanding of how regional and local tectonics influence fluvial terrace formation.

1.3 Thesis outline

This thesis is divided into 7 Chapters, with summaries in English and Dutch and a number of Appendices. Chapter 1 is an introduction to the thesis and explains its aims and objectives and gives a general outline of the study area in terms of tectonics, geology and geomorphology. Paragraphs 1.4 to 1.6 were published in the journals *Tectonophysics* and *Geomorphology*.

In Chapter 2, the tectonic framework of the study area is explored by means of tectono-geomorphic indices based on studies of DEMs, and field descriptions of faults and tectonic basins. This Chapter was published in the journal *Tectonophysics*.

In Chapter 3, a local fluvial terrace staircase of the lower Miño River is described, and an age assessment on the basis of thermoluminescence and Cosmogenic Ray Exposure (CRE) dating is presented. This made it possible to calculate incision rates, which serve as proxies for vertical tectonic uplift rates. A first hypothesis of how the lower Miño terrace record was formed, is presented. This Chapter was published in the journal *Global and Planetary Change*.

In Chapter 4, the hypotheses presented in the former Chapter are further explored and upscaled to a regional scale. Sections of the entire lower Miño terrace staircase are described as well as results from extensive terrace mapping. These are complemented by studies on weathering characteristics of the terrace deposits, and a numerical modelling exercise with the two-dimensional FLUVER2 model. The results are integrated to refine the vertical uplift rates of Chapter 3, and describe the evolution of the entire lower Miño River for the past 450 ka, with particular emphasis on the role of climate change and glacioeustacy. This Chapter was published in the journal *Geomorphology*.

In Chapter 5, all findings of the earlier chapters are summarised in a new, regional terrace map with a tectonic context. The map and accompanying paper were published in *The Journal of Maps*.

In Chapter 6, the terrace map forms the basis to explore new ideas on the activity of local tectonic block movements. The conclusions of Chapter 4 are re-assessed using a three-dimensional model that simulates terrace and tectonic basin formation. The interaction between terrace formation by the Miño River and tectonic basin activity is explored. New ideas are presented on basin activity in relation to the regional tectonic framework presented in Chapter 1. This Chapter has been submitted to the journal *Geomorphology*.

In Chapter 7, a Synthesis of the former Chapters is presented, leading to a better understanding of the complex interactions between climate change, glacioeustacy, regional and local tectonics and their effects on the development of a fluvial system. In the Appendices, all field data is presented as well as a fluvial terrace map of the lower Miño. Appendix 5 contains a CD-ROM with all Appendix data in GeoPDF format. Appendices 4 and 5 have been published in *The Journal of Maps*.

1.4 Tectonic setting

The NW corner of the Iberian Peninsula is part of the Iberian Massif (Fig. 1.1). It consists of Precambrian and Paleozoic rocks which were deformed and intruded by granitoids during the Variscan Orogeny (Fig. 1.2, Abril-Hurtado et al., 1972; Pliego-Dones et al., 1972, Teixeira, 1952). The Late Variscan mountain building phase in NW Iberia resulted in left-lateral NNE-SSW to ENE-WSW and right-lateral NNW-SSE to NW-SE strike-slip faults (Ribeiro, 1990). These were obliquely reactivated during the Mesozoic (Late Triassic) rifting phase, when the Atlantic Ocean opened up (Pinheiro et al., 1996). From the Cretaceous to the Early Cenozoic normal to oblique-normal, thrust and strike-slip faulting along NNW to E-W trends occurred (Anton et al., 2010).

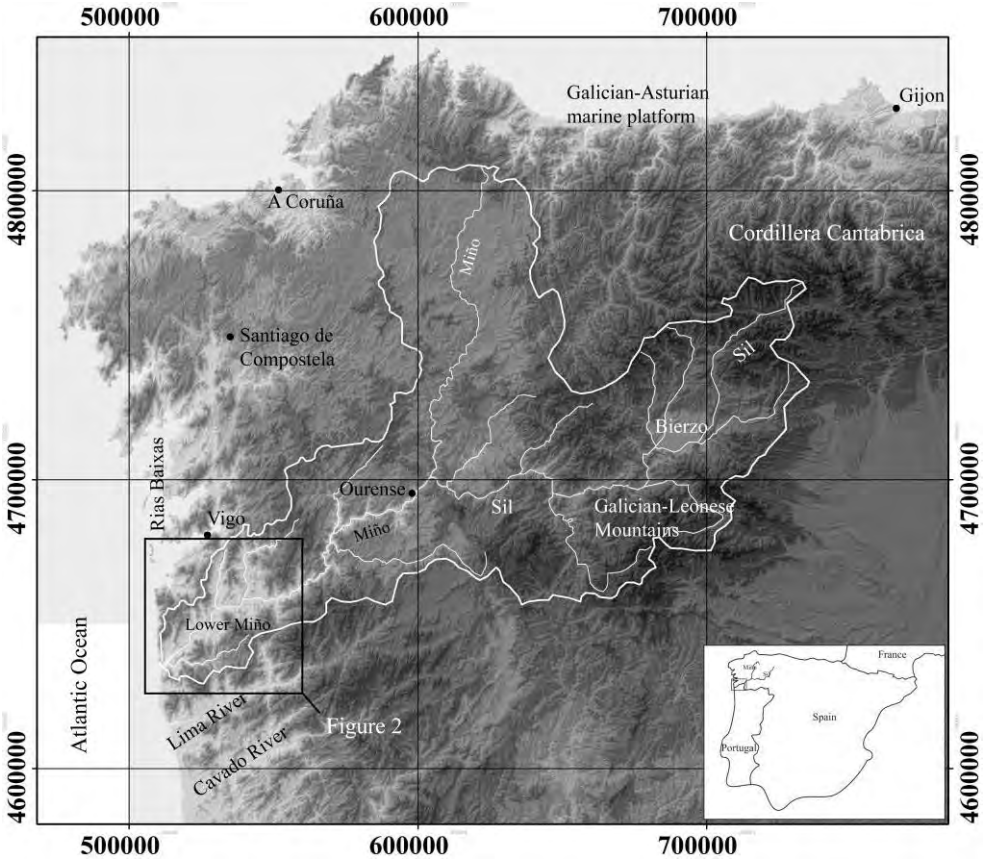

Fig. 1.1. The NW Iberian Atlantic Margin. The Miño-Sil catchment with main tributaries is delineated in white. The Figure is based on the ASTER DEM (USGS, 2009).

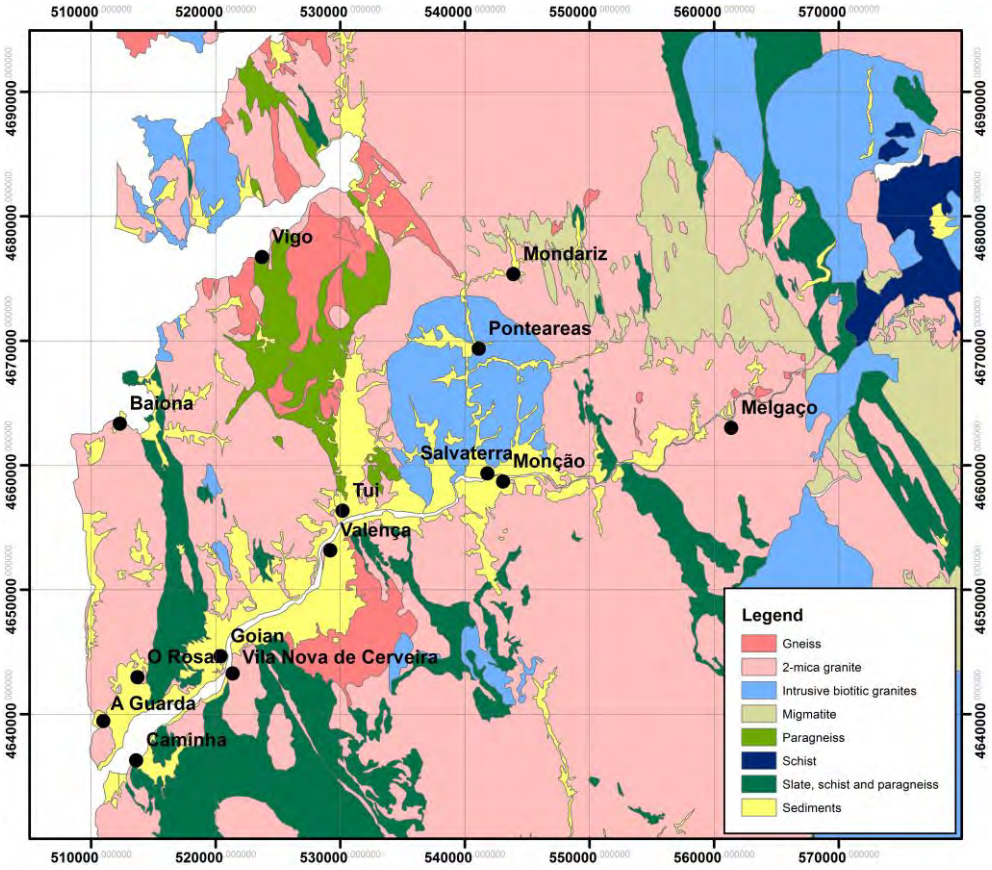

Fig. 1.2. Simplified geological map based on the 1:50.000 geological map series.

Collision of the Iberian and Eurasian plates during the Eocene resulted in the Pyrenean-Cantabrian mountain chain. This induced a N-S to NE-SW directed compressive force along the northern edge of the Iberian plate (Cloetingh et al., 2005), which reactivated the NNE-SSW strike-slip faults, mainly the left-lateral Vilariça and Regua strike-slip systems, and two right-lateral NW-SE transpressional strike-slip systems (Fig. 1.3); (Vegas et al., 2004; De Vicente and Vegas, 2009). Locally, thrust faults (Cabral, 1995; Pinheiro et al., 1996; Martin-Gonzalez, 2009) and normal faults (Yepes-Temiño, 2002) were also active. Associated with the right-lateral faults are the As Pontes and Meirama basins
(Santanach, 1994; De Vicente and Vegas, 2009).
From the Eocene to the Middle-Late Miocene the maximum horizontal stress direction became affected by the Atlantic ridge push from the NW (De Vicente and Vegas, 2009). This caused minor reactivation of old Variscan structures (Pinheiro et al., 1996). From the

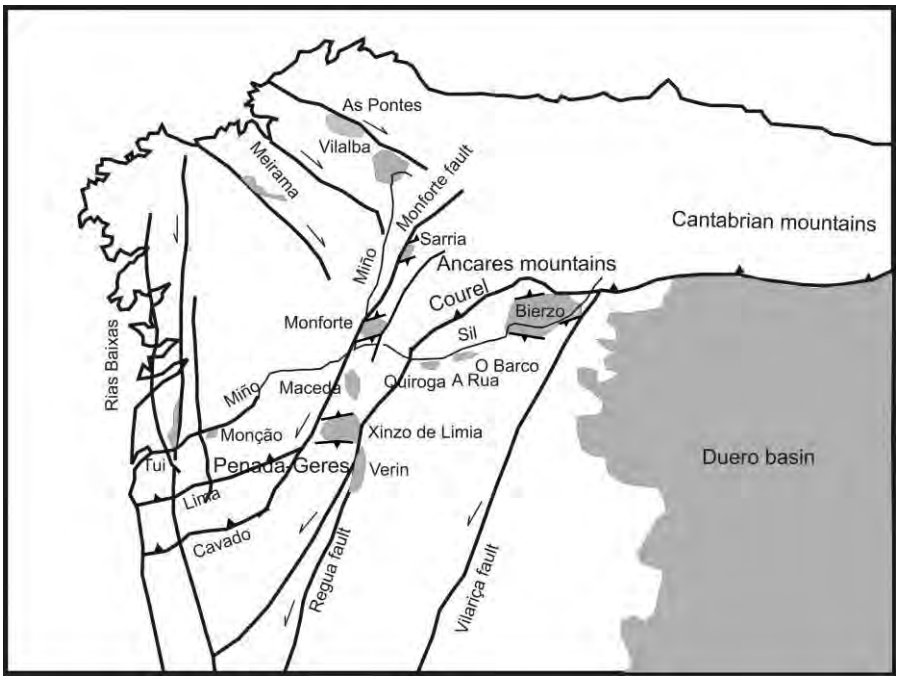

Fig. 1.3. Overview of the main basins (grey color), strike-slip and thrust faults and mountain blocks. For the sake of simplicity, NE-SW faults bordering the Rias Baixas are not drawn. Drawing adapted from Santanach (1994) and De Vicente and Vegas (2009).

Middle Miocene onwards a NW-SE to NNW-SSE compressive maximum horizontal stress has been acting (Andeweg et al., 1999; Cloetingh et al., 2002; Cloetingh et al., 2005; Casas-Sainz and De Vicente, 2009). The deformation in Galicia is a combination of compression, strike-slip and extension (De Vicente et al., 2008). This is due to the vertical stress and maximum horizontal stress being about equal in magnitude, and compressive. On the scale of NW Iberia, the stress conditions cause (re)-activation of the NW-SE normal faults, left-lateral NNE-SSW and right lateral ESE-WNW strike-slip faults and NE-SW thrust faults (De Vicente et al., 2008). Total Plio-Quaternary uplift for NW Iberia has been estimated at 100 m at the coast to 500 m landwards (Cabral, 1995). Indications that deformation is still ongoing are the seismic activity (Fig. 1.4; Pinheiro et al., 1996; Muñoz et al., 2003; De Vicente et al., 2008) and off-shore faulting in Pleistocene and Holocene sediments (Garcia-Gil et al., 1999). Documented evidence for onshore Pleistocene faulting is restricted to only two or three local sites (Carvalho, 1981; Ribeiro et al., 1986). In our study area the seismic activity is centered in the eastern sector where a large number of seismic events with small to moderate magnitudes have taken place (Fig. 1.4, Lopez-Fernandez, 2008).

At a large scale, the Oligocene-Late Miocene intraplate deformation of NW Iberia resulted in the formation of a number of basins (Martin-Gonzalez and Heredia, 2010; De Vicente et

al., 2011). The basins associated with the uplifted mountain ranges are generally thrust-related, whereas the large strike-slip systems are associated with both transtensional (Vilariça, Regua-Verin systems) and transpressional basins (Monforte system). Towards the western Iberian Atlantic margin, pull-apart basins along releasing bends are commonly associated with the NNE-SSW strike-slip systems, most notably the Vilariça fault system (Fig. 1.3). Strike-slip basins are generally elongated in shape, but rhomboid-shaped basins are also found, especially when a significant strike-slip offset is involved (De Vicente et al., 2011). For our study area, few tectonic basins have been documented. The N-S running Louro valley (Figs. 1.1 and 1.3) is considered to be a basin related to left-lateral strike-slip movements (Santanach, 1994; De Vicente and Vegas, 2009), but field evidence is inconclusive and the timing of formation not well constrained. Based on a fossil palm leaf in kaolinite clays underlying the siliclastic infill, Sos-Baynat (1965) suggested a Miocene age for this basin.

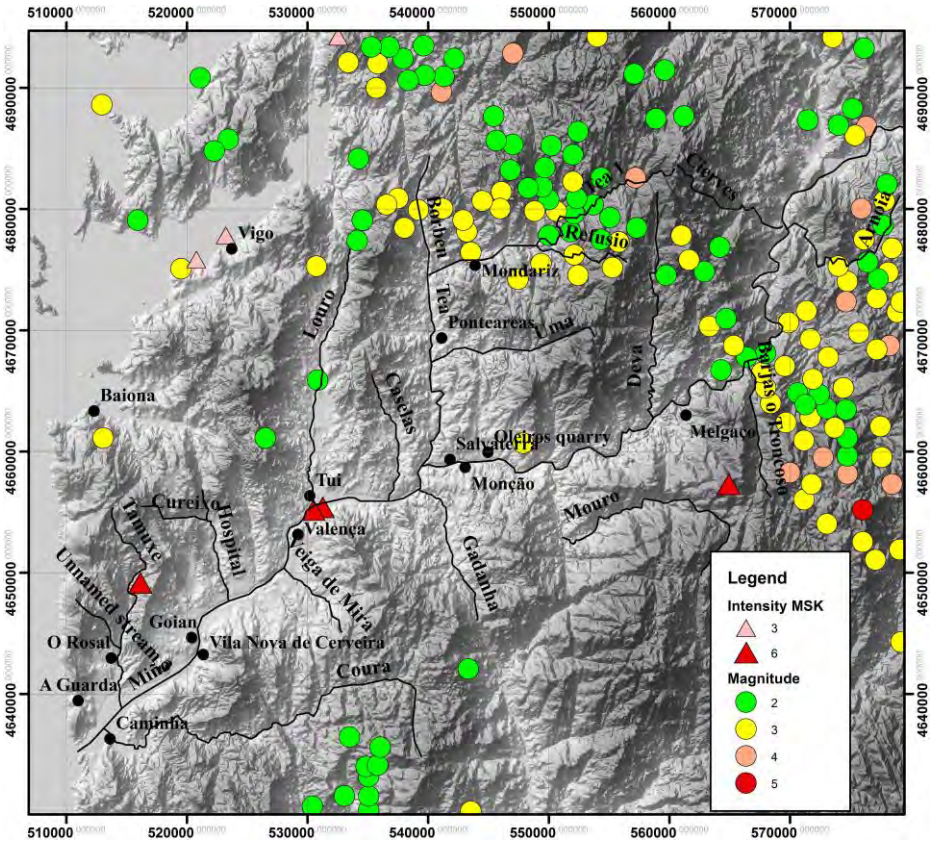

Fig. 1.4. Seismic activity in the study area (black square Fig. 1.1) over the past 50 years. Data obtained from the GASPI and RSNE-IGN programs. Adapted from Lopez-Fernandez (2008).

1.5 Morphologic setting

On a large scale, the landscape in northwestern Iberia is characterized by a large number of remnants of flat surfaces, which are interpreted as stepped etching surfaces (peneplains) that might date back from the Mesozoic. At least two clear stepped surfaces are easily recognised: a general level around 600 m close to the Atlantic coast, and a higher level around 1000-1400 in the east of our study area. Vidal-Romani and Yepes-Temiño (2001) suggest that 5 levels are present. In detail, the surfaces appear to be deformed. Originally, this was interpreted to be the result of horst-graben structures related to the Mesozoic rifting (Hernandez-Pacheco, 1949; Brum-Ferreira, 1991; Martin-Serrano, 1994), but more recent work suggests that compressive deformation and thrusting during the Tertiary were responsible for this morphology (Martin-Gonzalez, 2009; Martin-Gonzalez and Heredia, 2010).

The drainage network is deeply cut into the underlying bedrock. It is considered to be at least Late Neogene in age (Vidal-Box, 1941; Martin-Serrano, 1989; Pereira et al., 2000), but correlation to remnants of the erosion surfaces suggest a possible pre-Neogene age for some rivers such as the Miño (Vidal-Romani and Yepes-Temiño, 2001). The Miño has the most extensive terrace staircase of all rivers in NW Iberia with terraces up to 95 m above river level. Terrace ages are not known because until recently no suitable methods were available to date the terrace sediments, which consist entirely of quartz(ite) gravels and occasional sand layers. A tentative age of Pliocene-Quaternary has been proposed, based on fossil plant remains (Alves and Pereira, 2000; Vieira, pers. comm, 2010). The drainage network follows an intricate pattern of interlinked faults and Tertiary basins (Figs.1.1 and 1.3). Many rivers on the western Iberian shelf (e.g. the Miño, Lima, Cavado and Duero rivers) follow a NE-SW direction, which coincides with Variscan faults or large scale lithospheric folds (Cloetingh et al., 2002). Also, the Galician Rias Baixas (Fig. 1.1) follow this direction. The Rias Baixas are a series of inlets north of the Miño River that probably have a tectonic origin (Birot and Sole, 1954; Pannekoek, 1966; 1970; Nonn, 1966; Muñoz et al., 2003). They are most likely limited by reactivated N-S and NE-SW faults which caused subsidence of the enclosed central block (the area that now forms the estuary), resulting in tectonic depressions. Fluvial erosion may have been a contributing factor during glacial sea-level low stands (Garcia-Gil et al., 1999). It is not clear why the Lower Miño valley is not a ria, despite being situated in a geologically similar area. Perhaps no tectonic depression exists there, or maybe the depression is completely filled in with fluvial sediments and thus not discernible as such.

1.6 The Miño-Sil catchment

The Miño Sil catchment is the largest river catchment in NW Iberia with a surface area of 16,993 km2 (Fig. 1.1) and a mean discharge of 419.8 m3 s^{-1} at the river mouth (Rio-Barja and Rodriguez-Lestegas, 1992). The main river, the Miño Sil, has a length of 375 km and rises in the northwestern Spanish Cantabrian mountain chain and flows westward to the Atlantic Ocean. The Miño Sil system has a structurally controlled NE-SW direction that is caused by a number of partly reactivated Palaeozoic, Mesozoic, and Tertiary faults. These NE-SW trending faults are a common feature of the western Iberian Atlantic margin and almost all rivers and rias (marine embayments) follow this direction.

The lower Miño (Baixo Miño) is the final stretch of the Miño Sil River system. For the lowermost 80 km of its course, the Miño forms the natural border between Spain in the north (region of Galicia) and Portugal in the south (Fig. 1.1). Close to the Atlantic margin, the Miño changes direction from NE-SW and E-W to N-S a number of times where it crosses the reactivated Palaeozoic NNE-SSW bounded faults. For the lowermost 50 km of its course, the gradient of the Miño River is almost zero, and from the city of Tui to the Atlantic Ocean, the river is at sea level. Close to the coast the river valley opens up considerably and becomes a wide, tide-dominated estuary.

The present configuration of the Miño Sil catchment is the result of a number of processes that had already started in the Tertiary. Drainage reorganisation during the middle-late Miocene caused the Sil River to change drainage direction during the middle Tortonian from an easterly, landward direction toward the Atlantic Ocean (W to SW direction) (De Vicente et al., 2011; Martin-Gonzalez and Heredia, 2011). Subsequently, the Miño, which is considered to have a pre-Neogene age (Vidal-Romani and Yepes-Temiño, 2001), captured the Sil during the Pliocene by headward erosion (Pereira et al., 2000). This probably happened during the Pliocene (Pereira et al., 2000). Dated fossils in a kaolinite clay layer underlying the oldest terraces in the lower Miño catchment yield upper Pliocene ages, indicating that the oldest preserved fluvial terraces are upper Pliocene lower Pleistocene in age (Vieira et al., 2011). The Miño Sil mostly flows through bedrock canyons that are incised up to 600 m (Yepes-Temiño, 2002). Alluvial terraces in the Miño Sil catchment are restricted to a small number of fault-bounded tectonic basins (e.g., the Bierzo, O Barco, and A Rua basins), the Ourense basin (Yepes-Temiño, 2002), and the terrace staircase in the lower Miño area.

Chapter 2

Assessment of recent tectonic activity on the NW Iberian Atlantic Margin by means of geomorphic indices and field studies of the Lower Miño River terraces

Until recently, NW Iberia was assumed to be tectonically quiescent (stable). However, a combination of tectono-morphological analyses demonstrates that neotectonic movements do occur, which are in agreement with recent findings by other workers. We use a DEM-based tectono-geomorphic approach in combination with field work to assess the presence and nature of neotectonics in the Lower Miño catchment in NW Iberia. The area is characterized by clearly developed lineaments, coinciding with Paleozoic and Mesozoic faults and fractures and remnants of a peneplain stepping down towards the coast. Longitudinal river profiles show knick points where lithological control can be excluded. Valley shapes show that some valleys have recently been rejuvenated. Systematic asymmetry tendencies of river catchments indicate tilting of fault-bounded blocks. Finally, at several locations faulted terrace deposits of the Miño River have been found.

The types of motions that can clearly be evidenced by our analyses are normal faulting and tilting of fault-bounded blocks. Little clear evidence exists for strike-slip faulting, whereas reverse faulting has not been found in this study. A striking morphological feature of the study area is the presence of small fault-bounded basins, along the course of the river Miño. The tectonic movements take place along inherited, Paleozoic and Mesozoic faults, which apparently act as weakness zones. The reactivation of these faults under the present-day stress-conditions is probably the reason for the complicated pattern and style of present-day tectonic motions that we find. The small basins are particularly difficult to explain. They could result from the interaction of partially, obliquely reactivated strike-slip faults (step-over) and normal faults.

Published as: Viveen, W., Van Balen, R.T., Schoorl, J.M., Veldkamp, A., Temme, A.J.A.M., Vidal-Romani, J.R., 2012. Assessment of recent tectonic activity on the NW Iberian Atlantic margin by means of geomorphic indices and field studies of the lower Miño River terraces. *Tectonophysics* 544-545, 13-30.

2.1 Introduction

Tectonic activity during the Quaternary is still heavily debated amongst geomorphologists, which is partly due to the general scarcity of sedimentary deposits and fossils making it difficult to constrain time-limits on landscape evolution (Martin-Serrano, 1994). The presence of marine and fluvial terrace staircases and peneplain(s) suggests recent, neotectonic uplift, but some authors attribute these landforms either to a delayed incision response to earlier Alpine tectonics (Martin-Serrano, 1994; Martin-Serrano and Molina, 2005) or to not further defined, general vertical movements (Alonso and Pages, 2007). Others argue that tectonic processes might have been active up to the Tertiary/Quaternary transition but not afterwards (Abril-Hurtado et al., 1972ab; Rubio-Navas., 1981). Based on dated colluvia overlying a marine terrace, Trenhaile et al., (1999) and Blanco-Chao et al., (2003) argue that the area has been tectonically active up to the Eemian. From a structural geological perspective, recent findings indicate that Quaternary deformation does occur in NW Iberia (Santanach, 1994; Martin-Gonzalez, 2009; Martin-Gonzalez and Heredia, 2011), but no specific work has been carried out for the area studied in this paper.
The largest river in the region, the Miño-Sil system (Fig. 1.1), has a very extensive terrace staircase. Research of other fluvial systems elsewhere in Europe has demonstrated that contemporaneous climate change and uplift are required to develop and preserve a staircase of fluvial terraces (Veldkamp, 1992; Maddy, 1997; Bridgland et al., 2007; Van Balen et al., 2010). The Miño-Sil system with its terrace staircase could potentially preserve the most complete Cenozoic uplift record of NW Iberia, and makes it therefore a suitable area to investigate the presence and nature of neotectonic activity. Our research on the Miño-Sil terraces has revealed indications for young tectonic motions, like faulting and block-wise tilting of terraces. This indicates that apart from uplift the Miño-Sil is affected by local tectonics. In this paper we combine the field data with DEM-based tectono-geomorphic analyses to assess the presence and nature of neotectonics in the catchment of the Lower Miño River (this region is also known as the Baixo Miño). Research focusing on the Miño has traditionally been restricted to either the Galician side or the Portuguese side (e.g. Teixeira, 1952; Nonn, 1967; Alves and Pereira, 2000; Vidal-Romani and Yepes-Temiño, 2001). Our research integrates both sides resulting in a more coherent overview of the tectonic development of the lower Miño system. We will specifically pay attention to the role of faulting and tilting of fault-bounded blocks, and integrate the current state of knowledge on neotectonics of the area to form a coherent regional neotectonic framework.

2.2 Methodology

2.2.1 Field mapping of faults, basins and terraces

In 2 selected field sites in the Lower Miño River basin we investigated numerous gravel pits and road exposures on the presence and nature of faults and basins. Terraces were mapped based on field studies, aerial imagery and a 5-m DEM (see below).

2.2.2 Digital Elevation Model and lineament analyses

We used 3 different Digital Elevation Models (DEM's) for our tectono-morphic analyses, which comprises the entire area in Fig. 2.1, roughly 70 km by 70 km. The 30-m resolution ASTER DEM (USGS, 2009) was used for drainage basin delineation and the Asymmetry Factor (AF-factor) analysis. The ASTER DEM has a mean vertical error of 15 m. Because this is a large error for river profile analysis, we used a 25-m resolution DEM with a 2-3 m vertical error from the Spanish National Geographic Institute (IGN) for river profile analysis. Also, the 25-m DEM is based on topographic data pre-dating the large infrastructural and mining excavation activities in the area, which make the more recent 30-m DEM unsuitable for river profile analysis.

A 5-m resolution DEM from the Spanish CNIG was used for determining the VF- ratios. The vertical error is less than 0.1 m. The 5-m DEM covers the Spanish part of the Miño catchment and only the first two kilometers or so of the Portuguese side. This DEM as well suffers from artifacts (unremoved bridges, highways, large pits due to mining activities). For these two reasons this DEM could not be used for river profile analysis.

The DEM's were treated to remove sinks, flats and pseudo flats using the LAPSUS Arc Flat module (Schoorl et al., 2002).

On basis of all 3 DEM's and aerial photograph imagery, a map on a scale 1:100.000 was made of all major lineaments. The map was further combined with all known fault data taken from Spanish and Portuguese 1:50.000 geological maps and literature (Cabral, 1995; Martin-Gonzalez, 2009; De Vicente et al., 2009; IGME unpublished data). All the maps presented in this work use UTM N29, ED50 projection and datum.

2.2.3 Geomorphic indices

2.2.3.1 Valley Floor Height-to-Width Ratio

The Valley Floor Height to Width Ratio (VF-ratio) is used to distinguish deep and narrow valleys from broad-floored open valleys. The first tends to be associated with areas where the river is actively down-cutting and has no time to widen the valley (usually

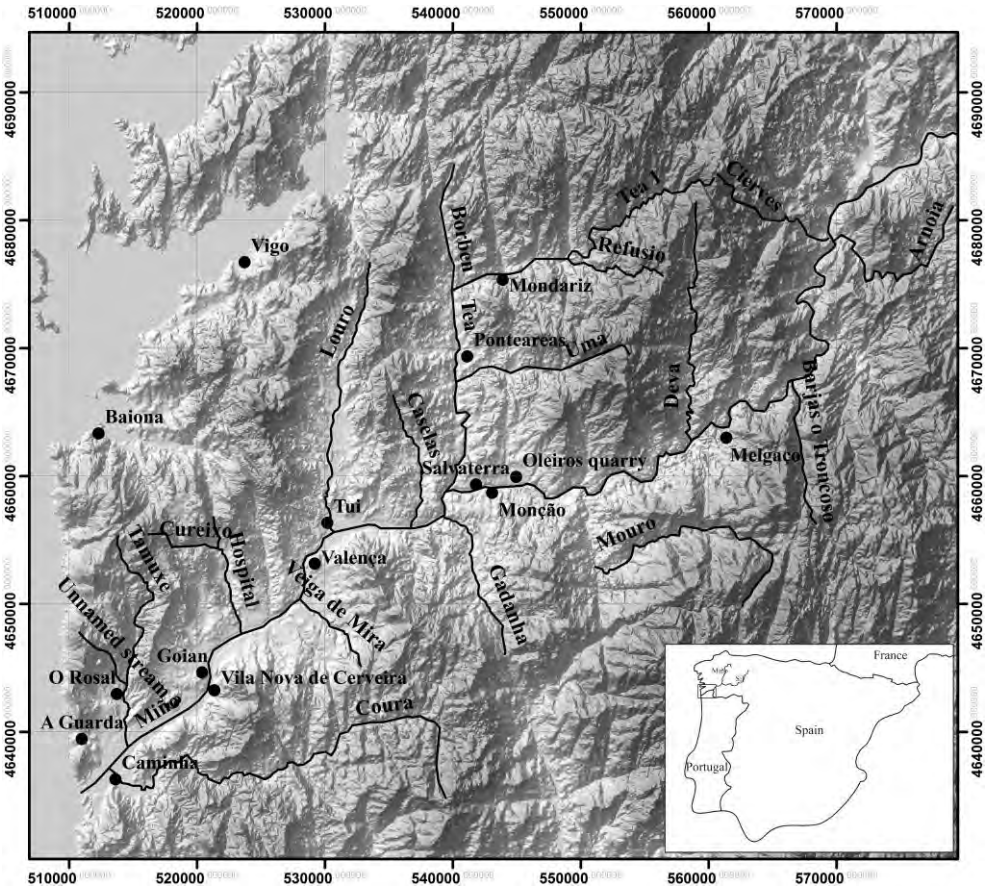

Fig. 2.1. Overview of the study area.

tectonically active regions), whereas the latter valley type is typical for regions where the river base-level has stabilised, for instance in tectonically less active regions. In general, the higher the river incision rate, the narrower and deeper the valley, which may reflect a higher uplift rate. The VF-ratio is usually calculated 500 m to 1000 m upstream from a mountain front (Bull, 2007). The VF-ratio can not determine tilting perpendicular to the stream flow direction.

The VF-ratio is calculated as follows (Keller and Pinter, 1999):

$$Vf = 2Vfw / [(Eld - Esc) + (Erd - Esc)]$$

Where *Vf* is the valley-floor width-to-height ratio, *Vfw* is the valley floor width, *Eld* and *Erd* are absolute heights of the left and right shoulders of the valley and *Esc* is the absolute height of the valley floor.

We calculated the VF-ratio for 35 tributaries of the Miño River. Each VF-ratio was measured 5 times 500 m to 1000 m upstream from a mountain front and then averaged to obtain a

statistically sound measurement.
The VF-ratios range from 0.08 to 9.46. Class boundaries are placed at 0.64 and 1.95 following division into one third quantiles. Silva et al. (2000) consider a value < 1 indicative of tectonically active areas, whereas Bull (2007) sets the limit at 0.5. Our class boundary of 0.64 is in between these limits.

2.2.3.2 T-vector

The Transverse Topographic Asymmetry Vector (T-vector for short) was first described by Cox (1994). It describes preferred stream migration within a catchment and can thus be used to detect block tilting. The T-vector is calculated as follows:

$$T = Da/Dd$$

Where *T* is the T-vector, *Da* is the distance from the active fluvial midline to the basin midline and *Dd* is the distance from the basin divide to the basin midline of the analyzed stretch. T-vectors can be calculated for any point along the river segments and have a magnitude and a bearing. The T-vector is thus more detailed than the Asymmetry Factor, because it works on segment-length scale rather than basin scale.
It is hard to calculate the T-vector in a GIS package, because it is difficult to automate the process of *Da* and *Dd* calculation. Therefore we wrote a script in C# that automatically calculates the T-vector. Input needed are a DEM and a file with catchment boundaries. The script can be downloaded as an executable from
http://www.lad.wur.nl/UK/Research/LAPSUS/T_Vector/

2.2.3.3 Stream Length Gradient Index

The Stream Length Gradient Index (SL-index) was first described by Hack (1973). It effectively analyses the gradient of part of a fluvial profile, corrected for the distance to the drainage divide. An undisturbed river profile will exhibit a typical concave profile with a progressive slope downstream. If the slope of the profile suddenly increases, the SL-index will suddenly increase, resulting in "spikes". Thus, it can be used to determine knick points in a longitudinal river profile. The SL-index is calculated as follows:

$$SL = (dH/dX) * L$$

dH is the height difference of the reach, *dX* is the length of the reach and *L* is the length of the entire reach from the drainage divide up the point halfway the reach of interest.
We selected 282 streams and rivers with lengths ranging from 2000 m to 50.000 m from the DEM with 25-m gridcel size, and calculated the SL-index for successive reaches of 100 m. This was done using ArcGIS Spatial Analyst and Hawth Tools (Beyer, 2004). For each river, the height values were averaged using a moving window of 5 neighbours. In total over 15.000 SL-index values were calculated. The values were then interpolated by means of block kriging. The semi-variogram was estimated using the VESPER package (Minasny et al., 2002). By these procedures, small narrow spikes in the SL-index that are the result of DEM artifacts have been smoothed out.

In general, low SL-index values are indicative for tectonically less active areas and for areas with bedrock which is less erosion-resistant. Low values are also found in subsiding settings, because river channels tend to be less steep.
High SL-index values are indicative for tectonically more active areas (Keller and Pinter, 1999), highly erosion-resistant bedrock, or migrating knick points due to base level lowering events in the past. If the latter two can be discarded, the high SL-index values can be used as indicator of vertical tectonic motions (Burbank and Anderson, 2001; Peters and Van Balen, 2007). The SL-index is thus a useful tool to differentiate between areas of varying tectonic activity.
We also visually inspected the 282 river profiles for the presence of knick points, because relatively low SL-index values that fall in the lowermost tectonic class may still indicate subtle tectonic activity, especially in areas of lower relief (e.g. Peters and Van Balen, 2007). We then checked if knick points coincided with filled-up areas in the DEM, boundaries between different rock types or infrastructure such as dams and bridges. They were considered tectonically-induced knick points if they did not coincide with any of the above and were located close to a lineament. It is possible that preferential erosion along a lineament could cause a knick point without the lineament being an active fault; the presence of a convex reach of the river profile bordering the lineament would therefore be an additional indication that differential uplift takes place instead of preferential erosion (taking into account that this cannot be applied to regions where two rock types of varying rock strength meet).

2.2.3.4 Asymmetry Factor
The Asymmetry factor (Hare and Gardner, 1985) is one of the most widely used tectonic indicators. It can be used to indicate the amount of tilting in a drainage basin. It is calculated as:

$$AF = (Ar/Al) * 100$$

where *Ar* is the area on the right side of the drainage basin, looking downstream and *Al* is the area on the left side. The main river serves as the divide between the two areas. In this study 250 drainage basins were analysed.

2.2.4 Channel steepness and basin asymmetry class map

We combined the maps of interpolated SL-indices and AF-values into a region-scale map with 5 classes. The map can be used to determine in which areas more marked channel steepness and basin asymmetry occur and in which areas less. In a later stadium, after discarding other possible explanations, this may be interpreted in terms of varying levels of tectonic activity.
SL-index values have been incorporated in these kinds of maps before (Bull, 2007). A

common problem when interpreting the SL-index values directly in terms of "tectonic activity level", (e.g. high values reflect high tectonic activity and low values little tectonic activity) is that the values may be dependent on rock type as more erosion-resistant rock gives higher values. Some authors therefore choose to evaluate a statistical relationship between the two (Hamdouni et al., 2008; Font et al., 2010). In our opinion this is not necessary for our study area as only 2 dominant rock types exist that are spread out more or less evenly throughout the region and a visual match between geology and tectonic class is clearly not present (Figs. 1.2 and 2.12).

So, first, both indicators are divided into classes of increasing intensity for both indices. Presently there are no absolute values available that distinguish between classes. Font et al. (2010) solved this problem by using the standard deviation as class boundaries. Our calculated SL-index and AF values show a strongly positively skewed distribution and therefore the standard deviation cannot be used. Instead we choose to divide the indices into three classes using quantiles at one third intervals. The classes of the two indices were simply added up and divided by 2, yielding 5 classes in total. These are 1) graded profiles and symmetric valleys, 2) graded to moderately graded profiles and asymmetric valleys, 3) moderately graded profiles and moderately asymmetric valleys, 4) moderately graded to strongly disturbed profiles and strongly asymmetric valleys, 5) strongly disturbed profiles and strongly asymmetric valleys. Because of the difference in detail between the Asymmetry factor (catchment scale) and the SL-index (100 m interval along a river profile), the resulting map can only be interpreted in broad terms.

2.3 Results

2.3.1 Field evidence for faulting and tectonic motions

2.3.1.1 Valença-Goian (western sector)

Several distinct groups of terraces exist in the region that are clearly separated by N-S, NW-SE and E-W trending lineaments (Figs. 2.2 and 2.3, and Fig. 2.4 for cross-section A-A'). A lineament is a structure on the DEM that follows a linear trend, but which cause is yet unknown, whereas a fault is a linear structure with clear tectonic activity associated to it. Associated with these lineaments are often steep bedrock scarps. Also, very large sub horizontal surfaces occur, whose extend nor height agrees with those of the general

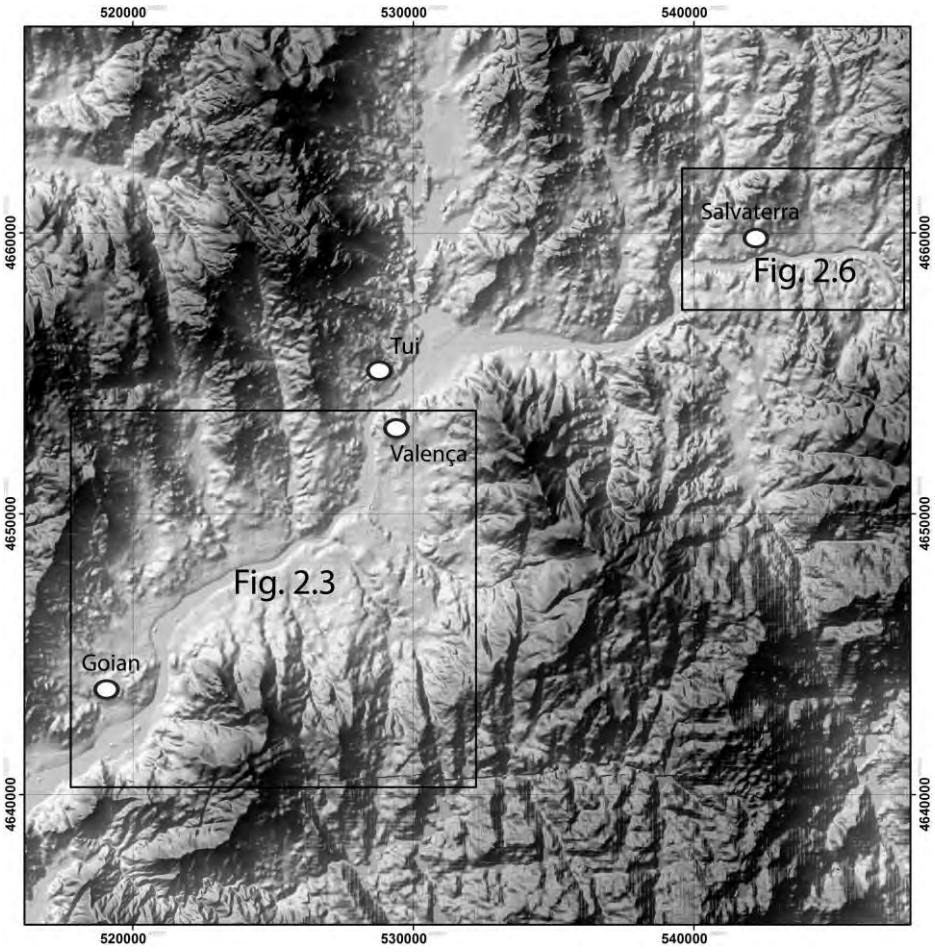

Fig. 2.2. Overview of field study locations discussed in Figs. 2.3. and 2.6.

terraces levels in the region. The large surfaces sometimes form the top of very thick gravel accumulations. For example, a quarry located in geomorphological depression 1 shows at least 13 m of gravel deposits and one in geomorphological depression 5 at least 11 m (Fig. 2.5A). Outside these areas terrace levels usually have a couple of meters of sediments at the most (Fig. 2.4). Therefore, we interpret these areas as tectonic basins. Moreover, in tectonic basin 2 we encountered an active sag pond along N-S and NW-SE trending faults. At the western side of tectonic basin 2, we found evidence of tilted layers which can be explained as the result of basin subsidence (Fig. 2.5B). Finally, in the tectonic basins, close to the DEM lineaments, we have found large quantities of kaolinite clays. Such clay accumulations are associated with thermal springs along (active) faults (Coelho et al., 2009).

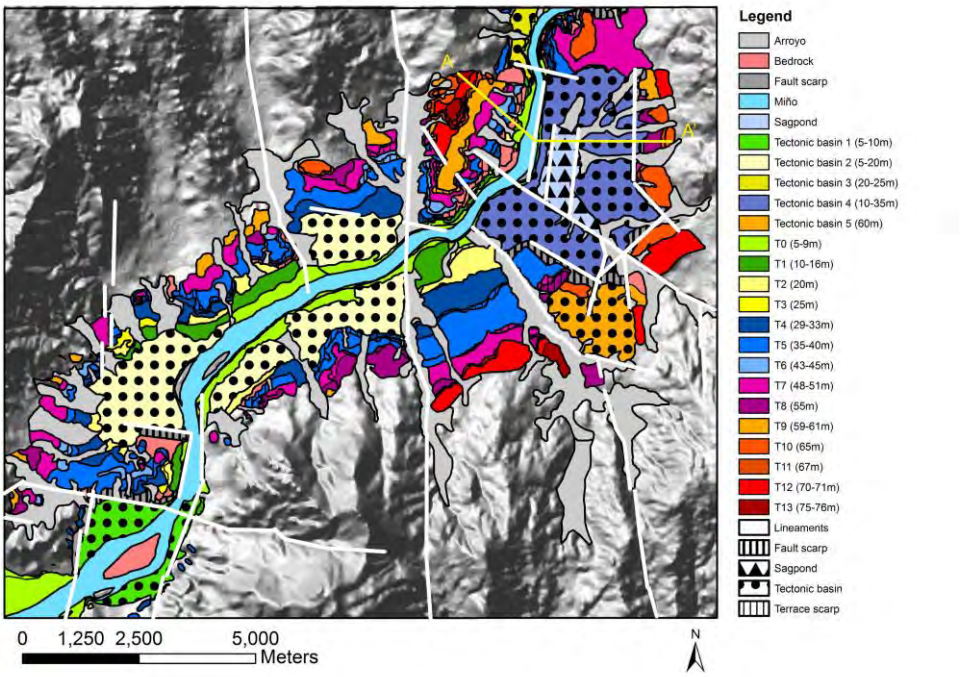

Fig. 2.3. Fluvial terraces in the Valença – Goian sector. Terraces were mapped using 5-m DEM and extensive field work. T0 is the current flood plain and not a real terrace yet. Therefore numbering starts with "0". Mapping of all lineaments is based on DEM-analysis and geological maps solely. Please note that an in-depth description of the Miño terraces is beyond the aim of this paper.

2.3.1.2 Salvaterra (eastern sector)

The terraces in this area appear quite regular with intervals of 5 m, but on the north bank an exceptionally large terrace is situated between 30 and 50 m (Fig. 2.4, cross-section B-B' and Fig. 2.6). A large mine is situated in the 30 – 50 m, 59 - 61 m and 70 -71 m terraces.

The gravelly deposits reach thicknesses of over 20 m in the deepest sections of the 30 – 50 m terrace and are associated with large quantities of kaolinite clays, hinting at thermal springs. The underlying bedrock is exposed in the northern part of the mine. In the quarry we have encountered 4 different faults. Fault 1 is a large NW-SE trending normal fault that can be followed throughout the mine. Evidence of striae has not been found. It marks the contact between the fluvial terrace at 65 m and the exceptionally large terrace at 30 – 50 m (Fig. 2.5C). Based on the faulted contact, the large thickness of the gravels and the large extent of the terrace surface, we interpret it as a tectonic basin. The

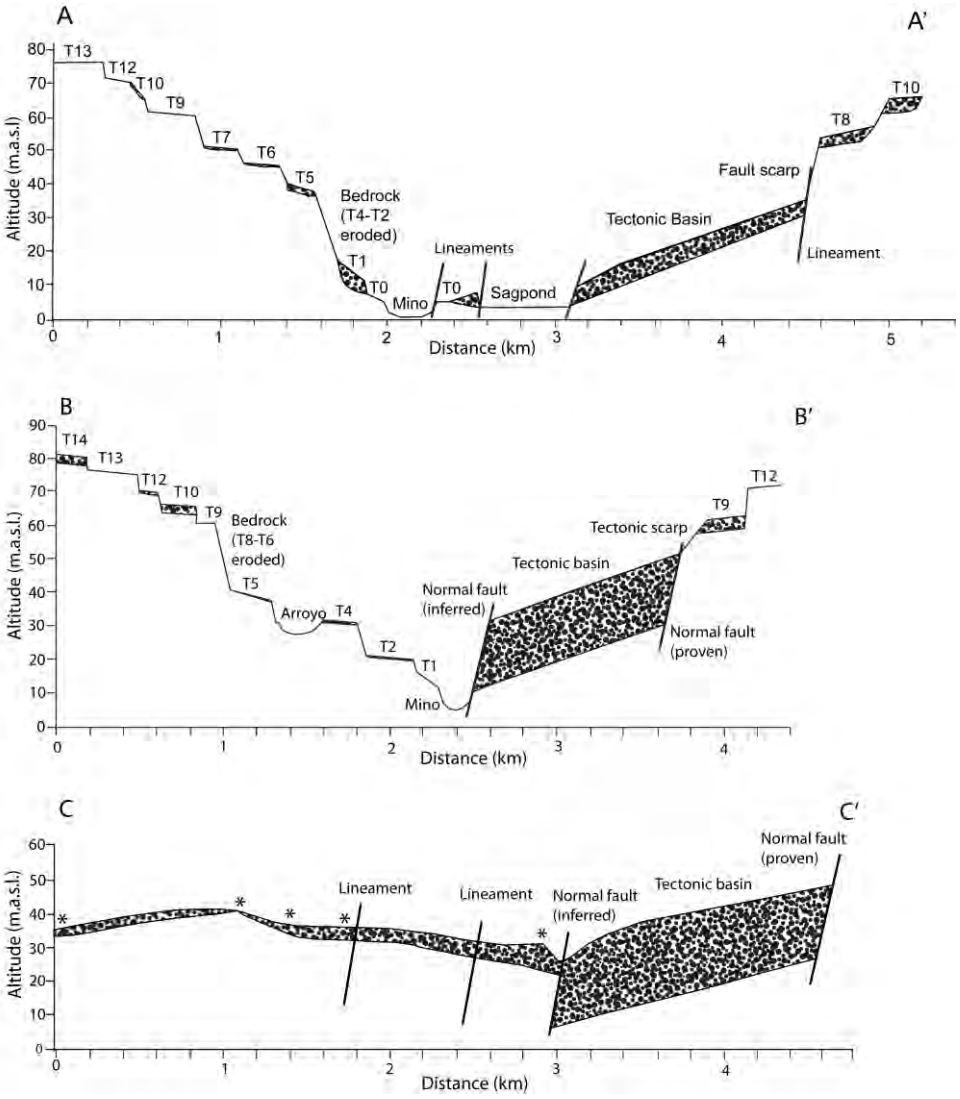

Fig. 2.4. Terrace transects of the Valença-Goian (A) and Salvaterra-Monção (B) sectors. Transect (C) shows gravel thickness of the large 30-50 m terrace. Gravel thickness determined by actual measurements along road cuts and in gravel mines. For every terrace at least one exposure was described. Depth refers to distance terrace surface – contact bedrock. Gravel thickness for the tectonic basins are minimum values, for the terraces exact values. Asterisks in transect C mark places where depth measurements were taken; the tectonic basin was inventoried entirely.

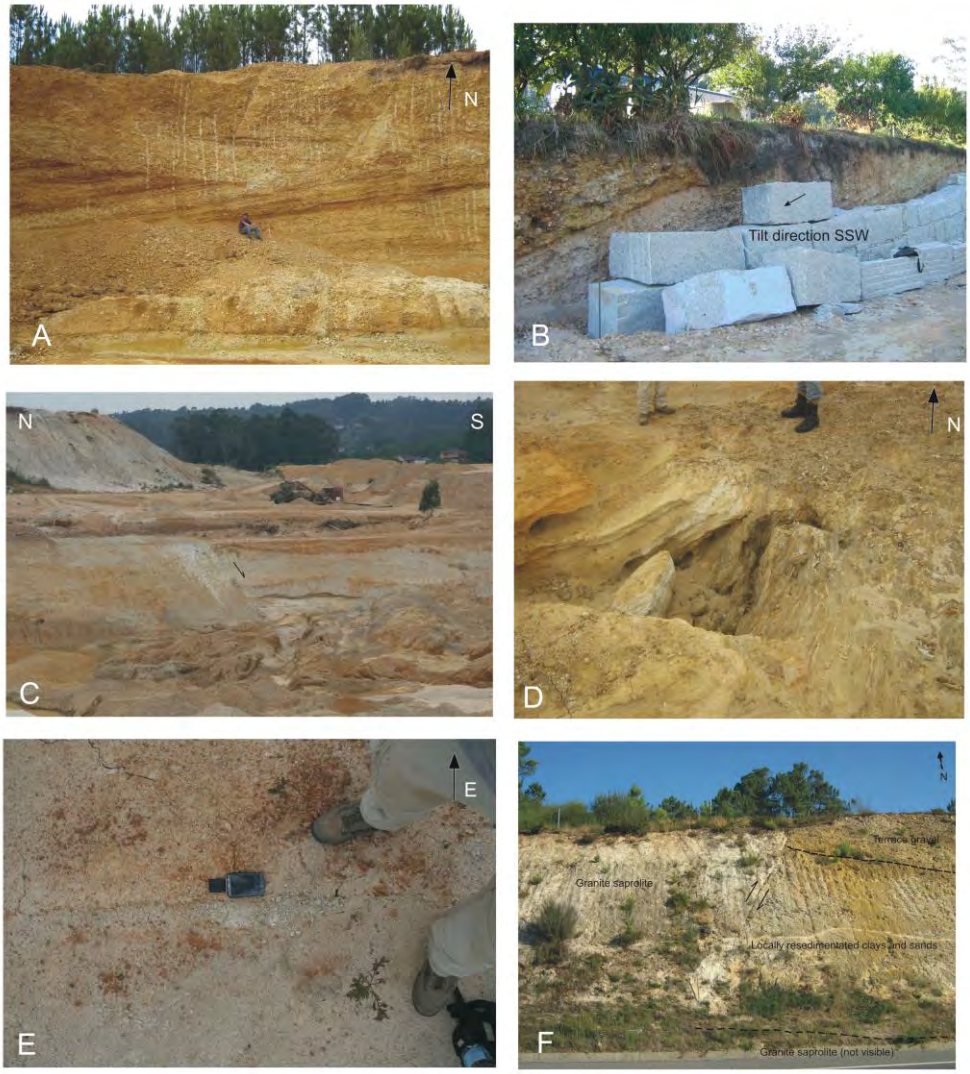

Fig. 2.5. Photo compilation of tectonic evidence. A) Quarry in tectonic basin 5 showing siliclastic gravel and large fore sets. Gravel thickness exceeds 11m. B) SSW-directed tilting of fluvial sediments indicates basin tilting. Exposure height is 4.5 m and total gravel thickness is 8 m. C) NW-SE directed normal fault (fault 1 in text) marking the border between the gneiss saprolite (left of fault) and the infilled tectonic basin (right of fault). Crane for scale. D) Contact between weathered gneiss and fluvial clay beds. Drag effect along an NW-SE axis indicates pure normal offset within the 70 -71 m terrace (fault 2 in text). E) N-S-directed normal fault, (Fault 3 in text). F) Normal fault with minimal 10 m off-set in fluvial terrace along new motorway, west of Salvaterra. The fault is almost vertical but this seems not to be due to the way in which the fault plane is cut.

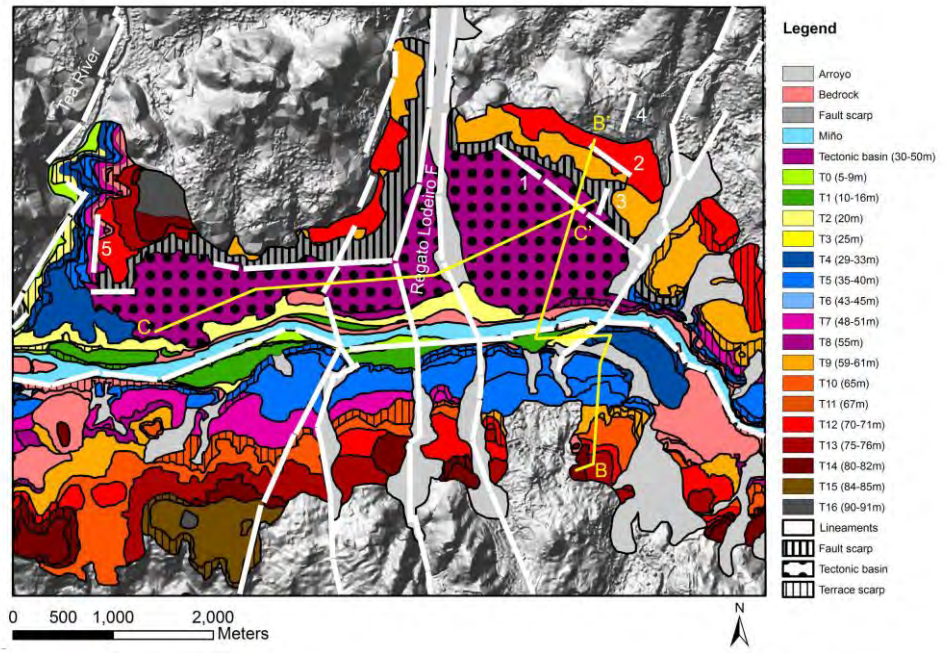

Fig. 2.6. Fluvial terraces in the Salvaterra-Monção sector. Terraces also mapped using 5-m DEM and field work. Mapping of lineaments and faults based on DEM and geological maps. Faults found in the field are numbered 1-5.

sediments in this basin are not tilted. The top of the 65 m terrace we thus consider to be the top of the basin fill. Fault 2 also trends NW-SE and forms a contact between weathered gneissic bedrock and the oldest fluvial terrace (70 - 71 m). Clear signs of drag in the fluvial fine sands indicate that the fault has a pure normal offset (Fig. 2.5D).
In the eastern sector of the mine we have observed 2 apparently normal faults (faults 3 and 4, Fig. 2.6) with a strike of 20 degrees N (Fig. 2.5E).

Results of mapping the gravel depths shows that only the part east of the N-S trending Regato Lodeiro fault has a large infill and has thus been subsiding long after the section on the west side ceased to subside (cross-section C-C', Fig. 2.4). Given that younger terraces formed (T1 and T2, see Fig. 2.6 and Fig. 2.4, cross-section B-B') we infer that the basin is no longer subsiding as terrace scarps are difficult to form in such a setting (Maddy, 1997).
Lastly, about half a kilometer east of the Tea River, a normal fault was exposed in a road cut. The fault forms the contact between granite saprolite and a fluvial terrace (fault 5, Fig. 2.6 and Fig. 2.5F). The fault trends 20 degrees N and has an estimated off-set of at least 10 m, with clear drag compatible with a normal faulting component.

2.3.2 VF-ratios

The VF-ratios are presented in Table 1 and in Fig 2.7. Low VF-ratios east of the Tea River point towards deeply incised V-shaped river valleys. These are interpreted to be the result of rapid tectonic uplift. Valleys in the A Groba and Argallo massifs also have low VF-ratios that indicate deeply incised valleys possibly resulting from uplift. Relatively high values west of the Tea River, for instance around the Louro and Caselas Rivers, could indicate absence of tectonic uplift or even subsidence. However, in this case another explanation lies in the erodibility of the subsurface consisting of terrace gravels. Valley numbers 23, 31, 33 and 35 with low VF-ratios are small tributaries in hard rock. This indicates that tectonic uplift is occurring or that stream power is sufficient to incise in the rock, but not enough to broaden the valley sides. The latter is contradicted by the high VF-ratios in the surrounding river valleys.

Table 2.1. VF-ratios. Numbers refer to locations where VF-measurements were taken.

Number	VF-ratio	Number	VF-ratio	Number	VF-ratio	Number	VF-ratio	Number	VF-ratio
1	0.18	8	0.35	15	1.32	22	1.20	29	3.02
2	0.72	9	2.87	16	1.52	23	0.17	30	0.29
3	0.39	10	1.96	17	4.06	24	3.50	31	0.09
4	0.64	11	3.07	18	1.26	25	4.15	32	9.47
5	0.28	12	1.08	19	2.16	26	2.73	33	0.40
6	0.23	13	1.70	20	2.76	27	1.70	34	4.49
7	1.27	14	1.52	21	1.98	28	0.24	35	0.31

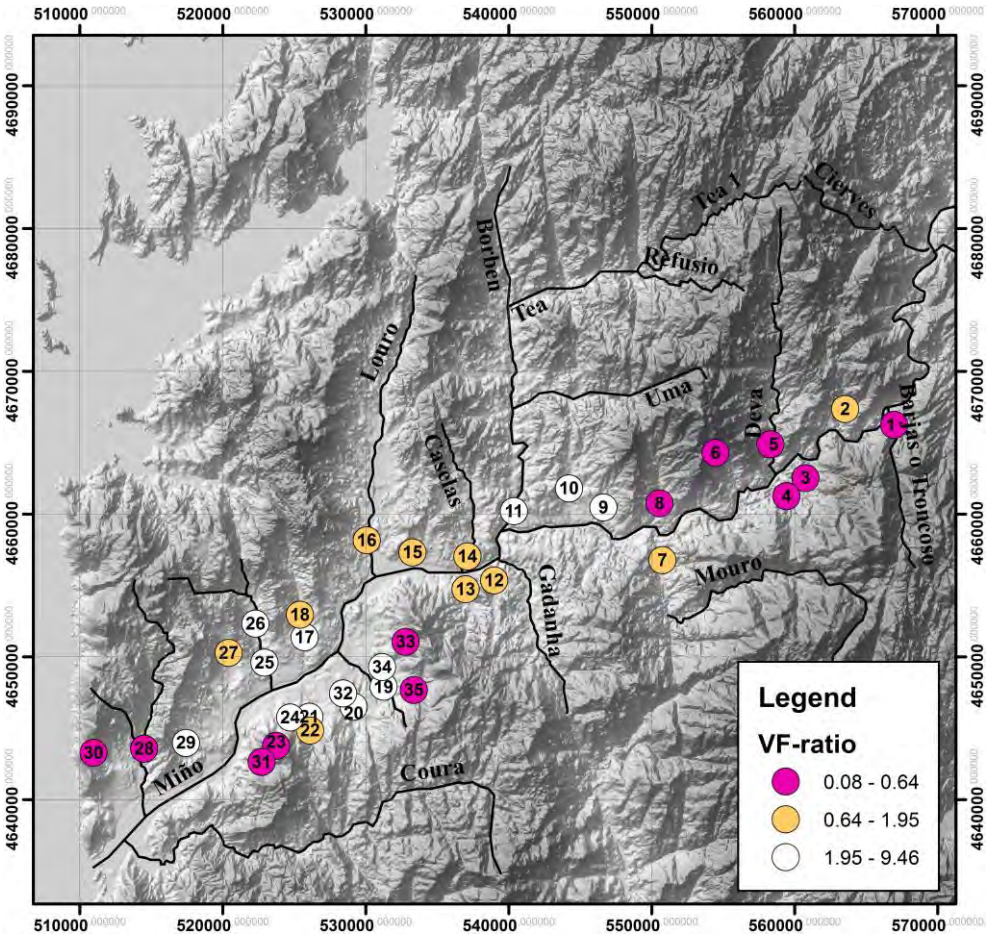

Fig. 2.7. VF-ratios taken in the Miño catchment. Numbers refer to Table 2.1.

2.3.3 T-vector

The T-vectors are presented in Fig. 2.8. Fig. 2.9 shows a rose plot with vector directions. The Figures show that most rivers are being oriented towards a NE-SW to ESE-WNW direction. In general, dip direction of rock strata may cause basins to develop a preferential asymmetry (Salvany, 2004; Khavari et al., 2009). However, this not the case in our study area, due to the homogenous geological build-up consisting of metamorphic rocks and granites (Fig. 1.2). As an example, the Tamuxe valley is indeed located in a zone of weaker rock (schist). However, the asymmetry of this valley is not related to the dip-directions of the lithological contacts.

The most intense asymmetry occurs in the eastern part of the study area and in the

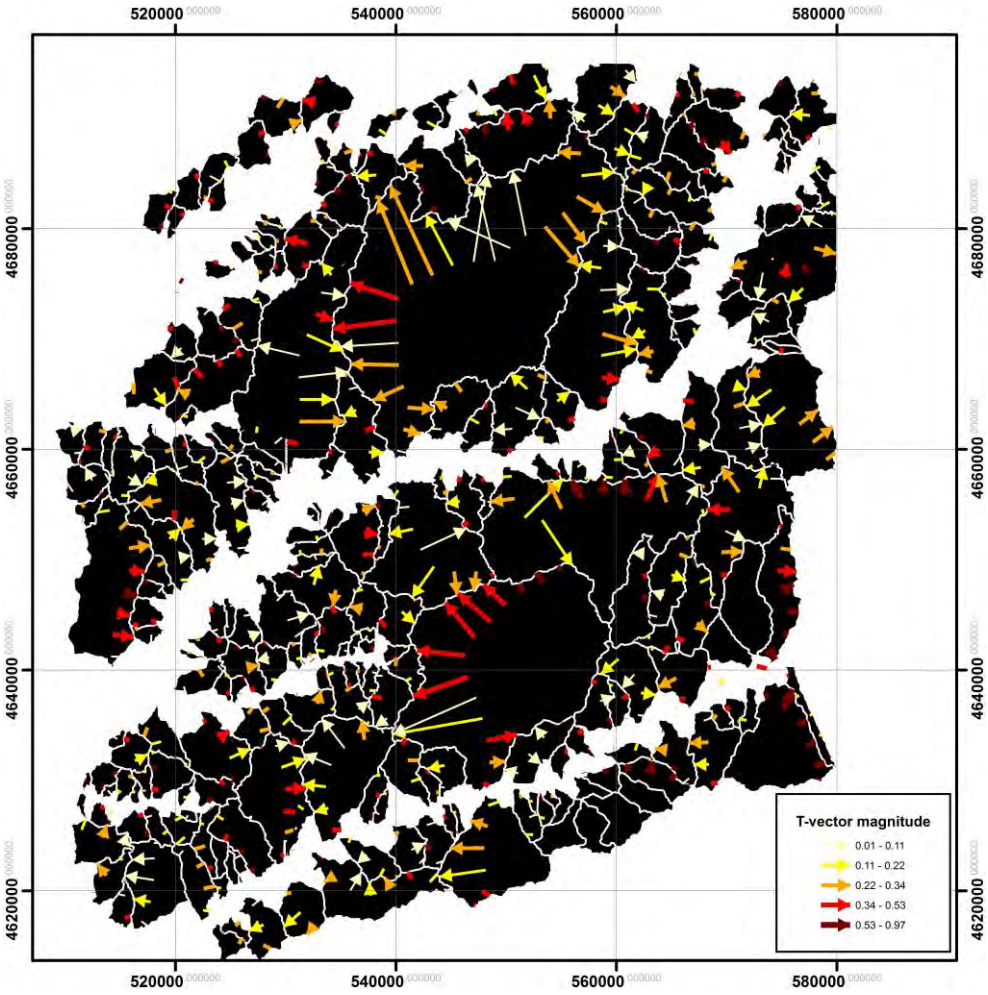

Fig. 2.8. T-vectors. Magnitude ranges from 0 (no tilting) to 1 (maximum tilting). Class interval based on quantiles. Color gives magnitude. Catchment boundaries shown by white delineations. Please note that the T-vectors cover a larger area than the tectonic class map; in this case the area around the Lima River is also included.

Tamuxe valley close to the Atlantic coast. In addition, in the eastern part neighbouring catchments have opposite asymmetries. This suggests tilting of the blocks delimiting the catchments in opposing directions. Timing of block tilting is not clear however. Drainage basin asymmetry may take a long time to develop in response to block tilting, for instance 100 ka to 200 ka (Burbank and Anderson, 2001). Basin asymmetry should therefore be used to assess block tilting on a Quaternary time scale and not so much on a Holocene timescale. A last note concerns the limitation of the technique to only be able to signal block tilting perpendicular to the main stream in a watershed. Tilt parallel to the direction of

the main stream cannot be assessed. It is therefore possible that areas that show small T-vector magnitudes, actually experience tilt.

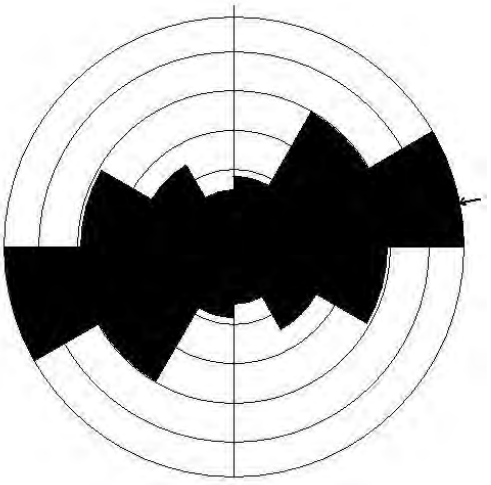

Fig. 2.9. Rose plot for 819 T-vector bearings (using GEOrient software (Holcombe, 2003)). Almost all vectors have a bearing from NE-SW to ESE-WNW.

2.3.4 SL-index

A selection of representative river profiles and their SL-index is presented in Figs. 2.10 and 2.11. We divided the profiles in two groups: A group with concave graded profiles without knick points; and a group with convex reaches and one or more knick points.
Some reaches, for instance the lower reach of the Louro River and the lower reach of the Tea and Borbon Rivers, have very little gradient and therefore SL-index values of 0. Others show combinations of (multiple) knick points and flat reaches. Many rivers in Galicia share the same characteristics (Nonn, 1966; Rio-Barja and Rodriguez-Lestegas, 1992). In principle they can have different causes, like head ward incision due to sea-level oscillations (suggested by Pannekoek (1970), lithological changes and tectonic motions. We do not consider intermediate-sized SL-spikes, since they reflect small irregularities in the river profiles that may or may not be related to small-scale faults. Other studies have

shown that the SL-index pattern usually has an oscillating character and that its best to focus on the larger spikes as they most likely represent the larger faults (Hayakawa and Oguchi, 2006; Peters and Van Balen, 2007; El Hamdouni et al., 2008). We proceeded by eliminating those knick points coinciding with lithological changes (Fig. 1.2), including terrace bodies of the Miño, although such knick points might actually still represent faulting activity if the lithological change is caused by a fault. A knick point was considered to be

caused by an active fault when it coincided with a lineament on the DEM (see below). By comparing Figs. 2.1, 2.10 and 2.11 it becomes apparent that most rivers with a graded profile are found in the western part of our study area. The rivers with unbalanced profiles are mostly found in the eastern sector, the area east of the Tea River. This pattern corresponds with the results of the VF and T-vector analyses.

2.3.5 Combined AF and SL-index results in map view

Fig. 2.12 shows the map with combined AF and SL-index values. Each of the underlying methods have their limitations (see methodology section), but by combining them into one map-based index these limitations are reduced. The map basically combines channel steepness and basin asymmetry in one, and as both are indicative for tectonic activity (other possible causes were already discarded), the map may be viewed as a tectonic activity class map. Note that the region experiences a low to moderate amount of tectonic activity and the tectonic activity classes should be viewed in that light.

The map shows that in a large part of the Baixo Miño area clear signs of block tilting and uplift are present, but there is a distinct separation between two different sectors. The sector east of the Tea River displays most indications for tectonic activity, due to the clear asymmetry in drainage basins and high SL-index values. West of the Tea River, fewer indications for tectonic tilt and differential uplift are found, even though they are still present as field evidence cleary shows. Neither SL-index analysis nor the VF-ratio has revealed these movements. These methods are good at highlighting relative uplift but not subsidence. It might even be that the streams are here in equilibrium with regional uplift and therefore have graded profiles, whereas in the eastern sector they are actively responding to perturbations (e.g. Whittaker et al., 2008). In the westernmost area, the A Groba massif north of A Guarda and the Argallo massif north of Goian, show indications of tectonic activity. The AF-analysis shows that 83% of the Tamuxe basin is located west of the Tamuxe and only 17% located east of the Tamuxe River. This suggests that the A Groba massif is tilting towards the east along a N-S axis.

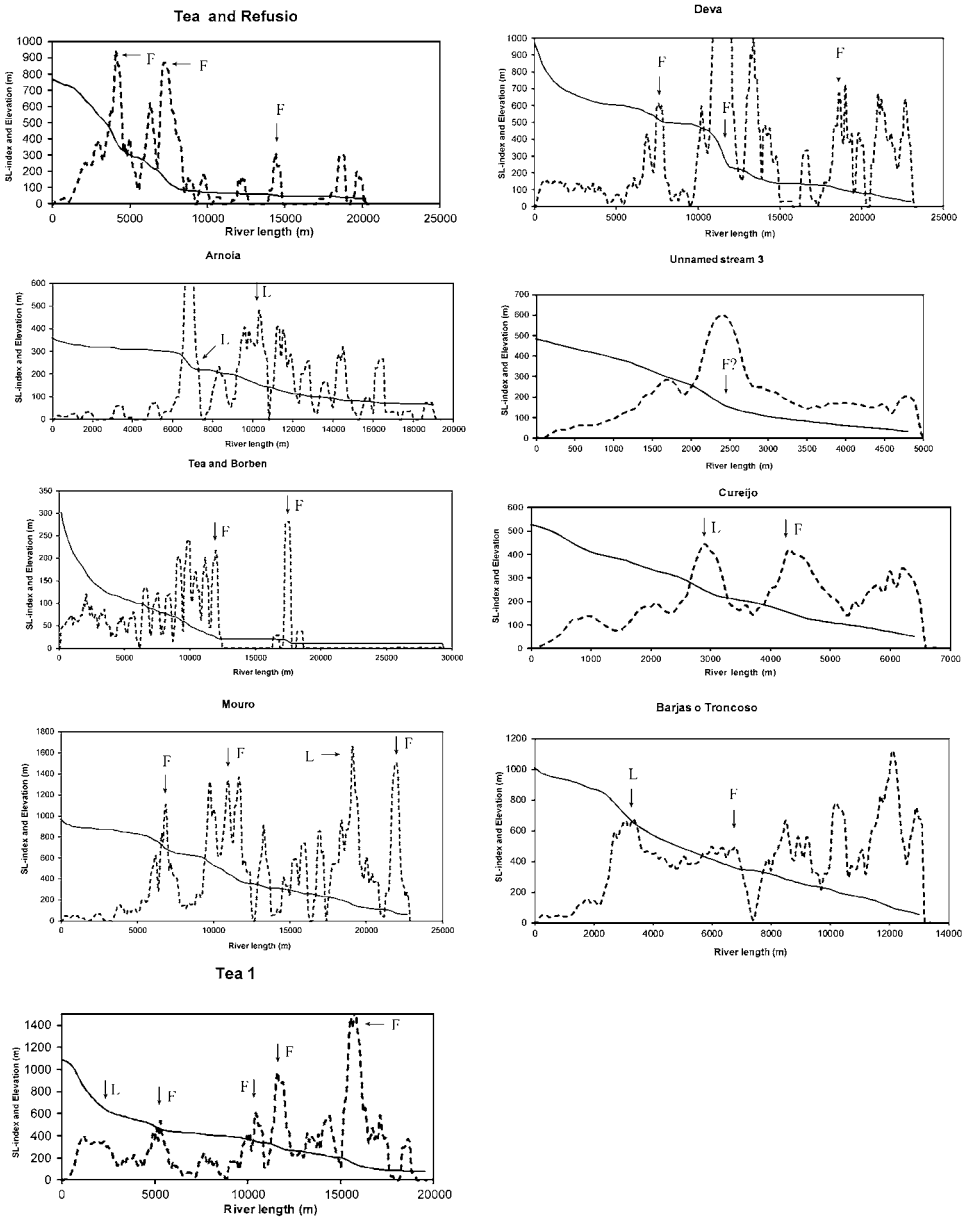

Fig. 2.10. Selected rivers that show signs of tectonic disturbance. They are mostly located in the eastern part of the study area. Black line = river profile; dashed line = SL-index. Knick points indicated by arrows. F = knick point due to active fault; L = knick point due to lithology; T= knick point due to fluvial terrace transition. Highest SL-value for Deva River attains a value of 3500, but has been cut off at for viewing purposes. Same for Arnoia River.

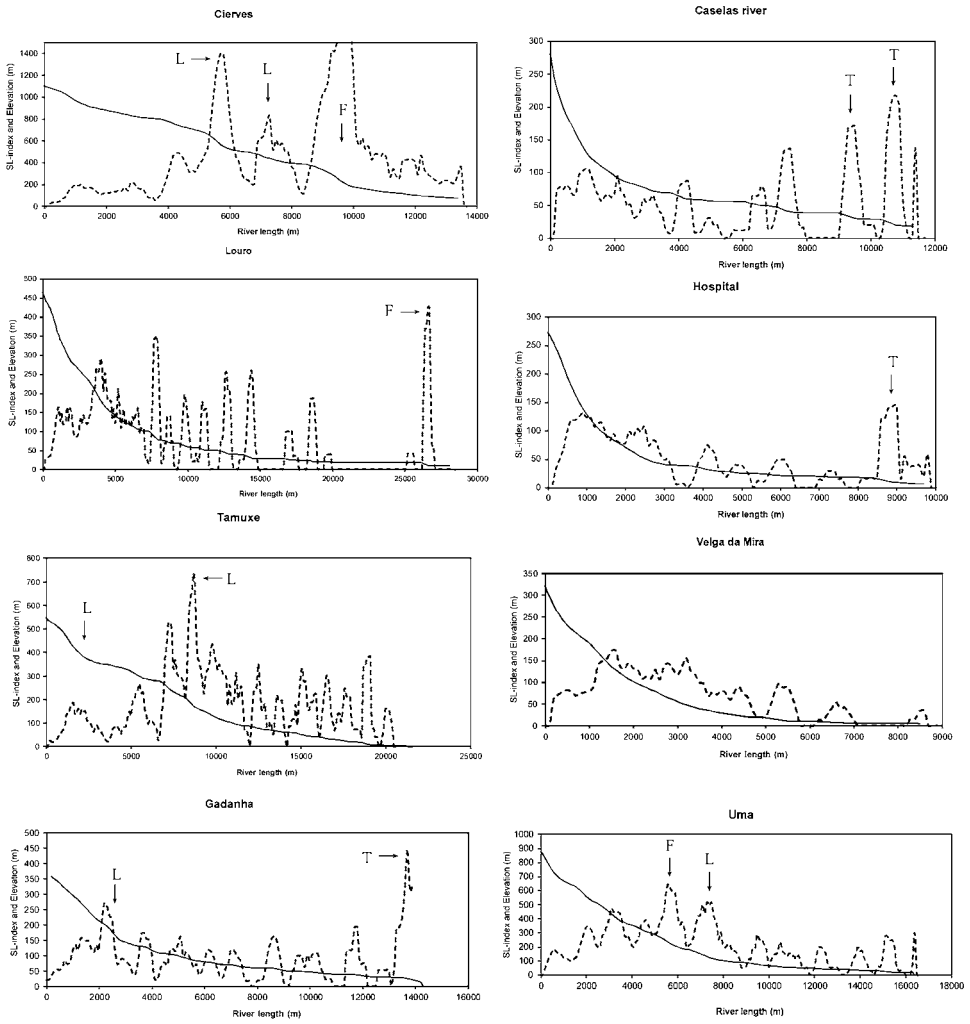

Fig. 2.11. Selected rivers that show a graded, non-disturbed profile. These are mainly found in the western sector of the study area. Exception is the Cierves River that does show tectonic influence.

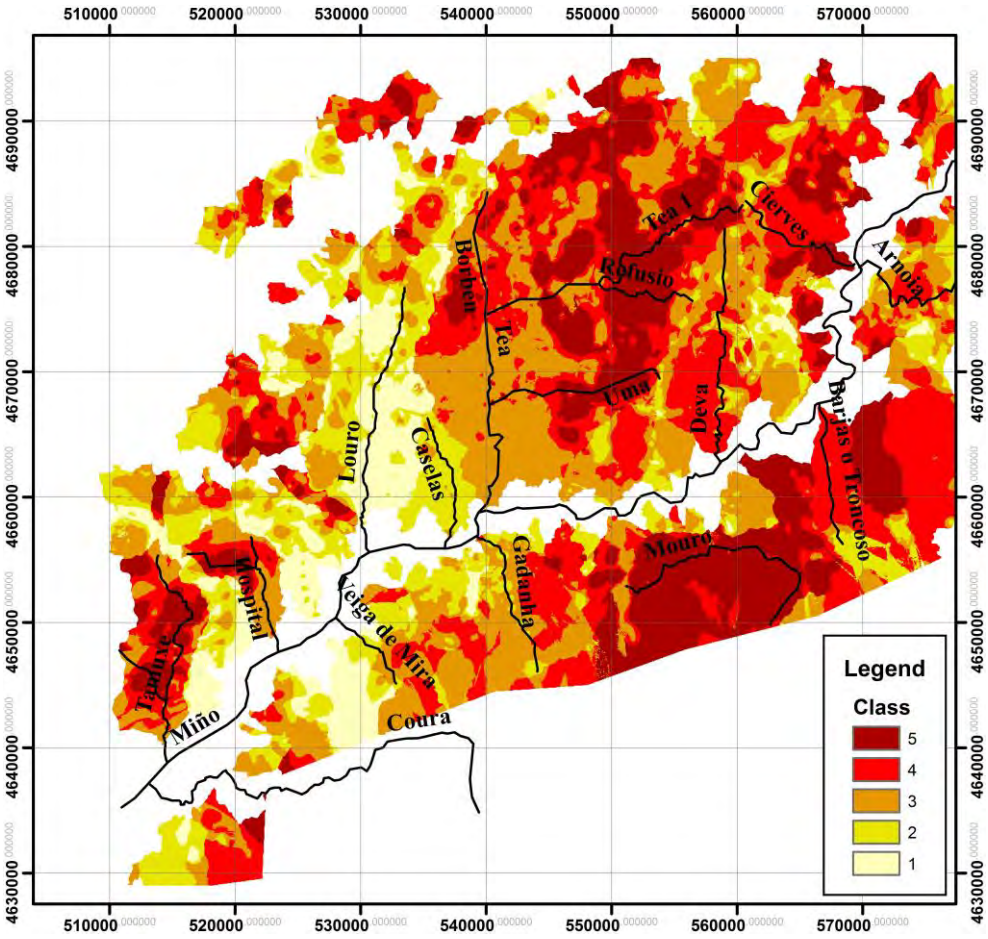

Fig. 2.12. SL-index and AF-values in combined map view. The map is divided into 5 classes with class 1 showing very little evidence for block tilting and differential uplift and class 5 showing strong indications for tilt and uplift.

2.3.6 Structural lineament map

The structural lineament map (Fig. 2.13) was constructed by mapping lineaments visually on the DEM. In the landscape these lineaments coincide with the courses of (fluvial) valleys. They thus represent areas of preferred fluvial incision. Most likely they coincide with faults and fractures in the subsurface as their overall direction and position coincides with known faults in the area (Abril-Hurtado, 1972ab; Pliego-Dones et al., 1972; Moreira and Simões, 1988; Rubio-Navas, 1981). Using results from our field observations and geomorphic indices, most importantly the SL-index and the VF-ratio, the lineaments have been interpreted as active and inactive faults. The analysis is thus restricted to faults with

vertical displacements; this method does not allow determining active strike-slip faulting. The results show that most of the active faults with a vertical component are situated east of the Tea river valley and north of A Guarda. Most passive faults are located in the Lower Miño estuary in between the Tea River and the massif north of A Guarda.
A rose plot was constructed for the active faults (Fig. 2.14). Most active faults trend NNW-SSE to NNE-SSW. A smaller but still notable population of active faults trends NE-SW and SE-NW. These faults occur in the eastern part of the study area. The east-west difference in strikes could reflect a difference in the structural grain of the crust. Only when strike-slip faulting is associated with block uplift, e.g. because of oblique movements, and only when also the SL-index for streams perpendicular to the strike-slip faults is taken into consideration, can wrench fault activity be accurately assessed. Keller and Pinter (1999) argue that constant low SL-index values in strike-slip systems also indicate fault activity, because brittle deformation along faults creates less erosion-resistant rock, but this is difficult to verify if other evidence is absent. So, although some of the streams in the studied area have low SL-index values and are aligned N-S to NNE-SSW, which is the main direction of the active strike-slip faults in NW Iberia, absence of conclusive field evidence, seismic activity and low T-vector and AF-ratios, suggests that strike-slip activity is low.

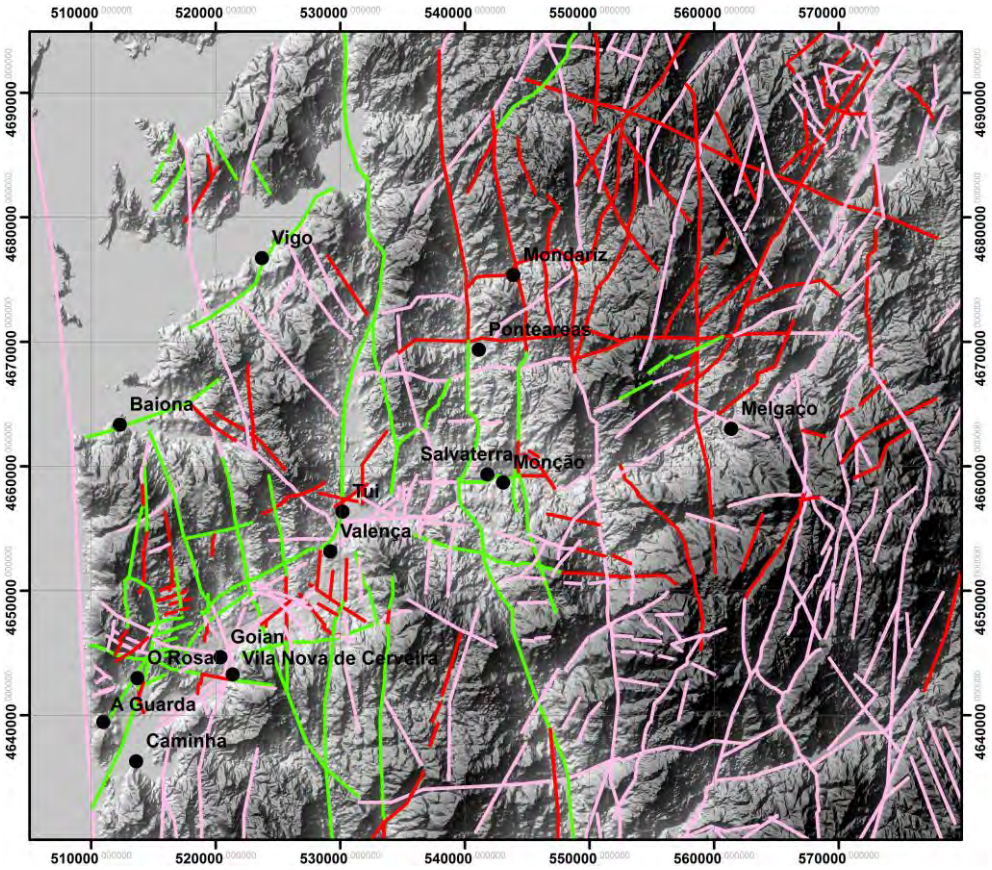

Fig. 2.13. Lineament map of the study area based on field studies, knick point analysis and lineament mapping. Red lines = active faults; Green lines = passive faults; pink lines = undetermined activity. Fault activity was undetermined in the southeastern sector (Peneda-Gerês mountain block) because we did not have a 25-m DEM for that area and could thus not calculate SL-indices. Activity for other lineaments was considered undetermined if the lineaments occurred where two rock types met.

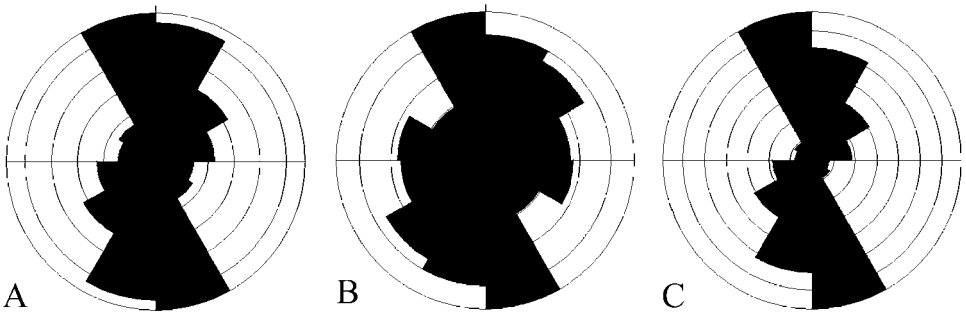

Fig. 2.14. Length-azimuth rose plots of lineaments constructed using GEOrient software (Holcombe, 2003). A) All lineaments; B) Active faults; C) Passive faults. Each segment represents 5% of total.

2.4 Discussion

According to our geomorphic analyses, faults are active in our study area. That is, fault lineaments are associated with vertical displacements. Our methods do not allow making inferences about strike-slip motions. In addition, tilting of fault-bounded block takes place, and locally fault-bounded basins subside. These vertical motions take place along pre-existing, Paleozoic and Mesozoic faults. Apparently, present-day stresses originating from far away plate-boundaries are capable of reactivating these faults. The present-day stress regime is characterized by a compressive maximum horizontal stress and an approximately equal vertical stress, whereas the minimum horizontal stress is tensile (De Vicente et al., 2008). The orientation and magnitudes of the present-day stresses are likely to be different from those which originally created the faults. According to our geomorphic analysis the N-S directed strike-slip faults play an important role in the present-day landscape development of NW Iberia. Parts of the faults are being reactivated. That is, along- strike parts of a pre-existing fault show evidence for vertical displacement whereas others do not (lateral motions can not be inferred). In addition, small subsiding basins occur, most of them along a N-S trending fault, like those south of Valença and east of Salvaterra. These tectonic phenomena probably occur due to the non-optimal angle between the orientation of the pre-existing faults and the present-day principal horizontal stress directions. We speculate that this results in a combination of local normal faulting (NW-SE faults), oblique slip motions and strain transfer from one N-S segment to the next via, for example, E-W faults. Alternatively, the small subsiding basins are pull-apart basins originating from active motions along strike-slip faults, for which we have not found evidence. More research is needed to elucidate the underlying mechanisms, but crustal shortening due to plate convergence along the Cantabrian-Pyrenean border seems plausible (De Vicente and Vegas, 2009).
It is possible that the course of the Miño River itself is also influenced by left-lateral strike-slip movements, as the Miño changes course from E-W to N-S at various confluences with N-S trending tributaries (e.g. the Tea and Louro Rivers). On the other hand, it may also be that the Miño simply runs through zones of weaker rock that are eroded preferentially along these N-S trending lineaments. There is also a striking coincidence between the most instrumentally seismic active zones in our study area and what we propose is the most active area of fault activity and block tilting (see Figs 1.4 and 2.12, the area around Mondariz). However, this study is not suitable to assess relationships between seismicity and faulting, therefore, future geomechanical modelling will need to study this topic further.

Vegas (2010) proposes that the Miño region is being uplifted. Cabral (1995) proposes a gradual increase in uplift from the west to the east in the Miño region. We partly agree with these inferences. The preservation of an extensive set of fluvial terraces in the Mino and its

tributaries and the remnants of a planation surface shows that uplift is occurring in the entire region.
However, contrary to Cabral (1995) we propose that a gradual increase is perhaps not the best uplift model since the Tea River clearly marks the transition from a 600 m remnant of a planation surface to the west to a higher elevated one to the east. Similarly, we have found terraces up to 90 m close to Salvaterra (near the Tea) and other authors have described levels up to 120 m (Teixeira, 1952). The terraces southwest of Valença are at an elevation of 76 m at the most. This might be explained by large-scale differential uplift of blocks. The tectonic block just north of A Guarda has been active until very recently as even the youngest terrace of the Tamuxe has a larger extent of the west side compared to the east side. This youngest terrace can be correlated to a nearby marine terrace that was inferred to be of Eemian age (Blanco-Chao et al., 2003). Thus, tilting has occurred after the Eemian as well.

2.5 Conclusions

NW Iberia is a tectonically active area. Tectonic motions occur along pre-existing faults and fractures, and the presence of fluvial terraces and stepped planation surfaces indicate that the area experiences tectonic uplift. Locally, basin subsidence is taking place due to fault interactions and local extension. The amount of uplift is more intense in the eastern part of our study area and lessens towards the west. The transition coincides with the location of the most active faults as the area directly east of the presumably active Tea fault forms an elevated block compared to the western part. The area can thus be subdivided into an eastern and a western sector, which behave differently from a tectonic point of view. Evidence stems from DEM- analyses as basin asymmetry, incised river valleys and occurrence of knick points demonstrate block tilting, differential uplift and active faults. In the sector west of the Tea river, few indications of differential tectonics have been found, based on our DEM analysis, but field evidence suggests that basin subsidence along pre-existing N-S faults does occur. The presented results demonstrate that along the NW Iberian Margin tectonic activity takes place, possibly because of strain transfer by plate convergence along the Cantabrian-Pyrenean border.

Chapter 3

A 0.65 Ma chronology and incision rate assessment of the NW Iberian Miño River terraces based on ^{10}Be and luminescence dating

In this work a series of 5 luminescence and ^{10}Be dated fluvial terraces of the Miño River (NW Iberian Atlantic Margin) is presented. The outcomes allowed answering the longstanding question whether the Miño valley infill has a fluvial or marine origin. The perfect exponential decrease in ^{10}Be concentrations with depth and a progressive increase in age with terrace altitude indicate that the Miño terraces are fluvial terraces rather than terraces incised in older marine basin infill. Accurate dating of the terraces was difficult due to saturation of the luminescence signal and high inheritance of ^{10}Be concentrations. Nevertheless, minimum ages of up to 650 ka could be determined and are very likely close to the real ages of the terraces. The age estimations and field evidence suggest that terrace formation and terrace incision occurred during eccentricity-forced cycles of glacio-eustatic sea level changes and tectonic uplift. The occurrence of a steep and narrow continental shelf probably favoured rapid and profound incision by the Miño River during periods of low sea levels. It is furthermore hypothesised that the transition periods between glacials and interglacials were especially important for terrace deposition and incision. Denudation rates of the terraces were calculated from the ^{10}Be data and do not exceed 1.30 m Ma^{-1}. These extremely low rates are probably the result of a combination of factors that favoured terrace preservation. Large, flat terrace surfaces with high permeability and continuous vegetation cover during the Quaternary stabilised the terrace surfaces.

Maximum incision rates, calculated from terrace age and altitude, are 0.07-0.09 m ka^{-1}. These values can be used as proxies for tectonic uplift rates. They are in agreement with published uplift rates along the northern Spanish coast and the westernmost termination of the Cordillera Cantabrica. This similarity most likely identifies a common tectonic regime leading to similar tectonic uplift rates. The results demonstrate that tectonic uplift occurs in a region that was until very recently considered as tectonically stable.

Published as: Viveen, W., Braucher, R., Bourlès, D., Schoorl, J.M., Veldkamp, A., Van Balen, R.T., Wallinga, J., Fernandez-Mosquera, D., Vidal-Romani, J.R., Sanjurjo-Sanchez, J., 2012b. A 0.65 Ma chronology and incision rate assessment of the NW Iberian Miño River terraces based on ^{10}Be and luminescence dating. *Global and Planetary Change* 94-95, 82-100.

3.1 Introduction

Fluvial networks and especially fluvial terraces are one of the most commonly used geomorphological systems to investigate the influence of climate and sea level changes on landscape development and to highlight the occurrence of neotectonic activity (Bridgland and Westaway, 2008a). It has for instance been shown that near-coastal fluvial terraces document the effects of sea level changes by their sedimentological and stratigraphical composition (Blum and Törnqvist, 2000), whereas terraces more upstream from the coast typically register climate-driven river discharge and sediment dynamics (Tebbens et al., 2000). Fluvial terraces also register tectonic activity in such a way that they can be used to quantify crustal uplift rates. It is thought that vertical crustal motions uplift the river bed above river level. Because the river tries to maintain a state of semi-equilibrium (Schumm, 1993), it will start to incise and form a terrace scarp. The position of the terrace surface with respect to a reference level, commonly the current floodplain, may be used to infer the vertical incision rate as a proxy for uplift rate (Van Balen et al., 2000; Bridgland et al., 2007; Peters and Van Balen, 2007; Claessens et al., 2009; Westaway et al., 2009). This is only valid if other factors that may lead to river incision, such as eustatic changes or glacio-isostatic adjustments can be discarded (Maddy, 1997). However, some workers argue that a river will almost never attain a state of semi-equilibrium and hence, river terraces cannot be used to infer exact rates of vertical deformation (Kiden and Törnqvist, 1998).

Much attention has been paid to the Quaternary history of the large Iberian river systems, notably the Tagus, Duero, Ebro and Guadalquivir rivers (Santisteban and Schulte, 2007; Martins et al., 2009). These river systems cover the larger part of the Quaternary and in some cases include the Miocene-Pliocene time period as well (Schoorl and Veldkamp, 2003; Cunha et al., 2008; De Vicente et al., 2011). They are therefore very suitable to study the long-term impact of climatic and tectonic changes on landscape evolution of the Iberian plate.

Little attention has been paid to the fluvial systems of the NW Iberian Atlantic Margin, mainly because of absence of fossils and other datable materials, making it difficult to establish a temporal framework. Another reason is that NW Iberia has a complicated tectonic history. Geologists and geomorphologists have only recently come to understand the tectonic mechanisms controlling its Late Cenozoic evolution (Cloetingh et al., 2011). In addition, a well-constrained geochronology that extends beyond the traditional ^{14}C-method is virtually absent for the area in between the Duero river and the Cantabrian coast. For this reason, the rates of vertical movements on the NW Iberian Atlantic Margin have not yet been time-constrained and are usually generalised as "Late Cenozoic vertical movements" (Cloetingh et al., 2005).

Recent advances in Optically Stimulated Luminescence (OSL) and cosmogenic nuclide dating methods now make it possible to date non-volcanic sedimentary landforms that formed throughout the Quaternary. The application of luminescence dating in fluvial

research has become widespread, because the timing of deposition of fluvial sediments can now be accurately assessed for the last glacial-interglacial cycle and even beyond. This in turn, makes it possible to infer which intrinsic and especially extrinsic factors (climate-driven changes in discharge or sediment load, eustacy and tectonic events) are responsible for long-term river dynamics (e.g. Wallinga, 2002). Cosmogenic nuclide dating has the added advantage that it covers a much larger time-span than luminescence dating (Siame et al., 1997). As such, it can be used to investigate the impact of tectonics and climate and sea level changes during a number of re-occurring glacial-interglacial cycles. This is still not very common in geomorphological research, where processes operating during the last-glacial interglacial cycle are usually used as a reference for all glacial-interglacial cycles. Studies that apply a combination of OSL and cosmogenic nuclide dating should yield more reliable age-constraints, because luminescence dating typically dates the timing of sediment deposition (Murray and Wintle, 2000), whereas cosmogenic nuclide dating (also called cosmogenic exposure dating or CRE dating) typically is used to date the timing of floodplain abandonment. This is considered to coincide with the start of river incision and hence, uplift (Brocard et al., 2003). For these reasons, the study presented here includes both methods. Studies combining both OSL and cosmogenic nuclides are still scarce however because of the high financial costs involved, the time needed to perform all the analyses and the usually limited number of suitable sample sites for both techniques (Pederson et al., 2006; De Long and Arnold, 2007; Gardner et al., 2009; Guralnik et al., 2011; Le Dortz et al., 2012).

The aim of this paper is to establish a first absolute terrace chronology of the NW Iberian Miño River, by means of a combination of ^{10}Be and luminescence dating. The presented ^{10}Be data will also allow deducting terrace surface denudation rates.
Because there is some doubt whether the Miño infill represents a fluvial or actually marine basin infill (Sos-Baynat, 1965, see paragraph 2.1), this question needs to be addressed first. The outcomes will then be used to propose a terrace formation model for the Lower Miño terraces. This will allow inferring incision rates that will serve as a first approximation for uplift rates on the NW Iberian Atlantic Margin.

3.2 The Miño terraces

Contrary to the Rias area just north of the Miño River and to the marine abrasion benches along the Galician coast (e.g. Garcia-Gil et al., 1999; Trenhaile et al., 1999), the Miño record has received little attention, despite the fact that the Lower Miño preserves an extensive morphological and sedimentary record. This record extends from the coast up to 70 km upstream (Fig. 1.2) and probably dates back to the Upper Pliocene (De Vicente et al., 2011; Vieira et al., 2011). Alluvial terraces are not found further upstream outside the tectonic basins, although a few flat surfaces without sediments have been described which were interpreted as erosive terraces (Vidal-Romani and Yepes-Temiño, 2001). The Miño record is exceptional in this sense that none of the larger NW Iberian rivers (e.g. the Duero, Lima, Cavado nor the Rias, see Fig. 1.1), contain such a well-defined sedimentary record that may be used to quantify regional uplift by means of fluvial vertical incision rates. Marine abrasion benches do exist, but their genesis is difficult to reconstruct due to the absence of datable sediments. In addition, the Miño terraces are made up of quartz and metamorphic quartzite gravels. This makes the application of CRE dating attractive because the quartz found in the clasts is the most suitable mineral for this method, making it possible to use the gravels directly for CRE dating. Also, quartzite bedrock is not found in the Lower Miño catchment. Quartzite is only present upstream in the Sil catchment, mostly in the vicinity of the small Bierzo basin (ITGE, 2001). So it is inferred that the Miño terrace gravels originate from this area. This ensures that all quartzite gravels selected for CRE dating originate from the same source. This is important for the calculation of source-sink travel time of the Miño gravels. Granites, gneisses and schists, which form the dominant rock type in the catchment (Fig. 1.2), are hardly present in the terrace deposits, although they are more commonly found in the current river bed. They may however have been weathered in situ in the terraces, leaving only quartz residues and kaolinite clays. This is evident in the youngest terraces that contain completely weathered granite and gneiss clasts and even boulders, that are still visible as ghost clasts. A decrease in feldspar content and an increase in (kaolinite) clays as a function of increasing terrace height have indeed been demonstrated (Pereira, 1991).

The Lower Miño terraces are observed at altitudes of up to 105 m above sea level. They are generally cut into the underlying, now weathered bedrock and form separate benches. On top of the terraces, several meters of gravel deposits are found. The terraces would classify as “strath terraces” according to the classification by Lewin and Gibbard (2010), but locally the gravel deposits attain thicknesses that are much greater than those normally observed for strath terraces. Terrace fills can reach a thickness of over 20 m in the localised tectonic basins (Viveen et al., 2012), whereas terrace gravel units outside the basins reach thicknesses up to 10 m. Further upstream the terraces become progressively thinner and grade into bedrock surfaces with only thin veneers of gravel. The terraces contain gravels with clast sizes of up to several decimetres. The gravels are generally rounded to well-

rounded and the terrace deposits are clast-supported with a sandy matrix. The gravels become increasingly weathered with altitude. It is common to find whitish or reddish completely weathered quartzite clasts that can be pulverised by hand in the higher terrace levels. The higher terrace levels may also contain decimetre-thick iron banks and iron-cemented quartzite conglomerates. Occasionally a sand layer is found in between the terrace gravel units. It is common to find deeply weathered granite saprolite underneath the terraces. In some cases, especially in the tectonic basins, large quantities of white kaolinite clays underlie the terrace gravels.

As previously mentioned, the Miño River is located directly south of a number of marine embayments (Rias). The fact that the Miño is not a Ria, despite being situated in a geologically similar setting, may be attributed to different tectonic conditions (Viveen et al., 2012). As the oldest infill of the Miño river basin dates from the Upper Pliocene (De Vicente et al., 2011; Vieira et al., 2011), it is feasible that the Miño gravels actually represent an older (marine) basin infill that was subsequently incised. Pliocene sea level was around 40 to 60 m above current sea level (Pais et al., 2012), which coincides with the altitude of the highest near-coastal fluvial terraces (Butzer, 1967). Additionally, the gravels are severely weathered and rounded to well-rounded and often show percussion marks, which are normally found on beach pebbles. This evidence may indicate a pre-Quaternary marine rather than fluvial depositional environment. The terraces could then result from Quaternary age incisions by the Miño River into the older, Pliocene marine sediments (Sos-Baynat, 1965).

The number of terrace levels and their spacing is still a topic of discussion. Most terraces have a 5 to 10 m high terrace scarp and up to 8 terrace levels have been described (Lautensach, 1945; Teixeira, 1952; Butzer, 1967; Nonn, 1967; Pereira, 1991; Alves and Pereira, 2000). The terraces have traditionally been studied in isolation, that is only on either the Galician or Portuguese side, and always only for a limited reach. For this reason, a detailed regional framework for the terraces is still lacking and no consensus exists on the number of terrace levels. The general belief is that the terrace deposits are of interglacial origin, because the terrace surface remnants are found at similar altitudes along the course of the Lower Miño. It was inferred that they run parallel to the current Miño River floodplain, which would indicate an interglacial base level (Lautensach, 1945; Butzer, 1967; Nonn, 1967). In addition, Butzer (1967) argued that in some of the terraces "red palaeosols" are found, which would typically point towards warm, humid and thus interglacial, climates during terrace formation. All things considered, dating the Lower Miño terraces with a combination of luminescence and CRE methods may lead to a better comprehension of their age and formation history. This will also allow quantification of the Miño incision rates.

3.2.1 The Vila Meã terrace sequence

This study focuses on the terrace staircase surrounding the Portuguese village of Vila Meã (20 km upstream from the Atlantic Ocean, Fig. 3.1). The site was chosen because it met the criteria needed to achieve the objectives of this study: 1) An intact terrace staircase not affected by differential tectonics (e.g. basin subsidence, see Fig. 3.1) to calculate incision rates; 2) high-quality exposures in a succession of terraces; 3) the presence of at least 3 m of gravel in each terrace level, which is a requirement for the CRE depth profiling technique (Braucher et al., 2009); 4) absence of colluvia and presence of intact soil profiles (required for CRE dating) and 5) the presence of sand layers in the younger terraces for luminescence
dating.

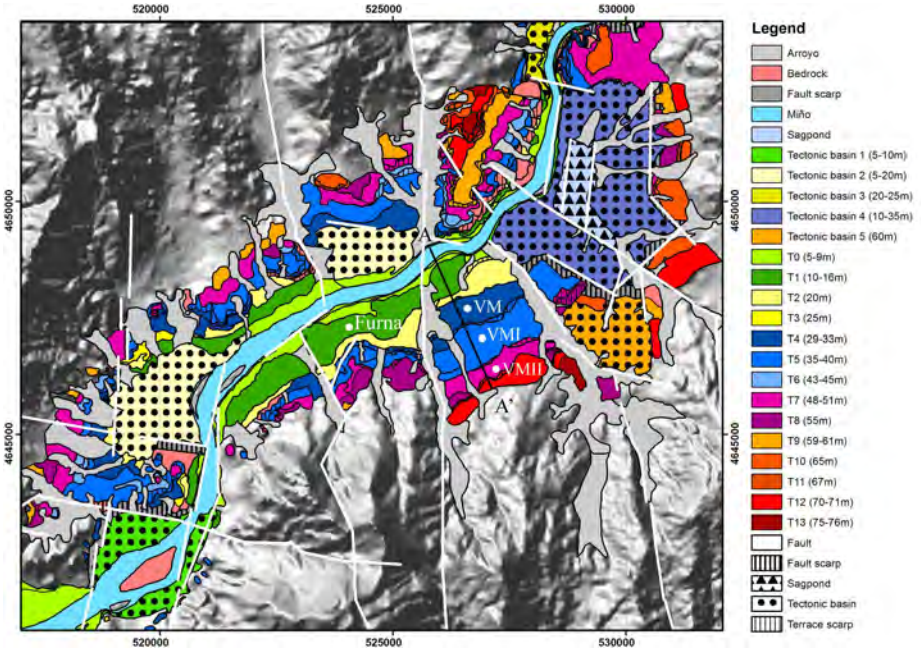

Fig. 3.1. Terrace map of the Vila Meã-Furna section and environments. Map updated from Viveen et al. (2012). Transect A-A' shows location of Vila Meã transect (Fig. 3.2). Terrace numbering is based on the assumption that terraces tread parallel to the current river level. This is probably incorrect (see discussion), but a revised correlation scheme is not yet available. Because of the necessity to maintain a regional correlation scheme, terrace heights and numbering are slightly different from the ones in Fig. 3.2.

Previous studies on the Vila Meã sequence reported the presence of 4 terraces between 5 and 55m and of one level at 100 m above sea level (Pereira, 1991; Alves and Pereira, 2000; Alves, 2004). In this study however, 7 levels are identified containing gravel up to 70 m.a.s.l., whereas evidence for the 100 m terrace level was not found (Fig. 3.2). Terrace

surfaces are sub horizontal and large (up to 838 m wide) with gradients ranging from 0.003 to 0.007 m km^{-1} perpendicular to the gradient axis of the Miño River. The construction of a small industrial park has led to the excavation of the terraces lying between 31 and 70 m altitude, making it possible to study the terrace sediments along a 1.5 km continuous outcrop. Because the Vila Meã terraces lack internal bedding and outstanding stratigraphical features, graphical log descriptions are not given.

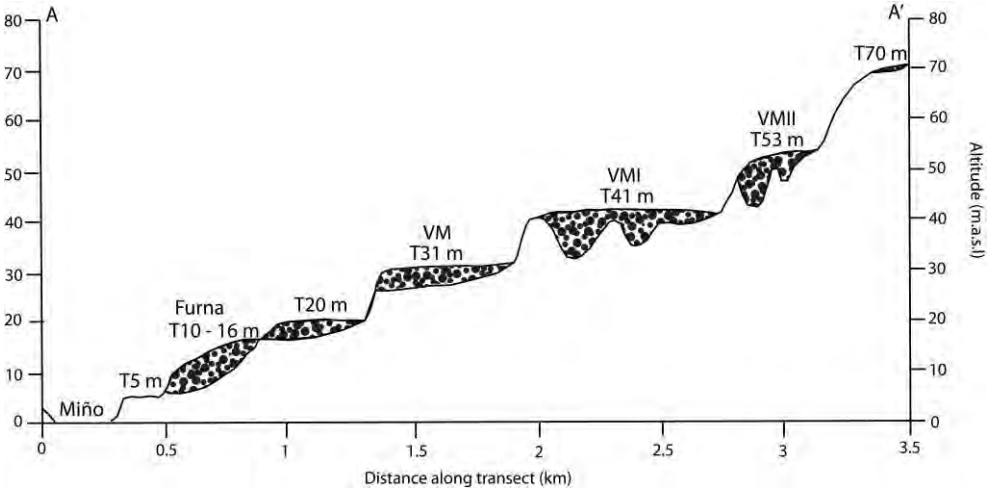

Fig. 3.2. Transect A-A'. A total of 7 terraces are evidenced between 5 and 70 m.a.s.l. T5 m is the actual river floodplain. Displayed gravel depths are based on actual measurements in the field.

What follows next, is a generalised description of the terraces. For an extensive overview of the sedimentological characteristics, see Table 3.1. The 70 m and 53 m terrace levels are, more than the other Vila Meã terraces, composed of completely weathered, white quartzites that sometimes can be crushed by hand, suggesting a prolonged weathering period for this terrace implying a considerable exposure age. The clasts may attain diameters of up to several tens of cm. Mean clast size is around 6 cm. The imbrication of the clasts shows a predominant SW direction, which is also the current flow direction of the Miño River. The clasts are embedded in a matrix of usually medium- to coarse-grained sand. The presence of occasional kaolinite lumps in the terraces suggests that feldspar-bearing rock types, such as granites, have completely weathered in situ. Occasionally, a local fine to coarse sand lens is found in the gravel bodies, but a clearly recognisable stratification is not present in any of the older terraces. The 53 m and 41 m terraces (VMII and VMI; Figs. 3.1, 3.2 and 3.3ABC) are made up of individual gravel bed channels that are incised up to 10 m into the underlying granite saprolite (Fig. 3A). The terrace deposits consist of rounded to well-rounded quartz and quartzite pebbles. Other rock types are not found, although the gravels in the current river bed further upstream demonstrate a variety

of rock types, such as quartzites, sandstones, gneisses, granites and the occasional schist. The terrace clasts demonstrate increasing degrees of weathering with altitude. Weathering rinds of pebbles of the 31 m and the 41 m terraces usually consist of an iron oxide rind and/or a white kaolinite coating and often the pebble core is oxidised as well (Fig. 3D). Completely leached, white quartzites are also found. The 31 m terrace level (VM; Figs. 3.1, 3.2 and 3.3e) consists of 4 m of gravel on top of weathered granite bedrock. All the terraces are overlain by an intact soil sequence which usually consists of an O-horizon, followed by an A- and sometimes spodic B-horizon, which ultimately culminates in the development of a Podzol soil profile (FAO, 2000).
In general, the granites below the terraces are deeply weathered. Other outcrops in the vicinity show that the granites may be weathered to depths up to 13 m below the surface.

Just 3 km southwest of the Vila Meã terraces another gravel pit is present in the 5 -16 m terrace (the "Furna" level; Figs. 3.4 and 3.5). The transition to the 20 m terrace is not very obvious here due to the absence of a discernible scarp, but a sudden change in terrace surface gradient may mark a possible terrace step. The quartz and quartzite clasts are also rounded to well-rounded and are up to several decimetres, with mean clast sizes of around 6 cm. Contrary to the Vila Meã terraces, the clasts hardly show any signs of weathering and are difficult to break. The Furna terrace gravels are also almost completely composed of quartzite and quartz pebbles, but a few granite and schist pebbles do occur. All this indicates that the Furna section is younger than the Vila Meã section. Sand lenses are also found in this terrace level, but again a clear stratification is not present. In total, 8 meters of gravel is present on top of deeply weathered granite. The saprolite is visible in several sections of the quarry.

Table 3.1. Sedimentological information on the Furna and Vila Meã terraces.

Site and coordinates (UTM N29, ED50)	General characteristics	Sedimentological composition	Internal bedding structures	Fluvial structures	Weathering characteristics
Furna (10-16 m) 523850 E, 4647354 N.	Predominantly gravel deposit; gravel thickness varies between 5 m (N side quarry) and 8 m (S side); Granite saprolite visible underlying gravels	Approximately 96 percent quartz and quartzite clasts. Mean size around 6 cm; maximum sizes up to 0.8 m. Clasts are rounded to well-rounded. Deposit is clast-supported with interstices of coarse-sand. Remaining clast types schist, slate, granite and gneiss.	In the SW section of quarry, a 0.7-m thick yellowish-red fine-sandy over bank deposit on top of gravel body.	A very few medium- to coarse grained sand lenses imbedded in the gravel. The lenses are 0.40 to 0.80 m thick and max. 4 m wide. Sand is not cemented. Imbrication in a few sites points towards S to SW palaeo-current direction.	The quartzite and quartz clasts are unweathered. Sometimes a less than 1 mm thick outer rind of iron-oxidation present. Very difficult to break with hammer. Ghost clasts of gneiss/granite present; weathered into kaolinite clay balls. Indicates that deposit is older than appears.
VM (31 m) 526030 E, 4647014 N.	Massive gravel deposit of 4 m thickness, no sand lenses, no fining upward/coarsening downward	Quartz and quartzite gravel, reasonably sorted, mean clast size around 6 cm. A few larger cobbles up to	No internal bedding	A few clast imbrications pointing SW	The quartzite clasts show signs of medium to advanced weathering. Clasts are either

	trends in gravel; Granite saprolite visible underneath terrace	30 cm. Rounded to well-rounded. No other rock types present. Clast-supported with interstices of yellowish fine-to medium grained sand.			completely iron-oxidized, giving a yellowish-brown color to the clasts; or completely oxidized with thin white weathering rinds due to silica-leaching and kaolinite formation. Easily crushable with hammer.
VMI (41 m) 526558 E, 4646837 N.	Massive gravel deposit with an overall thickness of 10 m. Granite saprolite visible at base. No stratigraphical features present.	Clast-supported gravel deposit with interstices of medium-to coarse grained sand. Reasonably sorted with mean clast size of around 5-6 cm. Only quartz and quartzite clasts, rounded to well-rounded.	No internal bedding	No fluvial structures present; palaeo flow direction could not be established, but is assumed to be SW based on terrace scarp alignment.	All clasts are covered by a thin patina of iron, presumably the result of iron-oxidation. Although clast-supported, the gravels are more loosely packed than in other terraces, which might explain the iron precipitation. Clasts are slightly weathered, presumably due to protection of the

					iron patina.
VMII (53 m) 526856 E, 4646161 N.	Mean gravel thickness around 2 m, but 2 large channels are incised more than 8 m into the underlying granite saprolite. No stratigraphical features present.	Only whitish quartz and quartzite clasts. Clast size highly variable with boulder-size quartzite clasts. Badly sorted. Clast supported with interstices of reddish kaolinite clay and sands of all fractions. Red color of matrix likely due to leached iron from quartzites.	No internal bedding	2 large palaeo-channels, whose direction of flow is estimated to be parallel to the terrace scarp (SW direction). The larger channel measures 75 m in width and at least 8 m in depth (Fig. 5c); the smaller one measures 15 m in width and 6 m in depth.	Extremely weathered terrace deposit. The smaller clasts are completely silica-leached and white. Crushable by hand. The larger cobbles and boulders have large, well-developed silica-leached and iron-oxidized weathering rinds (Fig. 5d).
70 m 526750 E, 4645742 N	Severely eroded, local gravel deposit max. thickness 1.5 m. Clasts are supported in a matrix of reddish clay.	Only a few small pebbles present. Largest clast size around 7 cm; mean clast size around 3.5 to 4 cm.	No internal bedding	No longer discernible.	Extremely weathered. Friable clasts difficult to extract from matrix. Most clasts have turned into white kaolinite balls.

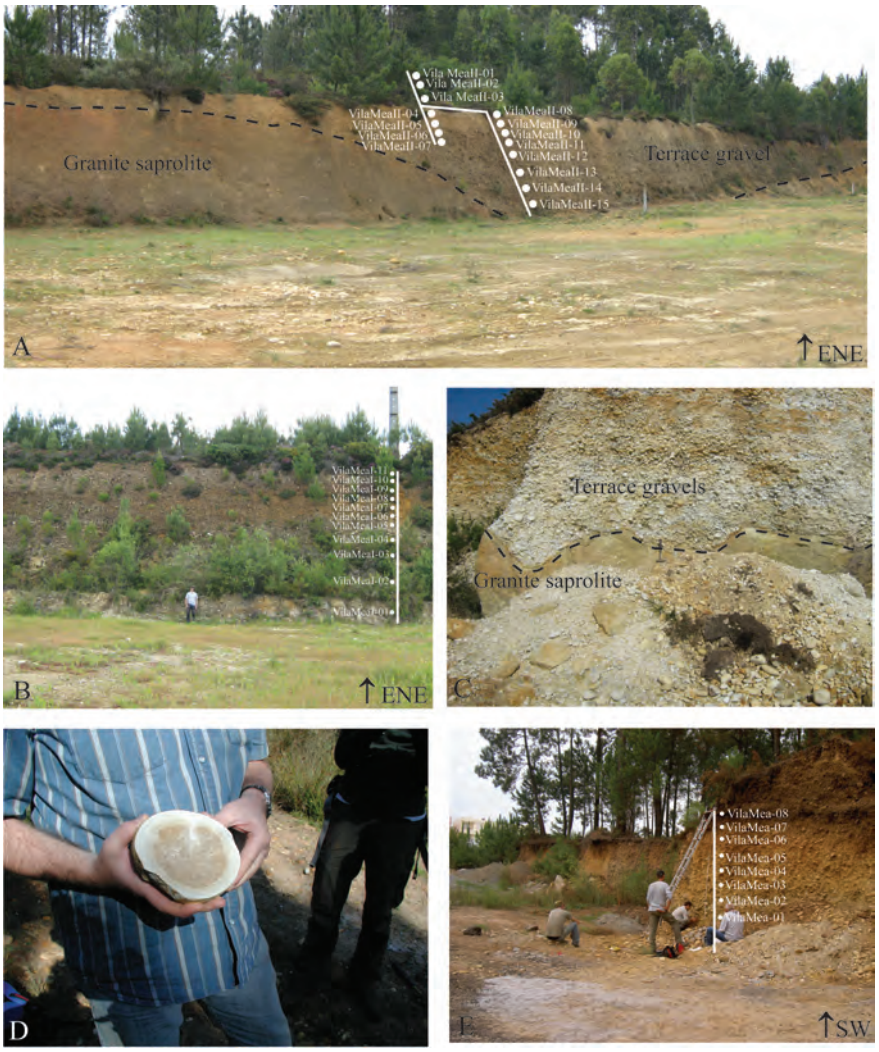

Fig. 3.3. A) Overview of the Vila Meã II site. Palaeo-channels incised in underlying, now weathered, granites. Terrace fill consists of completely weathered, white quartzites. The upper part of the section is located 2 meters away from the main section and not visible on the photo (samples VilaMeaII-01 to -07). Samples VilaMeaII-04 to -07 were taken in a trench at a depth similar to samples VilaMeaII-08 to -011. These samples were later compared against one another to ensure a correct fit of the upper and lower part of the VilaMeaII profile. B) Impression of the Vila Meã I section. The entire section consists of quartz and quartzite gravel without sand or clay lenses. Exposure measures 10 m from bottom to top. C) Detail of the Vila Meã I terrace. Erosive contact between silica-leached quartzites and granite saprolite. D) Detail of a weathered quartzite cobble. Core is oxidized; weathering rind is in a severe state of silica leaching and has turned white. E) Impression of the Vila Meã section (10Be depth profile Vila Meã (VM). Section measures 4 m from bottom to top ladder and consists entirely out of quartz and quartzite gravel. Note original soil sequence in top part of outcrop. On top of soil sequence, recently deposited soil is visible, which was not sampled.

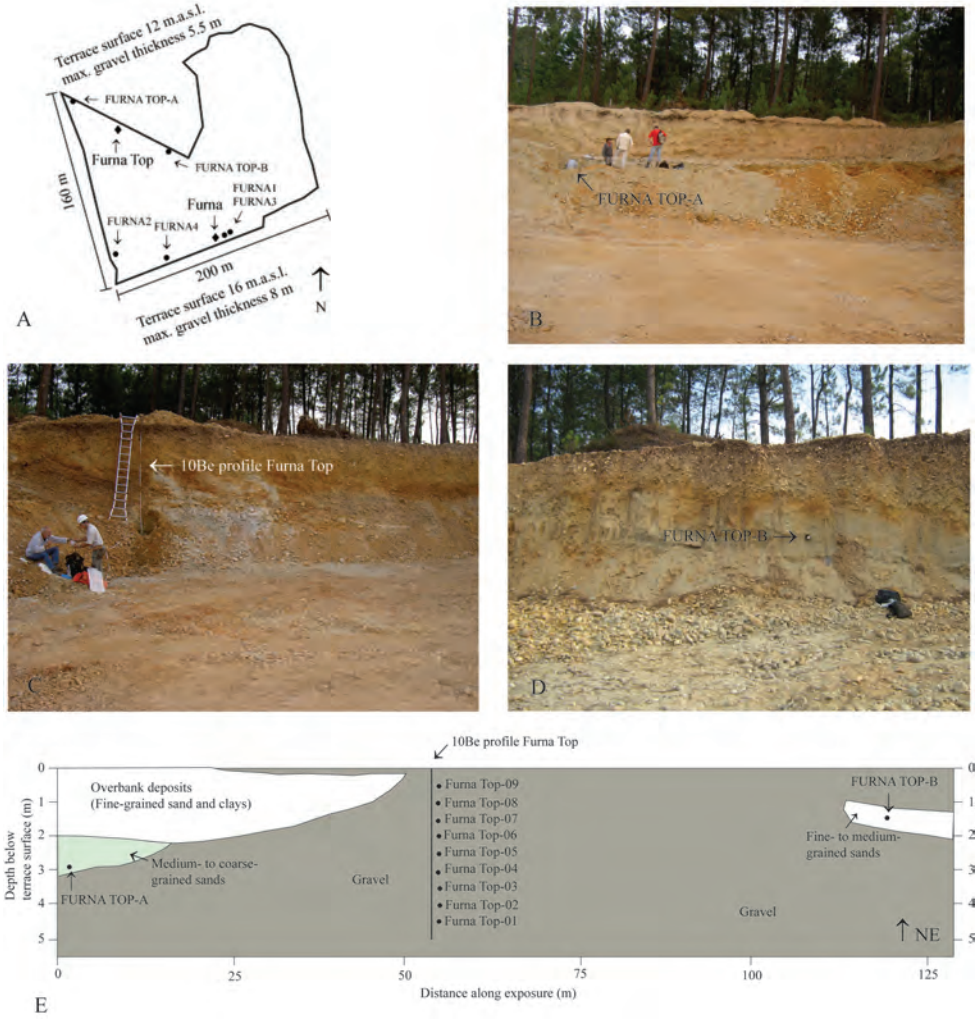

Fig. 3.4. A) Plan of the Furna mine. Locations of samples for luminescence dating are given (black dots), as well as locations for CRE dating (black diamonds). Terrace surface heights at north and south side of mine also given. B) Location of FURNA TOP-A sample site (luminescence dating). Note large over bank deposits in upper half of section. C) Sample site of ^{10}Be profile Furna Top. D) Sample site of FURNA TOP-B (luminescence dating). E) Reconstruction of the entire section along the NE wall of the mine where the 3 Furna Top samples were taken. As can be evidenced, conspicuous stratigraphical features or internal bedding are not present.

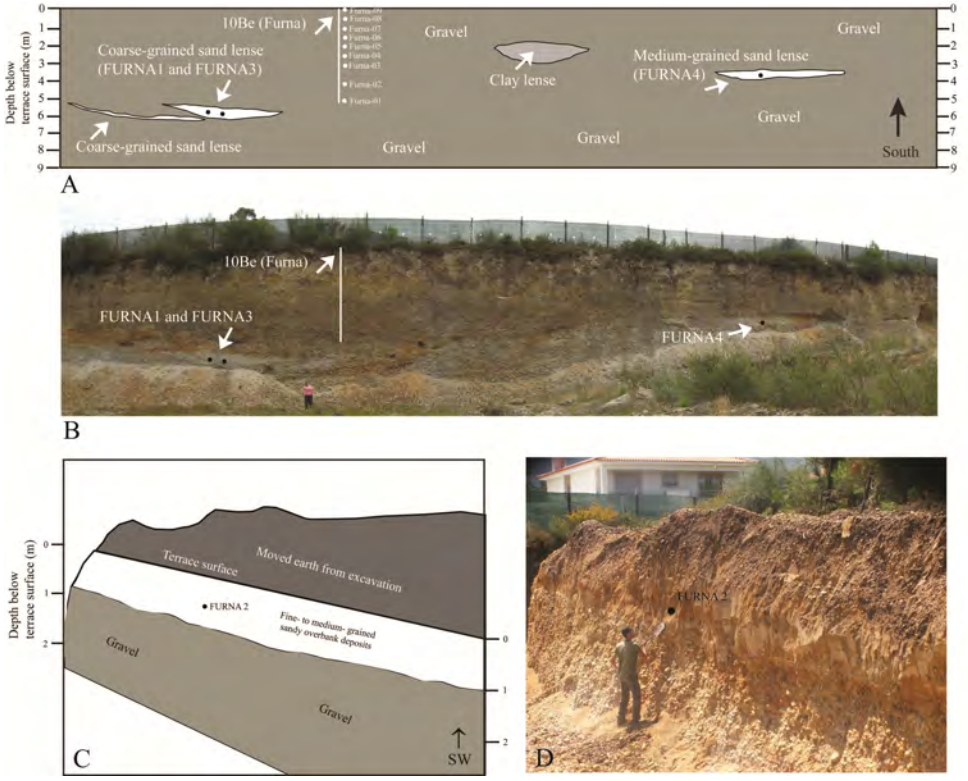

Fig. 3.5. A) and B) Cross-section of the south wall of the Furna mine (for location, see Fig. 3.4A). Locations of luminescence sample sites (FURNA 1,2 AND 4) and ^{10}Be depth profile (Furna) given. Internal bedding or important stratigraphical features are not present. The FURNA 1,2 and 4 sites seem to be part of a separate stratigraphical unit, because of a reddish iron bank separating the grey-colored unit from the more yellowish-reddish gravels in the upper part of the section. Closer inspection of the site however revealed that the iron bank is due to a former groundwater table, which has recently lowered due to drainage of the mine. C) and D) Western section of the Furna mine (for location see Fig. 3.4A). The section consists of a meter of yellowish-brown over bank deposits on top of gravel. The overbank deposit was sampled for luminescence dating (FURNA 3).

3.2.2 Terrace ages and chronology

Based on correlation with other tectonic basins in Portugal, the Miño basin is considered to be at least of Pliocene age (Pais et al., 2012) and an Upper Pliocene to Lower Pleistocene age has been assigned to the oldest Miño terraces. Due to the scarcity of fossils and chronostratigraphical markers (e.g. ash layers, palaeosols) and until recently due to lack of methods to date the ubiquitous quartz and quartzite gravels, accurate absolute terrace ages remain unknown. Based on a fossil leaf found in kaolinite clays underlying terrace gravels in the Louro valley, a confluent of the Miño, Sos-Baynat (1965) postulated a

tentative Miocene age for the clays. More recently, a palaeontological study of fossils in a clay bed underlying the older terrace gravels of the Vila Meã sequence suggested that the kaolinite clays were of Upper Pliocene age (Vieira et al. 2011). The Miño terraces at Vila Meã should therefore be younger than Late Pliocene.
Absolute dating has mainly been attempted on colluvium overlying nearby marine platforms. ^{14}C-results indicate that this colluvium originates from MIS 3 and 2, although some samples reached the limit of the ^{14}C method (Cano-Pan et al., 1999b; Trenhaile et al., 1999; Alonso and Pages, 2007). It was thus inferred that the lowest marine platform at 3.5 m.a.s.l. originates from the Eemian (MIS 5e) (Trenhaile et al., 1999; Blanco-Chao et al., 2003). Based on additional OSL- and TL-dating of fossil beach sediments overlying this platform, Alonso and Pages (2007) conclude that the platform originates from MIS 5a, but they cannot rule out the possibility of an older age, e.g. MIS 5c or MIS 5e. However, because of the very few marine platforms identified and dated, they cannot be used as a means to correlate the fluvial terrace section studied in this paper.

Moreover, scarcity of an absolute regional chronological framework extends well beyond the Lower Miño river valley. The only long-term regional records we are aware of encompass a cosmogenic nuclide dating study of deglaciation in the south-eastern Galician mountains (Fernandez-Mosquera et al., 2000) and a cosmogenic nuclide study of a 1 Ma marine terrace on the northern Galician-Asturian border (Alvarez-Marron et al., 2008). However, due to the different tectonic settings of these aforementioned locations, the resulting uplift rates can probably not be extended to our study area.

3.3 Materials and methods

3.3.1 Sampling strategy

For the Furna terrace level 6 samples were collected for quartz and feldspar OSL-dating. Two parts of the same terrace level (12 m and 16 m) were sampled (Furna Top and Furna; Figs. 3.4 and 3.5). Samples were taken from all sand lenses present in the predominantly gravelly deposit. These were taken at variable depths by inserting stainless steel and PVC-tubes of around 40 cm long and 5 cm in diameter in the medium- to coarse-grained sand lenses (Figs. 3.4 and 3.5).

When dealing with cosmogenic nuclides, one has two options to date exposed surfaces. Either collecting several samples from a depositional (e.g. terrace) surface, or several samples along depth profiles. In this paper, the second approach has been applied. Cosmogenic nuclide distribution with depth not only allows dating and determining the

mean denudation rate that has affected the surface since its exposure. It also allows the potential inherited concentration prior to deposition to be determined. This depth profiling technique is based on the fact that cosmogenic nuclides are produced by at least two types of particles: neutrons in the first meters and muons at depth (Brown et al. 1995, Braucher et al. 2011). This approach had been successfully applied to date fluvial terraces (Anderson et al., 1996; Repka et al., 1997; and Hancock et al., 1999; Siame at al., 2004). Because ^{10}Be produced by neutrons near the Earth's surface reaches steady-state with respect to denudational loss much more rapidly than ^{10}Be produced at depth from reactions with the more penetrating muons particles, it can be used to estimate the denudation rate. ^{10}Be produced at several meters depth by muons can be used to estimate the exposure time. To take these two types of particles into account, sampling must be as deep as possible (Braucher et al. 2009). This favours the muon contribution and near-surface samples (from 0 to ~3m) have to be relatively close to one another to be able to represent the neutron attenuation with depth. The shape of this attenuation is described by an exponential decrease and can be directly linked to denudation processes. Therefore, in this study, quartz and quartzite gravel were sampled every ~50 cm from 0 to 300 cm depth in order to constrain the spallogenic production; and every ~100 cm from 300 cm depth downwards to characterize the muon contribution. All samples were composed of 10- to 20 clasts.

At the Vila Meã site the terrace levels at 31 m, 41 m and 53 m (called VM, VMI and VMII respectively) were sampled (Figs. 3.1 to 3.3). The terrace at 70 m was not sampled as it did not contain enough gravel. As sand layers were not present in the deposits, we could not sample the Vila Meã section for luminescence dating.
At the Furna site, the Furna and Furna Top sections were sampled (Furna Top and Furna; Figs. 3.4 and 3.5). The sampling allowed the reliability of the selected ^{10}Be CRE dating technique to be tested in the studied area. The 20 m level was not sampled due to lack of a suitable outcrop.
Additionally, approximately 40 quartzite clasts were collected within the current Miño River bed to determine the current cosmogenic inheritance.

3.3.2 Luminescence dating

Grains within the range 90-180 μm were sieved for quartz OSL dating (samples FURNA1 and FURNA2) at the Luminescence Laboratory of the University of A Coruña (Spain). Acid wash was used to separate and to etch the surface of quartz grains (to eliminate the alpha contribution). Measurements were made in a Riso DA-15 automated TL/OSL reader system equipped with a 0.130±0.003 Gy s-1 90Sr/90Y beta-source and a 9235QA photomultiplier tube (PMT), using an optical Hoya U-340 filter (to measure the UV range emission) after optical stimulation with blue diodes. The single aliquot regenerative dose (SAR) protocol

(Murray and Wintle, 2000) was used to estimate the equivalent dose, performing OSL at 125°C during 40s after preheating at 220°C for 10s (preheat temperatures were chosen after preheat temperature tests). The natural dose-rate was estimated using a Canberra XTRA gamma detector (Ge Intrinsic) during 46-68 hours counting time (Hossain et al., 2002; Poręba and Fedorowicz, 2005). The factors of Adamiec and Aitken (1998) were considered to calculate dose-rates conversion.
A second batch of 4 samples was prepared for feldspar IRSL dating at the Netherlands Centre for Luminescence dating (NCL) of Delft University (samples FURNA 3, FURNA4, FURNA TOP-A AND FURNA TOP-B). K-rich feldspar grains of 180-212 µm were density separated at 2.58 g/cm3. A major problem with feldspar luminescence dating is that the signal may not be stable over geological timescales, referred to as anomalous fading (Wintle, 1973). A stable signal can be obtained from K-rich feldspars by infrared stimulation at elevated temperature after prior infrared bleach at lower temperature (Thomsen et al., 2008; Buylaert et al., 2009; Thiel et al., 2011). These methods are referred to as post-IR IRSL dating. A SAR method was used to estimate the absorbed dose. Two sets of samples were measured with post-IR IRSL methods using different measurement parameters. For samples FURNA3 and 4 (NCL 2208100-101) we used a 60s preheat at 260°C, followed by a 100s IR bleach at 100°C and then measurement of the post IR IRSL signal for 100s at 230°C. Subsequently, we applied a 100s IR bleach at 280°C to completely reset the pIR IRSL signal prior to the next SAR cycle. For FURNA Top-A and B (NCL-2110122-123) we used a 60 s preheat at 320°C, followed by a 100s IR bleach at 50°C and then measurement of the post IR IRSL signal for 100s at 290°C. We applied a 40s IR bleach at 330°C prior to the next SAR cycle. Three to five aliquots were measured for each sample and a fading rate of < 1% per decade was detected. Dose response curves were fitted with a saturating exponential plus linear response. Dose-rate samples were measured for at least 24 hours on a Canberra broad energy gamma spectrometer. The dose rate was calculated for 5 ± 2% water content (by weight) taking into consideration the contribution of cosmic radiation and internal alpha radiation was added. A K-content of 12.5% (Huntley and Baril, 1997) and a Rb content of 400 ppm (Huntley and Hancock, 2001) were assumed to calculate internal dose rates. We assumed a contribution of external alpha irradiation of 0.050 ±0.025 Gy ka^{-1} (Wallinga et al., 2007).

3.3.3 ^{10}Be dating

3.3.3.1 Samples preparation and measurement
Quartz was isolated and purified from samples and targets were prepared for Accelerator Mass Spectrometer (AMS) analyses of ^{10}Be following chemical procedures adapted from Brown et al. (1991) and Bourlès et al. (1989). Prior to initiating chemical procedures, all samples were crushed and sieved (250-1000 µm fractions). Successive leachings in H_2SiF_6 - HCL were performed to remove all mineral phases except SiO_2. Three partial dissolutions in

48% HF, dissolving each ~10% of the sample, were then required to decontaminate from potential atmospheric ^{10}Be and thus to ensure that only in-situ produced ^{10}Be is considered. After addition of 100 µl of a 3.10^{-3} g.g^{-1} ^{9}Be spike solution (Merchel et al., 2008), purified quartz was totally dissolved in excess 48% HF and the beryllium was isolated using ion exchange resin (DOWEX 1X8 100-200 mesh then DOWEX 50WX8 100-200 mesh) as described in Merchel and Herpers (1999). Targets of purified beryllium oxide were prepared for ^{10}Be measurements on the French AMS (accelerator mass spectrometry) ASTER national facility (Arnold et al. 2010) located at the CEREGE laboratory (Aix en Provence). The ^{10}Be data were calibrated directly against the National Institute of Standards and Technology (NIST) standard reference material 4325 by using an assigned $^{10}Be/^{9}Be$ ratio of 2.79 ± 0.03 10^{-11} and a ^{10}Be half-life ($T_{1/2}$) of 1.387 ± 0.012 10^{6} years, i.e. a radioactive decay of 4.997 ± 0.057 10^{-7} (Korschinek et al., 2010; Chmeleff et al., 2010). Analytical uncertainties include the counting statistics, the machine stability (~ 0.5%) and blank correction ($^{10}Be/^{9}Be$ blank ratios ranging from 0.29 to 2.10 *10^{-15}).

3.3.3.2 Data modelling

The equation used to model the data sums the exponential equations related to the considered particles that are neutrons, slow and fast muons:

$$C_{(x,\varepsilon,t)} = H.e^{-\lambda t} + \frac{P_{spall.}}{(\frac{\varepsilon}{\Lambda_n} + \lambda)}.e^{-\frac{x}{\Lambda_n}}\left[1 - e^{-t\left(\frac{\varepsilon}{\Lambda_n} + \lambda\right)}\right]$$

$$+ \frac{P_{\mu Slow}}{(\frac{\varepsilon}{\Lambda_{\mu s}} + \lambda)}.e^{-\frac{x}{\Lambda_{\mu s}}}\left[1 - e^{-t\left(\frac{\varepsilon}{\Lambda_{\mu s}} + \lambda\right)}\right] + \frac{P_{\mu Fast}}{(\frac{\varepsilon}{\Lambda_{\mu f}} + \lambda)}.e^{-\frac{x}{\Lambda_{\mu f}}}\left[1 - e^{-t\left(\frac{\varepsilon}{\Lambda_{\mu f}} + \lambda\right)}\right]$$

Where C(x, ,t) is the nuclide concentration as a function of depth x (g cm^{-2}), denudation rate (g cm^{-2}a^{-1}) and exposure time t (a). P_{spall}, $P_{\mu Slow}$, $P_{\mu Fast}$ and $_{n}$, $_{\mu s}$, $_{\mu f}$ are the production rates and attenuation lengths of neutrons, slow muons and fast muons, respectively. $_{n}$, $_{\mu s}$, $_{\mu f}$ values used in this paper are 160, 1500 and 4320 g cm^{-2}, respectively (Heisinger et al., 2002); λ is the radioactive decay constant. H is the inherited component from a previous exposure history. Surface production rates have been scaled using the polynomial from Stone (2000) based on a spallation Sea Level High Latitude production rate of (4.49 ± 0.30) atoms g^{-1}·a^{-1} and Sea Level slow and fast contribution of 0.012 and 0.039 at g^{-1} a^{-1} respectively, based on Braucher et al. (2011). Sample location and production information are presented in Table 3.2.

Table 3.2. Sample information and scaling factors for spallation and muon contributions.

Site	Altitude (m)	Spallation scaling	Slow muon scaling	Fast muon scaling
Furna	16	0.970	1.0077	1.0039
Furna Top	12	0.960	1.0039	1.0020
Vila Meã	31	0.976	1.0116	1.0059
Vila Meã I	40	0.988	1.0176	1.0090
Vila Meã II	53	1.001	1.0237	1.0120
Miño 0	9	0.960	1.0048	1.0025

As will be shown below, the high levels of inherited ^{10}Be concentrations complicate data modelling and therefore we use two different data modelling approaches. The first one is the depth profile approach as extensively described by Braucher et al (2009). It has been shown that ^{10}Be concentrations measured along depth profiles in terraces allow the CRE age and denudation rate of the deposits to be determined (Siame et al., 2004; Braucher et al., 2009; Hidy et al., 2010). In this modelling approach, a unique inherited component is determined for an entire depth profile and the concentration accumulated from previous cosmic ray exposure is assumed to be the same for all samples.

In this paper, the determination of the denudation rate, exposure age, inherited concentration and density follows the model of Braucher et al. (2009). This approach is based on Monte Carlo simulations where at least 100 depth profiles are generated by randomly selecting a concentration within the concentration ranges defined by the measured uncertainties (1s) at each sampling depth. Then loops on undetermined values are performed and for each quadruplet containing the parameters denudation, exposure age, inheritance and density, a total chi-square value is determined. In the end, the lowest total chi-square value for a given quadruplet is considered to be the best solution.

To estimate the model uncertainties, we applied the methodology described in Ward and Wilson (1978). From the minimum total chi-square determined above, a reduced chi-square (total chi-square divided by the degrees of freedom) is calculated and compared with the 0.05 critical value given by the chi-square table. In doing so, the model considers the degrees of freedom defined as the number of samples minus the number of free parameters. In this study, these are usually 4 (denudation, exposure age, inherited concentration and density). If the fit is correct, the reduced chi-square must be lower than the theoretical one. All quadruplets that yield reduced Chi-squares lower than the theoretical one are potential solutions.

The second approach is the rejuvenation method presented by LeDortz et al. (2012). This

method is valid only for places where the denudation rates are low, which is the case in the studied area (see Section 3.4). The main assumption is that at least one sample has been deposited without having experienced earlier exposure to cosmic rays. Thus, setting denudation at zero, CRE ages are determined considering no inheritance. Then, considering the age of the youngest sample for the entire profile, variable inheritance is calculated to make the modelled concentrations match the measured ones.

As the modelling approach is very sensitive to the density parameter, the densities of the terrace gravels were measured. Approximately 100 quartzite pebbles were collected along each studied depth profile and their densities measured. The collected pebbles all had similar characteristics to ensure that the density measurements were not biased. Only rounded to well-rounded pebbles with a spherical form and a diameter of 4 to 6 cm were collected. The current river bed was sampled 30 km upstream of the Vila Meã sequence, because the current Miño only transports sands at the Vila Meã site. The densities were measured in the laboratory by weighing the dry mass of the pebbles and the mass when submerged in water (the pebbles were covered by Parafilm to prevent water from entering the pores). Archimedes' Law was subsequently applied to calculate the density of the pebbles. All terrace gravels have densities ranging from 2.24 to 2.34 g cm^{-3}. The current river bed gravels have a mean density of 2.42 g cm^{-3}. As all terraces are clast supported, it was assumed that the major part of the terraces consists of gravel. Therefore the density has been imposed to evolve between 2 and 2.42 which appears to us to encompass the generally observed density range for the alluvial terraces. Consequently, four parameters (denudation, exposure age, inheritance and density) are thus taken into account in the modelling.

3.4 Results

3.4.1 Luminescence age determinations

Quartz OSL and feldspar post IR-IRSL have provided estimated EDs in the saturation zone of luminescence growth curves, i.e. greater than two times the onset of saturation (D0) of a saturating exponential fit of laboratory induced luminescence signals. In such cases, it is not possible to obtain reliable estimates of burial ages (Wintle and Murray, 2006). Minimum ages were obtained by dividing the minimum equivalent dose (i.e. 2* D0 value) for each aliquot by the sample dose rate (Fig 3.6).

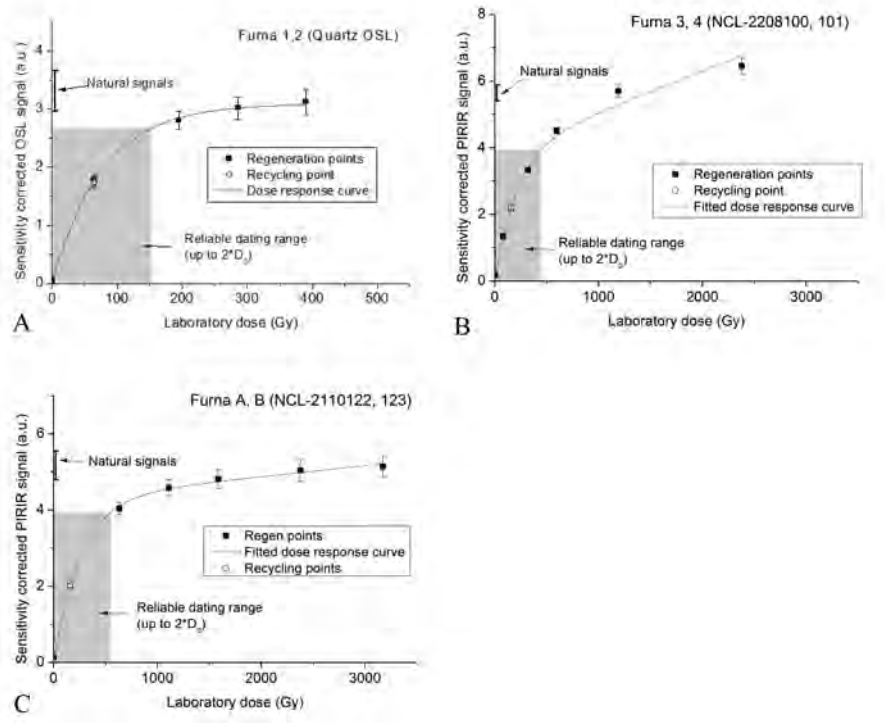

Fig. 3.6. Luminescence growth curves of A) Quartz from samples FURNA 1 and 2 (OSL), B) Feldspar from samples FURNA TOP-A and FURNA TOP-B (PIRIRSL), C) Feldspar from samples FURNA 3 and 4 (PIRIRSL).

Quartz OSL dating provided minimum ages of 37 and 45 ka. Feldspar post-IR IRSL dose response curves have greater saturation values than quartz OSL, and hence provide access to a greater age range (in spite of the higher dose rate of feldspar grains due to the contribution from internal K-40). Feldspar minimum ages centred around 120 ka (Table 3.3). The age range of luminescence methods in this area is affected by relatively high radiation levels of these deposits, resulting in high dose rates. Although the samples were

taken at variable depths, no trend was observed between sample depth and sample age (Table 3, Fig. 3.4 and 3.5), likely due to the minimum ages of the samples.

*Table 3.3. Maximum measurable dose based on criterion of 2*D0. For greater doses, the dose response curve is too flat to allow determination of De. Note that all estimated single aliquot equivalent doses are > 890 Gy (n=24).*

Sample	Sample depth below terrace surface (m)	Sample position in m.a.s.l.	Dose rate (Gy)	Max. measurable dose	Minimum age
FURNA TOP-A	3	9	5.45 ± 0.17	561 ± 88	103 ± 17
FURNA TOP-B	2.1	9.9	4.21 ± 0.13	567 ± 50	134 ± 13
FURNA1	5.5	10.5	3.43 ± 0.16	154 ± 40	45 ± 12
FURNA2	0.6	14.4	4.11 ± 0.15	154 ± 41	37 ± 10
FURNA3	5.5	10.5	4.05 ± 0.17	462 ± 18	114 ± 6
FURNA4	3.2	12.7	3.84 ± 0.16	463 ± 21	121 ± 7

3.4.2 ^{10}Be age determinations and denudation rates

3.4.2.1 Depth profile approach

As shown in Table 3.4 and Figs. 3.7 and 3.8, the ^{10}Be concentrations along a given profile decrease exponentially as a function of depth, as expected by theory. This demonstrates that the samples within each terrace level have undergone the same exposure history and have most likely been deposited during a single aggradation event. However for all studied sites, the ^{10}Be concentrations measured at depth below 300 cm are higher than expected and roughly constant. This reveals that the sediments in the studied terraces have been exposed to cosmic rays prior to deposition (inheritance). Applying the procedure explained above, denudation, exposure age, density and inheritance have been determined and solutions are presented in Table 3.5. Due to the high inherited content, the associated uncertainties linked to exposure ages are non-symmetric and lead to lower limits in the order of 20 to 30 ka but to upper limits of several hundred ka. This informs us that most of the studied sites have almost reached steady state denudation.

Allowing the four unknowns (i.e. density, denudation rate, CRE age, inheritance) to evolve freely, the best fit models yield CRE ages ranging from 418 ka up to 5 Ma for the Vila Meã terraces with denudation rates ranging from 0.3 to 1.15 m Ma^{-1} (see Table 3.5). The low denudation rates indicate that the terraces are pristine landforms which experienced very little surface erosion. For the same terraces, the inherited concentrations range from 81 to 130 kat g^{-1}. No realistic inherited concentrations could be determined for the VMII site. The two Furna terraces appear significantly younger (154 and 151 ka for Furna and Furna Top,

respectively). Here again, high inherited concentrations have been determined (100 and 67 kat g^{-1}) that are of the same order as the Vila Meã ones.

The unrealistic CRE age (>5Ma) determined for the VMII terrace strongly suggests that that steady state may have been reached at this site. Following the approach of Lal (1991) but considering the muon contributions, the maximum denudation rate determined for the VMII site (1.3 m Ma^{-1}) implies a minimum integration time of 650 ka, which can be considered as a minimum age.

Because the modelled CRE ages have high upper limit uncertainties, but at the same time very low denudation rates that may approach zero denudation, a second fit has been performed. In this fit, the denudation is fixed at 0. This approach leads to minimum exposure ages with well constrained upper and lower age uncertainties of 458 ± 40 ka for VM; 563 ± 30 ka for VMI and 530 ± 120 ka for VMII. In the latter case, inheritance could be modelled at 82 kat g^{-1}.

Considering that the three VM profiles may have reached the steady state, a third fit has been performed considering the exposure duration as infinite. In that case, the four initial unknowns are becoming only two as the inherited component is now meaningless and the exposure time set as infinite. This yields to maximum denudation rates ranging from 1.05 to 1.3 m Ma^{-1} and densities varying from 2.16 to 2.36, thus confirming the low denudation rates modelled by the other approaches.

Table 3.4. ^{10}Be samples measurement information. (: outlier).*

Site	Samples	Depth (cm)	Dissolved mass (g)	^{9}Be (g)	^{10}Be (at g^{-1})
Furna	Furna-01	490	32.6587	0.1020	100 000 ± 6 406
	Furna-02	400	30.6738	0.1007	104 649 ± 8 634
	Furna-03	300	28.0781	0.0998	91 765 ± 6 870
	Furna-04	250	27.8566	0.1004	113 174 ± 3 512
	Furna-05	200	27.4063	0.1005	165 840 ± 8 982
	Furna-06	150	30.0381	0.0995	145 500 ± 6 827
	Furna-07	100	31.6194	0.0995	235 909 ± 10 335
	Furna-08	50	44.3369	0.1004	397 615 ± 12 219
	Furna-09	10	34.6417	0.1003	864 547 ± 31 975
Furna Top	FurnaTop-01	460	24.3145	0.1003	66 999 ± 3 840
	FurnaTop-02	410	28.7303	0.1006	79 460 ± 4 213
	FurnaTop-03	360	30.2767	0.1004	91 035 ± 4 136
	FurnaTop-04	310	24.687	0.1001	77 510 ± 3 630
	FurnaTop-05	260	26.9691	0.1007	135 204 ± 8 323
	FurnaTop-06	210	31.3794	0.1001	167 192 ± 10 083
	FurnaTop-07	160	24.8533	0.1001	214 981 ± 7 712
	FurnaTop-08	110	23.6981	0.1008	379 007 ± 11 732
	FurnaTop-09	60	35.7092	0.1006	865 177 ± 26 506
Vila Mea	VilaMea-01	350	25.4237	0.1003	111 989 ± 8 233
	VilaMea-02	300	21.0714	0.1006	119 877 ± 6 487
	VilaMea-03	250	28.762	0.1005	113 284 ± 4 981
	VilaMea-04	200	35.5059	0.1007	177 394 ± 13 347
	VilaMea-05	150	27.0295	0.1006	297 128 ± 12 295
	VilaMea-06	100	33.9973	0.1001	520 732 ± 17 443
	VilaMea-07	50	29.6363	0.1004	862 493 ± 27 382
	VilaMea-08	0	25.1884	0.1007	1 557 262 ± 60 113
Vila Mea 1	VilaMeal-01	900	35.9499	0.0990	93 367 ± 7 556
	VilaMeal-02	700	44.4545	0.1009	120 491 ± 6 181
	VilaMeal-03	500	45.4135	0.1010	122 604 ± 3 629
	VilaMeal-04	400	42.8678	0.1019	104 731 ± 4 623
	VilaMeal-05	300	47.668	0.1016	125 236 ± 3 758
	VilaMeal-06	250	44.4302	0.1012	186 265 ± 8 334
	VilaMeal-07	200	59.9979	0.1003	262 091 ± 9 085
	VilaMeal-08	150	38.7709	0.1020	468 167 ± 13 616
	VilaMeal-09	100	14.1683	0.1008	736 149 ± 21 203
	VilaMeal-10	50	44.3708	0.1008	1 166 479 ± 33 266
	VilaMeal-11	20	54.2833	0.1010	1 451 939 ± 29 299

Vila Mea 2	VilaMeaII-01	20	17.9785	0.0989	1 713 407 ± 53 371
	VilaMeaII-02*	50	17.5063	0.0979	2 414 310 ± 69 018
	VilaMeaII-03	120	25.5951	0.0986	461 208 ± 15 734
	VilaMeaII-04	150	20.2395	0.0999	349 114 ± 12 135
	VilaMeaII-05	200	20.8465	0.1000	230 086 ± 13 614
	VilaMeaII-06	250	17.1461	0.0943	167 475 ± 19 000
	VilaMeaII-07	300	14.6992	0.1022	85 297 ± 22 529
	VilaMeaII-08	150	23.6053	0.1007	336 648 ± 11 952
	VilaMeaII-09	200	16.996	0.1002	236 554 ± 7 771
	VilaMeaII-10	250	18.3943	0.0999	199 675 ± 6 429
	VilaMeaII-11	300	26.0973	0.0999	139 536 ± 4 348
	VilaMeaII-12	350	24.1886	0.1004	99 310 ± 5 031
	VilaMeaII-13	450	16.6721	0.1001	87 227 ± 4 074
	VilaMeaII-14	550	25.4272	0.0998	87 706 ± 4 073
	VilaMeaII-15	650	19.2003	0.1003	67 281 ± 3 745
Actual river	Miño 0	0	23.1819	0.1586	55 247 ± 5 843

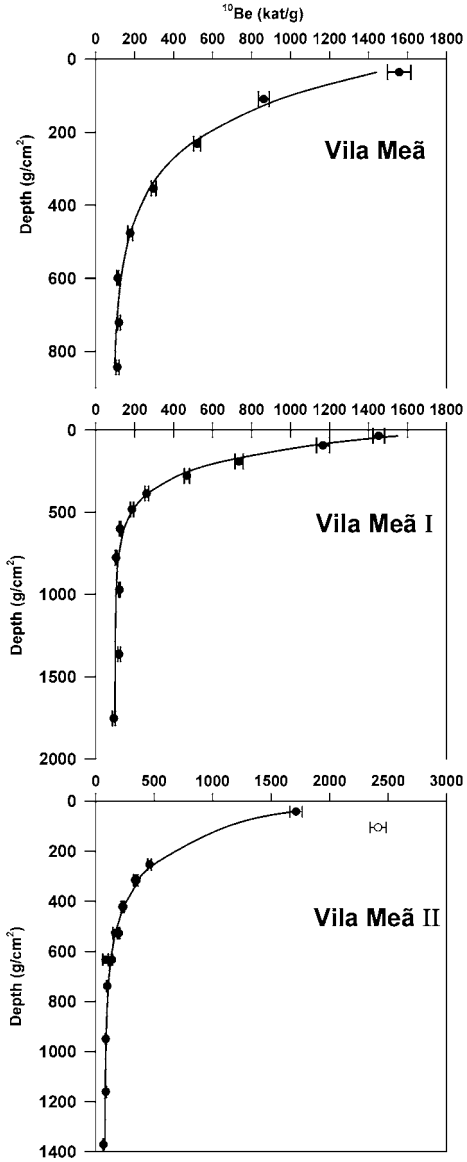

Fig. 3.7. ^{10}Be concentrations as function of terrace depth for the Vila Meã profiles. Depth in g cm^{-1}.

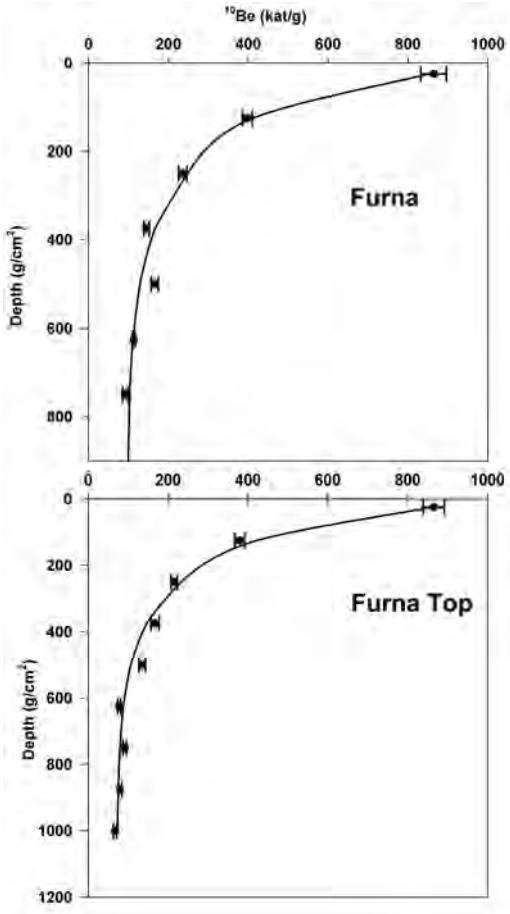

Fig. 3.8.^{10}Be concentrations as function of terrace depth for the Furna profiles. Depth in g cm^{-1}.

Table 3.5. Best fit ^{10}Be ages for the data. With d, T, and H as density, exposure time, denudation and inheritance, respectively. When the d, T, and H boxes are empty, the four parameters are considered as unknown and are to be determined by the model. When at least one box is filled, the corresponding parameter is forced into the model calculation (for example T=Inf implies infinite time corresponding to denudational steady state). The reduced Chi-square value corresponds to the sum of all individual sample chi-squares divided by the degrees of freedom (number of samples less the free parameters).

Site	**Model input**				**Inheritance (kat g^{-1})**	**Density (g cm^{-3})**	**Reduced Chi^2**	**Denudation (Modelled, min max), (m Ma^{-1})**	**Exposure age (Best fit, min; max) (ka)**	**Integration time (ka)**
	d	T	ε	H						
VM					81 ± 4	2.35	8.11	0.7 ± 0.7	475; -30; +4000	
VM			0		81 ± 4	2.36	6.37		458 ± 40	
VM		Inf.			Meaningless	2.36	10.55	1.3±0.1	Meaningless	
VMI					130 ± 6	2.20	9.65	0.3 ± 0.03	780 ± 250	
VMI			0		123 ± 8	2.20	10.24		563 ± 30	
VMI		inf			Meaningless	2.16	12.18	1.05± 0.05	Meaningless	
VMII					Meaningless	2.16	13.4	1.15 ± 0.15	>5000	650
VMII			0		82 ± 3	2.16	5.38		530 ± 120	
Furna					100 ± 6	2.42	5.67	0.6; -0.6; +4	154; -30; +800	
Furna Top					67 ± 4	2.12	9.14	0.7; -0.7; +4.8	151 ;- 20; +1300	

3.4.2.2 The rejuvenation approach

Minimum ages ranging from 414 to 579 ka are calculated for the three VM sites, and minimum ages ranging from 187 to 196 ka for the Furna sites (Table 3.6). The slightly higher CRE ages for the Furna sites compared to the depth-profile approach may be explained by an overestimation of inheritance by the depth profile approach. In all cases the CRE age estimations are in agreement with both data modelling approaches. The modelled inherited concentrations range from 32 to 279 kat g^{-1}, with the majority of concentrations centring around 93 kat g^{-1} (Table 3.6). Thus, modelling of the inheritance by two different approaches yields similar results. This confirms that the inherited concentrations at the studied sites are constant and similar.

Table 3.6. Inherited concentrations and minimum CRE ages resulting from the rejuvenation method.

Samples	Inheritance (kat	Minimum age
Furna-01	102	196 (± 5.9)
Furna-02	105	
Furna-03	81	
Furna-04	93	
Furna-05	126	
Furna-06	52	
Furna-07	44	
Furna-08	0	
Furna-09	172	
FurnaTop-1	63	187 (± 5.8)
FurnaTop-2	74	
FurnaTop-3	81	
FurnaTop-4	55	
FurnaTop-5	94	
FurnaTop-6	82	
FurnaTop-7	32	
FurnaTop-8	0	
FurnaTop-9	220	
FurnaTop-11	52	
VilaMea-01	80	414 (± 13.1)
VilaMea-02	101	
VilaMea-03	64	
VilaMea-04	82	
VilaMea-05	105	
VilaMea-06	120	
VilaMea-07	0	
VilaMea-08	279	

VilaMeaI-01	100	450 (± 9)
VilaMeaI-02	131	
VilaMeaI-03	122	
VilaMeaI-04	77	
VilaMeaI-05	50	
VilaMeaI-06	52	
VilaMeaI-07	36	
VilaMeaI-08	82	
VilaMeaI-09	126	
VilaMeaI-10	128	
VilaMeaI-11	0	
VilaMeaII-01	0	579 (± 17.9)
VilaMeaII-02	n.a.	
VilaMeaII-03	65	
VilaMeaII-04	101	
VilaMeaII-08	84	
VilaMeaII-05	117	
VilaMeaII-09	125	
VilaMeaII-06	118	
VilaMeaII-10	161	
VilaMeaII-07	49	
VilaMeaII-11	121	
VilaMeaII-12	88	
VilaMeaII-13	87	
VilaMeaII-14	92	
VilaMeaII-15	67	

3.4.2.3 Effective sediment transport time deducted from inherited ^{10}Be concentrations

As shown above, the inherited components determined for the 5 depth profiles range from 69 to 130 kat g^{-1} when considering a constant inherited concentration. When compared with other studies (Vassallo et al., 2011, Le Dortz et al., 2012), the inherited component in the Miño river system appears to be temporally quite constant. To validate this conclusion, the ^{10}Be concentration has been measured in an amalgamated sample of ~40 quartzite pebbles that are currently transported by the Miño River (Miño 0, Table 4). The concentration measured in this sample (~55kat g^{-1}) is of the same order of magnitude as the inherited component determined in the Vila Meã and Furna profiles. This observation seems obvious, but to our knowledge, this is a unique case where the inheritance determined from a depth profile is in agreement with the concentration accumulated in the actual river bed. This suggests that the current source of pebbles of the Miño river as well as their transport time has not significantly varied over the last few hundreds ka. As quartzite bedrock is present only upstream of the Sil River, with the Bierzo basin being the

main source of quartzite clasts, it seems reasonable to suggest that the quartzites of the Vila Meã sequence originate from the Bierzo and surroundings (Fig. 1.1). The maximum integration time for the VMII terrace thus indicates that the Sil and Miño rivers became connected at least 650 ka ago.

It is unlikely that lateral erosion of the valley sides led to an enrichment of current river bed gravels by older quartzite gravels, thus yielding similar inheritance values for the contemporaneous gravels. We have not observed any weathered quartzite gravels while performing the density measurements nor when we inspected the floodplain. Also, just upstream of where we took the gravels from the present river bed, the Miño no longer contains any terraces, but only a long bedrock canyon of at least 150 km length, before connecting with the Bierzo basin.

It is possible to estimate the effective travel time from source to sink using equation 1 (assuming no denudation and no storage) and the Miño 0 sample concentration (Table 3.4). Considering an average altitude of 600 meters for the entire Miño watershed, yielding a ~7.2 at g^{-1} yr^{-1} production rate, gives transport ages ranging from 8.7 ka to 15 ka. Taking into consideration that exposure also occurred during exhumation of the quartzite bedrock, the travel time should be considered a maximum travel time.

3.5 Discussion

3.5.1 Fluvial terraces or marine basin infill?

The high and constant inheritance component revealed by the beryllium profiles and the fact that many of the older quartzite clasts are deeply weathered and well-rounded could be indicative of a pre-Quaternary (marine) basin infill. However, the CRE age estimated from the profiles (Fig. 3.7 and 3.8) clearly indicates an increasing CRE age with increasing terrace altitude, which suggests cyclic deposition instead of one large depositional event. In addition, Quaternary-age fluvial aggradation on top of an older basin infill before incision of the terraces would yield ^{10}Be profiles evidencing at least 2 different exponential decreases. The presented profiles however, clearly show a decrease of the ^{10}Be concentrations with depth that can be satisfactorily modelled with a unique exponential decrease, indicating a single depositional event. The idea of an older basin infill that was subsequently incised can therefore be rejected.

3.5.2. Terrace ages

It has been observed all over the world that fluvial terraces in general have a cyclic character (Bridgland and Westaway, 2008a). That is, terrace deposition and incision within a terrace staircase occur at regular temporal intervals that are caused by a rhythmic pattern of climate and/or sea level changes. For the last 800 ka or so these changes were forced by the 100-ka eccentricity-driven Milankovitch cycle; for the remainder of the Quaternary a 41-ka obliquity-driven cycle prevailed (Maddy et al., 2005; Bridgland and Westaway, 2008a). Especially along the Western European Atlantic coast, many river systems show a regular terrace staircase with roughly 5- to 10-m intervals that extend back to the Mid-Pleistocene climate revolution or beyond (e.g. Veldkamp and Van den Berg, 1993; Antoine et al., 2007; Santisteban and Schulte, 2007). Because the Vila Meã staircase also exhibits a regular pattern and is closely situated to the ocean, the CRE and luminescence ages are compared to the benthic record of Lisiecki and Raymo (2005, Fig. 3.9). It is clearly shown that independent of the method used, the different terrace levels form separate groups based on age differences. Terrace age also increases with terrace altitude. The Furna and Furna Top terraces cluster around the MIS 7 to 6 transition and MIS 6. The oldest minimum luminescence age obtained (FURNA TOP-B, 134 ± 13 ka) situates the timing of terrace deposition at the end of MIS 6 and seems to agree well with the CRE ages for the Furna level. It is likely however that the timing of terrace deposition occurred closer to the MIS 7 to 6 transition instead of the final stage of MIS 6 because CRE dating typically gives terrace abandonment ages. The timing of deposition should therefore be slightly before the timing of the CRE ages. This would be additional evidence that the luminescence ages underestimate the timing of deposition of the Furna terrace. The 3 different age estimations for the Vila Meã terrace (VM) all centre on MIS 12 and the transition to MIS 11. The CRE ages for VMI centre on MIS 15 and 14, when only the overlapping age interval between the 2 depth profile techniques is taken into account. The rejuvenation approach seems to underestimate the CRE age. For the VMII terrace, the rejuvenation approach seems to underestimate the age as well and the minimum age of 650 ka seems a better match, which places the VMII terraces in MIS 16. By this way of reasoning, it becomes apparent that the VM, VMI and VMII terraces are all spaced a 100-ka glacial-interglacial cycle apart. Fig. 3.9 indicates an age gap of over 200 ka between the Furna and VM terraces. Interestingly enough, morphological evidence between 16 and 20 m points towards a terrace level that has not been dated (Fig. 3.1). No terrace level younger than the Furna level has been dated, although morphological evidence shows that a younger terrace exists (Fig. 3.1). It has recently been shown that just offshore the Miño River, fluvial gravel deposits from the Last Glacial Maximum are overlain by Holocene muds (Lantzsch et al., 2009, 2010). It is most likely that this

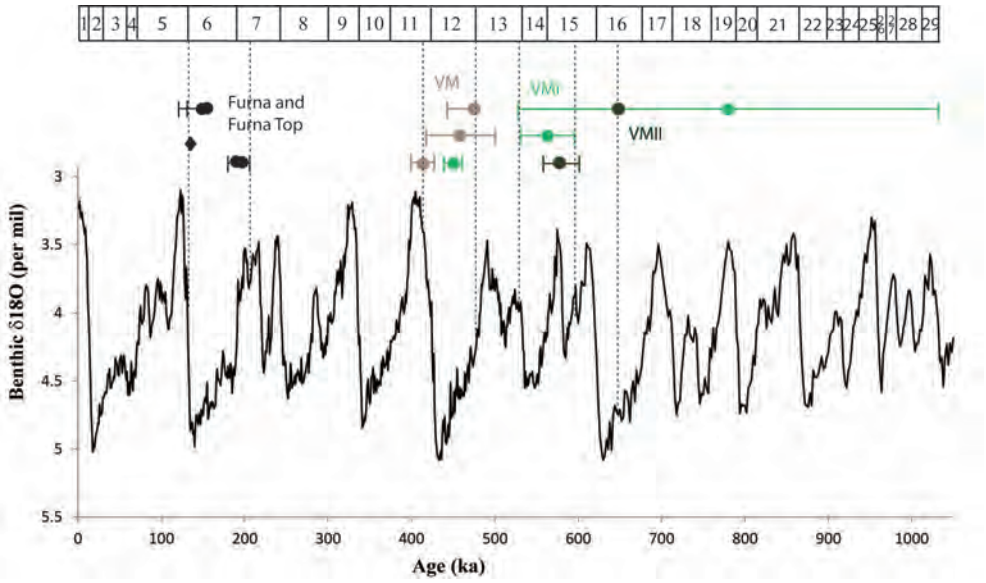

Fig. 3.9. CRE and luminescence ages compared against benthic ^{18}O stack (Lisiecki and Raymo, 2005). The Y-axis is inverted. MIS boundaries given in upper part of Figure. Dots indicate the estimated CRE ages (Tables 3.5 and 3. 6) and have associated error bars (min/max age) for the depth profile approach. The rejuvenation approach ages are strictly minimum ages. Max. age error bar for Furna, Furna Top and VM terrace not given because these maximum ages are unrealistic and obstruct the clarity of the drawing. The black diamond indicates the oldest minimum age obtained for the Furna site, the sample Furna Top-B (Table 3.4). The dashed lines indicate the most likely age interval for each terrace level. The Figure clearly shows that The Furna and VM terrace levels have their own specific cluster of estimated ages. The situation for VMI and VMII is less obvious, but it is shown that the ages progress with terrace altitude. It can be observed that the VM, VMI and VMII terraces are possibly spaced approximately 100 ka apart, which may indicate eccentricity-forced terrace formation.

situation extends to the lowermost area of the Miño River, as the Rias Baixas show a similar pattern of Holocene muds on top of glacial gravel (Pannekoek, 1970 ab; Garcia-Gil et al., 1999). This would imply that a terrace level formed during MIS 2-5d has not yet been uplifted sufficiently above the Miño River level to be recognisable as such. The terrace is probably overlain by Holocene deposits and visible in the field as the 5 m terrace (Fig. 3.1 and 3.2). The CRE ages obtained by the depth profile method (denudation set at 0) and the integration time for VMII, yield ages that fit best the above described scenario of 100 ka eccentricity-driven forcing. This should not be surprising, as the depth profile method with 4 free parameters has shown that denudation is very low and might even approach 0 (Table 3.5). It may therefore be concluded that the ages of the depth profile technique (denudation parameter set at 0) are actually very close to the real ages. The rejuvenation approach on the other hand, seems to work better for the Furna terrace as the depth profile approach probably overestimates the amount of inheritance.

It follows that the undated 70 m terrace would be situated around at least around MIS 18.

The large interval of 17 m between this terraces and the 53 m level, as compared against the roughly 10-m intervals between the other terrace levels, suggests that at least one terrace level may not be registered in the terrace staircase (Fig. 3.2). This would place the oldest 70 m terrace even further back in time, possibly around MIS 20 or MIS 22. It has been shown that around this time many river systems in Europe changed from broad, shallow laterally eroding river systems to deeply incising river valleys because of a change towards 100-ka eccentricity-forced cyclicity (Gibbard and Lewin, 2009). This would make the Lower Miño staircase considerably younger than the Upper Pliocene to Lower Pleistocene age proposed by Vieira et al. (2011). The Miño terraces have therefore most likely been formed due to climatic forcing similar as elsewhere along the European Atlantic Margin (Antoine et al., 2007; Bridgland and Westaway, 2008a; Martins et al., 2010). These causes are further explored below.

3.5.3 Driving forces behind terrace formation

The uncertainties of the CRE and luminescence age estimations do not allow inferences to be made about a glacial or interglacial origin of the terrace gravels. But based on field observations and a comparison with fluvial terrace systems elsewhere along the European Atlantic Margin, a terrace formation model for the Lower Miño is proposed.

Interglacial deposits have not been observed underlying the terrace gravels. The contact between the gravels and the underlying saprolite is always erosive as can be evidenced from the large channels cut deeply into the granite saprolite (Fig. 3.3A and 3.3C). It has been observed in other river systems in the world and especially Europe that a change in river style may lead to profound erosion and to a complete removal of sediments on the flood plain (Blum and Törnqvist, 2000). This is especially the case when rivers change from a meandering channel style to a braided channel type during the transition from an interglacial to glacial (Gibbard and Lewin, 2002). The current Miño River only transports fine- to medium-grained sand on the lower 25 km reach of its course, whereas the older terrace gravels are found up to 2 km from the coastline. The Miño thus had more stream power during development of the terraces, because it was able to transport coarser gravel calibre bed load. A glacial sea level low stand would induce a steeper river gradient and thus more stream power. This would indicate that the Miño gravels were deposited around an interglacial-glacial transition period, but after removal of the former interglacial flood plain sediments. Because the ^{10}Be-concentrations in the terraces show a perfect exponential decrease with depth, it is proposed that sedimentation of the gravels occurred during a short time period. This differs from the ideas of other workers who argue that gravel deposition in fluvial terraces may occur over extended time periods of several 10 ka (Bridgland and Westaway 2008a). Deep and prolonged incision occurred after gravel deposition, probably around a glacial-interglacial transition period. This may be evidenced

from the steep, intact bedrock scarps that would otherwise have a much lesser slope due to lateral erosion of the river. The proposed model of terrace formation and incision agrees with the model proposed by Bridgland (2000) and shows that during a glacial period both lateral erosion and sedimentation can occur (Gibbard and Lewin, 2009). The important difference with the model by Bridgland (2000) is that interglacial floodplain deposits are not formed on top of the glacial terraces. The ^{10}Be profiles at least have not indicated any major erosion phases after gravel deposition (Figs. 3.7 and 3.8). This also indicates that gravel deposition should have occurred relatively early during a glacial period, when base level was sufficiently high. Only then could the Lower Miño deposits have been uplifted above an interglacial base level and thus effectively have prevented interglacial sedimentation on top of the glacial gravels. The only exception could possibly be the Furna terrace, which contains a metre of overbank deposits on top of the gravels (Figs. 3.4 and 3.5). These deposits could possibly be a consequence of the MIS 5e sea level high stand, although the luminescence ages cannot confirm this. A second important difference is that climate change-induced variations in discharge and sediment load are probably not as important for the Lower Miño as elsewhere (e.g. Vandenberghe, 1995; Busschers et al., 2007; Bridgland and Westaway, 2008a). The greater part of the catchment was always vegetated and relatively humid (Desprat et al., 2005; 2009), which probably restricted the occurrence of major flood events. Small glaciers were present in the upper catchment (Vidal-Romani et al., 1999; Jalut et al., 2010; Rodriguez-Rodriguez et al., 2011), but to such a small extent that glacier retreat probably has not caused significant changes in water discharge and sediment load dynamics of the Miño-Sil River. Sea level change however, is proposed to play an important role in sediment transfer, valley incision and terrace scarp formation because of the close proximity to a very narrow continental shelf (Talling, 1998; Meijer, 2002; Törnqvist et al., 2006). Indeed, many passive margin fluvial systems around the world have deeply incised river valleys, especially if the shelf gradient is steeper than the coastal plain gradient (Blum and Törnqvist, 2000). Such incised valleys are also common along the Iberian Atlantic Margin which has a narrow continental shelf. Examples include the Tagus River valley (Vis et al., 2008) and the Duero River valley (Naughton et al., 2007). Bathymetry data indicate that the 35-km wide continental shelf in front of the Miño River mouth drops to 200 m below sea level just before the shelf break (Lantzsch et al., 2009; 2010). The shelf has a mean gradient of 4 m km^{-1} compared to a coastal plain gradient of 0 m km^{-1}. Sediment transfer and terrace incision are therefore most likely a direct consequence of river gradient changes induced by eustacy and differ in this sense from the other European Atlantic systems in northern/central France, Benelux and the UK. There, a glacial fall in sea level led to a lengthening of the river profiles by several hundreds of kilometres due to the relatively shallow North Sea basin (De Mulder et al., 2003). Base level changes did propagate upstream (Tebbens et al., 2000), but in a much less aggressive way when compared to base level changes in the Lower Miño River.

A steeper gradient than the present one during terrace deposition also implies that the present Lower Miño River gradient cannot be used as a means for long distance terrace remnant correlation (see correlations made by for instance Lautensach, 1945; Butzer, 1967, Nonn, 1967). This seems to be confirmed by remnants of the oldest terrace which have a height difference of 40 m between the near-coastal ones and the more upstream remnants. The current Miño has almost no gradient along this interval. It is possible that this height difference is caused by fault activity (Viveen et al., 2012a, see Chapter 2), but valley incision during periods of glacio-eustatic low sea level thus seems a more likely alternative. This circumstantial evidence in combination with the new luminescence and CRE ages suggests that the Miño terraces may have formed due to a 100 ka eccentricity-driven cycle of sea level changes in combination with tectonic uplift, which has shown to be a prerequisite for terrace formation (Maddy, 1997; Bridgland and Westaway, 2008a).

3.5.4 Miño terrace denudation rates

The calculated denudation rates are very low considering that the Miño experiences a moderate amount of tectonic activity and high annual rainfall with catchment-wide mean precipitation of up to 1100 mm yr^{-1} for the past 430 ka (Desprat, 2005; Desprat et al., 2005; Sanchez-Goñi et al., 2005). It is likely that the low gradient of the terraces (0.003 to 0.007 m km^{-1}) in combination with high infiltration capacity of the terraces, prevented overland flow. Additional factors may be that the underlying granites weathered rapidly, thus preventing water stagnation, also that the Miño catchment has always been vegetated, even during the coldest spells of the glacial periods (Sanchez-Goñi et al., 2008; Desprat et al., 2009). It has also been demonstrated that fluvial systems with moderate vertical uplift rates (typically 0.08 to 0.11 m ka^{-1}) have the largest potential for alluvial terrace preservation (Veldkamp and Van den Berg, 1993). Likely because of these exceptional circumstances, the Vila Meã sequence experienced very little erosion.

3.5.5 Miño incision rates

The minimum luminescence and ^{10}Be ages of the terraces allow estimating maximum incision rates. Because the terraces most likely have a glacial origin, the current Miño floodplain cannot be used as a reference level for incision calculation. Therefore only maximum incision rates between the dated terraces can be estimated. The incision rates are calculated based on what are considered the best age estimations for the terraces (see paragraph 3.5.2). These are the ages obtained from the depth profile method (denudation set at 0) for the VM and VMI terraces, the integration time for VMII and the rejuvenation approach ages for the Furna terrace. Over the period 650 – 563 ka, the maximum incision rate is estimated at 0.13 m ka^{-1}; over the period 563 – 458 ka at 0.09 m ka^{-1}; and over the

period 458 – 196 ka at 0.07 m ka^{-1}. Because the ^{10}Be concentrations measured along the VMII terrace have reached steady state, the 650 ka integration time for this terrace should be considered as a minimum age and the calculated incision rate is very likely severely overestimated. These assumptions lead to an estimated maximum mean incision rate of 0.07 – 0.09 m ka^{-1} over the time period 196 – 650 ka. Because the spacing of the terraces in the staircase is more or less equal, and taking into consideration climate-driven terrace cyclicity, it is assumed that the incision rate has remained constant over time (Burbank and Anderson, 2001). The calculated incision rates can be considered as average values when compared to calculated incision rates elsewhere along the European Atlantic Margin. Middle to Late Quaternary values ranging from 0.07 to 0.12 m ka^{-1} have been found in the Netherlands, France and the UK (Veldkamp and Van den Berg, 1993; Maddy, 1997; Westaway, 2002; Westaway et al., 2006). A link has been made between accelerated surface erosion and a change to the more intense 100 ka climate cycles, leading to isostatic rebound and adaptation by fluvial systems through incision (Westaway et al., 2009). We propose that the reconstructed neotectonic movements of the north Iberian plate edge (Viveen et al., 2012a, see Chapter 2) are more likely to have caused the reconstructed incision by the Miño River. These are further explored in the next paragraph.

3.5.6 Tectonic uplift rates

Incision has been shown to be a good approximation for tectonic uplift (Maddy, 1997; Burbank and Anderson, 2001), if it can be assumed that incision kept pace with regional uplift. This is often the case with larger fluvial systems such as the Miño, and equal sized rivers have even been able to keep up with uplift despite significant external disturbances such as volcanic eruptions (e.g. Veldkamp et al. 2012). That this is not always the case has been demonstrated for instance by Kiden and Törnqvist (1998). We argue that the incision of the Miño is a direct response to glacio-eustatic changes and crustal uplift. The aforementioned proximity to the continental shelf and the steepness of the shelf probably cause a profound change in river gradient and most likely led to rapid incision by the Miño (Veldkamp and Tebbens, 2001). A delayed response is therefore unlikely. All terrace levels are well above current and MIS 5e (+ 3 to 6 m.a.s.l.) sea levels. As sea level has not been higher, it is obvious that tectonic uplift has occurred. This is further demonstrated by the presence of a flight of at least 4 marine terraces along the Portuguese coast just south of the Miño (Candido de Medeiros., 1970). Marine terraces have been shown to be a reliable proxy for crustal uplift (e.g. Maddy et al., 2000; Claessens et al., 2009). Our only concern is that fluvial incision caused by eustacy in combination with the relatively high stream power of the Miño River actually outpaced the rate of vertical crustal uplift; that is, the rate of vertical incision is exaggerated because the river profoundly incised to grade towards a new equilibrium profile (Maddy, 1997). For these reasons, and the fact that the ^{10}Be ages are minimum ages, we believe that our incision rates can only be used as proxies for

maximum uplift rates. The estimated maximum incision rates can be compared to the few regional available uplift rates:
The only long-term uplift estimation in the studied area has been published by Cabral (1995), who estimated that the uplift rate over the last 2 to 3 Ma should approximately range between 0.033 and 0.05 m ka^{-1} based on undated geomorphological markers. A multiple cosmogenic nuclides study by Alvarez-Marron et al. (2008) reveals uplift rates ranging from 0.07 to 0.15 m ka^{-1} for a 1 Ma wave-cut platform on the Galician-Asturian coast (Fig. 1.1). Recently, a modelling study of apatite-fission track data combined with structural mapping for the Galician-Leonese Mountains (westernmost extension of the Cordillera Cantabrica; Fig. 1.1) suggests Neogene uplift rates of 0.08 m ka^{-1} (Martin-Gonzalez et al., 2011). The maximum uplift rates presented by us are in agreement with those proposed in the latter two studies and do not exclude the estimations made by Cabral. This similarity along the Northern Spanish coast, the westernmost termination of the Cordillera Cantabrica and in the studied area strongly suggests that the deformation along the northern edge of the Iberian plate leads to comparable vertical deformation rates and extends as far as the Western Iberian Atlantic Domain (De Vicente and Vegas, 2009; Viveen et al., 2012a, see Chapter 2). The causes for this deformation are not well understood, but lithospheric folding causing crustal shortening seems a plausible hypothesis (Cloetingh et al., 2005).
The presented CRE ages in this work allow us to challenge the findings of Trenhaile et al. (1999) and Alonso and Pages (2007) claiming that the south-western Galician coast has not experienced tectonic uplift since at least MIS 5e, because colluvium overlying a fossil beach at 3.5 m.a.s.l. yield ages from the last glacial period. As the MIS 5e sea level was likely about 3 to 6 m higher than nowadays, they argue that the fossil beach has not experienced uplift. The data presented in this work however, show that tectonic uplift occurred before MIS 5e and, as the present-day stress field remained more or less equal throughout the Late Cenozoic, that tectonic conditions have not changed. This is further demonstrated by the presence of (unpaired) fluvial terraces and active faults and blocks (Viveen et al., 2012a, see Chapter 2). It therefore appears logical to conclude that tectonic activity is still present nowadays.

3.6 Conclusions

This work presents a first assessment of the Miño River terrace chronology and incision rates based on a combination of luminescence and ^{10}Be dating. Due to the high inherited concentrations, all ^{10}Be CRE ages are considered minimum ages, but there are strong indications that they are very close to the real ages of the Miño terraces. Minimum ages of up to 650 ka have been calculated. Furthermore, the ^{10}Be profiles indicate that the Miño terrace deposits have a fluvial origin and are not an older, marine basin infill as suggested by some workers. As the gravels originate from the headwaters of the Sil River, this work also demonstrates that the Sil and Miño rivers became connected at least 650 ka ago. The terraces are likely of glacial origin and may have formed due to a 100 ka eccentricity-driven cycle of sea level changes in combination with tectonic uplift. The oldest terraces are suggested to date back from the Lower to Middle Pleistocene transition period. This makes the terraces considerably less old than previously thought.
The denudation rates affecting the fluvial terrace sequence range from 0.30 to 1.30 m Ma^{-1}. These surprisingly low denudation rates considering the climate and tectonic activity in the region, most likely result from favourable conditions preventing surface erosion. The almost flat surfaces, high permeability and continuous vegetation cover during the Quaternary stabilised the terrace surfaces.

The reconstructed incision rates can be used as proxies for tectonic uplift rates. The ages obtained from the terraces allow estimation of a maximum uplift rate of 0.07 – 0.09 m ka^{-1} for the period 196 – 650 ka. This work presents the first maximum uplift rates for the NW Iberian Atlantic Margin and shows that moderate amounts of uplift occur in a region that until recently was considered tectonically stable.

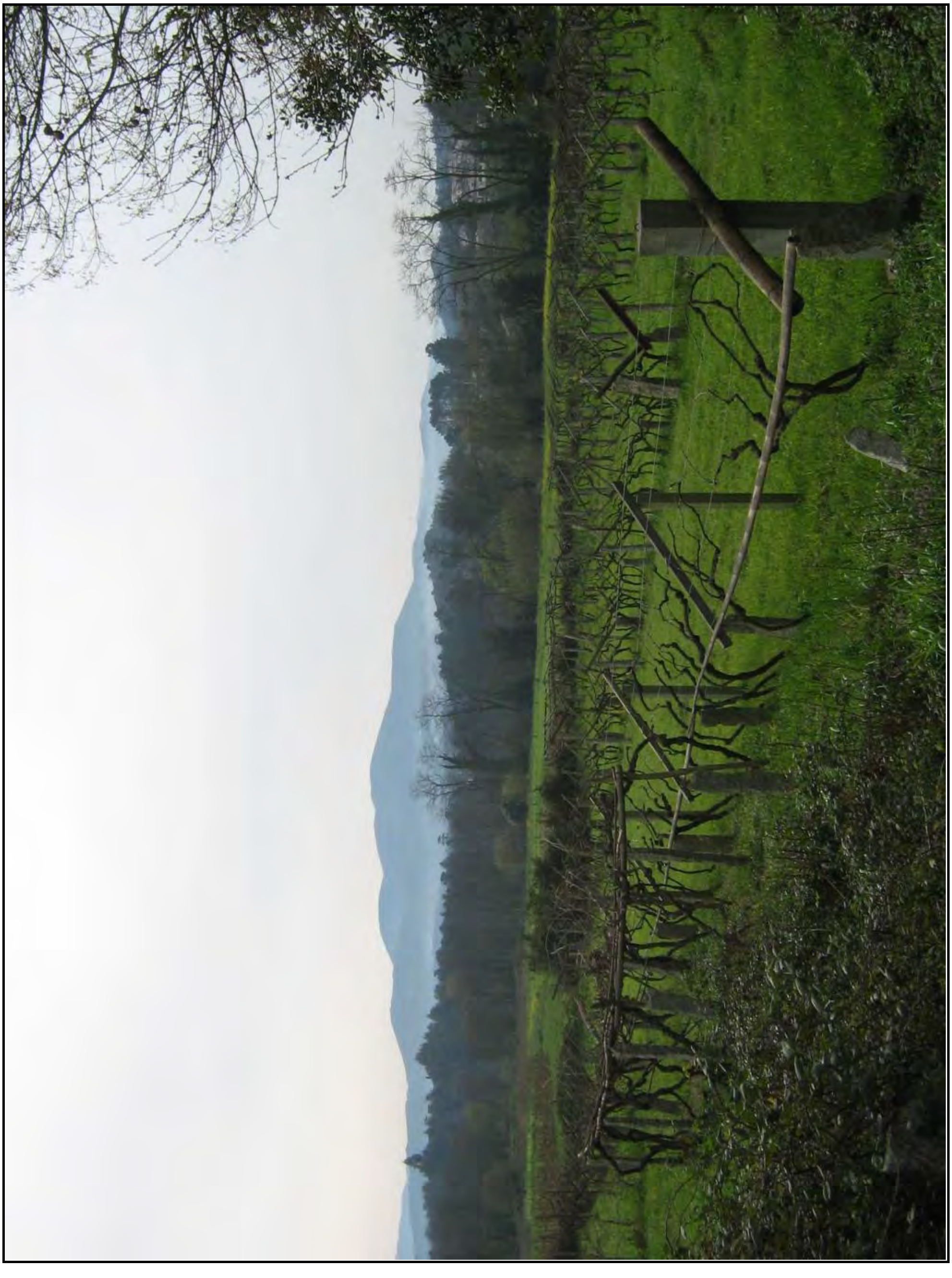

Chapter 4

Reconstructing the interacting effects of base level, climate, and tectonic uplift in the lower Miño River terrace record: a gradient modelling evaluation

The origin of the lower Miño River terraces in the NW Iberian Peninsula has been a topic of debate since the 1940s. Various hypotheses about their main controlling factors have been put forward, but general consensus is still lacking. Field studies of terrace distribution and the weathering of quartzite pebbles in the terrace deposits demonstrated that terrace longitudinal correlation is not parallel to the current river bed. In addition, the longitudinal profile model FLUVER2 was used to simulate the profile evolution of the Miño River over the past 450 ka. A reconstructed longitudinal profile and an offshore climate record were used as inputs. Several scenarios with variable uplift rates were investigated and evaluated against properties of four selected reaches along the river for a match with the number of terraces, their relative altitude, timing, and sediment thickness. An uplift scenario with a net constant vertical uplift rate of 0.08 m ka^{-1} yielded the best results. The best fit scenarios indicate that base level changes from glacioeustatic changes in combination with tectonic uplift are the main driving forces of the observed terrace formation and valley incision. Contrary to most NW European fluvial systems, the timing of upstream-controlled sediment supply has a less dominant effect on terrace formation. This can be explained by the close proximity to the narrow passive Atlantic margin.

Published as: Viveen, W., Schoorl, J.M., Veldkamp, A., Van Balen, R.T., Desprat, S., Vidal-Romani, J.R., 2013. Reconstructing the interacting effects of base level, climate, and tectonic uplift in the lower Miño River terrace record: a gradient modelling evaluation. *Geomorphology* 186, 96-118.

4.1 Introduction

River gradient modelling may be a useful technique to help deduce which extrinsic factors (climate, tectonics, and base level changes) are responsible for the contemporary fluvial longitudinal profile of a river (Schumm, 1993; Boogaart and Van Balen, 2000). Individual factors may have more influence depending on the river reach (Tebbens et al., 2000) and often interact in a nonlinear way, leading to delayed response times along different reaches (Schumm, 1977). In this sense, longitudinal profile modelling over large temporal scales for instance may lead to a better understanding of the shape of the palaeoriver profile and how it responded to various degrees of tectonic uplift (Gargani et al., 2006). Furthermore, the effect of abrupt Quaternary climate changes on fluvial profile dynamics may be better constrained (Veldkamp and Tebbens, 2001), and numerical modelling even has the potential to provide evidence that different reaches along a river profile react differently to extrinsic and intrinsic changes (Tebbens et al., 2000). The effect of knickpoint migration along a profile under the influence of changes in uplift and sediment flux may also be better understood by numerical modelling (Gasparini et al., 2006).

In this paper we investigate how the longitudinal profile of a river system close to a narrow, steep passive margin may respond to changes in climate, sea level, and tectonics. The studied area is the NW Iberian lower Miño River. The lower Miño has been the subject of studies for over 70 years (e.g., Lautensach, 1945; Teixeira, 1952; Butzer, 1967; Nonn, 1967; Cano-Pan et al., 1997, 1999a); but there is still disagreement on many important topics, such as under what climatic conditions the terraces were formed, the exact number of terraces and how they should be correlated, and the rate of vertical uplift in the area. All these issues can be addressed by simulating the longitudinal profile development of the river. Our approach is based on a combination of techniques: field studies on terrace spacing and their deposits are combined with a quantification of the degree of gravel weathering. This will hopefully allow a preliminary correlation of terrace remnants in the studied river system. Then the evolution of the river system is modelled over a period of 450 ka using a river gradient modelling program, FLUVER2 (Veldkamp and van Dijke, 1998, 2000).

The main focus of this paper is on three key elements: (i) to establish a new longitudinal terrace correlation based on field evidence, (ii) to deduct which uplift range fits best with the observed terrace distribution; and (iii) gain more insight in how river systems near passive margins develop under the influence of climate, sea level, and tectonic changes.

4.2 The lower Miño terraces

In the lower Miño, a number of terrace fragments are situated up to 110 m above current river level (Fig. 4.1). A continuous set of terraces can be found up to 70 km upstream, but from there on sediments become scarcer and are only found in the wider parts of the Miño valley where the potential for terrace deposition and preservation is largest, such as in tectonic basins. The terraces are predominantly strath terraces, whereby the terraces are the resultant of progressive incision into the bedrock and not so much of coupled fill-and-incision processes (Lewin and Gibbard, 2010).

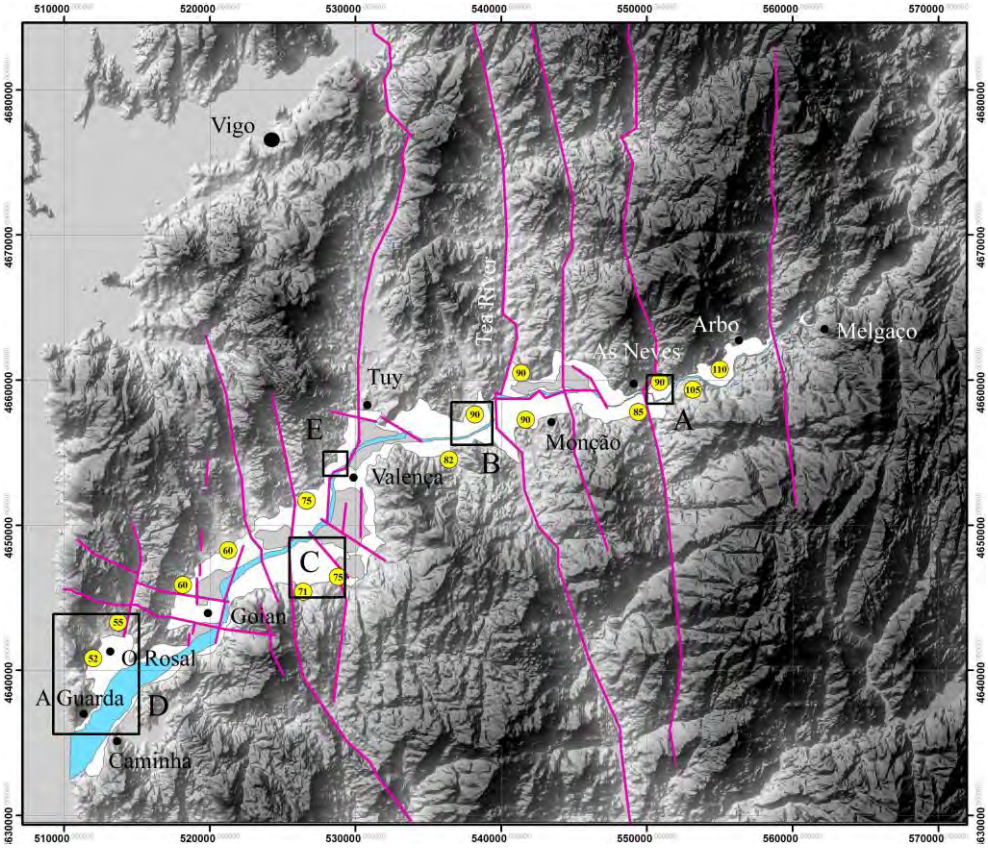

Fig. 4.1. The lower Miño (Baixo Miño) area. Distribution of fluvial deposits (white colour), tectonic basins (grey colour), and faults (purple colour) based on Viveen et al. (2012a) and detailed mapping based on fieldwork and DEM interpretation. Yellow round markers indicate maximum surface height in metres of the highest mapped fluvial terraces. A clear decreasing downstream trend is evident. The rectangles show where the Chan de Vide, Caldelas, Vila Meã, and O Rosal sites (Figs. 4.3 and 4.4) are located and where the seismic profiles were undertaken (Figs. 4.3 and 4.9).

The lower Miño terraces have very thin sediment covers upstream in the studied area, but attain sediment thicknesses of up to 10 m close to the coast. The terrace deposits contain quartz and quartzite gravels and cobbles that may reach diameters of several tens of centimetres. Sand or clay lenses are not very common. Age indicators such as ash tephra layers, fossils, archaeological artefacts, and palaeosols are absent, making long distance terrace correlation very difficult (cf. Briant et al., 2012). The terraces have traditionally been studied in isolated areas, and for that reason there is considerable disagreement on the number of terraces and the underlying mechanisms for terrace formation (Lautensach, 1945; Teixeira, 1952; Butzer, 1967; Nonn, 1967; Cano-Pan et al., 1997, 1999a). Table 4.1 gives an overview of all terrace studies carried out in the region. A tentative correlation is made for the levels observed by the various authors, leading to at least 10 terrace levels in the Baixo Miño. All these authors reconstructed the terraces parallel to the current river bed (Table 4.1).

Terrace deposition has been proposed to have occurred during interglacial periods (Lautensach, 1945; Butzer, 1967; Nonn, 1967) and glacial periods (Viveen et al., 2012b, see Chapter 3). The interglacial hypotheses is based on the observation that terraces with similar positions above the present (interglacial) Miño River can be found throughout the studied area. Also, Butzer (1967) made a tentative correlation of the fluvial terraces with 'interglacial marine platforms' (coastal terraces) close to the coast, but the absence of marine sediments on these platforms means that a fluviomarine correlation is speculative at best. At present, only the most recent marine platform has been identified with certainty (Trenhaile et al., 1999; Blanco-Chao et al., 2003). The idea of a cold-climate origin is based on the observation that currently the Miño mainly transports suspended load (sand and clay) in the lower 25 km of its course; whereas coarse gravels are found up to 3 km from the coast, evidence of past higher stream power conditions. We hypothesised that an increase in stream power induced by a glacioeustatic fall in sea level would provide sufficient stream power to carry the gravels close to the coast (Viveen et al., 2012b, see Chapter 3). To add to the confusion, the presence of small tectonic basins that are also filled up with fluvial deposits (Viveen et al., 2012a, see Chapter 2) cause additional misinterpretations regarding the number of terraces, terrace heights, and terrace correlations.

We further postulated that the narrowness of the NW Iberian continental shelf would surely lead to dramatic changes in the glacial longitudinal profile gradient of the river (Viveen et al., 2012b, see Chapter 3). This would lead to a deeply incised river valley, which is a common configuration for river systems elsewhere along the western Iberian Atlantic margin (Vis et al., 2008). We therefore postulate that terrace formation was not parallel to the current river bed (Viveen et al., 2012b, see Chapter 3), as evidenced by a downstream decrease in position of the highest terrace levels (Fig. 4.1). Consequently, additional field

observations are required that allow terrace remnant correlation based on specific measurable properties.

*Table 4.1. Comparison of terrace height mapping in the study area by other workers. Based on the compilation, a revised chronology of 10 terrace levels (T0 to T9) is proposed (first column); (P) stands for Portuguese bank of the Miño River, (G) stands for Galician side. Only Lautensach (1945) investigated both river banks. *** indicates that the terrace level was not described by the author.*

Author	Lautensach (1945)	Teixeira (1952)	Butzer (1967)	Nonn (1967)	Geological maps Spain 1:50,000	Geological maps Portugal 1:50,000	Cano-Pan et al. (1997)	Cano-Pan et al. (1999a)	Alves (2004)
Area investigated	Cortegada-A Guarda (GP)	Melgaço-Caminha (P)	Porto-A Guarda (G)	As Neves-A Guarda (G)	Arbo-A Guarda (G)	Melgaço-Caminha (P)	Tuy-A Guarda (G)	Chan de Vide-Salvaterra (G)	Valença-Vila Meã (P)
T0	5-10	5-12	3-10	***	0-10	5-8	2-9	5	5
T1	20	15-20	***	15-20	***	15-20(25)	10-19	8-10	15
T2	***	***	22-24	25	10(13)-25(30)	***	19-28	***	***
T3	***	***	34-36	30-35	***	***	***	***	***
T4	40-45	30-40	42-44	35-45	30-45(50)	30-40(45)	32-42	30-40	45
T5	***	50	52-59	50-55	***	45-50(55)	42-55	***	55
T6	***	60-70	65-68	65	50(55)-70	60-70	52-62	69-75	***
T7	***	75-80	76-80	***	***	75-80	65-72	75-80	***
T8	***	***	***	***	***	***	***	80-90	***
T9	***	90-100	***	***	***	90-100	76-95	100	100

4.3 Methodology

4.3.1 Terrace inventory

Terrace surfaces were mapped based on field campaigns in the years 2007 and 2009-2011 and interpretations of a 5-m digital elevation model (DEM) with a vertical accuracy of 0.10 m from the Spanish National Geographic Institute (IGN). The terraces investigated will serve to validate the longitudinal profile modelling results. These transects are situated at the localities of O Rosal (3 km upstream from the Atlantic Ocean), Vila Meã (22 km upstream), Caldelas (36 km upstream), and Chan de Vide (55 km upstream) (see Fig. 4.1). An important criterion for selecting these terrace transects is the avoidance of tectonic basins that might disturb the terrace order and spacing (Fig. 4.1). The transects were also chosen in such a way that they are distributed at more or less equal distances along the lower Miño valley. Because the sedimentological composition of the terraces is exceedingly simple (only clast-supported, coarse quartz, and quartzite gravels) without any outstanding stratigraphical features (sand or clay lenses, fining or coarsening upward sequences), stratigraphical logs were not useful as a distinctive characteristic and only a summary of field observations is given (see Table 4.2).

4.3.2 Quartzite pebble weathering

Quartzite pebble weathering is still not completely understood, but it has been shown that two important processes in quartzite weathering are (i) oxidation and leaching of Fe (Molina-Ballesteros and Cantano-Martin, 2002; Tripathi and Rajamani, 2003) and (ii) silica leaching (Howard et al., 1995), which leads to an increase in the porosity of the pebbles causing a decrease in bulk density. During fieldwork it was observed that quartzite pebbles become more weathered with increasing age and terrace altitude. In order to allow reproducible quantification of the weathering state, pebble bulk density differences might be sufficiently characteristic to correlate the different terrace threads.

A total of 17 terraces were sampled for density measurements of quartzite pebbles at the localities of O Rosal, Vila Meã, and Chan de Vide. Because the Caldelas terraces only contain thin sediment covers, terraces were sampled upstream close to Monção (45 km upstream, Fig. 4.1). The terraces were sampled up to a depth of 3 m (in some cases 2.5 m when not enough sediment was available) at every 0.5 m along the depth profile. Samples were only taken where a continuous gravel deposit was available, that is, gravel deposits with sand or clay lenses were not sampled as they might influence water flow through the terrace deposit and, hence, the weathering rate of the pebbles. Because larger pebbles tend to weather more slowly compared to smaller ones, care was taken to only select quartzite

pebbles of equal sizes in the range of 4 to 6 cm. For this reason, the O Rosal 11-21 m level was not sampled (mean size 3.6 cm). To ensure that all pebbles had a similar transport history, only rounded to well-rounded spherical-shaped pebbles were selected. Per sample level 15 to 20 pebbles were selected.

An important assumption is that all quartzite clasts have a more or less similar initial mineralogical composition. Tripathi and Rajamani (2003) showed that quartzites with an association of weathering-prone minerals, such as micas or pyrites, weather more rapidly than quartzites with a more resistant mineralogy. The quartzite pebbles in the lower Miño terraces originate from the same source, namely the Bierzo basin and surroundings (Viveen et al., 2012b, see Chapter 3). In this area, river captures by the Miño–Sil rivers have not been reported for the middle Pleistocene (Garcia-de Celis, 1997). For this reason we argue that the type of quartzite in the lower Miño terraces has not significantly varied through time.

The samples were cleaned with a steel brush and oven-dried at 80°C during 24 h. The samples were then wrapped with a thin waterproof foil, Parafilm; and the dry mass and the mass in water were determined. Based on the Archimedes' principle, the density was determined (Kueppers et al., 2005) and the mean density per terrace level calculated.

4.3.3 Modelling

For the modelling exercise, the numerical model FLUVER2 is used. The model calculates erosion and sedimentation dynamics along a two-dimensional longitudinal profile. A full description of the model structure, functioning, and parameter calibration is provided by Veldkamp and Van Dijke (1998, 2000), Tebbens (1999), and Stemerdink et al. (2010). The main equations are summarised in Appendix 1.

Although the oldest and highest fluvial terraces are thought to date back to the lower–middle Pleistocene transition period (Viveen et al., 2012b, see Chapter 3), the model in this study is used to simulate terrace formation for the past 450 ka for the lower Miño catchment. The extent of the modelling time window is restricted to 450 ka by the available climate input derived from three marine cores and is likely shorter than the time period investigated for the terrace inventory and quartzite weathering. The complete river profile is divided into segments of 0.34 km length, and for every segment new calculations are made for time steps of 20 years. These calculations comprise the incoming and outgoing fluxes of water and sediments as well as the segment sediment transport capacity. The balance between sediment in transport and the local capacity determines the lowering (erosion) or raising (sedimentation) of the profile and, consequently, sediment input or output. Because the lower Miño region was always vegetated, also during glacials

(Desprat et al., 2007) and bedrock-dominated, sediment input from small local tributaries or slope processes is ignored. The entire profile measures 408 km and consists of 1201 segments.

Below we discuss the main model inputs and assumptions. These comprise an initial longitudinal profile, sea level input, a palaeodischarge model, and vertical tectonic uplift rates. The modelled height and number of terrace surfaces and the timing of terrace formation is then compared against field evidence from the four selected sites discussed in the previous section (Chan de Vide, Caldelas, Vila Meã, and O Rosal terrace transects).

4.3.3.1 Initial longitudinal profile and sea level input

FLUVER2 is based on a forward-modelling approach, so an initial longitudinal profile is needed before the start of the modelling exercise. We assume that the lower Miño was able to keep up with regional uplift by incising at a similar rate, resulting in a state of semi equilibrium (Bull, 1991). This seems justified because the lower Miño is a large river with considerable stream power, and uplift rate is moderate (Viveen et al., 2012b, see Chapter 3). For this reason, the average shape of the longitudinal profile and its altitudinal position will remain approximately constant throughout the modelling exercise. The longitudinal profile was extracted from an SRTM DEM with a grid cell size of 90 m (NASA, 2000). The DEM has a theoretical vertical accuracy of 30 m, which might lead to problems as accurate simulations of the lower Miño River bed requires more precise altitudinal values. Comparison to a 5-m DEM with a vertical accuracy of 0.10 m shows that the values of the 90-m DEM are quite similar. However, the 5-m DEM could not be used because many small artefacts such as bridges and dams were present in the grid. The profile measures 375 km from its source in the Cordillera Cantabrica to the Atlantic Ocean. An additional 33 km are added to account for lengthening of the profile during periods of glacial sea level fall, resulting in a profile of 408 km total length. Seismic profiles available for the continental shelf just north and south of the Miño show that the Holocene and glacial fluvial deposits are parallel to the current sea bed (Lantzsch et al., 2009, 2010). For this reason the height of the current sea bed was used as an approximation for the now submerged Miño River bed during glacial low stand (Rodrigues et al., 1991).

Table 4.2. Field observations of the terrace transects discussed in the text; the locations and the terrace transects can be found in Figs. 4.1 to 4.3.

Site and coordinates (UTM N29, ED50)	Site description	Sedimentological composition terrace	Internal bedding structures	Weathering characteristics	Fluvial structures
Chan de Vide T0 (27-28 m) 550578 E, 4658836 N	A small terrace located direcly above the Miño canyon.	A shallow exposure shows 0.3 m of fine, organic-rich Holocene? sand.	Not visible	Not applicable	Not visible
Chan de Vide T1 (40 m) 550735 E, 4658878 N	Just SW of Chan de Vide a railroad cuts through the terrace. Fluvial material found between 3.5 and 8 m below surface; granite saprolite underlies terrace.	Massive quartz and quartzite gravel deposit in an unconsolidated white to light yellow clayey to coarse sandy matrix.	No internal bedding	Quartz and quartzite clasts hardly weathered. Difficult to break with hammer. Break into shards when broken.	Variable clast imbrications (S to W) due to proximity of small tributary.
Chan de Vide T2 (50-53 m) 550861 E, 4658932 N	Roadcut shows 2.5 m of gravel on top of granite saprolite.	Quartz and quartzite gravels in yellowish fine sandy matrix.	No internal bedding	Quartzite clasts are either unweathered (dark grey) with thin iron oxidation rinds, or completely iron-oxidised (brown) with sometimes a reddish-brown iron-oxidation rind. Not easy to break with hammer.	Not present
Chan de Vide T3 (60-64 m) 550901 E, 4659197 N	Palaeochannel cut into granite. Deepest incision reaches 2.5 m below surface; shallowest point 0.5 m below terrace surface.	Rounded to subrounded quartz and quartzite gravels of around 4 cm diameter in a fine sand to clayey matrix. Iron oxidation in large parts of the matrix.	No internal bedding	Quartzite gravels have iron-oxidation (brown) or iron leaching (white) rinds. Cores are brown to light brown to white. Easy to break with hammer.	Palaeochannel cut into underlying granite.
Chan de Vide T4 (71-73 m) 550732 E, 4659520 N	A small gravel mine shows 10 m gravel overlying weathered granite.	Massive quartz and quartzite gravel deposit. Mean clast size 4-6 cm, but large cobbles up to 30 cm present.	No internal bedding	Quartzites quite weathered in upper part of profile, less so in lower part. Quartzites have a predominantly light brown-white to white core. Brown cores are in smaller amounts present. Weathering rinds are either brown or	At 3 m below terrace surface, a 1-m thick clay bank is found; extent 10 m.

				white. Easy to break with hammer.	
Chan de Vide T5 (81 m)	Roadcut of only 1 meter. Base terrace not visible.	Quartz and quartzite gravel in upper part of intact soil profile.	No internal bedding	Quartzites in Ah-soil horizon show deep dissolution pits.	Not visible
550810 E, 4659716 N					
Caldelas T0-T9 (11-85 m)	No mines or gravel pits present, only small road cuts. All terraces very similar and situated on steep slopes. The terrace base is visible for all terraces and situated on top of granite.	All terraces are very shallow, with maximum gravel depths of ± 1 m. In some cases 1-m thick colluvia overly the terraces. Gravel consists of quartz and quartzite, matrix is medium to fine sand. Color not visible because of soil development.	No internal bedding	All terraces appear to be quite weathered, the older ones more so than the younger ones. In older terraces the gravels are friable and completely white or brownish-white.	Not present
537854 E, 4656567 N; 537264 E, 4656795 N; 537943 E, 4657090 N; 538068 E, 4657563 N; 535786 E, 4657197 N					
Vila Mea terraces (13-70 m)	For a full description see Viveen et al. (2012b).	For a full description see Viveen et al. (2012b).	For a full description see Viveen et al. (2012b).	For a full description see Viveen et al. (2012b).	For a full description see Viveen et al.(2012b).
Vila Meã (64 m)	A small industry park contains a couple of exposures in this terrace. In all exposures the gravel deposit is about 3 m thick. Base not visible.	Rounded to well-rounded quartzite and quartz gravels. Mean size around 6 cm. Matrix is a brownish-yellowish mixure of fine sand, clay and iron oxides.	No internal bedding	Quartzites have light brown, thin outer rinds and white-brown to white cores. Clasts are very fragile but cannot be pulverised by hand.	Not present
531227 E, 4649965 N					
O Rosal T0 (0-1 m)	Current floodplain, is a tide-dominated wetland.	Holocene overbank deposits (muds and fine sand).	Not visible	Not applicable	Not applicable
513036 E, 4639542 N					
O Rosal T1 (3-10 m)	No outcrops or exposures present.	Unknown	Unknown	Unknown	Unknown
O Rosal T2 (11-21 m)	A 4-m outcrop behind the LIDL shows fluvial gravels.	Rounded to well-rounded quartz and quartzite gravels with a mean diameter of	No internal bedding	Upper metre clasts have well-developed iron-oxidation rinds and brown, orange	Clasts too small and too rounded to be useful
513411 E, 4640707 N					

	Base terraces not visible.	3.6 cm. Matrix terrace is white to yellow kaolinite clay with fine sand. In upper metre of profile the clasts are larger (4-6 cm) and appear more intact.		or yellow-red cores. Difficult to break. Lower 2 m of profile contain extremely weathered completely white quartz and quartzite gravels. Can be crushed by hand.	for palaeocurrent analyses. Clay or sand wedges not present.
O Rosal T3 (24-34 m) 513178 E, 4641262 N	Roadcut (± 100 m long and 10 m high) where new highway is constructed; 8.5 m of quartz/quartzite gravel. Base on top of kaolinte clays.	Quartz and quartzite gravels with a mean diameter of 4-6 cm in a grey to white coarse-sandy matrix. Exposure gives a 'washed' impression; no iron oxidation in matrix.	Massive kaolinite banks in some parts of the exposure.	Quartzite gravels are all completely white or white-brown. No traces of iron oxidation. Easy to break with hammer, but not fragile.	Not present
O Rosal T4 (36-41 m) 512905 E, 4642945 N	Gravel depth is 6-7 m. Terrace base is underlain by weathered granite.	Rounded to well-rounded quartz and quartzite gravels in a yellow-red clayey and fine sandy matrix. Mean clast size 4-6 cm. Iron oxidation evenly throughout outcrop.	No internal bedding	Quartzites have a thin outer rind of iron-oxidation and a whitish-brown, light brown or white inner core. Lower part of profile only white or whitish-brown clasts. Clasts difficult to remove from outcrop without breaking them.	Palaeocurrent direction could not reliably be established, but imbrication suggests a general direction of SSW to SSE.
O Rosal T5 (50-55 m) 513692 E, 4643220 N	A construction site shows at least 8 m of gravel. Base not visible.	Massive quartz and quartzite deposit in a yellowish-reddish clay matrix. Iron banks present. Terrace is almost a conglomerate.	No internal bedding	Completely white quartzites; extremely difficult to remove from outcrop; pulverised when broken by hand.	Palaeocurrent on basis of clast imbrication cannot be reliably established. Apparently many directions.

The FLUVER2 model also needs sea level input to be able to induce base level changes. To this end, the modelled sea level time series from Bintanja et al. (2005) was used. The data is available in regular timesteps of 0.1 ka, making it very suitable for the modelling exercise. The data were transformed to timesteps of 20 years by means of linear interpolation between data points.

4.3.3.2 Palaeo-discharge

The reconstructed palaeodischarge model used in this modelling exercise is based on the approach developed by Stemerdink et al. (2010). This method is based on the assumption that sea surface temperature (SST) is a proxy for precipitation. The latter is important for transpiration estimates. Based on three marine pollen records from the NW Iberian margin, changes in terrestrial vegetation have been shown to be synchronous with variations in oceanic conditions and especially with SST in that region (deep sea cores MD99-2331, MD04-2747, MD03-2797; see Desprat et al., 2005, 2006, 2007, 2009, Desprat, unpublished data; Sanchez-Goñi et al., 2005, 2008; Naughton et al., 2009). Palaeoprecipitation reconstructions based on these three pollen records show a similarity in amplitude and timing of precipitation patterns when compared to SST records from the same sequence (Fig. 4.2A; Desprat, 2005; Desprat et al., 2005; Desprat, unpublished data; Sanchez-Goñi et al., 2005; Sepulchre et al., 2007).

The SST record from the NW Iberian margin is a composite record based on the three above-mentioned deep sea cores retrieved at the same coordinates. The SST are derived from the relative abundances of planktonic foraminifera species using the modern analogue technique (details of the procedure in Matsuzaki et al., 2011). Chronology is based on radiocarbon dating for the interval 0-26 ka (Naughton et al., 2007a) and on graphical correlation of botanical events detected in the pollen records from the NW and SW Iberian margin cores, MD99-2331 and MD95-2042, for the interval MIS 26-135 ka (Sanchez-Goñi et al., 2008). For the interval 135-425 ka, the planktonic $\delta^{18}O$ curves of the MD01-2447 and MD03-2697 cores and that of the SW Iberian margin core MD01-2443 (Tzedakis et al., 2004; Martrat et al., 2007) were correlated to establish the age model.

Palaeoprecipitation estimates inferred from pollen are not continuous, whereas the SST data are. For the timespans where palaeoprecipitation data are available, they show a good correlation. Therefore, the SST is used as a basis to further develop the palaeodischarge model. Fig. 4.2A shows that a good agreement exists between the SST scaled by a factor [100 + (800/15)] and the palaeoprecipitation. The SST data set covers the last 425 ka. Because the model needs over 100 ka to initialise and spin up, we extended the series with SST data from the SW Iberian Atlantic margin (the SST records from SW Iberia are

derived from alkenones from core MD03-2699; Rodrigues et al., 2011).

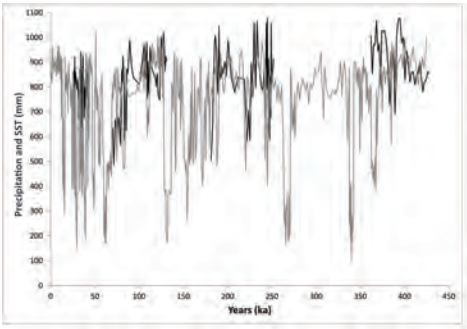

(A) Precipitation and SST compared

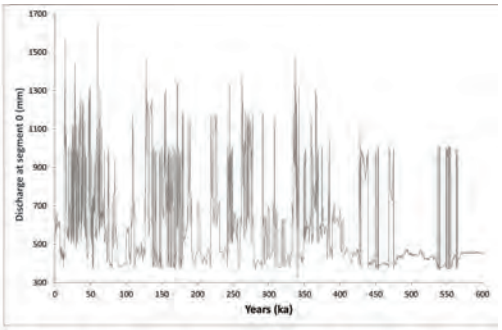

(B) Palaeodischarge through time

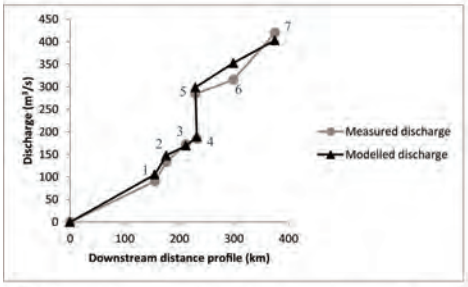

(C) Measured and modelled discharge compared

Fig. 4.2. Palaeodischarge reconstruction for the Miño–Sil catchment. A) The SST for NW Iberian Atlantic Ocean compared against reconstructed precipitation, based on marine pollen records for the Miño–Sil catchment. B) Reconstructed palaeodischarge for the past 600 ka at segment 0 along the longitudinal profile of the Miño–Sil system. The curve is based on the combined scaled SST records for the NW and SW Iberian margin, vegetation filters and seasonal factors (Stemerdink et al., 2010), and a glacial meltwater pulse. The palaeodischarge has not yet been converted to catchment-wide discharge. C) Modelled catchment-wide discharge at time-step 0 (contemporary value), compared against measured weir data from several water reservoirs and dams along the Miño–Sil River system (Rio-Barja and Rodriguez-Lestegas, 1992). Numbers refer to the following reservoirs and dams: 1. San Martiño; 2. Seguieros; 3. San Estevo; 4. San Pedro; 5. Miño–Sil confluence at Os Peares; 6. Frieira; 7. confluence Miño and Atlantic Ocean.

This effectively lengthens the simulation timespan to 600 ka. Because the amplitude of the SW Iberian SST curve is much less pronounced than the one for NW Iberia, probably due to the latitudinal difference of the site locations or to different proxies used to reconstruct SST, the palaeodischarge reconstruction based on the SW Iberian SST can at best be considered as approximate. Therefore, only the modelling results for the past ± 450 ka will be discussed.

The palaeoprecipitation estimates have to be corrected for vegetation and climatic conditions before they can be converted to runoff estimates. The corrections are carried out using multiplication factors and are discussed below.

Part of the precipitation is converted into evapotranspiration by vegetation that considerably lessens discharge, depending on vegetation type. In the Miño–Sil catchment, three principal vegetation groups can be distinguished: (i) Atlantic forest during warm, humid interglacial and sometimes interstadial conditions; (ii) heath vegetation during humid but cooler conditions and (iii) dry-grassland during the coldest and driest conditions (Desprat et al., 2005, 2006, 2009; Sanchez-Goñi et al., 2005, 2008; Naughton et al., 2007a). Based on the pollen and SST records from the NW Iberian margin, we have made the following inferences: Atlantic forest when SST is > 12°C, heath when it is 6–12°C; and grassland when it is < 6°C. Following the approach by Stemerdink et al. (2010), the following factors were applied to account for the loss of precipitation by transpiration: Atlantic forest = 0.5; heath = 0.68; and grassland = 0.8 (Soegaard et al., 2001; Ladekarl et al., 2005). This means that, for instance for the Atlantic forest, 50% of total precipitation ends up as discharge.

Stemerdink et al. (2010) discussed the influence of seasonality on river runoff. Under glacial conditions, for instance, snow melt during summer causes all the discharge to concentrate in just 3 months; whereas under a more temperate climate, discharge is more or less continuous the whole year round. This effect will be neglected in the FLUVER2 modelling of the Miño because the model works with timesteps of 20 years, thus effectively smoothing out seasonal effects. However, these seasonal effects may have a profound influence on the erosion and transport capacity of a river because of the increase in stream power (Kettner and Syvitski, 2008, 2009). Therefore, we apply a multiplication correction factor of 1 for interglacial climates (SST < 12°C); a factor of 2 for intermediate climate conditions (SST 6–12°C), and a factor of 4 for full glacial conditions (SST < 6°C).

Part of the upper Sil catchment has been glaciated during the coldest phases of the glacials (Fernandez-Mosquera et al., 2000; Rodriguez-Rodriguez et al., 2011). Glaciations occurred only at altitudes above roughly 1000 m, which comprises 22% of the entire Miño–Sil catchment area. The glaciers did not form a continuous ice cap, neither in space nor time, and reached a mean thickness of around 300 m (Vieira, 2008; Cowton et al., 2009; Rodriguez-Rodriguez, 2011). The north Iberian glaciers were very sensitive to minor climatic changes and have been shown to have responded rapidly in terms of advancing and retreating (Jalut et al., 2010; Moreno et al., 2010, 2012; Delmas et al., 2011). However, the exact timing and extent of glaciation and deglaciation events remain poorly constrained, and knowledge of glacial dynamics extending beyond the last glacial is scarce (Fernandez-Mosquera et al., 2000). Therefore the assumption was made that a glacial

meltwater pulse occurs after the SST temperature was below 6°C for at least 5 ka and the SST temperature subsequently rises above 6°C. Assuming a melting rate of 300 mm y^{-1} (Ohmura, 2011), the 300m-thick Iberian ice caps produce an extra pulse of meltwater during a period of 1 ka.

In order to convert the palaeoprecipitation and meltwater pulse to catchment-wide discharge, a flow accumulation model was created based on the 90m SRTM DEM (NASA, 2000). The downstream increase in catchment size was calculated for various steps along the Miño–Sil channel, taking into account the attributions of the 10 largest tributaries (see also Fig. 1.1). To prevent model instability, the discharge from individual tributaries was added evenly through the Miño–Sil channel between tributary confluences.

The palaeodischarge time model and the catchment model were then combined, yielding discharge rates in $m^3 y^{-1}$ per segment along the longitudinal profile. The resulting palaeodischarge curve, which includes all the factors described in this paragraph, can be found in Fig. 4.2B. The reconstructed palaeodischarge values at timestep 0 (present) compare well to measured discharge rates for the past half century at various points along the Miño–Sil (see Fig. 4.2C; Rio-Barja and Rodriguez-Lestegas, 1992).

4.3.3.3 Sensitivity analysis on discharge

To check the sensitivity of FLUVER2 to the reconstructed palaeodischarge module, a sensitivity analysis was performed consisting of two main experiments: (i) to check the sensitivity to changes in the amount of discharge. Therefore the reconstructed palaeodischarge was increased with factors of 1.10 and 1.50; and the discharge was decreased with factors of 0.90 and 0.50; and (ii) to check the sensitivity to changes in timing of the mean discharge peaks. A model was reconstructed whereby the main discharge peaks occur during the interglacial periods, which is different from the palaeodischarge model where low discharges occur during the interglacials. As input, the $\delta^{18}O$ benthic stack of Lisiecki and Raymo (2005) was used. The data were first normalised and then inverted to obtain high $\delta^{18}O$ values during interglacials and low values during glacials. The curve was then linked to the hydrological catchment model as used for the main palaeodischarge model to obtain real-world discharges.

4.3.3.4 Tectonic uplift

Few estimations for uplift rates are currently available. Cabral (1995) proposed, based on undated geomorphological markers, Plio-Pleistocene uplift ranging from 0.033 to 0.05 m ka^{-1} for the studied area. Late Cenozoic uplift rates of 0.08 m ka^{-1} for the Cordillera Cantabrica were proposed recently by Martin-Gonzalez et al. (2011). Recently, a maximum tectonic uplift rate of 0.07-0.09 m ka^{-1} was proposed by Viveen et al. (2012b, see Chapter 3) and uplift rates of 0.07-0.15 m ka^{-1} for the northern Iberian coast by Alvarez-Morran et al. (2008). For this reason a range of eight different tectonic uplift rates ranging from 0.04 to 0.14 m ka^{-1} were investigated. Uplift for the first 190 km of the longitudinal profile was kept constant at 0.08 m ka^{-1} because of the uplift estimations in this area by Martin-Gonzalez et al. (2011).

4.4 Results

4.4.1 Terrace inventory

The locations of the selected areas are shown in Figs. 4.1 and 4.3. Table 4.2 gives a summary of sedimentological and weathering characteristics of the terraces. The Chan de Vide transect is the most upstream area studied. Here, the Miño flows through a deeply incised granite bedrock gorge, and the current river bed contains a mixture of coarse sand and gravel. Nowadays, the Miño River level is much lower than it used to be because of the construction of several hydroelectric dams upstream. In total seven terrace levels are present between 30 and 90 m asl (Figs. 4.3, 4.4, and 4.5A), with vertical terrace level spacing ~ 10 m. In general the outcrops show that the amount or depth of gravels varies widely. The highest terrace at 90 m is visible as a flat surface in the landscape with a distinct terrace scarp, but fluvial sediments are no longer present. The 81-m terrace contains at least 1 m of sediment and is also very degraded and found as an isolated hill on which the village of Chan de Vide is built. A small gravel pit in the 71-73 m level shows 10 m of quartz and quartzite gravel on top of weathered bedrock.

The terraces at 60-64, 50-53, and 40 m contain 2.5 to 3.0 m of gravel above weathered bedrock, but in some outcrops just downstream of Chan de Vide the 40-m level has up to 8 m of gravel. All the gravels are made up of quartz and quartzite pebbles, but rounding is less than for the pebbles in the downstream transects. The pebbles in the oldest terraces, at 60-64 and 71-73 m, show the most advanced signs of in situ weathering (weathering rinds, iron-leaching, easy to break), whereas the lower terrace gravels show hardly any sign of in situ weathering. The lowest terrace level, situated at 27 to 28 m, does not contain gravel. Instead, it is an unweathered bedrock surface with a fine, organic-rich sand deposit on top with a minimum thickness of 1 m.

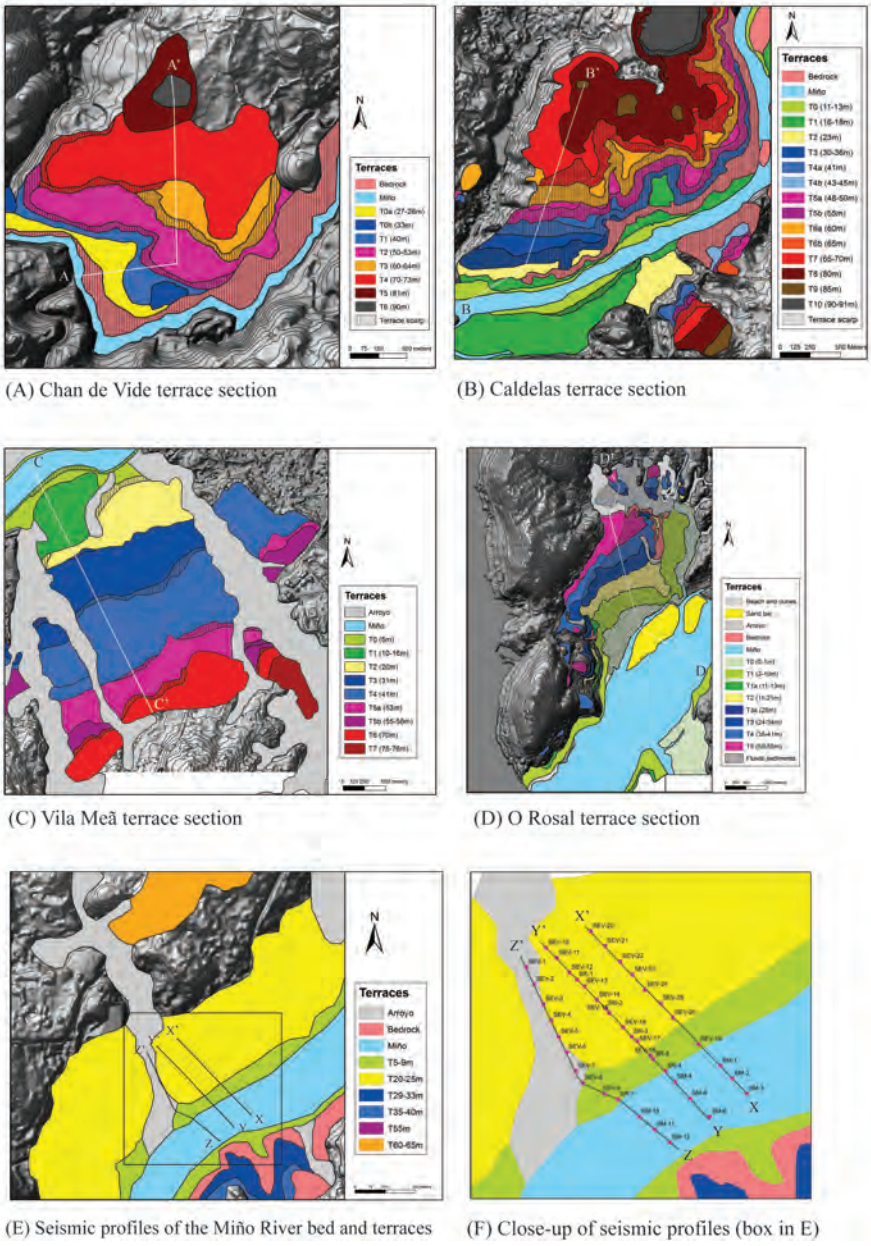

(A) Chan de Vide terrace section

(B) Caldelas terrace section

(C) Vila Meã terrace section

(D) O Rosal terrace section

(E) Seismic profiles of the Miño River bed and terraces

(F) Close-up of seismic profiles (box in E)

Fig. 4.3. Detailed mapping of terrace surfaces at four selected sites, based on extensive fieldwork and DEM interpretation. A) Chan de Vide site; B) Caldelas site; C) Vila Meã site (Viveen et al., 2012b); D) O Rosal site; E) location of seismic profiles and boreholes (MOPU-CEAT, 1982); F) detail of the three seismic and borehole profiles. Original numbering by MOPU-CEAT (1982) maintained. For coding details see Fig. 4.9.

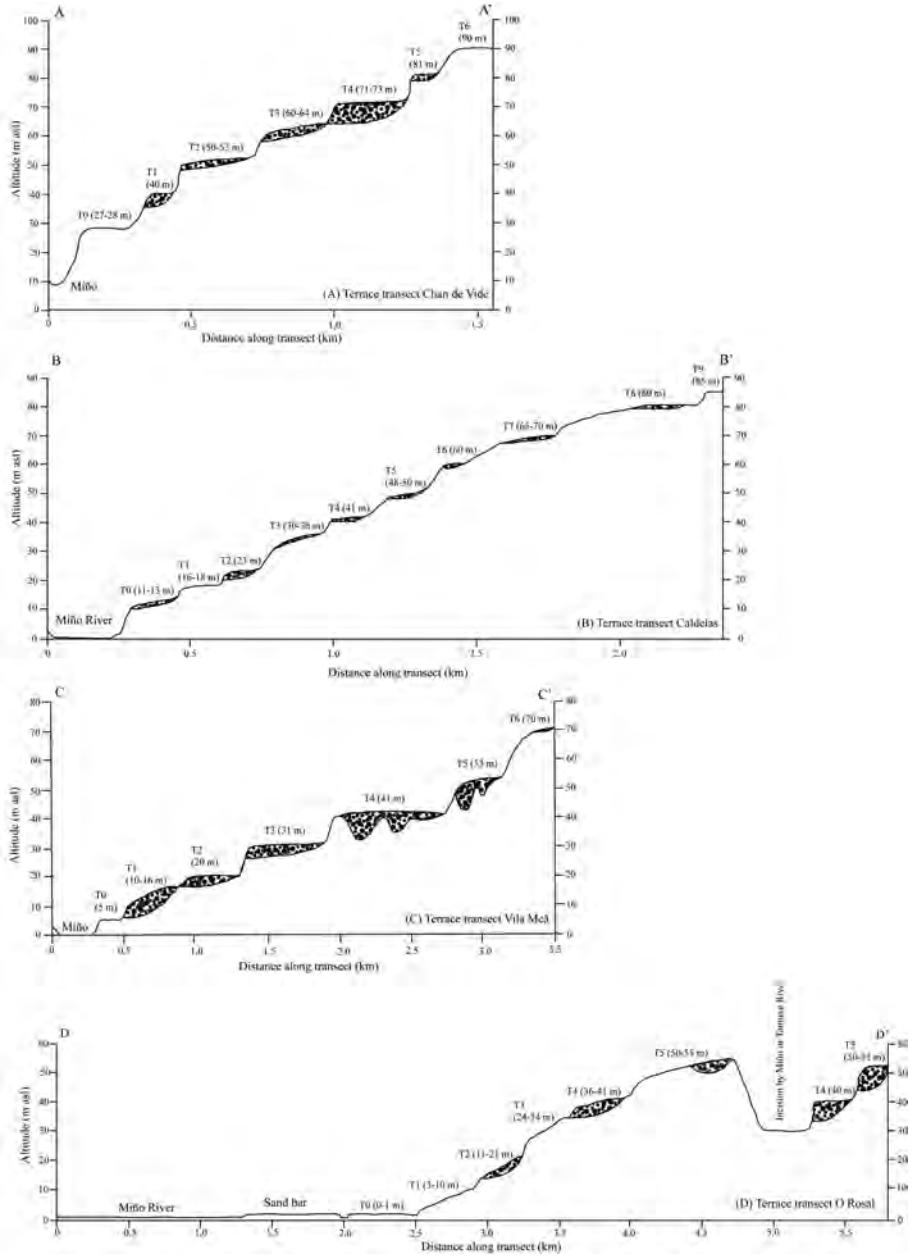

Fig. 4.4. Selected terrace transects in the lower Miño region. Terrace mapping based on fieldwork and DEM interpretation. All mapped terrace gravel depths are based on field observations, unless otherwise stated in the text. The locations of the four profiles are shown in Figs. 4.1 and 4.2A-D.

Fig. 4.5. A) unweathered quartzite gravels and sand on the current Miño floodplain. B) strath terrace close to Caldelas. Terrace deposit measures 0.7 m from top to base. C) outcrop in the O Rosal 50-55 m terrace. D) outcrop in the O Rosal 11-21 m terrace. Quartzite clasts are completely weathered and partly integrated into the terrace matrix. E) intermediate weathering of quartzite clasts (0 cm level in the O Rosal 11-21 m level). The most important process is iron oxidation, causing a yellow-brown core colour and brown-red Fe oxidation rinds. F) advanced weathering of quartzite clasts (O Rosal 50-55 m level). Quartzites are completely leached of Fe, causing the white colour, and silica leaching causes extreme friability, leading to disintegration of the clasts.

The Caldelas transect includes eight terraces up to 80 m asl and is located some 36 km upstream from the river mouth. Vertical terrace spacing is also around 10 m, and the terraces appear to be incised into the underlying bedrock. A large flat surface without sediments was found at 90-91 m. This may possibly be an eroded terrace level. In the vicinity of the transect a number of smaller terraces are found, which may be sublevels of other terraces; therefore a subdivision into 'a' and 'b' levels was made for the terraces around 60, 50, and 40 m. In terms of number of individual levels, the Caldelas terrace staircase contains the most complete record studied in this paper. A reason for the completeness may be that the Miño had to incise asymmetrically into a narrow bedrock canyon with limited accommodation space. The river repeatedly incised into the southern side of its valley floor and thus migrated progressively in that direction, causing incision phases to be recorded as incised benches in the underlying bedrock. Most terrace levels are represented by outcrops, which reveal only a thin gravel deposit of 1 m maximum thickness above weathered bedrock (Fig. 4.5B). The gravels are usually capped by a metre of colluvium.

The Vila Meã transect was extensively described in Viveen et al. (2012b, see Chapter 3). The transect contains seven terraces up to 70 m asl. The terraces were dated using a combination of ^{10}Be cosmogenic ray exposure (CRE) and luminescence techniques and revealed minimum ages of up to 650 ka for the 53-m terrace. For an overview of the age estimations, see Tables 3.5 and 3.6 of Viveen et al. (2012b, see Chapter 3).
In addition, a level at 64 m was described, located some 3 km farther upstream. It appears to be the missing terrace level between the 53- and 70-m terraces as suggested by Viveen et al. (2012b, see Chapter 3). Some 3 m of quartz and quartzite gravels is present in a yellowish-reddish clay matrix. The base of the terrace deposit is not visible. The quartzite clasts are rounded to well-rounded, very friable and have a brown to white colour.

The O Rosal transect consists of 5 to 6 terraces up to 55 m asl, again with vertical spacing of around 10 m. The individual terrace scarps are difficult to distinguish because an up to 2-m-thick layer of colluvium covers the entire section, which is bisected by a widely incised valley floor. It is not clear whether this incision was by the Tamuxe River or by the Miño, but the terrace gravels all contain quartz and quartzite clasts, indicating that they originate from the Miño. In this northern section, a staircase with three terraces at 50-55, 36-41, and 24-34 m asl is present. An outcrop in the 50-55 m level reveals a minimum 8 m of gravel (Fig. 6C), and a collection of outcrops in the 36-41 m level indicates 6-7 m of gravel. In the latter case, the base of the gravel deposit is underlain by weathered granite. Both terraces consist of rounded to well-rounded quartz and quartzite pebbles with a mean diameter of around 4 cm. The pebbles in the 50-55 m terrace are completely white and can be crushed by hand; the quartzite pebbles of the 36-41 m terrace have predominantly light brown to white colours.

In the southern section, an outcrop in the 24-34 m terrace shows 8.5 m of gravel on top of white kaolinite clay. The gravels are made of well-rounded quartz and quartzites in a matrix of white kaolinite clay and coarse sand. The gravels themselves are completely white, but not friable. Closer investigation of the kaolinite revealed remnants of angular quartz and, in some cases, traces of gneissic banding are visible. This indicates that the kaolinite is the in situ weathering product of the gneissic bedrock.
Another outcrop in the 11-21 m terrace shows at least 4 m of rounded to well-rounded fluvial gravel in a clast-supported matrix (Fig. 4.5D). The upper metre is made up of slightly larger clasts (4-6 cm) that have a brownish aspect with well-developed, brown-red weathering rinds (Fig. 4.5E). The pebbles in the lower part of the profile are smaller than in the upper part (mean clast diameter 3.6 cm), completely weathered, white, and can be crushed between thumb and index finger. Extracting the pebbles from the matrix without breaking them proved to be very difficult.

4.4.2 Bulk densities of terrace quartzite pebbles

The calculated densities of the quartzite pebbles vary from 2.42 g cm^{-3} for the unweathered, current Miño River bed to 2.04 g cm^{-3} for the extremely weathered O Rosal 51-m terrace. Per terrace level, between 40 and 116 pebbles were measured with a mean count of 91 pebbles per terrace level. A total of 1553 pebbles were measured. Standard deviations range from 0.07 to 0.14 with a mean deviation of 0.11 (Table 4.3), which implies that the correlation between the four transects is an approximation. Each individual transect (Chan de Vide, Monção, Vila Meã, and O Rosal) show a decrease in density with increasing terrace altitude, confirming that progressive weathering causes a loss in mass of the quartzite pebbles (Fig. 4.6). This loss in mass is in agreement with the various field observations. The changes in density in general agree with the changes observed in friability of the pebbles as well as colour changes (Tables 4.2 and 4.3; Figs. 4.5E, F). Assuming that the gravel deposits with a similar bulk density have a similar weathering age, allows a correlation of the different deposits between the four transects. It becomes apparent in Fig.4.7 that the traditional reconstruction of terraces parallel to the current riverbed does not hold up. We observe that the closer a terrace transect is to the ocean, the lower the position in the landscape of the individual terraces and the lower the density (Fig. 4.7). At the Chan de Vide transect for instance, the 60-m terrace has a pebble density of 2.25 g cm^{-3}, whereas at Monção the 49- and 42-m terraces have a comparable pebble density of 2.24 to 2.23 g cm^{-3}. The Vila Meã 31-m terrace has a similar pebble

Table 4.3. Statistical information for the quartzite density measurements of the lower Miño terraces; n means number of measured samples per terrace level, and σ^2 is the standard deviation of the mean density value.

Transect	Terrace	Coordinates (UTM N29, ED50)	Sampled depth	n	Density (g cm^{-3})	σ^2
CDV	13 m (floodplain)	550551 E, 4658563 N	0	40	2.42	0.07
CDV	35 m	547157 E, 4658686 N	3	87	2.42	0.09
CDV	50 m	550861 E, 4658932 N	2.5	73	2.38	0.11
CDV	60 m	550901 E, 4659197 N	2.5	107	2.25	0.13
CDV	71 m	550732 E, 4659520 N	3	92	2.22	0.13
Monção	42 m	541193 E, 4658599 N	3	101	2.24	0.12
Monção	49 m	542122 E, 4658411 N	3	84	2.23	0.11
Monção	63 m	544315 E, 4658378 N	2.5	82	2.18	0.14
Monção	80 m	544371 E, 4657852 N	3	91	2.18	0.12
Vila Meã	13 m	526500 E, 4649280 N	3	96	2.33	0.11
Vila Meã	31 m	526030 E, 4647014 N	3	89	2.26	0.12
Vila Meã	41 m	526303 E, 4646580 N	3	105	2.23	0.12
Vila Meã	53 m	528643 E, 4647919 N	3	107	2.13	0.11
Vila Meã	64 m	531227 E, 4649965 N	3	102	2.09	0.11
O Rosal	33 m	513178 E, 4641262 N	3	116	2.19	0.13
O Rosal	40 m	512905 E, 4642945 N	3	110	2.18	0.11
O Rosal	50 m	513692 E, 4643220 N	3	71	2.04	0.11

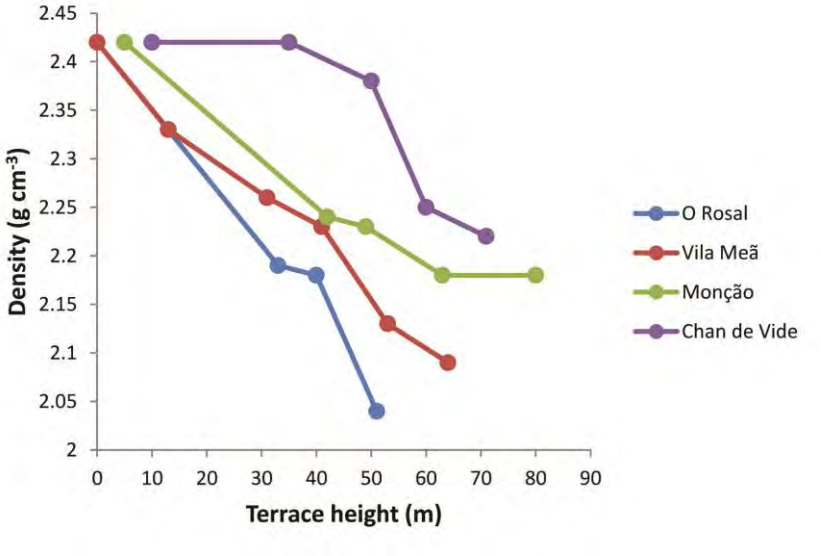

Fig. 4.6. Quartzite pebble densities versus terrace altitude for four terrace transects at Chan de Vide, Monção, Vila Meã, and O Rosal. For each transect, the value of 2.42 g cm-3 for unweathered quartzite was added, although this value was only measured at the Chan de Vide site.

density of 2.26 g cm^{-3}, and at O Rosal not a single terrace has a pebble density above 2.19 g cm^{-3}. This trend continues for the next higher terraces that have quartzite pebble densities around 2.22 to 2.23 g cm^{-3} (CDV 71-m terrace, Monção 49-m terrace, Vila Meã 41-m terrace and O Rosal 33-m terrace) and the terraces with pebble densities of around 2.18 g cm^{-3}. Lines connecting terraces with similar pebble densities indicate that long-distance terrace correlation is not parallel to the current Miño floodplain. Rather, a gradient of ~ 1 m km^{-1} for the terraces between Chan de Vide and O Rosal (Fig. 4.7) represents the best fit. The proposed terrace correlation gradient is quite coherent with the distribution pattern of fluvial terraces in the region. The height and occurrence of the oldest terraces in the lower Miño fit exactly with projections based on a downstream gradient of 1 m km^{-1} (Figs. 4.1 and 4.7). Notably at the Chan de Vide site only terraces up to 90 m asl were found; but the higher terraces are probably eroded, as 2 km upstream of Chan de Vide terraces have been observed up to 105 m asl (Fig. 4.1).

Based on the new terrace correlation scheme and the new terrace inventory, the number of terraces in the lower Miño can also be established. We propose that 9 or 10 terrace levels exist (Fig. 9, T0 to T9; there is doubt about the mapped level T8 because it is a discontinuous surface), and one Holocene floodplain level. The terrace levels correspond well with the terrace sequence derived from a composition of mapped terraces by other workers (Table 4.1).

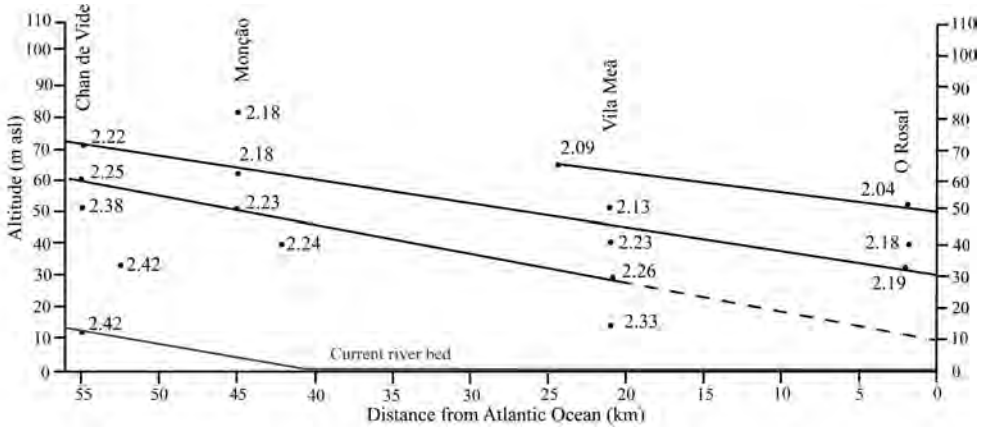

Fig. 4.7. Quartzite pebble densities (numbers next to dots) projected against a terrace altitude – downstream distance plot. The diagonal lines indicate the most likely long-distance terrace correlation based on the densities. The dashed line is added to facilitate comparison of the gradient of the lower terraces with the higher ones.

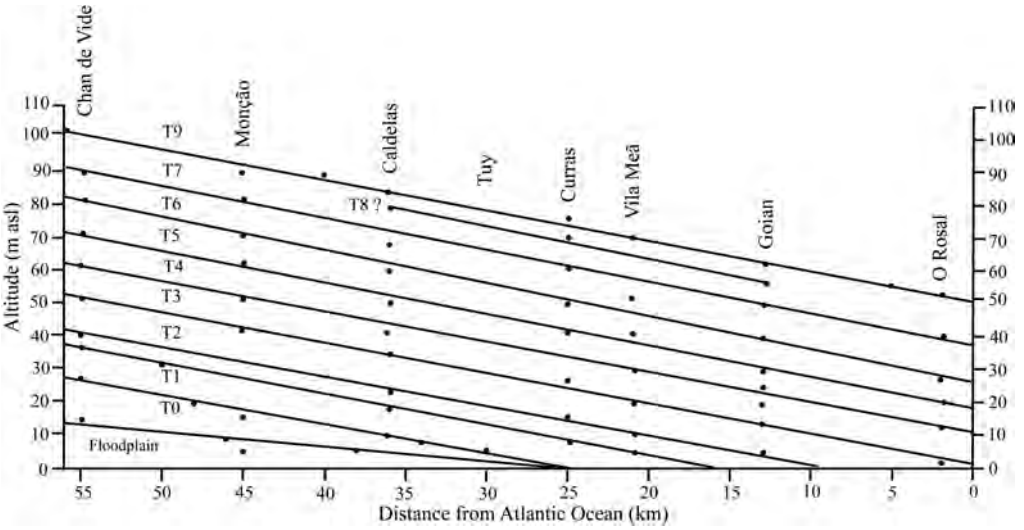

Fig. 4.8. Long-distance terrace correlation of the lower Miño terraces in the area between Chan de Vide (55 km upstream) and the Atlantic Ocean (0 km upstream). Terrace correlations are based on continuous mapping of fluvial terraces along the lower Miño River by means of DEM-interpretation (5-m grid), quartzite weathering characteristics and terrace distribution. For simplicity, only a selection of terrace transects is shown here. The Goian, Curras, and Monção terrace sequences are shown by Viveen et al. (2012a); the other transects are described in Figs. 4.2 and 4.3 and Table 4. 3.

4.4.3 Modelling results

4.4.3.1 Simulated terrace levels

The modelled outcomes show that, independent of any tectonic uplift scenario, six terraces are simulated between 0 and ± 450 ka (Fig. 4.9). For three locations along the fluvial profile (Chan de Vide, Caldelas, and Vila Meã), an uplift rate of 0.08 m ka^{-1} reproduces terrace levels at similar heights as found in the field (Figs. 4.3, 4.4, and 4.9). The O Rosal terraces cannot be used for validation purposes because the modelling results indicate that, for uplift scenarios with a rate equal to or lower than 0.08 m ka^{-1}, the terraces for the last 450 ka are located below the current river bed. Uplift rates higher than 0.08 m ka^{-1} seem unlikely because of the good fit of the other three terrace transects with lower uplift rates. The O Rosal terraces described in the previous section are therefore assumed to be older then terraces at similar heights in the other sections.

For an uplift rate of 0.08 m ka^{-1}, the timing of the formation of the Vila Meã terraces is in close agreement with the proposed ages by Viveen et al. (2012b, see Chapter 3). The other uplift rates simulate terrace surface heights that are either too high when

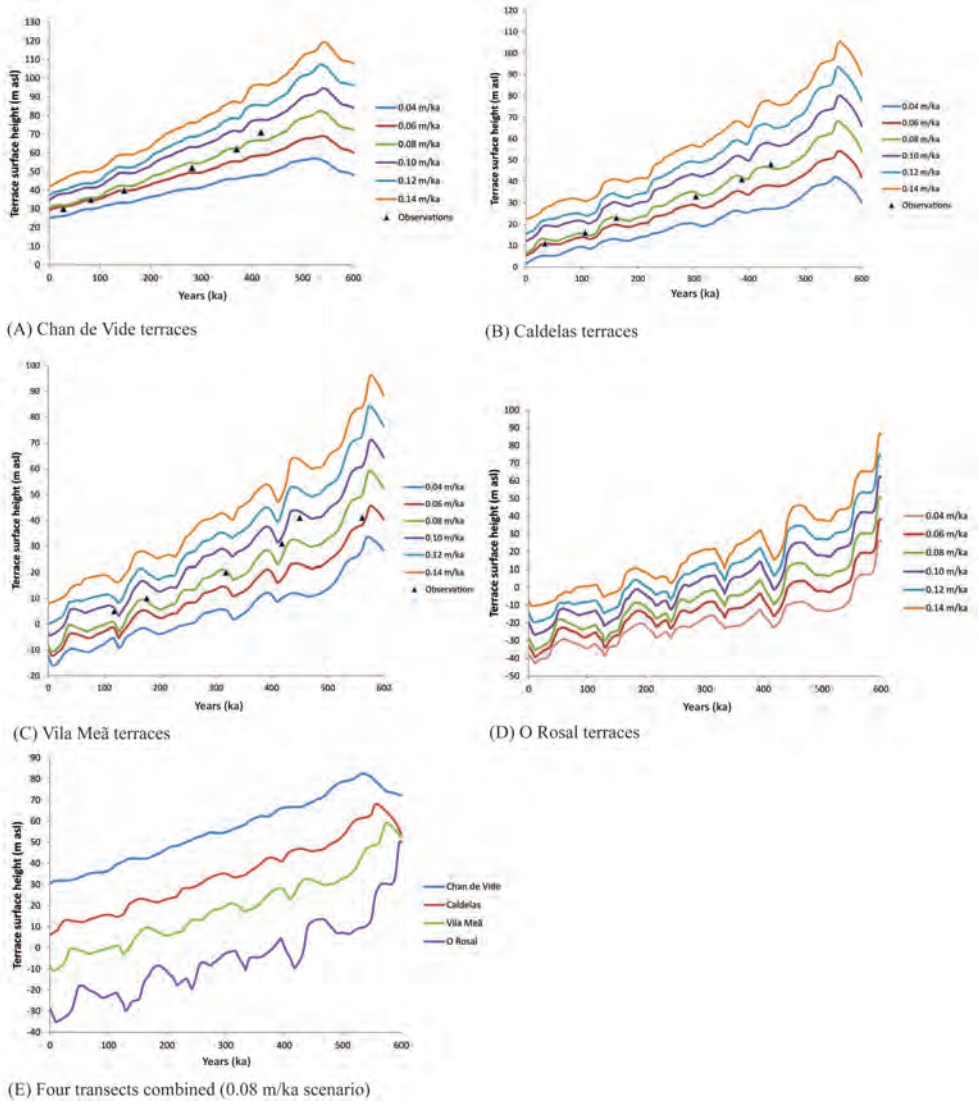

Fig. 4.9. A to D) results from modelled terrace surface heights at four locations compared to terrace surface heights evidenced in the field (Fig. 4.3). A total of six scenarios with different uplift rates ranging from 0.04 to 0.14 m ka^{-1} are shown. The simulated terrace surface heights with an induced vertical uplift rate of 0.08 m ka^{-1} compare very well to field observations (black triangles) for all four selected sites. E) superposition of the modelled Chan de Vide, Caldelas, Vila Meã, and O Rosal terrace profiles for the 0.08 m ka^{-1} uplift scenario. Terrace altitudes clearly decrease downstream along the river profile. A gradient of 55 m is calculated for the longitudinal profile section between Chan de Vide (55 km upstream) and O Rosal (2 km upstream), which translates to a downstream terrace gradient of 1 m km^{-1}.

compared to field evidence or too low. The 0.04 and 0.06 m ka^{-1} scenarios in addition yield terraces below the current river bed, which is not in agreement with available seismic sections and borehole data (Figs. 4.3E, 4.3F and 4.10).
At the Vila Meã site, FLUVER2 predicts terraces formed during the last glacial cycle (T0 and T1 terrace at 0 and 1 m, respectively). These terraces were not found in the field, but we propose that terrace gravels from the last glacial period could be present below the Holocene overbank deposits of the current river bed (Viveen et al., 2012b, see Chapter 3). The two simulated terraces experienced only a small incision event and most likely would occur in the field as one terrace.
The terrace levels at 9.5 m and between 14 and 20 m were found in the field, although the incision phase between two subsequent terrace levels was modelled at a slightly lower position of 9.5 m compared to field evidence (Fig. 4.4). For the terrace level at 41 m, two possible options are given because there is a 100 ka age difference between the two modelled ages for the rejuvenation and depth profile approaches (Viveen et al., 2012b, see Chapter 3). In this case, there is good agreement for the younger age option of around 450 ka, but the terrace altitude is simulated at too low an elevation. Possible causes are explained in the next section.

4.4.3.2. Terrace deposits
The thickness of terrace sediment also has to be taken into account (Fig. 4.11). A bedrock surface without sediments may be simulated at the correct position, but if field evidence indicates several metres of sediment above a bedrock surface at the same height, then we have to conclude that the position of the simulated bedrock surface is actually too high. The modelled deposits for the Chan de Vide and Caldelas sites agree well with field evidence, although the model slightly underestimates the sediment thickness for all tectonic uplift ranges at the Chan de Vide site. On the other hand, the given sediment volumes are maximum values as the measurements were made where the gravel beds cut deepest into the underlying saprolite. The 0.08 and 0.14 m ka^{-1} scenarios compare best to field evidence, and for the Caldelas site even slightly overestimate the sediment thickness observed in the field. The deposits for T5 at Chan de Vide are underestimated in all cases. It is very likely that the site we visited (a gravel quarry) is not representative of the overall amount of gravel of this terrace level. The thick stack of sediment could be the result of a local channel that incised in weak, fragmented bedrock, thus creating accommodation space for a thick gravel fill. The other Chan de Vide terraces can be seen to have significantly thinner sediment.

The sediment thicknesses at the Vila Meã site are also modelled in agreement with field observations for most uplift scenarios (Fig. 4.11). Because post-depositional erosion of

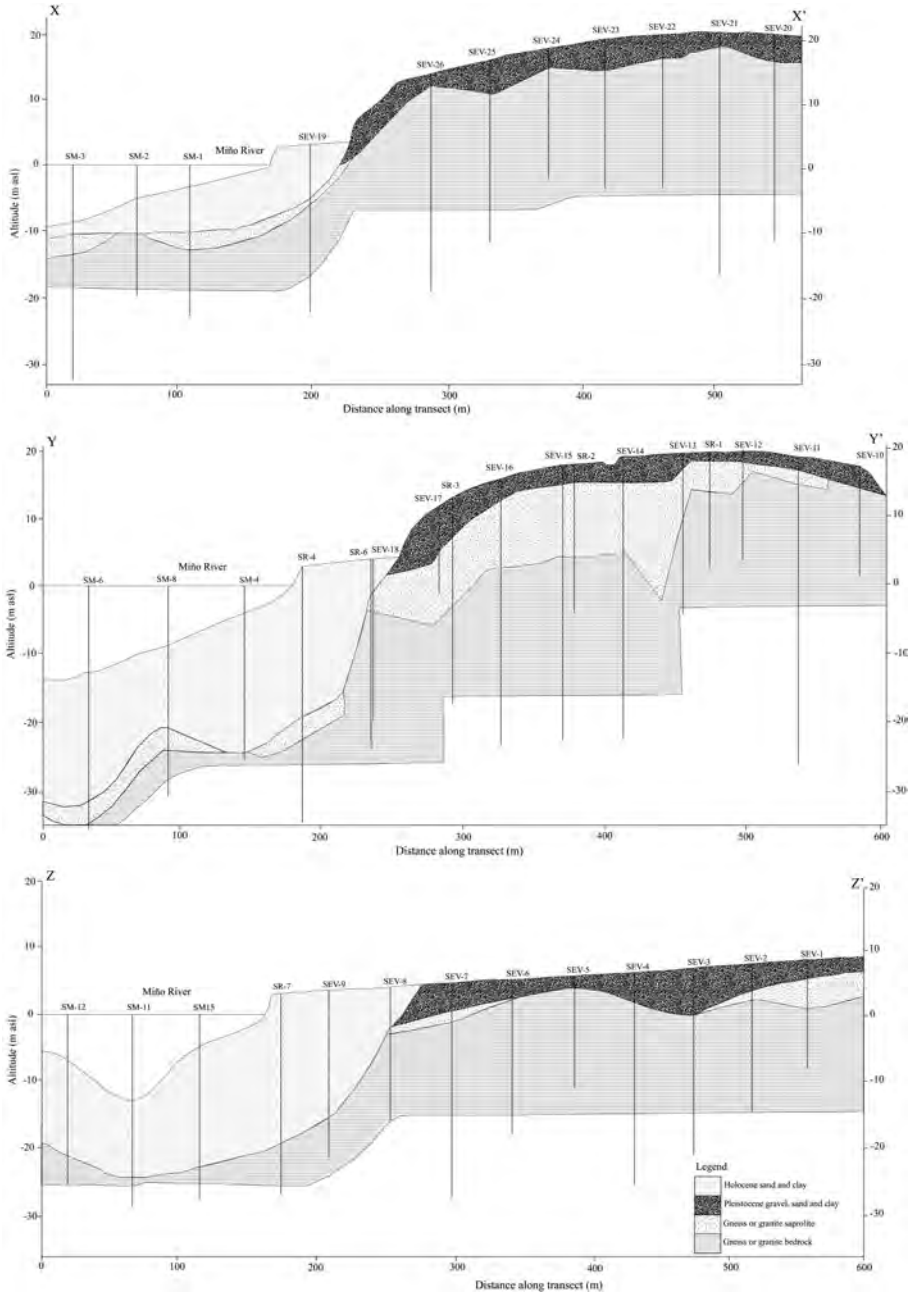

Fig. 4.10. Cross sections adapted from three seismic profiles (MOPU-CEAT, 1982; see Fig. 3EF). SEV = Sondeo Electrico Vertical terrestre; SR = Sondeo de Reconocimiento (borehole); SM = Sondeo Electrico Marino. The three profiles clearly show that the Miño River has incised deeply in the underlying saprolite and that the Miño channel is filled with ~ 20 m of Holocene sediments. The incision decreases considerably in profile X-X' and is expected to converge with the current river bed just east of the city of Tuy (Fig. 4.1).

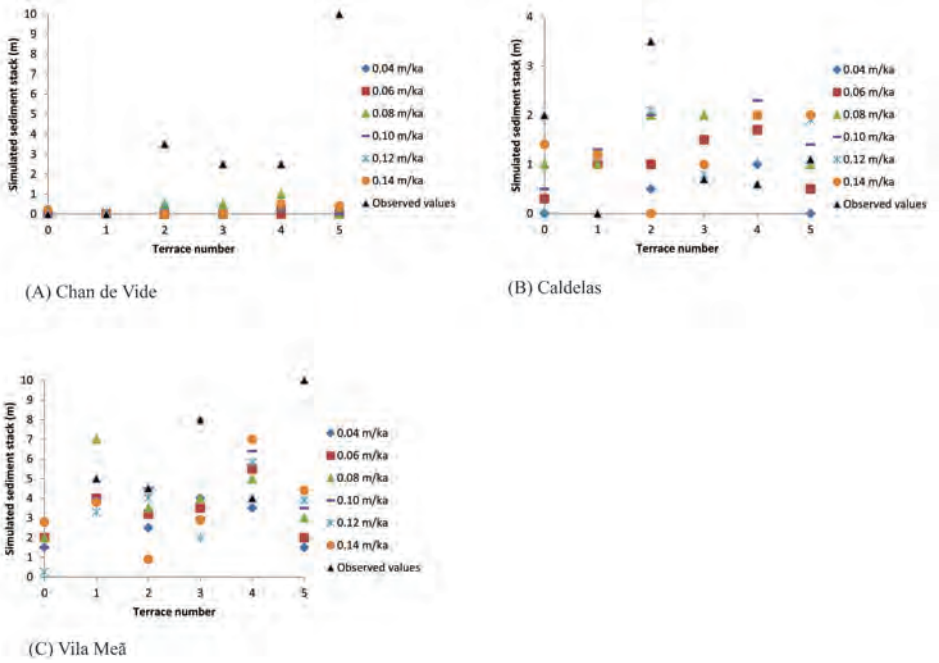

Fig. 4.11. Modelled sediment stack for the simulated terraces at Chan de Vide, Caldelas, and Vila Meã compared to measured gravel depths in the field. A comparison for the O Rosal site is not made because no data is available for sediment stacks of terraces below the current river level.

the terraces (Caldelas site excluded) may be neglected (Viveen et al., 2012b, see Chapter 3), themodelled volumes should be as close to the observed values as possible.
Sediment volume for the T5 terrace at Vila Meã is strongly underestimated however. A possible cause for the height disparity might be that we used the SW Atlantic SST curve for the period of 425-600 ka, which has a low temperature amplitude. The translation to a discharge curve leads to an underestimation of discharge and also sediment delivery. The amount of simulated sediment deposition for this terrace is only 3 m, whereas in the field 10 m was observed. The difference of 7 m precisely makes up for the simulated terrace height difference between 33 m and the observed terrace altitude of around 40 m.

4.4.3.3 Long-distance terrace correlations

The modelled profile strongly resembles the modern river profile up to the confluence with the Tea River (Fig. 4.12). For the lowermost part, the situation is different as strong

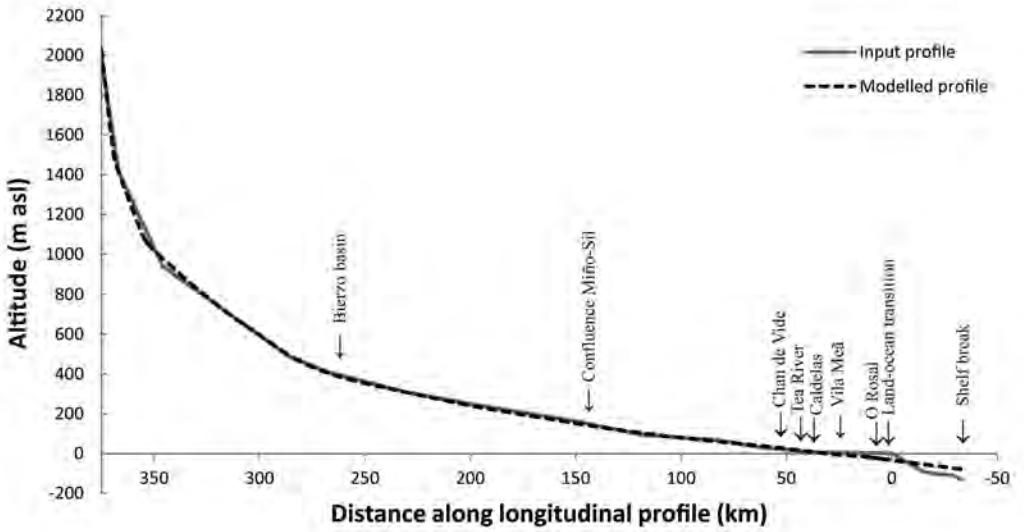

Fig. 4.12. Modelled profile (0.08 m ka-1 uplift scenario) for the past 450 ka compared against the actual profile (input profile) of the Miño Sil River system. The modelled profile closely resembles the actual profile for the first 340 km along the downstream length. At 340 km (at the Tea River confluence), the model predicts the beginning of incision by the Miño River. Close to the Tea River, the modelled profile slowly incises below the level of the current river bed. The shelf break coincides with the lowest glacial sea level low stand (e.g., the LGM low stand). Geographical locations (e.g., Bierzo basin and confluence Miño Sil are given to make locating the position along the profile easier (see Fig. 1.1).

incision occurs. Borehole data and seismic sections (Fig. 4.10) show deep incision of the current river channel just north of Vila Meã. The model reproduces this incision, confirming a steeper, glacial gradient. This incision also exerts an important effect on the distribution of fluvial terraces along the profile. Based on the gravel density correlations we observed that the terraces do not trend parallel to the current river bed. This steeper gradient is confirmed by all FLUVER2 simulations that demonstrate a graded profile with a gradient of 55 m between Chan de Vide and the O Rosal terraces (1 m km^{-1}; Fig. 4.9E).

4.4.3.4 Sensitivity analysis on discharge

Two plots of the erosion and sedimentation dynamics at the Vila Meã site are presented (Fig. 4.13). Increasing the discharge with a factor of 1.10 and 1.50 (Fig. 4.13A) does not significantly alter the erosion and sedimentation dynamics. The erosion and sedimentation peaks are slightly more pronounced, which would be expected because of an increase in discharge, but the main sedimentation events occur during the same time periods as the standard scenario of 100% discharge. There is however a slight difference in the timing of the major erosion phases, which still occur during the climate transitions. A similar trend is observed when discharge is decreased by a factor of 0.90. Reducing the discharge with a factor of 0.50 however, has large consequences. Aggradation hardly occurs and erosion

prevails, likely because the Miño has no longer sufficient capacity to transport sediments. This is, however, an extreme case and not representative for the real-world situation, as clear evidence of sedimentation events in the form of terraces exist. Changing the timing of the main discharge peaks (Fig. 4.13B) does not significantly alter the timing of erosion and sedimentation events when compared to the standard scenario of 100% discharge. There is a lag in some of the erosion peaks, but the sedimentation peaks occur at exactly the same moments as in the standard scenario. In both scenarios there is a small difference in the intensity of erosion and sedimentation events, but this is the result of the procedure that we adapted here. The sensitivity analysis is based on the same parameter set as for the standard scenario, which was optimised for that specific scenario. The differences in erosion and sedimentation intensity are therefore an artificial result of a non-optimal parameter combination.

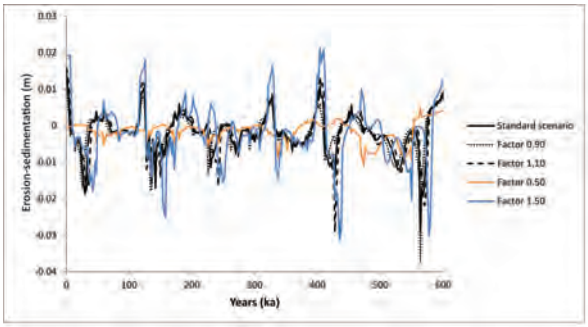

(A) Sensitivity analysis applying various discharge factors

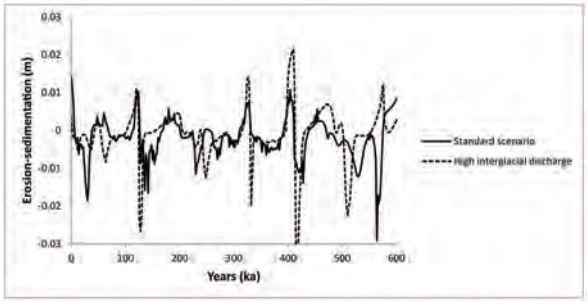

(B) Sensitivity analysis with changes in the timing of peak discharges

Fig. 4.13. Sensitivity plot of erosion (Y-axis, negative values) and sedimentation (Y-axis, positive values) events for the past 600 ka at the Vila Meã site. A) Sensitivity analysis whereby the palaeodischarge is increased and decreased with factors of 1.10, 1.50, 0.90 and 0.50. The standard scenario is the 100% discharge scenario, B) sensitivity analysis whereby high discharge peaks occur during interglacials and low peaks during glacials.

4.5 Discussion

4.5.1 Long-distance terrace correlations

Suggested correlation at a gradient of 1 m km^{-1} was obtained by comparing changes in the density of the systematically weathered quartzite pebbles in the various terrace levels. We demonstrated that in each terrace transect, quartzite pebbles decrease in density with increasing terrace altitude and that the density values can be used to correlate the terrace levels between the four studied transects. The FLUVER2 modelling results from all uplift scenarios indicate a similar gradient for the terrace treads in the studied area. Adapting the results from the 0.08 m ka^{-1} uplift scenario, a gradient of 1 m km^{-1} was modelled for the 55-km-long trajectory between O Rosal and Chan de Vide. The long-standing idea of terrace reconstruction parallel to the current Miño River bed can therefore be rejected (cf. Lautensach, 1945; Butzer, 1967; Nonn, 1967; Cano-Pan et al., 1999a). The 1 m km^{-1} gradient is slightly steeper than fluvial gradients elsewhere along the western Iberian Atlantic margin. An LGM gradient of 0.6 m ka^{-1} was recorded for the lower Tagus River (Vis et al., 2008), although the continental shelf width is of the same dimensions as in NW Iberia. This suggests that factors other than continental shelf dimensions may also be important. Mattheus and Rodriguez (2011) suggested that discharge is of importance to valley incision depth, but as the Miño and the Tagus have similar discharges at their mouths (Rio-Barja and Rodriguez-Lestegas, 1992; Benito et al., 2003), this cannot be an explanation. The explanation probably lies in the fact that the Miño catchment experiences much higher elevations close to the coast, whereas the lower Tagus is situated in a large, almost flat, estuary and overlies a basin fill of unconsolidated Tertiary sediments (Vis et al., 2008). For the lower Duero River basin, very little data are available. However, bathymetry data indicate that the surface of the LGM river bed is situated at a maximum depth of 50 m below sea level close to the river mouth (Carvalho and Rosa, 1988, in Naughton et al., 2007b), which is a similar value as the top of the simulated last glacial O Rosal terrace (± 35 m below sea level), which could indicate a comparable glacial river bed gradient. As both the northern and western Iberian margins have steep and short continental shelves and relatively high mountain ranges close to the coast, it is very likely that not only the aforementioned examples but most near-coastal river systems are strongly influenced by glacioeustatic sea level variations (e.g. Vis et al., 2008; Ramos et al., 2012) and that terraces may not have trends parallel to the current river bed. Care should therefore be taken in using terrace altitude as a criterion for long-distance terrace correlations.

4.5.2 Uplift rates in the lower Miño basin

The presented uplift scenarios show that the longitudinal profile can be modelled satisfactorily independently from uplift rate, so this cannot be used as a criterion to identify the best-fit uplift rate. In all cases, six terraces were modelled, which also agrees with field evidence if we assume that, for the Vila Meã site, the two small terraces that were formed during the last glacial appears as one terrace because of the small height differences between them. The timing of terrace formation at the Vila Meã site in combination with the simulated terrace heights for the 0.08 m ka^{-1} scenario agrees well with the ^{10}Be cosmogenic ray exposure (CRE) age estimations, but the timing of terrace formation for the 0.04 m ka^{-1} and 0.06 m ka^{-1} scenarios cannot be proven wrong because the CRE age estimations are minimum ages only. On the other hand, the uplift ranges between 0.10 and 0.14 m ka^{-1} can be proven wrong because the position of the simulated terrace surfaces is much too high when compared to the position of the dated terraces. The 0.08 m ka^{-1} uplift scenario also gives the best results when it comes to simulated terrace heights. Even more important is that lower uplift scenarios yield terraces at the Vila Meã site below the current river bed, which is not in agreement with the borehole and seismic profiles (Fig. 4.10). The results show that with decreasing uplift rate, as expected, the terrace staircase decreases in altitude as well. The amount of simulated terrace deposits is also best represented in the 0.08 m ka^{-1} uplift scenario, although the Vila Meã deposits are never simulated entirely correctly, as is also the case in the other uplift scenarios. However, an increase in simulated sediment volumes to match the volumes found in the field will lead to 3 to 4 m of sediment for some terraces (e.g., the T2 terrace at Vila Meã site), which will still lead to terrace surface heights as found in the field but is not enough to compensate for a lower uplift scenario (e.g., the 0.06 m ka^{-1} scenario). All in all, the 0.08 m ka^{-1} uplift scenario fits best to the observations made in the field and agrees well with the aforementioned proposed 0.07-0.09 m ka^{-1} uplift rate in the lower Miño region (Viveen et al., 2012b, see Chapter 3). Because the terrace staircase exhibits a regular pattern (Fig. 4.4) and the oldest terraces probably date back to the lower to middle Pleistocene transition, the mean uplift rate of 0.08 m ka^{-1} can be extended at least to the entire middle Pleistocene. Similar uplift rates were found in the westernmost termination of the Cordillera Cantabrica (0.08 m ka^{-1} for the Neogene; Martin-Gonzalez et al., 2011) and on the northern Spanish coast (0.07-0.15 m ka^{-1}; Alvarez-Morran et al., 2008). This suggests a similar tectonic mechanism controlling the deformation along the northern and northwestern Iberian plate edges, for instance lithospheric folding causing crustal shortening (Cloetingh et al., 2005; De Vicente and Vegas, 2009).

The good agreement between the modelled timing of terrace formation and the CRE ages suggests that the minimum CRE ages are actually close to the exact timing of terrace abandonment. This was already suggested by Viveen et al. (2012b, see Chapter 3) and appears to be confirmed by the FLUVER2 modelling outcomes.

4.5.3 Controls on terrace formation and valley incision

It has been shown that many river systems near passive continental margins react in a generalised way to glacioeustatic changes in sea level, and variations depend mainly on the angle and length of the continental slope versus the angle of the coastal plain, drainage area, and most importantly, whether sea level drops below the shelf break (Talling, 1998; Blum and Törnqvist, 2000; Törnqvist et al., 2006; Mattheus and Rodriguez, 2011). The lower Miño is not an exception in this sense, and we propose that it follows the pattern of incision and deposition predicted by Posamentier and Vail (1988). During sea level high stands, the Miño is aggrading and a coastal prism made up of fine-grained sediments is formed in the drowned glacial low stand valley (Fig. 4.14).

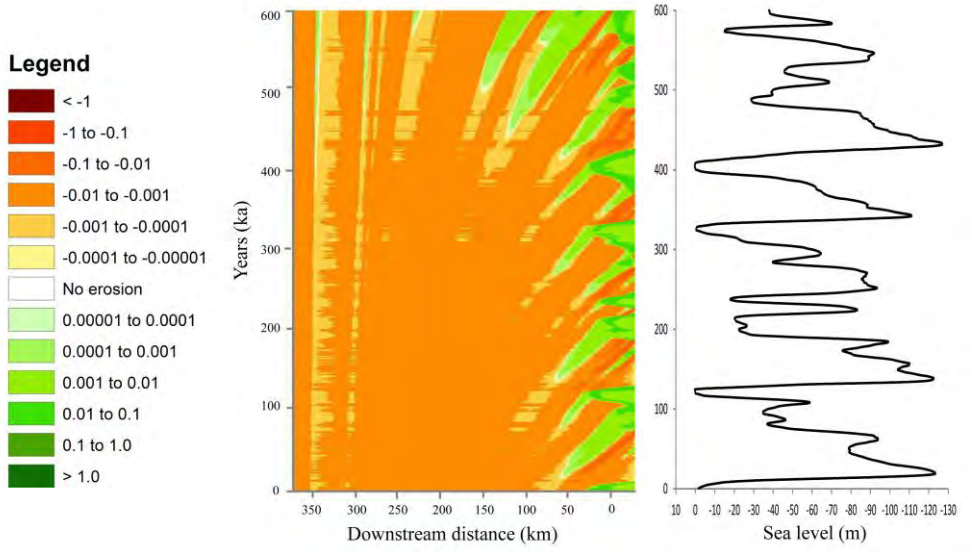

Fig. 4.14. Profile evolution map (PEM) showing erosion (orange colours) and sedimentation phases (green colours) in m y-1 against a plot of time and downstream distance to the river mouth. Sedimentation and erosion phases are in line with glacioeustatic changes.

In the lower Miño, the coastal prism extends from the Atlantic Ocean up to the city of Tuy (Figs. 4.1 and 4.10). During glacial sea level fall, the Miño river channel lengthens and its gradient increases, causing an increase in stream power. Because the Miño River is not actively incising at the initial falling stage, large-scale lateral erosion of the interglacial deposits occurs, followed by rapid aggradation because of a combination of increased sediment availability and an increase in river gradient (Blum and Törnqvist, 2000; Meijer, 2002; see Fig. 4.15A). This is the phase when the main bodies of the fluvial terraces are

formed. FLUVER2 correctly predicts the occurrence of terraces up to 60 to 70 km upstream, which is in agreement with the mapped terrace distribution (Figs. 4.1 and 4.14). In the field, the contact between terrace gravels and underlying saprolite is clearly erosive (Figs. 3.3A and 3.3C in Viveen et al., 2012b, see Chapter 3), indicating that the scour depth exceeded the base of the interglacial deposits. The exponential decrease of the ^{10}Be signal in the Vila Meã deposits (Viveen et al., 2012b, see Chapter 3) confirms that deposition would have been rapid. Then, when sea level falls even farther (Figs. 4.15B and 4.15C), the Miño switches to incision mode because the continental shelf gradient (± 4 m km^{-1}) is steeper than the gradient of the coastal plain (0 m km^{-1}) (Blum and Törnqvist, 2000). Because sea level does not drop below the shelf edge, an across-shelf valley is not formed and a 'drainage connectivity' (Meijer, 2002) between the fluvial and deep sea realm is not established. Sediments therefore do not bypass the continental shelf but are deposited upstream of the shelf edge. This might explain why the gravel-rich O Rosal terraces are found so close to the coast and why so little sediment is found on the NW Iberian continental shelf, which has been designated as a 'low-accumulation' shelf (Lantzsch et al, 2009; 2010).

The period of fluvial incision is much longer than the period of fluvial aggradation (~ 80% of the time, see Fig. 4.15A), which is ample time to form the fluvial terrace scarps, which are, according to the modelling results, the resultant of tectonic uplift superimposed on a 100-ka eccentricity-driven cycle of glacial-interglacial eustacy. This is a common mechanism for fluvial terrace formation along the Iberian Atlantic continental margin (e.g., Martins et al., 2010), but elsewhere along the European Atlantic margin climate-driven discharge changes are the main controlling factor (e.g., Antoine et al., 2007). Both settings have in common however, that because of the dominant 100-ka eccentricity modulation very often 8 to 10 fluvial terraces are found that date back to the mid-Pleistocene revolution (Bridgland and Westaway, 2008a).

When sea level rises again, the Miño River responds by renewed aggradation, which results in a backfilling sedimentary wedge of fluvial or fluviomarine overbank deposits on top of the glacial deposits in a funnel-shape drowned river valley (Merritts et al., 1994; Blum and Aslan, 2006; Mattheus and Rodriguez, 2011). Marine seismic profiles and borehole data from the NW Iberian shelf indeed confirm the existence of Holocene sands and muds on top of glacial sand and gravel (Garcia-Garcia et al., 2005; Lantzsch et al., 2009, 2010), although submarine data for the Miño River mouth are not available. This succession has also been observed at a few sites in fluvial terraces between the Miño River mouth and Tuy (see for instance Figs. 3.4 and 3.5 in Viveen et al., 2012b, Chapter 3), but only in the youngest terraces and tectonic basins that have not experienced any

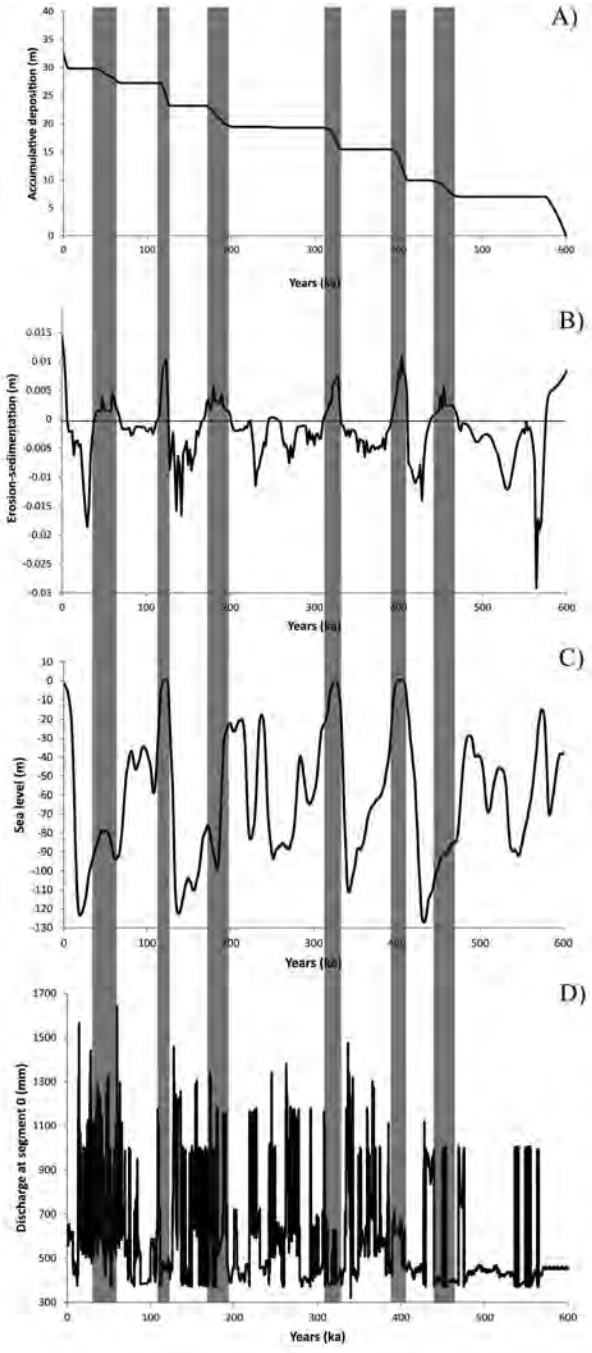

Fig. 4.15. A) Accumulative deposition of fluvial sediments compared against B) timing of erosion/sedimentation events, C) timing of sea level changes, and (D) discharge. Grey bars show timing of terrace deposition.

erosion. North of Tuy, overbank deposits are never found on top of the terraces, probably because the glacial river bed is never situated below the interglacial river level and, hence, it is unlikely that thick stacks of interglacial deposits are aggraded and preserved on top of the glacial terrace.

Erosion and sedimentation phases are not synchronous along the fluvial profile. Rather, deposition and incision are delayed when knickpoints move upstream along the profile. The delay may be as much as almost a full glacial-interglacial cycle (Fig. 4.14). Similar delays in knickpoint migration were already observed in other fluvial systems (e.g., Tebbens et al., 2000; Van Balen et al., 2010). This indicates that long-distance terrace correlation based on age estimations and altitude alone may not be sufficient to correlate terraces along the near-coastal parts of these fluvial systems.

A remarkable result of the modelling exercise is that the period of rapid aggradation does not correspond to periods of increased discharge but rather the opposite (Fig. 16D). Changing the intensity of the discharge or the timing of discharge peaks makes no difference (Fig. 4.13). This indeed suggests that for the lower Miño the effects of glacioeustatic changes on river gradient modulation are more important than upstream controls by, for instance, climate change-driven discharge (Tebbens et al., 2000; Bridgland and Westaway, 2008a). This situation can probably only be extended to settings similar to the lower Miño area with a steep and narrow continental shelf. It is therefore not correct to speak of 'glacial' or 'interglacial' terraces, as terrace formation can occur in both periods (Fig. 16), but rather, glacioeustatically controlled terraces.

4.6 Conclusions

Field evidence, weathering characteristics of the terrace deposits, and simulations with the river gradient modelling program FLUVER2 have given a coherent picture of the evolution of the lower Miño River system. Model simulations for the past 450 ka with various rates of tectonic uplift indicate that model runs with an uplift rate of 0.08 m ka^{-1} mimic best the development of fluvial terraces in the lower Miño. The number of terraces as well as terrace height, timing of terrace formation, and the amount of sediment are correctly simulated. The best-fit uplift rate is in agreement with the earlier proposed maximum uplift rate of 0.07-0.09 m ka^{-1} and can be considered the best estimation of the average uplift rate for the lower Miño region for at least the period since the beginning of the middle Pleistocene.

Bulk density measurement correlations of terrace quartzite pebbles suggest a gradient of 1 m km^{-1}, which agrees with the surface gradient of the highest terrace levels in the lower

Miño. FLUVER2 simulates a similar gradient. Based on these findings, a revised correlation scheme is presented for the lower Miño River terraces; 9 to 10 fluvial terraces and a Holocene floodplain level have been reconstructed.

In addition, model simulations indicate that glacioeustatic changes in sea level exert a primary control on terrace formation. The terrace gravels are deposited during a short time period when a glacioeustatically controlled fall in sea level is initiated. During the remainder of the time, incision prevails, resulting in terrace scarp formation and valley incision. A rise in sea level creates a backfilling sedimentary wedge that is deposited on top of the near-coastal gravel bodies.
The 100 ka eccentricity-driven changes in sea level, in combination with crustal uplift, are considered the dominant factors for terrace formation; climate-induced changes in discharge and sediment supply have been shown to exert only a minor influence on near-coastal terrace formation. We hypothesise that this is because of the narrow continental shelf offshore from the Miño River.

Chapter 5

Fluvial terrace map of the northwestern Iberian lower Miño River

A new fluvial terrace map with a tectonic framework for the northwest Iberian lower Miño River is presented. It is the first integrated map to cover the entire lower, 67-km reach of the Miño River, and to cover both the Spanish and Portuguese side of the river. The map is presented on a scale of 1:200,000, although its features were mapped on a scale of 1:5,000. Various map layers can be viewed, such as a digital elevation model (DEM), fluvial sediment thickness layers, a palaeoflow direction layer, a lineament and fault layer, and two terrace and tectonic basin layers, showing up to 10 fluvial terraces and a floodplain level. Interpretation of the map shows that next to regional tectonic uplift and glacioeustacy, local basin subsidence and small-scale block movement are very important for the fluvial network, localised fluvial terrace formation, and preservation.

Published as: Willem Viveen, Jeroen M. Schoorl, Antonie Veldkamp, Ronald T. van Balen, Juan R. Vidal-Romani, 2013. Fluvial terrace map of the northwest Iberian lower Miño River, *The Journal of Maps*, in press.

5.1 Introduction

River terraces are former river channels and floodplains that are situated at positions above the present river bed. They are either aggradational or erosive geomorphological surfaces that were subsequently incised. The incision forms a terrace riser or terrace scarp. Incision can be caused by changes in the ratio sediment load: water discharge, which is normally a climatically-induced change (e.g. Starkel, 2003); or because of changes in base level, induced by either sea level changes or tectonic uplift (Bridgland and Westaway, 2008a). Tectonic uplift is considered a prerequisite in preserving terraces above the current river bed (Maddy, 1997; Viveen et al., 2013a, see Chapter 4). A distinction is made (cf Leopold et al. (1964) as cited in Lewin and Gibbard, 2010) between "fill-cut" terraces, whereby incision occurs after sediment deposition; "cut-fill" terraces whereby multiple incision and aggradation events occur within one terrace level; and "strath" terraces, the resultant of purely lateral planation and vertical incision into bedrock. These strath terraces usually only have a thin sediment cover, or sediments are lacking at all.
Because river terraces can be formed by a variety of regional or even global factors (climate changes, tectonics), they are often used to assess the importance of these factors on landscape formation (Bridgland and Westaway, 2008a). Studies on river terrace formation usually involve a plethora of research techniques (Stokes et al., 2012b). These include remote sensing of Digital Elevation Models (DEMs), aerial photographs, topographical and geological maps to get an overview of regional terrace distribution; GPS-based field work to map terrace distribution more accurately (e.g. Meikle et al., 2010), and to collect sediment samples for laboratory analysis; dating of fill and strath terraces using fossils or radiometric techniques (e.g. Cordier et al., 2012); and more recently, numerical modelling to investigate the processes behind terrace formation (Viveen et al., 2013a, see Chapter 4).

In this paper, the terraces of the lower Miño River are presented. The Miño terraces recorded base level changes, climate changes and a variety of tectonic influences that makes it an important example for further studies on terraces world-wide (Viveen et al., 2012ab; 2013a, see Chapters 2 to 4). The lower Miño River has been a topic of study for over 70 years (e.g. Lautensach, 1945; Teixeira, 1952; Butzer, 1967; Nonn, 1967; Cano-Pan et al., 1997, 1999; Yepes-Temiño, 2002; Alves, 2004), but a detailed, regional terrace map covering both the Spanish and Portuguese river bank has been lacking so far. This has impeded a coherent, regional overview of the lower Miño River terraces and their palaeoenvironmental significance (Viveen et al., 2013a, see Chapter 4). For this reason, a new map for the entire area is presented here. The new terrace map had to fulfil a number of objectives, which are outlined below:
(i) refinement of the terrace stratigraphic framework; (ii) improvement of terrace correlations along the entire lower Miño River; (iii) revised chronology based on recent luminescence and cosmogenic ray exposure dating, and numerical modelling results; (iv)

correct depiction of the newly discovered tectonic basins (Viveen et al., 2012a, see Chapter 2); and most importantly, (v) give an insight into where and in what structural context the terraces were formed. For this reason we have added several other map layers. There is a terrace map layer that shows terrace scarps, bedrock gorges, and tectonic elements, a lineament and fault layer, a palaeoflow direction layer and fluvial sediment thickness layers. Earlier versions of parts of the map were already published in Viveen et al. (2012ab, 2013a, see Chapters 2 to 4), but the map presented in this work contains a fully updated terrace numbering, positions of tectonic basins as well as previously unpublished sediment thicknesses and palaeoflow directions.

5.2 Methodology

The Miño terrace map is drawn on a scale of 1:5,000 and primarily based on a DEM with 5-m grid cell resolution (MDT5, IGN) and a vertical precision of 0.10 m. The spatial extent of the fluvial terraces was, in first instance, based on the 1:50,000-scale geological map series of Spain and Portugal, and later on refined on the basis of a large number of field observations. Approximately 400 site descriptions were made during the years 2007, and 2009-2013 (see Appendix 2). Their locations were mapped with a Garmin eTrex Summit HC Handheld Global Positioning System (GPS) with a differential GPS signal receiver. Signal precision was up to 1 m, although in most cases, precision of the signal was around 4 m. In total, over 1.500 hours of fieldwork were invested in the lowermost 55 km of the lower Miño region. The terrace section in the uppermost 12 km of the area was mapped purely on basis of the geological maps and DEM. Fieldwork was aimed at the following characteristics, which are visible as separate map layers: (i) Fluvial sediment thickness. A differentiation is made between “exact” and “minimum” thickness, whereby in the case of exact thickness, the basel contact between fluvial gravels and underlying bedrock or saprolite was found; and not found in the case of minimum thickness. All terrace sediments consist of quartz and quartzite gravel (Viveen et al., 2012b, 2013a, see Chapters 3 and 4), sometimes interbedded with clay or sand lenses; (ii) lineaments and faults. All faults are described in Viveen et al. (2012a, see Chapter 2); all other elements are lineaments, which have been mapped from the DEM; (iii) palaeoflow directions (see Appendix 3). These are mainly based on clast imbrication in the terrace sediments and occasionally on foresets in sand beds; (iv) terraces and tectonic basins. Only the larger terrace surfaces were mapped, although sublevels have been reported (Viveen et al., 2013a, see Chapter 4). These were grouped together into a single terrace level. Only terraces with fluvial sediment (fill-cut terraces) were mapped, but in a few rare cases strath terraces as well, if this improved the visibility of the terrace level on the map. Tectonic basins were mapped on basis of the criteria in Viveen et al. (2012a, see Chapter 2): large flat surfaces with surface positions not

in agreement with local terrace staircase positions; presence of lineaments and fault scarps; fluvial sediment thicknesses surpassing 8 to 10 m.

The number of terraces and their correlations (Fig. 4.8) are based on Viveen et al. (2013a, see Chapter 4). Up to 10 terraces and the floodplain level were mapped. Terrace correlations were based on observed systematic changes in the density of quartzite pebbles in the terrace deposits, which were caused by weathering processes; and river profile modelling. Long-distance terrace correlations are approximate because terrace levels do not always perfectly fit the calculated correlation gradient of 1 m km^{-1}. Their position can be situated above or below their ideally estimated position at that location, but this is never more than ± 1 terrace level T0 is the youngest terrace and T10 the oldest. The ages for T0 to T4 are based on results from a terrace formation modelling exercise (Viveen et al., 2013a, see Chapter 4) and in agreement with CRE ages (Viveen et al., 2012b, see Chapter 3). Ages of T2-T6 are based on CRE ages (Viveen et al., 2012b, see Chapter 3). Ages of the more upstream terraces may differ significantly from the downstream ones, because the more upstream reaches of the river need more time to adapt to glacioeustically-induced variations in base level (Viveen et al., 2013a, see Chapter 4). The resulting map is projected in UTM N29, ED50 and is available in GeoPDF format, making it possible to turn on and off the various map layers, and to overlie the map with other georeferenced data.

5.3 Results of the fluvial terrace map

5.3.1 Mapped terrace levels

A continuous series of fluvial terraces is present in the lower Miño valley (see Appendices 4 and 5). Terraces often occur as small groups or blocks of terraces, that are separated from other terrace blocks by tectonic basins and lineaments. Terraces tend to have larger surfaces in the wider valley sections, and smaller surfaces in the narrower sections. Terrace scarps are often well preserved and mapped accordingly, especially in the upstream areas where they are cut into bedrock, and not as easily eroded as downstream, where they are cut from thick stacks of alluvium. In terms of terrace levels, the most complete terrace staircases are found in the narrower valley sections. There, the Miño could probably only laterally migrate in one direction, and responded by asymmetric vertical incision to changes in sediment load and discharge. This resulted in a complete sequence of strath terraces incised into the underlying bedrock. East of Monção, the older terrace levels are not found, likely because the mountainous terrain and generally thin sediment covers favoured rapid erosion. In the uppermost reach (55-67 km), a bedrock canyon and very few

terrace levels are found, probably because the influence of glacioeustacy is waning due to distance to the coast (Viveen et al., 2013a, see Chapter 4); and because of increased uplift which hampered terrace formation (Viveen et al., 2012a, see Chapter 2). In the most downstream section, the youngest terrace levels are not found. They are probably buried below the current river bed (Viveen et al., 2013a, see Chapter 4). In one occasion, a T10 terrace is mapped (39 km, south bank), but it is not clear if this is a Miño terrace as it is not directly situated in the Miño valley. Terrace distribution, development of the fluvial terrace scarps and sediment thickness also indicate the sometimes wandering pattern of the course of the Miño, e.g. at 55 - 44 km. The terraces are alternating between the north and south bank, before the Miño enters a tectonic basin. While the Miño flowed through the tectonic basin, only one or two terrace levels (T3 and T4) were formed on the south bank.

5.3.2 Sediment thicknesses and palaeoflow directions

Terrace thicknesses show a variable pattern (see Appendix 5). There is a weak observed trend of thicker sediment stacks downstream (2 – 6 m) compared to upstream (0 – 2 m), but a more obvious observed trend is visible when comparing sediment thicknesses to fluvial terrace form. Areas with narrow, equally spaced terraces (e.g. at 38-40 km upstream from the ocean, and at 22-26 km) contain less sediment (0 – 2 m) than the areas with large, broad terrace surfaces where thicknesses reach up to 10 m (e.g. 50 km north bank) , 19-23 km south bank and at 3 km).

Palaeoflow directions (79 observations of imbrications and foresets, see Appendices 3 and 5) indicate that the reconstructed flow was always directed downstream and observed flow directions were in general (sub)parallel to the downstream axes of the terraces. Exceptions are found in tectonic basins (e.g. 23 km south bank and 14 km north bank), most likely because they are local depressions.

5.3.3 Lineaments, faults and basins

A total of 9 tectonic basins were mapped (see Appendices 4 and 5). All basins are rhomboid-shaped, similar in size and very small (< 5 km2). The basin at 29-34 km contains a structure on the north side that is visible as a depression in the landscape. Pliego-Dones et al. (1972) mapped the structure as an alluvial fan, but it is more likely a sag pond (sensu Burbank and Anderson, 2001). This interpretation is based on its form, small extent and the fact that the nearby N-S trending lineament was interpreted as a left-lateral strike-slip fault (De Vicente and Vegas, 2009). Another sag pond is found at 25 km. Palaeoflow directions in the tectonic basin north of the sag pond at 31 km, indicate a northward direction. This shows that the basin was indeed filled up with Miño sediments, as already suggested by Sos-Baynat (1965). The basin is part of a larger N-S trending valley, but as fluvial terraces of

the Miño are only found close to the Miño River, the remainder of the valley is not mapped. In many cases, the basins are subdivided into smaller basins, leading to a system of individually subsiding compartments, or blocks, for instance between 22-26 km (east bank), and 29-33 km.

The terrace distribution and tectonic basins are clearly structurally-controlled. Three types of lineament directions delimit the tectonic basins (see Appendices 4 and 5). These are (i) E-W to ESE-WNW lineaments; clear examples are the lineaments controlling the basins between 22 and 0 km; (ii) NW-SE trending faults (e.g. the basin at 47-48 km (Viveen et al., 2012a, see Chapter 2); and (iii) approximately N-S-trending lineaments. The E-W and N-S trending lineaments are also responsible for faulting of terrace surfaces. A clear example is found at 34-35 km (south bank), where the western part of the T3 terrace surface has subsided 10 m.
Structural control on the terraces is evident from the sometimes long, narrow and straight configuration of the terraces without any obvious meandering. Between 22 and 31 km (north bank) all terraces (T0 to T9), are aligned in a NNE-SSW; and at 21-23 km, all terraces are of similar size and trend NE-SW.

5.4 Discussion and conclusions

The results indicate that the occurrence of terraces and their sediment thicknesses depends on more factors than downstream distance alone. The most well-developed terraces are situated in wider parts of the Miño valley, where a well-developed network of lineaments is present (typically the N-S oriented parts, see Appendices 4 and 5). In areas where these structures are absent, less fluvial terraces are found. This is obvious for the lowermost 15 km, where no well-developed network of lineaments exists on the south bank, and only terraces on the north bank are preserved. It is likely that former strike-slip activity along these faults caused weakening of the bedrock by cataclastic shearing. Strike-slip activity may be deducted from the broad and flat-bottomed tributary valley at 40 km (south bank) which may be the result from sheared bedrock; and the two structures interpreted as sag ponds along a N-S trending lineament. This supports the hypothesis that left-lateral strike-slip faulting was occurring along the N-S trending lineaments (De Vicente and Vegas, 2009).

The three lineament orientations (E-W to ESE-WNW, NW-SE and N-S) isolate a large number of small blocks that form separate entities in the landscape (tectonic basins and small blocks of terraces). The results indicate that the Miño, while flowing across such blocks, was often forced to migrate in a predetermined direction. Another clear example is found

between 40 and 50 km, where the oldest terrace levels on the south bank have positions that are consistently 10 m higher when compared to the terraces on the north bank. In this reach, the Miño likely flows across an active E-W trending fault. This suggests unequal uplift on both sides of the river bank, possibly induced by a northward tilt of the south block. In response, the Miño shifted northward. This and other examples on the map suggest that local block movement was also an important factor for terrace formation and preservation. Differential uplift of blocks has been observed in other river systems, for instance in southern Iberia (Stokes, 2008; Cunha et al., 2008; Martins et al., 2009), Germany (Peters and Van Balen, 2007), and the Netherlands (Veldkamp and Van den Berg, 1993), but always on a larger spatial scale or over longer time periods (e.g. Bridgland et al., 2012; Demir et al., 2012). As far as we are aware of, such potentially small-scale differential block movements affecting terraces in such a persistent manner have not yet been reported. The results from our map also indicate that faulting has been active during terrace formation in the Miño valley, which is from the Mid-Pleistocene transition period until now (Viveen et al., 2012b, see Chapter 3).

The influence of glacioeustacy has been thoroughly investigated in Viveen et al. (2013a, see Chapter 4), and is clearly visible on the terrace map (see Appendix 4), where terraces increase in altitudinal positions from the coast towards the more upstream reaches. The proximity of a narrow, steep continental shelf caused profound changes in river gradient when sea level dropped, as the Miño had to adapt to the new base level by incision. This led to terrace threads with a much steeper gradient than the current floodplain. Similar strong control of base level has been reported for other areas with short steep continental shelves around the world, for instance in southwest Iberia (Vis et al., 2008) and the United States (Blum and Törnqvist, 2000; Blum and Aslan, 2006). Climate-induced variations in discharge and sediment supply on the other hand, seemed to have had a less important effect on terrace formation as suggested by modelling experiments (Viveen et al., 2013a, see Chapter 4).
In this sense, the Miño River system is very different from many other river systems in the world, where climate change is a major driver for terrace formation and base level has a less prominent (but still important) influence (Bridgland and Westaway, 2008a). Tectonic uplift is becoming more and more accepted as another important driver for terrace preservation (Bridgland and Westaway, 2008b). Now, the results for our terrace map suggest that local, small-scale tectonic motions may also be of importance, something that until now has remained poorly investigated within the fluvial terrace community. This opens up new possibilities of integrating fluvial terrace research with the field of tectonic geomorphology. Concluding, glacioeustacy, vertical tectonic motions, small-scale block movements, downstream distance, and structural basin control are all important factors for terrace formation and preservation.

Chapter 6

Modelling the impact of regional uplift and local tectonics on fluvial terrace preservation

A terrace formation model (TERRACE) combined with a longitudinal river profile model (FLUVER) were used to simulate fluvial terrace formation in the northwest Iberian lower Miño River basin under influence of three tectonic conditions, namely regional vertical uplift, local basin subsidence and localized differential uplift. The simulation results were compared against mapped terrace altitudes and deposit thicknesses. The best results were achieved by combining all three tectonic factors, indicating that specific terrace formation is a complex interplay of regional and local tectonics. The best fit regional uplift rate of 0.10 m ka^{-1} over the past 600 ka is higher than previously estimated for a section further to the west, which can be attributed to an increase in tectonic uplift from the NW Iberian Atlantic margin towards the east. Local relative subsidence causes sediment accumulation in local basin, and sediment starvation of the fluvial terraces on the surrounding uplifting blocks. Differential uplift on both river banks causes unpaired terraces, which are fill terraces on one side of the valley, and strath terraces on the other side. Usually, the formation of fill or strath terraces is considered to be climate-dependant. Our results indicate that local tectonics can be important, and that therefore many current terrace correlations based on deposit thicknesses might be over-simplified.

Based on: Viveen, W., Schoorl, J.M., Veldkamp, A., Van Balen, R.T., *Submitted to Geomorphology*. Modelling the impact of regional uplift and local tectonics on fluvial terrace preservation.

6.1 Introduction

Tectonic motions are an important factor on river terrace formation. Firstly, terrace staircases are formed as a result of regional uplift (Bridgland and Westaway, 2008a; Cunha et al., 2008; Claessens et al., 2009). Secondly, differential tectonic movements may cause the formation of unpaired terraces along a river (Peters and van Balen, 2007; D'Allesandro et al., 2008; Larue, 2009; Martins et al., 2009; Ramos et al., 2012) or cause differences in terrace dimensions because the river is forced to migrate in a predetermined direction (e.g. Cox, 1994; Salvany, 2004). Differential uplift may also cause differences in fluvial sediment thicknesses between terrace levels, especially if one or several of the terraces are located in relatively subsiding locations, causing a local depression in which large amounts of sediments can accumulate (Stange et al., 2012; Viveen et al., 2012a, see Chapter 4). The influence of tectonic movements on terrace formation and preservation is however always registered as an end result, without clear indications for the relative contributions of the different tectonic components (e.g. local, regional, and tilting). Thus, in most case studies the exact effects of tectonic motions on terrace formation remain poorly understood.

In this paper we use a forward model to simulate the effects of various tectonic processes on terrace formation and preservation, in order to deduct what their individual contributions are to the observed net results. A terrace staircase from the NW Iberian lower Miño River is used as a case study, because the terrace ages are well-constrained by cosmogenic ray exposure (CRE) and thermoluminescence dating (Viveen et al., 2012b, see Chapter 3), and because the influence of other external factors such as base level change and climate change on the regional terrace sequence is well understood (Viveen et al., 2013a, see Chapter 4). Lastly, an extensive dataset based on field observations such as mapped terraces and terrace deposit thicknesses, and tectonic basins (Viveen et al., 2012a; 2013b, see Chapters 2 and 5), makes it possible to compare the modelled results against real-world data.

6.2. Study area

The area studied in this paper is located some 40 to 50 km upstream from the Atlantic Ocean and centres around the small cities of Salvaterra on the north bank and Monção on the south bank (Fig. 6.1). The terraces and the tectonic basin in this area were studied in detail in Viveen et al (2012a, see Chapter 2); later, a revision of the terrace chronology was given in (Viveen et al., 2013ab, see Chapters 4 and 5; see Fig. 6.2A). Apart from the tectonic basin, the other outstanding feature in the area is the unequal distribution of

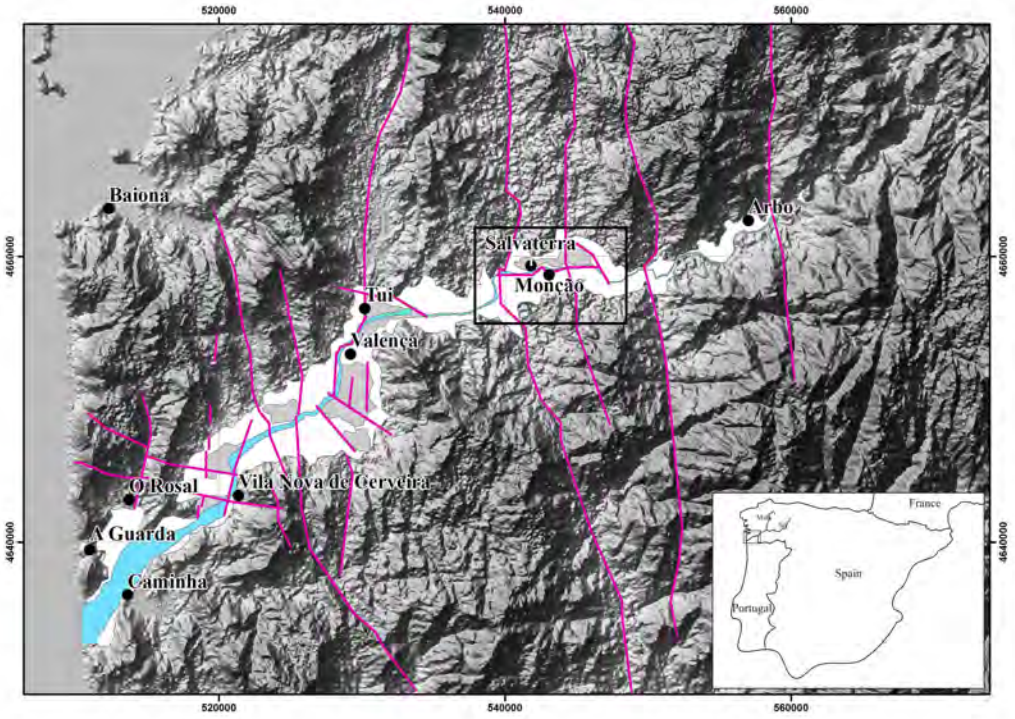

Fig. 6.1. Overview of the lower Miño River basin. Blue area shows the Miño River, white area shows fluvial terrace distribution, grey areas are the mapped tectonic basins and the purple lines are active tectonic lineaments and faults. Black square indicates the area studied in this paper. Figure adapted from Viveen et al. (2013a).

terrace levels on the north bank and the south bank (Fig. 6.3). On the south bank, the highest and oldest terrace fragments are located 10 m higher in the landscape compared to the highest terraces on the north bank, suggesting about 10 meter of differential uplift since the formation of the oldest terrace. In addition, thicknesses of the fluvial terrace deposits on the south bank are less compared to the north bank (Viveen et al., 2013b, see Chapter 5), see Fig. 6.2B). On the south bank, terrace sediment is restricted to small, local channel infills cut into the underlying bedrock, whereas on the north bank, the terraces are made up of large, continuous gravel beds (Fig. 6.3). These observations also suggest the presence of higher uplift rates on the south bank of the Miño River. This seems plausible, since local block tilting was demonstrated in an earlier paper (Viveen et al., 2012a, see Chapter 2). In addition, it was hypothesised that the Miño runs across a series of active faults, which could form the separation between the north and south bank tectonic domains.

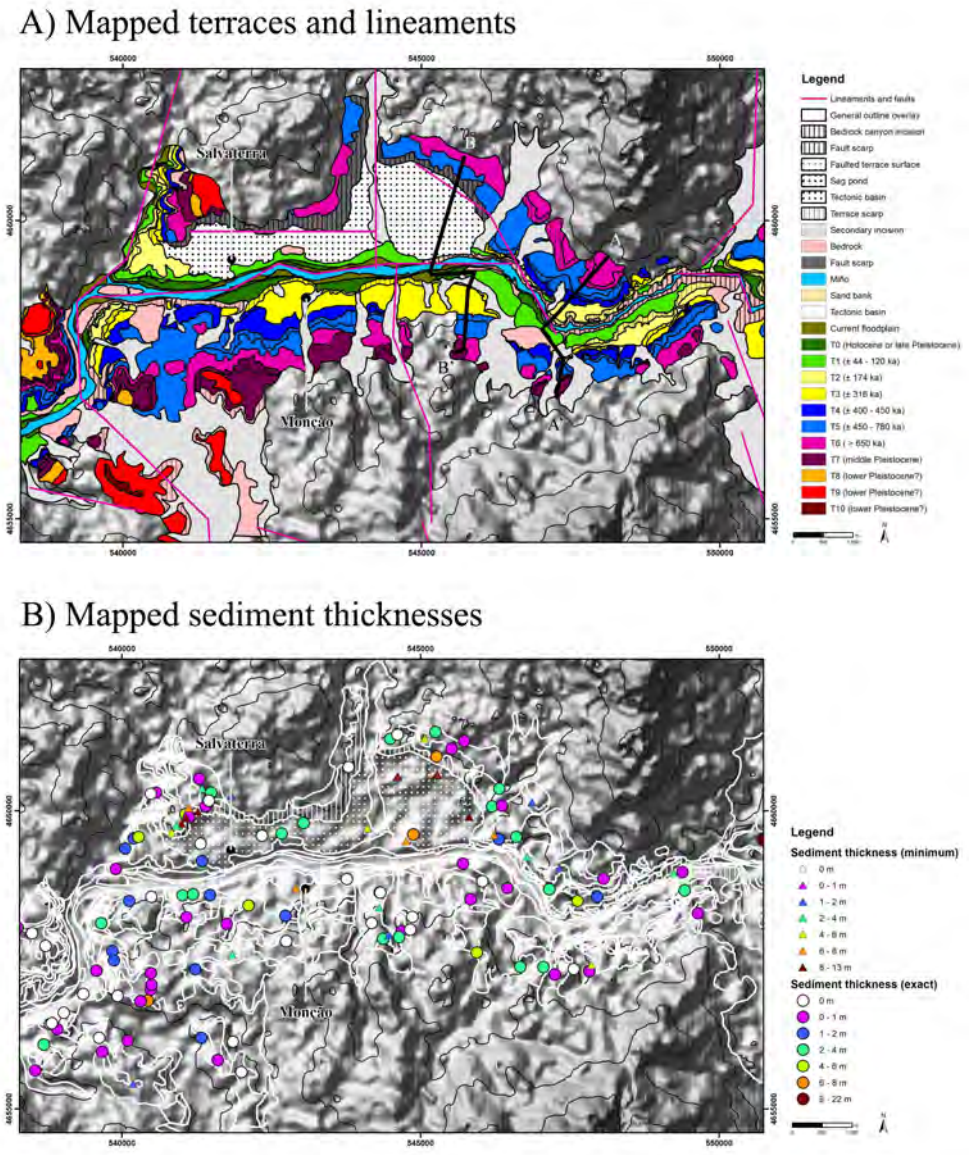

Fig. 6.2. A) Mapped terraces in the studied area (black square Fig. 1). The two black lines show the terrace transects of Fig. 3. A first version of this figure was published in Viveen et al. (2012a), and later on refined in Viveen et al. (2013b). B) Mapped sediment thicknesses (Viveen et al., 2013b). For minimum sediment thicknesses, the base of the deposit was not found. For exact thicknesses, the base was found. White lines show the outline of the terraces in Figure A.

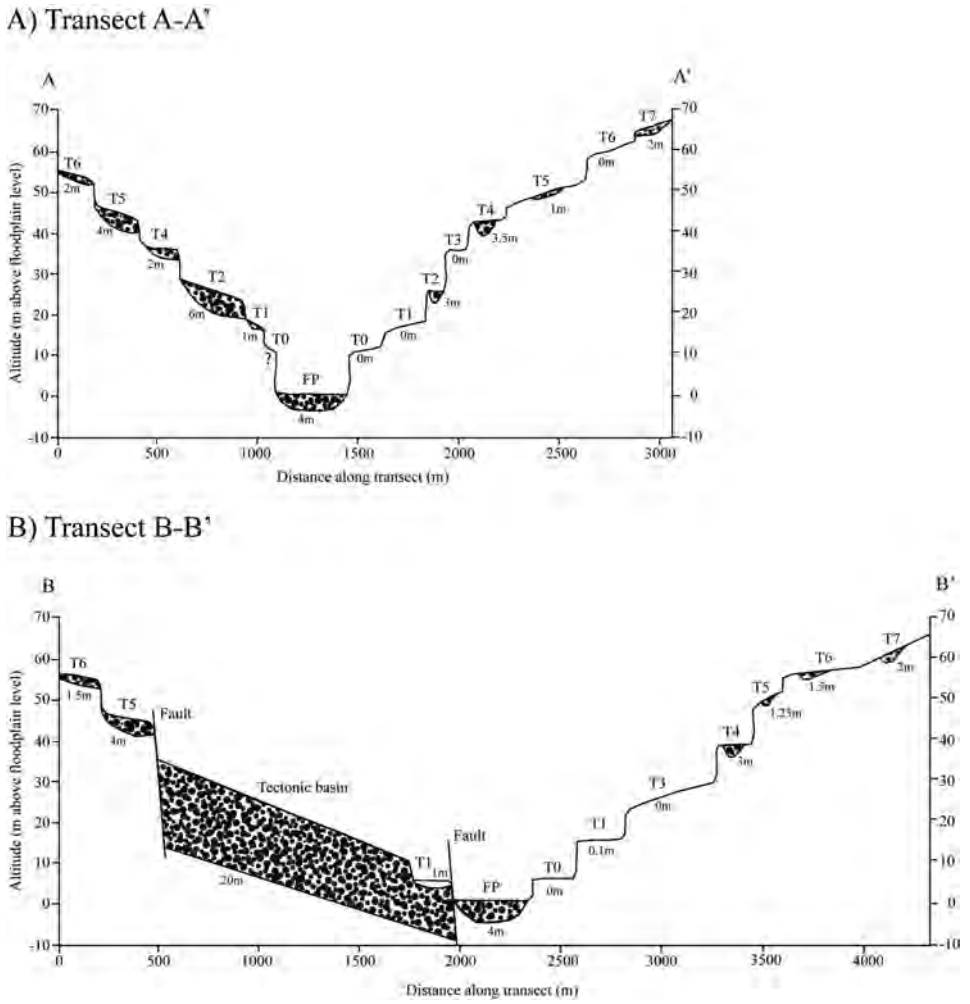

Fig. 6.3. A) Terrace transect used for modelling scenario 1. See Fig. 6.2A for location of the transect. B) Terrace transect used for modelling scenarios 2 and 3. See Fig. 6.2A for location transect. This transect is an improved version of Fig 2.4B in Viveen et al. (2012a, see Chapter 2).

6.3 Methods

6.3.1 Modelling methodology

We used the two models from the FLUVER2 modelling set (Veldkamp and van Dijke, 2000),

that consist of a numerical longitudinal profile evolution model (FLUVER) and nested within this basin wide model, a coupled valley-scale terrace formation model (TERRACE), based on expert system principles. The longitudinal model FLUVER was already extensively calibrated for the Miño system, yielding the vertical fluvial dynamics along the longitudinal profile as a function of discharge, sediment load, base level changes and uplift (Viveen et al., 2013a, see Chapter 4). The existing TERRACE model (Veldkamp and Vermeulen, 1989; Veldkamp, 1992) required some modification in order to be able to deal with local tectonic effects. The TERRACE model simulates the effects of vertical and lateral erosion and deposition on valley development, using expert system decision rules. The quantitative input parameters, river discharge (Q, in m3 s^{-1}), sediment load (Qs in m3 s^{-1}), valley gradient (m m^{-1}), and erosion and deposition quantities (m3 s^{-1}), are provided by FLUVER simulations (Fig. 6.4), which was calibrated and quantified by previous simulations (Viveen et al., 2013a, see Chapter 4). In TERRACE, changes in discharge (Q) and sediment load (Qs) determine which channel type is valid (see Schumm (1977, p. 135):
IF Q(t-1) < Q(t) and Qs(t-1) > Qs(t) THEN channel type is meandering
IF Q(t-1) < Q(t) and Qs(t-1) < Qs(t) THEN channel type is not changing and remains what is was
IF Q(t-1) > Q(t) and Qs(t-1) > Qs(t) THEN channel type is not changing and remains what is was
IF Q(t-1) > Q(t) and Qs(t-1) < Qs(t) THEN channel type is braiding

For each system state the effective floodplain (in m) is determined in a different way. In a braided system, the whole space between the lowest terraces account as floodplain. This implies that the physical constraints, the terraces scarps, or the valley side, determine the floodplain width. The effective floodplain width of a meandering river system is calculated using the sinuosity formula of a meandering river from Schumm (1977, p. 115):
Effective floodplain width = 15 * (Q/0.028)0.5

Previous simulations with FLUVER have already determined when and how much the system erodes or aggrades (Fig. 6.4). Deposition migrates downstream along the valley axis with adding one grid layer on 1 m until a terrace scarp or valley side is met. Erosion migrates upstream along the valley axis by removing one grid layer on 1 m (if river incises, see Fig. 6.5) until terrace scarp or valley side is met. When the river has also bank erosion (Fig. 6.5), the valley is widened with one grid unit (200 m) on both sides. The river behaviour states 'incision' and 'bank erosion' are determined by the following decision rules:

IF 'erosion' and 'uplift' and 'meandering' THEN 'incision'
IF 'erosion' and 'uplift' and 'braided' THEN 'incision' and 'bank erosion'
IF 'erosion' and 'no uplift' and 'meandering' THEN 'incision' and 'bank erosion'

IF ‘erosion’ and ‘no uplift’ and ‘braided’ THEN ‘bank erosion’

The condition uplift is true when the river is not able to compensate the uplift by erosion. This condition acts with a threshold of 1 m.

The TERRACE model is not attempting to mimic real valley morphology in detail, but displays the morphological probability expression of alternating erosion and depositions events including preservation potential. Only terrace units of 200 m * 200 m (x,y) dimensions are significantly large enough to be considered as a relevant unit. This size is derived from a Monte Carlo sensitivity analysis made for a previous application in Germany (Veldkamp et al., 2002).
The TERRACE model has as main limitation that it is not process-based, and that no feedbacks back to the longitudinal profile model can occur. Localized increase in accommodation space, due to block subsidence, would in a process model lead to more localized deposition. But this effect is not accounted for, or fed back in the longitudinal profile FLUVER, causing systematic underestimations of deposit volumes and thickness.
Preservation is the main characteristic that the terrace model adds to simulations with the longitudinal profile evolution model FLUVER. FLUVER simulates the alternating erosion and deposition events that can lead to a terrace, while TERRACE mimics the net effects of these events as preserved in a valley.
There are three different tectonic controls that can be simulated. General uplift or subsidence (Veldkamp and van Dijke 2000), unequal uplift rates of left/right half of the valley (see Veldkamp, 1992), and local uplift or relative subsidence (Veldkamp et al., 2002).

6.3.2 Modelling scenarios

Our previous studies showed that regional uplift, local basin subsidence and fault motions are affecting the landscape. Applying these three tectonic ingredients at once might obscure their separate effects. Therefore we decided to introduce tectonic complexity stepwise in the modelling. Firstly, we start with the regional tectonic uplift rate. Secondly, we introduced local, vertically subsiding basins. Thirdly, we introduce differential uplift/subsidence caused by faults. The latter also accounts for unequal amounts of subsidence in the basins, for example due to the vertical geometry of the faults, in a strongly simplified way. We use this approach since all tectonic motions in TERRACE are vertical and homogenous over large distances; we cannot model lateral

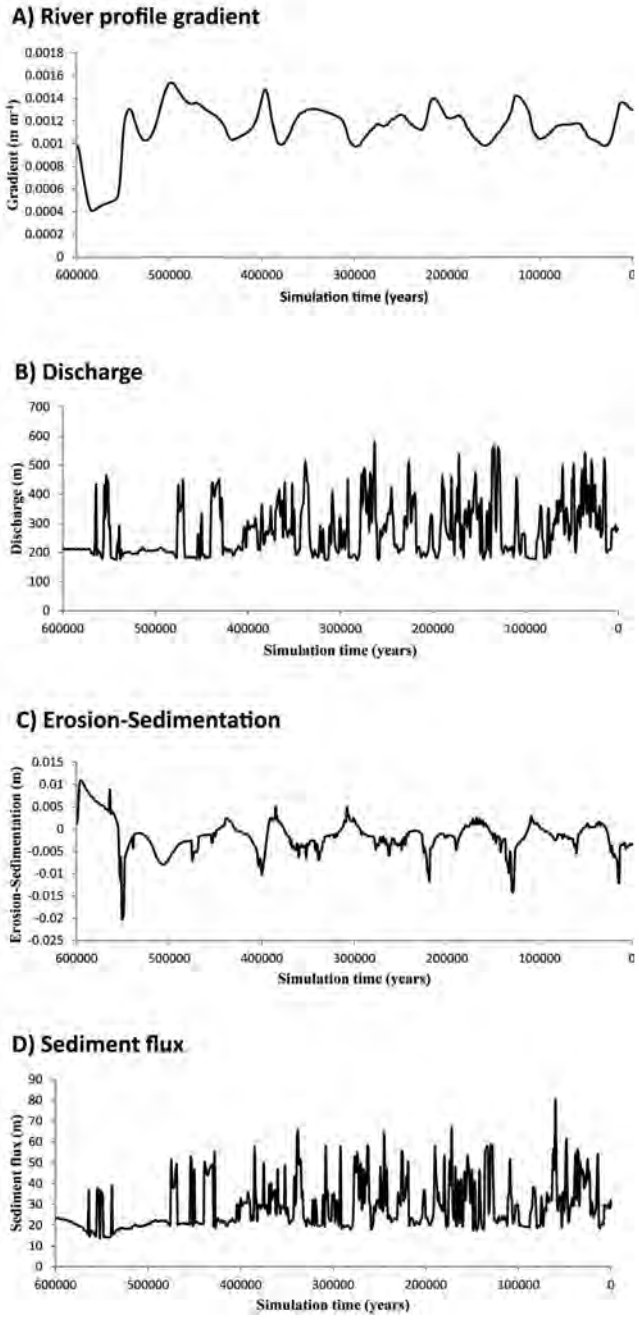

Fig. 6.4. TERRACE model input derived from an earlier modelling exercise with the FLUVER model (Viveen et al., 2013a) for the studied section of the Mino River with A) gradient, B) Discharge, C) erosion sedimentation dynamics and D) sediment flux.

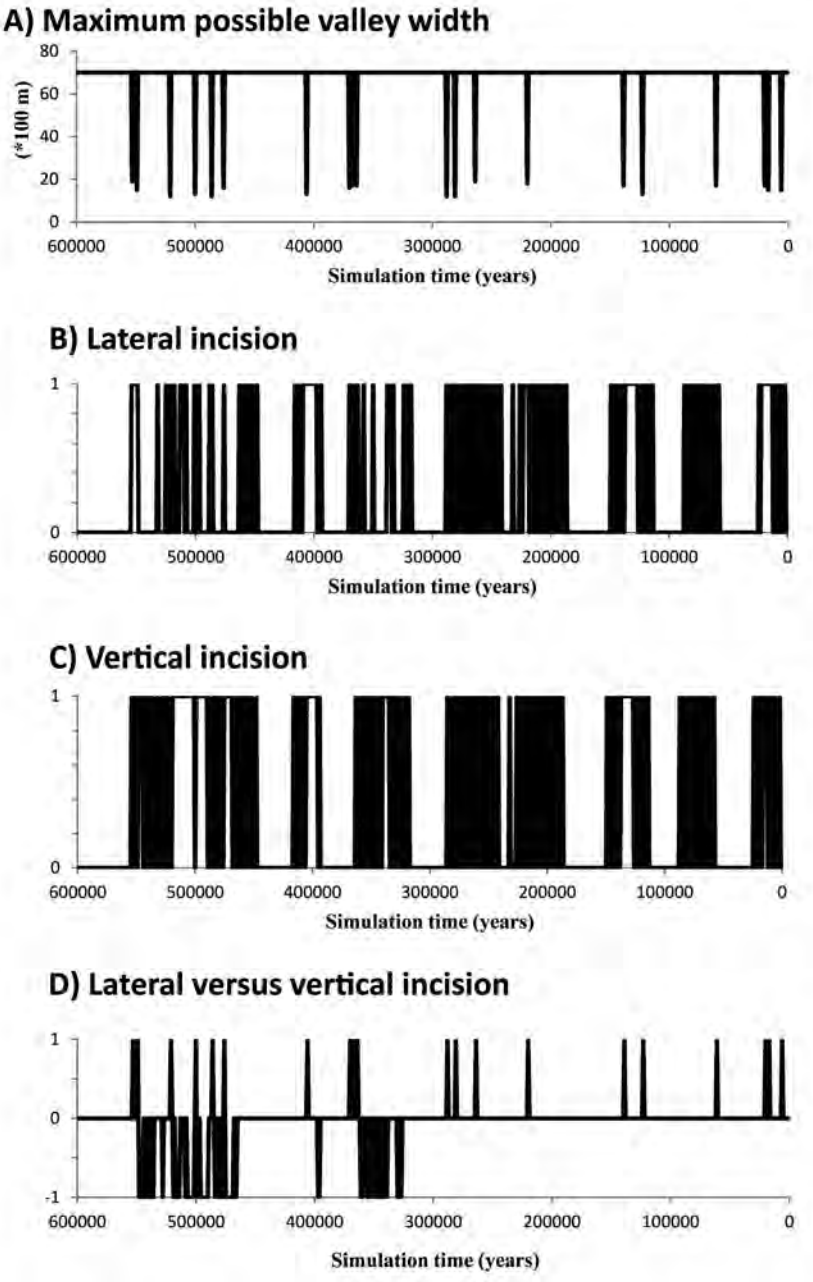

Fig. 6.5. Parameter switches for the TERRACE model. A) Variations in maximum floodplain (valley) width over time; B) lateral incision events. These are either true (black lines with value 1), or false (value 0). C) Vertical incision events (true when black lines have value 1, and false when 0). D) Phases of either lateral incision (value is +1) or vertical incision (value is -1).

motions involved with listric faults or half grabens.

The first step of the modelling exercise is to determine the regional vertical uplift rate required for terrace formation and preservation. In an earlier paper (Viveen et al., 2013a, see Chapter 4) we demonstrated that a regional uplift rate of 0.08 m ka^{-1} corresponded best with the observed terrace sequences in the lower Miño valley, based on a river profile model. Thus, we apply a range of uplift rates from 0.08 m ka^{-1} to 0.12 m ka^{-1}. The decision on which results best matches observations, is based on i) terrace altitudes; and ii) terrace deposit thicknesses. Observed terraces and their depositional thicknesses were previously published in Viveen et al. (2012a, see Chapter 2) and later on refined in Viveen et al. (2013b, see Chapter 5). The initial match is based on a terrace section with an (almost) complete terrace sequence where no tectonic basin is present (Fig. 6.3A). Because there is a height difference of 10 m between the highest terraces on the north and south bank, which might be caused by unequal uplift on both sides of the river, only the terraces on the north bank are used to calibrate vertical uplift rates in the first scenario. Also, only the terraces up to T5 are used for a match as the T6 terrace is older (> 650 ka) than the simulation time (600 ka).

Once the best-matching vertical uplift rate has been established, this rate will be used as input for the next scenario in which a tectonic basin is introduced. The surface of the basin is characterized by a lack of terraces, since it is an area of accumulation. The basin surface covers a flat section of 1.5 km wide and 10 km long, extending from the west to the east along the north bank of the river. The age of this surface, and thus of the tectonic activity, is constrained by the ages of the terraces lying higher and lower than this depositional surface (Fig. 6.2A). It should be noted that the creation of local basins can happen by localized less uplift, so-called down-lifting. So the whole area experiences uplift, but specific blocks lag somewhat behind creating relative basins.

We assume that basin subsidence took place between 500 ka and 100 ka. This is based on the observation that before 500 ka a terrace was formed (T5 terrace), whose minimum age was established with 10Be dating at either ± 450 ka or ± 563 ka (Viveen et al., 2012b, see Chapter 3). The lower limit of 100 ka for basin subsidence is based on the occurrence of a T1 terrace, which was formed between ± 44 ka and ± 120 ka (Viveen et al., 2013ab, see Chapters 4 and 5). Also, thermoluminescence dating of a sand lens at a depth of 6 m below the tectonic basin surface gave a minimum age of 105 ± 4 ka (Wallinga and Johns, 2011; Wallinga, pers. comm). A minimum subsidence rate of ± 0.05 m ka^{-1} is calculated from a mapped minimum sediment thickness of 20 m and the time period in which basin subsidence was supposedly active. Using the 0.05 m ka^{-1} subsidence rate as a starting point, a range of subsidence rates between 0.05 and 0.15 m ka^{-1} is investigated. The most likely subsidence rate is based on a good match between i) surface position of the tectonic basin

and terraces on the north bank of the river (again only the terraces up to the T5 level); and ii) a minimum sediment thickness of 20 m for the tectonic basin. The results are compared to a new terrace transect (Fig. 6.3B). It should be noted that a local subsidence of 0.05 m ka^{-1} in a regional uplift of 0.1 m ka^{-1} still means a net uplift 0.05 m ka^{-1} compared to the Atlantic base level.

The third step in the modelling exercise is to introduce the effect of differential uplift rates, which is implemented by unequal uplift on both sides of the river. The difference in uplift is calculated from an accumulated 10 m difference between the highest terraces on the north and south bank over the modelled time period of 600 ka. This yields a difference in uplift of ± 0.017 m ka^{-1}. This additional uplift is then added to the tectonic block on the south bank. Again, a range of uplift differences ranging from 0.010 to 0.020 m ka^{-1} is explored and tested against i) best match between modelled and mapped terrace positions (Fig. 6.3B); this time both on the north and south bank. For the north bank we again look at the terraces up to the T5 level, but for the south bank we compare with the terraces up to the T6 level, because if there is indeed differential uplift, then this level will most likely fall within the simulation time; and ii) mapped sediment thicknesses on the north and south bank.

To summarise, the following modelling scenarios will be investigated (Fig. 6.6):

1. Varying regional vertical uplift rates;
2. (Best result vertical uplift rate) + varying basin subsidence rates;
3. (Best results vertical uplift rate and block subsidence rate) + varying differential uplift rates.

6.4 Results

6.4.1 Scenario 1: regional uplift

Regional uplift rates of 0.08 m ka^{-1} and 0.10 m ka^{-1} both yield 6 terraces on the north bank, which is in agreement with the mapped terrace staircase (Fig. 6.7A). An uplift rate of 0.12 m ka^{-1} yields 8 terrace levels, which is too much. In addition, an uplift rate of 0.10 m ka^{-1} results in terrace altitudes at similar heights as observed in the field, whereas an uplift rate of 0.08 m ka^{-1} yields terraces below the observed terrace positions. Thus, an uplift rate of 0.10 m ka^{-1} gives the best results.

Simulated sediment thicknesses for terraces at the north bank either overestimate or underestimate mapped thicknesses by a few meters, although the order of magnitude is the same (Fig. 6.7C). Varying uplift rate does not lead to significant improvements in values.

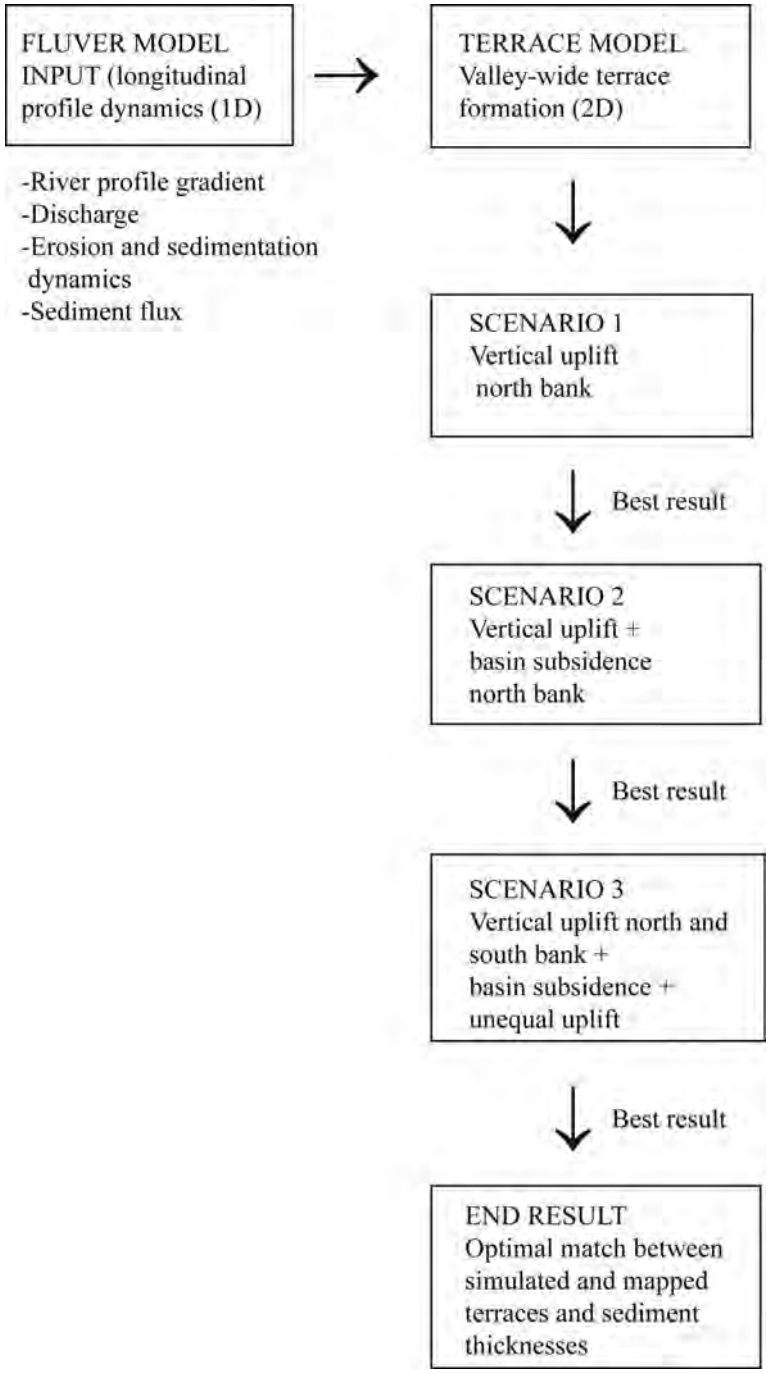

Fig. 6.6. Flow chart showing the 3 modelling scenarios and their input conditions.

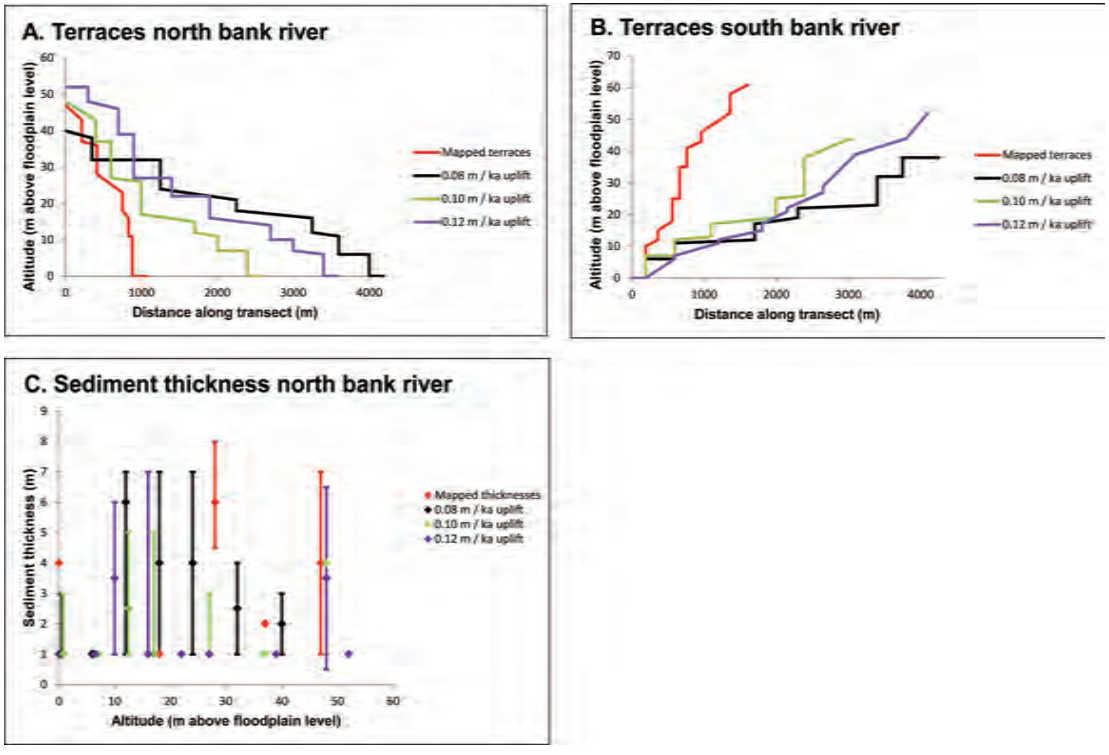

Fig. 6.7. Results from Scenario 1 where variable uplift rates between 0.08 m ka^{-1} and 0.12 m ka^{-1} are simulated on both banks of the Miño River and compared against mapped terrace levels and sediment thicknesses in the field. A) Simulated terrace altitudes on the north bank of the river. B) Simulated terrace altitudes on the south bank of the river. C) Simulated sediment thicknesses of the north bank of the river. Only values for the various terrace levels are compared that were also observed in the field. The most observed value, the median, is displayed as a dot, and the minimum and maximum values are given by the error bars. Terrace sediment thicknesses of the south bank are not given, because terrace altitudes do not compare well against field evidence, which makes it not useful to compare sediment thicknesses.

6.4.2 Scenario 2: basin subsidence

Adopting the 0.10 m ka^{-1} regional uplift, in scenario 2 a relative subsiding tectonic block (basin) was introduced on the north bank, and various relative subsidence rates were investigated (Fig. 6.8A). A model applying a relative subsidence rate of 0.05 m ka^{-1} does not predict a morphology in agreement with observations, as various terrace steps are still formed. The model should at least predict a large, flat surface between 10 and 35 m above floodplain level, which is the top of the basin fill. Increasing relative subsidence rates to 0.075 and 0.10 m ka^{-1} does lead to a clear large tectonic basin surface (around 10 m above floodplain level), although also a terrace step is formed around 20 m above floodplain level, which was not observed in the field. In addition, a terrace step is formed just below and above the tectonic basin surface, which is in agreement with field evidence. Increasing relative subsidence to 0.15 m ka^{-1} also leads to a distinct basin surface, but the surface is situated at too low in the valley. We conclude that a relative basin subsidence rate of 0.10 m ka^{-1} leads to the modelling results which are best in agreement with observations.
In terms of sediment thicknesses (Fig. 6.8B), a relative basin subsidence rate of 0.05 m ka^{-1} leads to an underestimation of sediment thicknesses for the terraces and the tectonic basin. Simulations adopting subsidence rates of 0.075 and 0.10 m ka^{-1} give values that are in agreement with mapped thicknesses; increasing the subsidence rate to 0.15 m ka^{-1} causes too much deposition in the tectonic basin. Based on terrace altitudes, the predicted basin surface height, and the sediment thicknesses, a relative subsidence rate of 0.10 m ka^{-1} gives results that match well with field evidence.

6.4.3 Scenario 3: unequal uplift

In this scenario, differential uplift was added to the model. The south bank of the Miño was uplifted more than the north bank. This mimics the effect of a probable important fault below this part of the Mino. Fig. 6.9A shows that an uplift increase of 0.010 to 0.020 m ka^{-1} of the south bank leads to an improvement of the simulated terrace staircase on the north bank, when compared to the mapped terraces, as the terrace step at 20 m above floodplain level is no longer formed. At differential uplift rates of 0.010 and 0.015 m ka^{-1}, two terraces are formed above the position of the basin surface, whereas a model assuming a differential uplift rate of 0.020 m ka^{-1} predicts a simulated terrace staircase that matches very well with the mapped staircase.
On the south bank (Fig 6.9B), increasing the differential uplift leads to an increasingly better match with the mapped terraces; the differential uplift rate of 0.020 m ka^{-1} yields the best results.

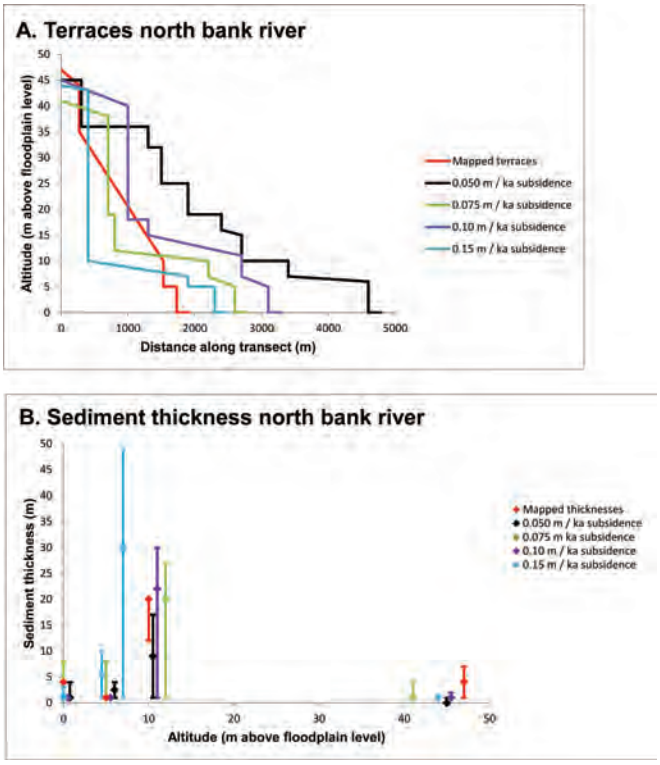

Fig. 6.8. Results from Scenario 2, where the best result of scenario 1 (0.10 m ka-1 regional uplift rate) is complemented by the implementation of a tectonic basin on the north side of the river. In this scenario, various rates of basin subsidence are investigated. A) Simulated terrace altitudes on the north bank of the river, compared against field evidence. B) Simulated terrace and tectonic basin sediment thicknesses, compared against field evidence. The tectonic basin surface is found at altitudinal values of ± 10 m above floodplain level. Terraces and sediment thicknesses of the south bank are not given, because the terraces are still not predicted at the right positions above floodplain level.

Sediment thicknesses for all differential uplift rates on both the north (Fig. 6.9C) and south (Fig. 6.9D) bank correspond well with the mapped thicknesses, even though sediment thicknesses on the south bank are overestimated by a metre for some terraces.

6.4.4 Terrace and sediment distribution scenarios 1, 2, and 3

The step-wise presented results show that by applying a uniform uplift without tectonic basin activity, paired terraces are formed on both sides of the river (Fig. 6.10A), and sediment distribution is uniform on both river banks (Fig. 6.11A). The terraces are also more or less equal in size. When the local basin is introduced (Fig. 6.10B), terraces are no longer paired, and a large flat tectonic basin surface develops in the valley. The basin

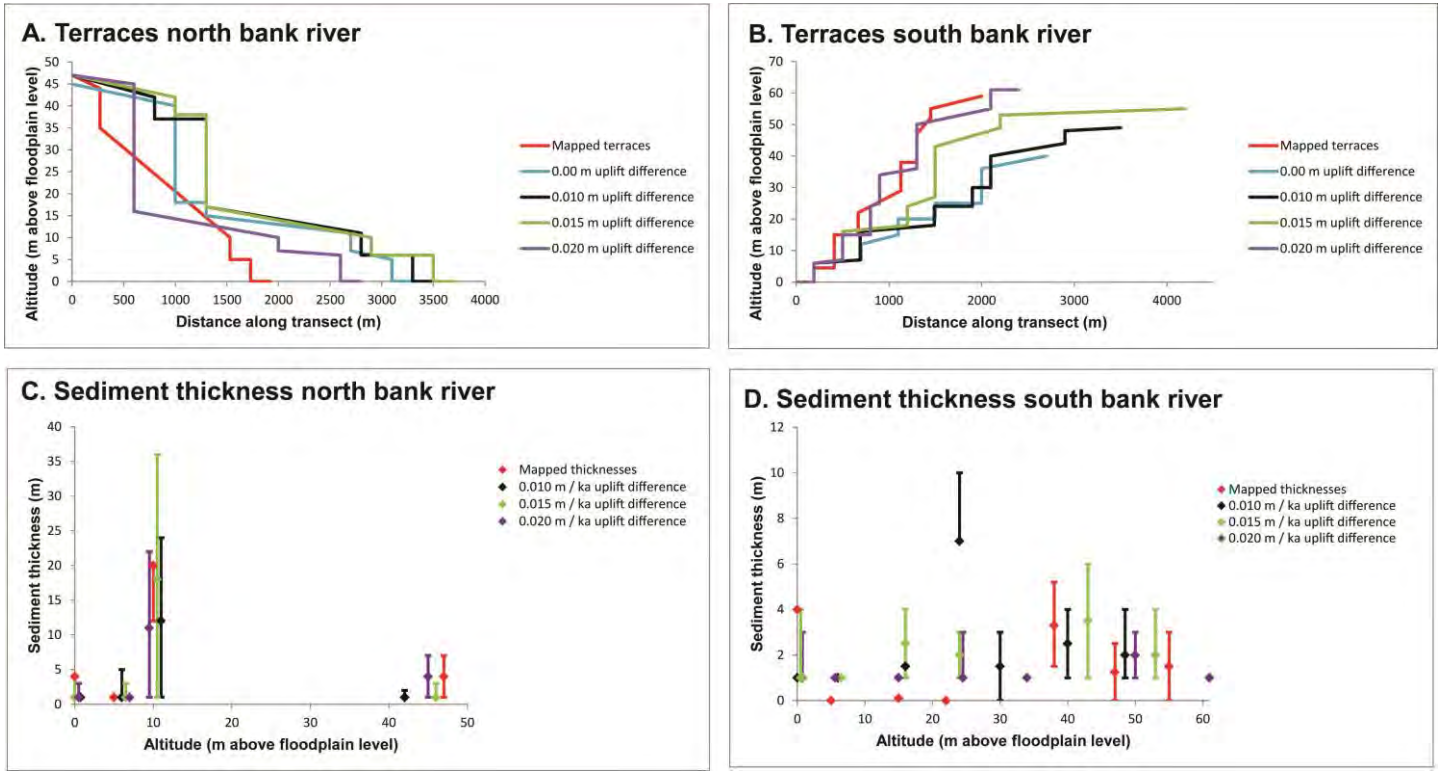

Fig. 6.9. Results from Scenario 3, where the best result of scenario 2 (0.10 m ka-1 basin subsidence), is complemented by varying the uplift rate on both sides of the river. A) Simulated terrace altitudes on the north bank, compared against field evidence. B) Simulated terrace altitudes on the south bank, compared against field evidence. C) Simulated sediment thicknesses on the north bank, compared against field evidence. D) Simulated sediment thicknesses on the south bank, compared against field evidence.

Fig. 6.10. Preserved terrace remnants (in colour coding according to height above floodplain level in m). The X-axis represents distance along the Miño River (10 km in total) and the Y-axis valley width (in km). See Fig. 2A for a comparison with the mapped terrace distribution. A) Best result from Scenario 1, where an equal uplift of 0.10 m ka-1 on both sides of the river was simulated. B) Best result from Scenario 2, with a regional uplift rate of 0.10 m ka-1 and a basin subsidence rate on the north bank of0.10 m ka-1. C) Best result from Scenario 3, with a regional uplift rate of 0.10 m ka-1 and a basin subsidence rate on the north bank of 0.10 m ka-1. On the south bank an additional uplift rate of 0.020 m ka-1 has been added.

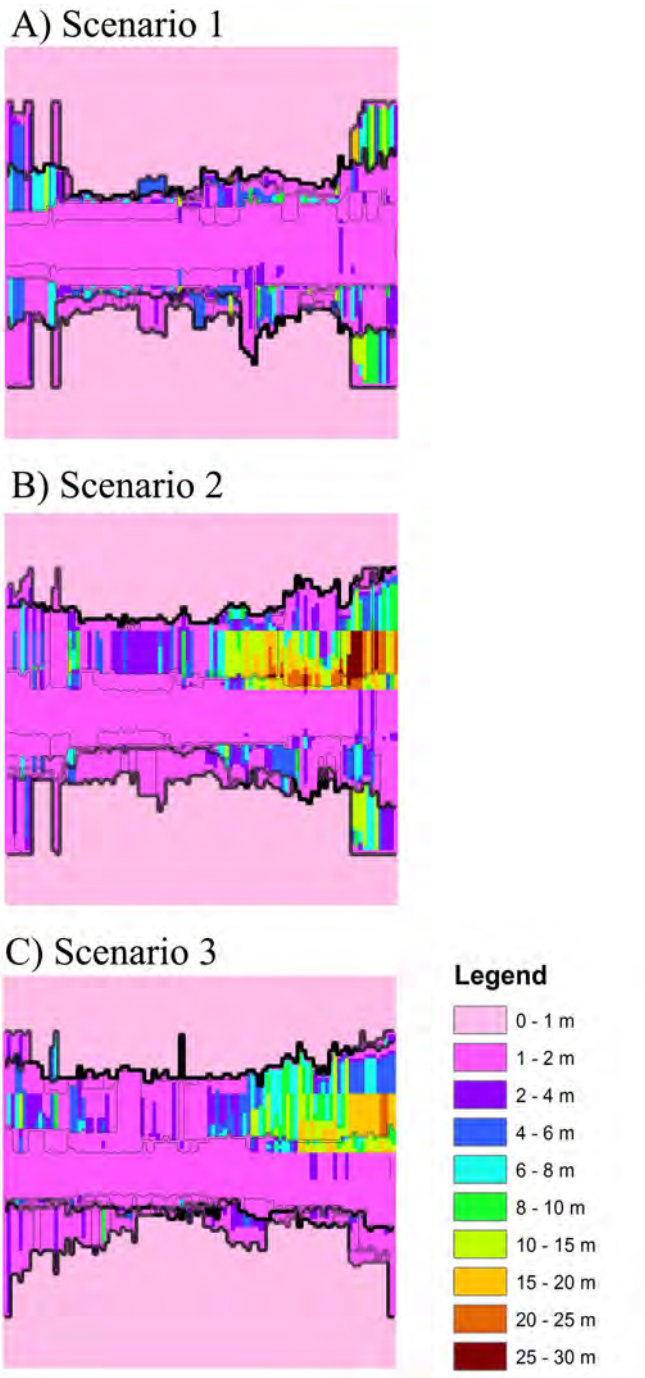

Fig. 6.11. Semi-spatial representation of fluvial sediment thickness distribution for A) Scenario 1; B) Scenario 2; and C) Scenario 3.

accumulates a large amount of sediment, which leads to unequal sediment distribution on both river banks (Fig. 6.11B). Adding more uplift to the south bank of the river (Fig. 6.10C) leads to even less paired terraces, and the terraces on the south bank are conspicuously narrower in form. Unequal uplift also leads to less sediment on the faster uplifting south bank, and also to less sediment accumulation in the tectonic basin (Fig. 6.11C).

6.5 Discussion

Our results indicate that relative subtle tectonic motion differences can leave a clear imprint on the preserved terrace record. A certain amount of vertical uplift is required for the formation of a terrace sequence as found in the field. The best matching uplift rate is 0.10 m ka^{-1}, whereas in an earlier work we reconstructed a regional best matching uplift rate of 0.08 m ka^{-1} (Viveen et al, 2013a, see Chapter 4). However, in that earlier modelling exercise, it was assumed that incision by the Miño-Sil system was able to keep up with uplift, and the model was calibrated accordingly. This condition was not imposed on the terrace model in this paper and suggests that even large river systems such as the Miño are not able to always maintain their state of semi-equilibrium, as Kiden and Törnqvist (1998) already argued, leading to underestimation of the uplift rate. Another reason may be that uplift is slightly higher in the study area, when compared to the area more to the west, where we originally dated the Vila Meã terrace section using CRE techniques (Viveen et al., 2012b, see Chapter 3). This notion is supported by evidence such as deeply entrenched river valleys which do not occur west of the studied area (Cabral, 1995). Earlier neotectonic reconstructions (Viveen et al. 2012a, see Chapter 2) also suggested an eastward increase of regional uplift rate.

The inclusion of block subsidence to the modelling exercise strongly affected the terrace configuration and preserved sedimentation thicknesses. The scenarios demonstrated that, as the rate of downlift increases, terraces are no longer able to form at the location of the tectonic basin, and a clear basin surface develops. The modelled surface height (11-15 m above floodplain level) does not entirely agree with the observed position (10-35 m above floodplain level), see Fig. 6.9A, indicating that other, not simulated factors may play a role. We hypothesise that in reality the tectonic block did not only subside, but was also partially tilted along the fault through which the Miño flows. Partially tilted terrace surfaces have been observed at other locations in the lower Miño (e.g. Fig. 2.5B in Viveen et al., 2012a, see Chapter 2) and thus seems to be a fairly common tectonic mechanism in the area. Since the block tilt was not directly simulated, the simulations do not take these tilt effects into account. The simulated sediment thicknesses clearly indicate that the presence of a downlifting tectonic block cause sediment accumulation in these basins, which causes sediment starvation in other parts of the river valley (Fig. 6.11). This might explain why

there is less sediment in the synchronous terraces on the other side of the river. These results suggest that basin subsidence rates based on sediment thicknesses in the basin only, can severely underestimate the real subsidence rates. Again, the net result, sediment thickness, does not account for the amount of sediment removal by lateral river erosion.

Differential uplift rates on both sides of the river will cause unpaired terraces and confirms similar observations by other authors (Veldkamp and Van den Berg, 1993; Peters and van Balen, 2007; D'Allesandro et al., 2008; Larue, 2009; Martins et al., 2009; Ramos et al., 2012). Terraces are narrower on the faster uplifting block, likely because the river had less time to laterally erode the river valley and create accommodation space. This also affects sediment thicknesses, because the river had less time and space to deposit fluvial sediments. This leads to less sediments on the faster uplifting south bank, something that was in our case study augmented by the presence of the subsiding basin on the north bank, which acted as a sediment trap. It is possible that less sediment generation due to decreased lateral valley wall erosion on the south bank causes an overall decrease in sediment availability, as observed in Fig. 6.11C.

The results clearly indicate that the net effect of the three simulated tectonic processes together (vertical uplift, basin subsidence and differential uplift), leads to the terrace sequence and sediment thicknesses that best match the real-world situation. It is therefore likely that these three tectonic conditions are indeed present in the studied area. This has theoretically consequences for the long-distance terrace correlations we made (Viveen et al., 2013a, see Chapter 4) and for the fluvial terrace map (Viveen et al., 2013b, see Chapter 5). But because the terrace levels on both sides of the river mis-match each other by maximally 10 m positional difference, which equates ± 1 terrace level, our correlations and terrace map are still valid. Local tectonic processes may thus be of influence on terrace formation, and this is something that is not always taken into account when correlating terraces over longer distances, which is usually done on basis of altitudinal positions above a reference level and limited dating results (Bridgland and Westaway, 2008a; Stokes et al., 2012b; Perez-Alberti et al., 2013).

Throughout the lower Miño River valley, unpaired terrace sequences with small altitudinal differences are found, as well as a number of tectonic basins (subsided blocks) (Viveen et al., 2013b, see Chapter 5). This reinforces the idea that the area is a made up of individually moving (uplifting and subsiding) tectonic blocks (cf. Birot and Solé-Salabris, 1954). Noteworthy is the observation that the unpaired terrace sequences along the river always occur where a tectonic basin is present (Viveen et al., 2013b, see Chapter 5). The observed and inferred tilted terrace and basin surfaces suggest a regime of local movements along faults. Terraces and sediment thicknesses were correctly simulated by imposing upper and lower temporal boundaries (based on CRE and thermoluminescence dating) on tectonic

basin subsidence. This suggests that the reconstructed time period of basin activity based on the occurrence of terraces at positions just above and below the basin surface, may be a good method to estimate basin activity, so we proceed to extend the method to all tectonic basins in the lower Miño valley. All subsided block (basin) surface positions in the lower Miño region (Viveen et al., 2013b, see Chapter 5) are plotted against longitudinal terrace profiles (Fig. 6.12), showing that almost all basin surfaces are located at positions at or below the T5 terrace. This suggests that enhanced extension along the predominantly N-S trending faults occurred over a relatively short time span of the past ±500 ka, and thus has not been continuous through time. The only exception is the small basin directly below the T7 terrace (Fig. 6.12), but this basin is located in a N-S trending valley that is likely dating back from the Miocene and where possible strike-slip activity might have been active since then, as evidenced from the thick infill of kaolinite clays and fluvial sediments (Sos-Baynat, 1965; De Vicente and Vegas, 2009). These inferences indicate that strain transfer from the northern Iberian plate boundary toward the northwestern Iberian Atlantic margin (De Vicente and Vegas, 2009) still occurs and locally re-activates faults and block tilt. It also indicates that relatively subtle tectonic motions already have a profound influence on the composition and distribution of terrace staircases and tectonic basins.

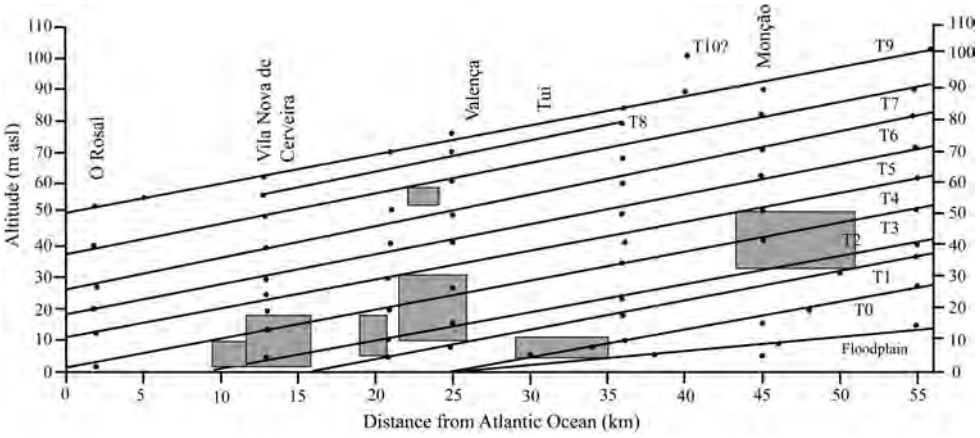

Fig. 6.12. Long-distance terrace correlations for the lowermost 55-km reach of the Miño River (Viveen et al., 2013a). Grey squares show where tectonic basins are located and at what position with respect to the terrace levels. The tectonic basin surfaces are not flat, but grade towards the river. Therefore, the top part of a grey square shows the highest position of a tectonic basin surface (typically away from the river, in a perpendicular position with respect to the river); and the bottom part of a grey square shows the lowest tectonic basin surface height (part of the basin surface closest to the river).

In long-term fluvial research, much attention has been paid to the influence of climate change (Vandenberghe, 2008; Bridgland and Westaway, 2008a; 2012), and more recently, to regional tectonic motions (Bridgland and Westaway, 2008b). Little attention has been paid so far to small-scale tectonic influences on terrace formation, even though they apparently exert a first-order control on terrace formation. We therefore foresee a stronger need for the integration of fluvial terrace research with the field of tectonic geomorphology in the near future. Our reconstructions demonstrate that regional calculated uplift rates in tectonically active areas can easily yield underestimations of uplift rates affected by local tectonic activity. The differences in uplift rates of different tectonic blocks leading to unpaired terraces can still be relatively well estimated from the terrace altitudinal differences with again a tendency to underestimate the rate difference. The occurrence of localised tectonic block subsidence leading to basins has a strong effect on the sediment distribution and preservation in a river valley. The observed sediment thickness is an underestimation of the actual amount of subsidence. Perhaps the most important insight of our simulations is that terrace correlations using sediment thickness as correlation measure may be wrong in settings with differential block movement. Until now, terraces along and across a river tend to be correlated on basis of similarities in sediment thicknesses and stratigraphy (Cunha et al., 2008; Martins et al., 2009; Briant et al., 2012). Fill and strath terraces across a river are therefore considered to have formed in different time periods under different climatic conditions, whereby fill terraces are considered the result of periods of aggradation and strath terraces of lateral erosion (Hancock and Anderson, 2002; Gibbard and Lewin, 2009). But this may not be necessarily true as relative subtle differential uplift may form both fill and strath terraces at the same time. It is therefore possible that many current fluvial terrace correlation schemes world-wide are too simplistic, as fill and strath terraces are not considered synchronous.

6.6 Conclusions

Integrated modelling of terrace formation for the studied area in the lower Miño River valley demonstrate that only scenarios with the combined influence of regional tectonic uplift and localized differential crustal block uplift including subsidence, yield realistic modelling outcomes. Leaving one of these tectonic factors out of the modelling scenarios, leads to the formation of terrace staircases and sediment distribution outputs that do not compare well with mapped terrace levels and sediment thicknesses. The three tectonic components together influence fluvial terrace formation, making the situation more complex than previously suggested. The results indicate that a vertical regional uplift rate of 0.10 m ka^{-1} over the past 600 ka, gives the most realistic results. This rate is slightly higher than earlier reconstructed uplift rates just west of the studied area, but fits in the overall tectonic context of increasing uplift from the Iberian Atlantic margin eastwards. The localized block subsidence occurs at similar rates as the regional uplift. It is hypothesised

that localised block (basin) subsidence in the region occurred predominantly during the past 500 ka, indicating non-continuous fault activity during the Quaternary. The effect of the localized subsidence is that the majority of the fluvial sediments are stored in the local basin, inducing sediment starvation of the surrounding uplifting blocks, and in turn causing synchronous strath terrace formation across the valley. The lower Miño River runs across an active fault, and delimitates two tectonic blocks on the north and south bank, that experience a subtle difference (0.10 versus 0.12 m ka^{-1}) in tectonic uplift rates. This causes unpaired fill and strath terraces with altitudinal differences of in total 10 m. The formation of both fill and strath terraces in the same time period shows that terrace correlation schemes on basis of similarities in sediment thicknesses and facies is a too simplistic approach.

Chapter 7

Synthesis

7.1 The effects of climatic change on river development

Climate change is a major driver for terrace formation in many river systems world-wide (Bridgland and Westaway, 2008a). Although in Europe glacial periods tend to be generally drier than interglacial periods, they experience higher annual peak discharges and an increase in hill slope-derived sediment supply. This causes an increase in the ratio sediment load: discharge during glacials and also stadials (Bogaart and Van Balen, 2000). Consequently, many river terraces in for instance NW and central Europe register terrace aggradation during glacials and stadials (Starkel, 2003; Cordier et al., 2009) and interglacial terraces are generally limited (Gibbard and Lewin, 2002). Often, these cold-climate terraces are made up of gravels and coarse sands (Gibbard and Lewin, 2009). Additionally, the headwaters of European river systems were often glaciated, and glacier retreat during climate amelioration resulted in increased discharge and sediment load (Starkel, 2003; Harmand and Cordier, 2012; Stange et al., 2013). Climate transitions, especially the warm-cold transitions, are the periods in which often terrace incision occurs. These transitions are usually characterised by degradation in vegetation and the instable climate causes more frequent peak discharges, resulting in lateral and vertical erosion (Antoine et al., 2007; Vandenberghe, 2008). Alternatively, terrace incision events have also been reported during the cold-warm transitions. Large quantities of glacial melt water and an initial sediment pulse were followed by a stabilisation of vegetation, leading to a drop in sediment load, and causing pronounced incision (Bridgland, 2000; Maddy et al., 2001; Stange et al., 2013). Climate changes in the Miño-Sil basin were expressed by changes in vegetation from deciduous forest to open grassland, and from wetter to drier conditions (Desprat et al., 2005, 2006, 2007, 2009, Desprat, unpublished data; Sanchez-Goñi et al., 2005, 2008; Naughton et al., 2009). The upper Sil catchment experienced frequent phases of glacier advance and retreat (Jalut et al., 2010; Moreno et al., 2010, 2012; Delmas et al., 2011), but the extent of the glaciers was always relatively small (Vieira, 2008; Cowton et al., 2009; Rodriguez-Rodriguez, 2011). Thus, because of the highly unstable past climate in northwestern Iberia, one would expect that the Miño-Sil system responded to these changes and that these changes are preserved in the fluvial terrace facies, just like in terrace deposits from river systems elsewhere. In northwestern mainland European river systems for instance, climate fluctuations within a glacial cycle are visible as alternating layers with different grain sizes and as local incisions in the underlying sediments (Vandenberghe, 2002; Kasse et al., 2003; Vandenberghe, 2003). In the United Kingdom for instance, terraces are usually glacial, coarse-grained sediment bodies, showing distinct phases of river activity within one terrace body (Lewin and Gibbard, 2010). Such a distinct stratigraphy is lacking in the Miño terraces. The Miño terraces are always made up of coarse gravels without changes in facies distribution, and sometimes interbedded with small sand or clay lenses. These gravelly terraces are also considered of cold-climate origin, because the current lower Miño River only transports fine sands and lacks the stream power and

capacity to transport gravels all the way to the coast. Additional evidence stems from changes in ^{10}Be concentrations with depth that are clearly exponential without any obvious trend breaks (Viveen et al., 2012b, see Chapter 3). This indicates that the terrace gravels were deposited within a very short time period, instead of over a large part of a glacial cycle as envisaged by Bridgland (2000). This seems further confirmed by calculations of the transport time of the Miño gravels (Viveen et al., 2012b, see Chapter 3): all gravels investigated have a similar history of inherited ^{10}Be concentrations, which was caused by transportation of the gravels from the head waters of the Miño-Sil system towards the coast. The calculated maximum transport times on the basis of the inherited concentrations range from 8.7 to 15 ka, again indicating that the gravels were deposited during a relatively short time. The terrace gravels were probably deposited during the transition to a glacial period, just after removal of any earlier interglacial floodplain deposits, which were subsequently incised. A similar model was presented by Bridgland (2000), although in his model, sedimentation occurs throughout a glacial period. However, the increase in stream capacity of the lower Miño River does not seem to be controlled by an increase in discharge related to changes in rainfall, vegetation or glacial melt. Model simulations show that neither a change in discharge rate, nor a change in discharge timing had an effect on the timing of sedimentation and erosion events (Viveen et al., 2013a, see Chapter 4), although it may of course be assumed that the transport capacity of the river is discharge dependent, and thus, controls the thickness of the fluvial deposits (Bogaart and Van Balen, 2000; Van Balen et al., 2010). It appears that another controlling mechanism is responsible for an increase in stream power of the river and thus, terrace formation. This is in agreement with reconstructions made for the Mondego and Tagus River systems along the western Iberian margin. There, terrace formation is either attributed to tectonic causes or glacioeustacy, but never to climate fluctuations (Cunha et al., 2005; 2008; Martins et al., 2010; Ramos et al., 2012). These factors are discussed in the next paragraphs.

7.2 The effects of glacioeustacy on river development

Glacioeustatic changes play an important role in the development of downstream reaches of fluvial systems (Blum and Törnqvist, 2000), but the exact extent of glacioeustic influences very much depends on local factors such as the drainage area, continental shelf dimensions versus coastal plain dimensions, and whether sea level drops below the shelf break during sea level fall (Talling, 1998; Blum and Törnqvist, 2000; Meijer, 2002; Törnqvist et al., 2006; Mattheus and Rodriguez, 2011). River systems near broad, sub horizontal continental shelves, such as the North Sea basin, or the Caspian Sea (Overeem et al., 2003) experience negligible effects due to relative fall in sea level, because these rivers mainly adapt by lengthening their channels several hundreds of km instead of adapting by incision

(Tebbens et al., 2000; Gargani et al., 2006; Antoine et al., 2007). A different situation exists where the continental shelf is short, and steeper than the coastal plain, because in these settings, a river cannot adjust its profile by channel lengthening and instead, will compensate by incising (Merritts et al., 1994; Blum and Törnqvist, 2000; Vis et al., 2008; Viveen et al., 2013a, see Chapter 4). Here, incised valleys will form (Blum and Törnqvist, 2000). This setting is more common in the USA, but rare in Europe, where they are predominantly found in the Bay of Biscay (Törnqvist et al., 2006), the northern and western Iberian margins, and in some parts of the Mediterranean, such as in south eastern France (Kettner and Syvitski, 2009). Therefore, river systems near short, steep continental shelves are suggested to follow a generalised pattern to glacioeustatic changes: During the initial fall in sea level, the river is not yet incising and responds by large-scale lateral erosion, thus removing any former (often interglacial) deposits, because the erosion base exceeds the base of the fluvial deposits (Gibbard and Lewin, 2002). At such transitions, the river tends to change from an interglacial meandering style to glacial braided style (Gibbard and Lewin, 2002). A similar change in style was also observed for the lower Miño River, based on changes in sediment calibre (Viveen et al., 2012b; 2013a, see Chapters 3 and 4). This indicates that during this stage of falling sea level, large quantities of sediments were deposited during a relatively short time period (Martin et al., 2011; Viveen et al., 2013a, see Chapter 4), which were subsequently incised to form cold stage, coarse-calibre, fluvial terraces (Viveen et al., 2013a, see Chapter 4). As discussed earlier, fast deposition is also suggested by the perfectly exponential decrease in ^{10}Be concentrations for the fluvial terraces in the lower Miño (Viveen et al., 2012b, see Chapter 3). When sea level rises again, the river responds by re-adjusting its profile, leading to a much lower gradient and less stream power. This in turn leads to the formation of a thick succession of fine-grained, fluvio-deltaic deposits at the transgressive shore line in the formerly incised valley. As the shoreline moves upstream due to increasingly rising sea level, so does the area where aggradation occurs. This results in the formation of a backfilling sedimentary wedge that fills up the formerly incised valley. The final thickness of this wedge may be several tens of m thick at the present-day (high stand) shore line, and taper out to zero m thickness more upstream where the influence of sea level is no longer present (Merritts et al., 1994; Blum and Aslan, 2006; Vis et al., 2008; Viveen et al., 2013a, see Chapter 4). Modelling results also show that the glacioeustatically-induced incision and deposition events travel 100 – 150 km upstream and are thus not confined to the near-coastal reach (Blum and Törnqvist, 2000; Tebbens and Veldkamp, 2000; Viveen et al., 2013a, see Chapter 4). There is also a significant lag in response times to glacioeustatically-induced base level changes along the river reach (Tebbens et al., 2000). The difference in response time to the same event between the most upstream and downstream parts, may be as much as a full glacial-interglacial cycle (Viveen et al., 2013a, see Chapter 4), confirming that fluvial terrace deposition and incision are diachronous events.

In this thesis the focus is placed on the large, glacial-interglacial events, but also sub events,

possibly related to minor sea-level fluctuations, appear to be registered in the terrace record. They usually occur as small, isolated terrace fragments at positions in between the larger terraces (Viveen et al., 2013a, see Chapter 4). They are, however, often difficult to distinguish, not only because of their local extent, but also because they are often partly eroded by lateral erosion of the river (cf Vandenberghe, 2008). The registration of even small sea level fluctuations in the terrace record again suggests the sensitivity of the fluvial system to glacioeustatic variations. Because glacioeustacy has such a dominant influence, and fluvial system response may lag so much behind the initial event that triggered the response, it is proposed that the standard denomination of "glacial" and "interglacial" terraces (cf Bridgland and Westaway, 2008a) in settings similar to the lower Miño River, is replaced by "glacioeustatically-controlled terraces" (Viveen et al., 2013a, see Chapter 4). Martin et al. (2011) argue that valley narrowing by glacioeustically-triggered incision is decoupled from terrace formation and that, hence, terraces, if already formed, are short-lived features. The well-defined, long-lived terrace staircase in the incised valley of the lower Miño (Viveen et al., 2012a; 2012b; 2013a, see Chapters 2 to 4), demonstrates that this is not true, at least in tectonically active settings. The effects of tectonics on terrace formation are explored in more detail in the following paragraphs.

7.3 The effects of vertical tectonic movements on river development

Over the past two decades, more and more evidence started to appear that tectonic uplift is a pre-requisite for fluvial terrace preservation, as this is the only way in which terraces can be preserved above the current river level (Veldkamp and Van den Berg, 1993; Maddy, 1997; Bridgland and Westaway, 2008b). Temporary terraces may be formed due to a drop in base level, usually because of sea level lowering. As sea level rises again, the terraces become submerged and are buried under a new stack of (finer) fluvial sediments (Blum and Törnqvist, 2000). Despite these findings, the idea continues to linger that terraces can be formed without uplift, for instance because of glacioeustatic motions only, or because of fluvial incision as a delayed response to Tertiary tectonics (e.g. Martin-Serrano and Molina, 2005). To demonstrate whether tectonic uplift is occurring, a variety of methods can be applied. In this thesis, cosmogenic ray exposure (CRE) and thermoluminescence dating were performed on a fluvial terrace staircase in the lower Miño. On the basis of the dating results, maximum incision rates of 0.07 to 0.09 m ka^{-1} for the past 650 ka were calculated. It was proposed that these could serve as proxies for tectonic uplift, if assuming that fluvial incision could always compensate for tectonic uplift (Viveen et al., 2012b, see Chapter 3). To further investigate this hypothesis of tectonic uplift, the formation of fluvial terraces was simulated under varying rates of tectonic uplift, using a numerical model that simulates river profile development. The modelling outcomes showed that a regional uplift

rate of 0.08 m ka^{-1} yielded terrace staircases and fluvial sediment thicknesses similar to the ones mapped in the field (Viveen et al., 2013a, see Chapter 4). Because this model was not capable of simulating terraces taking preservation potential into account, a different, quasi two-dimensional model was used that simulates terraces in the context of valley width (Viveen et al., submitted, see Chapter 6). These modelling outcomes show that an uplift rate of 0.10 m ka^{-1} gave the best match with the field situation. These slightly higher rates, compared to previous reconstructions can be explained by two factors: i) either the Miño River was not able to compensate all uplift by incision; or ii) uplift rate increases from the west towards the east in the Miño-Sil catchment. The latter trend was also proposed by Cabral (1995) and Viveen et al. (2012a, see Chapter 2), because towards the east, studied river profiles are ever less graded, show many knick points, and river valleys are ever more incised. Either way, the combination of the dating results and the two modelling exercises shows that calculating tectonic uplift rates solely on basis of dated terraces, leads to reasonable (cf Bridgland and Westaway, 2012b), but not always entirely accurate results. The often-used assumption of river incision being able to keep up pace with tectonic uplift (e.g. Maddy, 1997; Bridgland and Westaway, 2008b) is an over-simplification, even for large river systems such as the Miño-Sil system (cf Kiden and Törnqvist, 1998).
The assumption of homogenous regional uplift is often based on long-distance terrace correlations that tread parallel to a reference level, for instance the floodplain, or that at least have a similar gradient throughout the studied reach (cf. Briant et al., 2012). In this thesis, a long-gradient of 1 m km^{-1} was calculated for the entire lower Miño valley from positions of the oldest terraces, changes in quartzite pebble densities, and river profile gradient modelling (Viveen et al., 2013a, see Chapter 4). The different types of evidence seemed conclusive, and even resulted in a coherent, very detailed terrace map of the area (Viveen et al., 2013b, see Chapter 5). Still, the terrace modelling exercise indicated that the most upstream part of the lower Miño area possibly experiences higher uplift rates, and that the terrace correlations made earlier (prior to the modelling) are not entirely correct there, because then we assumed a regional, homogenous uplift rate of 0.08 m ka^{-1}. This shows that correlating terraces over larger distances in tectonically active areas should be done with great care, and preferably not solely on basis of a limited set of dating results (Martins et al., 2009; Briant et al., 2012; Perez-Alberti et al., 2013), and the assumption of regional uplift. Instead, the hypotheses of incision keeping pace with regional uplift, and the occurrence of homogenous regional uplift, should be tested beforehand. Numerical modelling has been shown to be a good tool for this.

7.4 The effects of local block movements on river development

One of the reasons why there has been so much disagreement between authors on the number of terraces and their positions in the lower Miño valley is because they did not take

the presence of local differential tectonic block movements into account (Viveen et al., 2012a, see Chapter 2). The presence of active normal and possibly left-lateral strike-slip faulting along N-S, NE-SW and E-W trending faults, caused relative subsidence of tectonic blocks, resulting in local tectonic basins (Viveen et al., 2012a, see Chapter 2), and locally more uplifted blocks (Viveen et al, 2013b, see Chapters 5 and 6). The tectonic basins were subsequently filled with fluvial sediments from the Miño River, and because of their flat surfaces and small dimensions, not distinguishable from normal fluvial terraces. Earlier authors did recognise that the Miño possibly runs across a series of faults because of the many sudden 90 degree turns the course of the river makes (Yepes-Temiño, 2002). But they did not infer that this might have had implications for the fluvial terrace distribution as well. In this thesis it was first shown that in the lower Miño valley, many tributaries have asymmetrically-developed catchments, which indicates the presence of active tilting of tectonic blocks (Viveen et al., 2012a, see Chapter 2). In a subsequent paper (Viveen et al., submitted, see Chapter 6), we demonstrated that tilting of some of these blocks was expressed through unequal uplift on both sides of the Miño River. This resulted in unpaired terraces, and an accumulated height difference of 10 m between the oldest terraces. Terraces on the faster uplifting block are also narrower, with less sediment preserved, mostly confined to small, incised gullies perhaps because the Miño had less time to laterally erode the valley wall and deposit sediments. Sediment starvation on the faster uplifting block was further exacerbated due to the presence of a relatively subsiding block on the other side of the river, which locally accumulated over 20 m of sediments. Such significant effects of small, fault-bounded blocks on terrace distribution have only been reported sparsely in the literature. One of the few examples is found in the SW Iberian Tagus River, where terrace mapping and dating with thermoluminescence techniques demonstrated that terraces were severely off-set because of active faulting (Cunha et al., 2008; Martins et al., 2009). Correlating terraces was only possible by dating terraces on each individual tectonic block. Other examples are the Segre and Gallego Rivers in NE Iberia (Stange et al., 2012). Similarly, the Dutch Maas River is proposed to run through an active fault, delimiting two separate tectonic blocks that caused unpaired terraces on both sides of the river (Veldkamp and Van den Berg, 1993). In the German Upper Rhine Graben, terraces were clearly displaced because of active faulting, again causing unpaired terrace sequences (Peters and Van Balen, 2007). These examples show that movements of local fault-bounded blocks are important factors in terrace distribution and sediment thicknesses.

7.5 Separating the effects of glacioeustacy, climate change, and tectonic movements

Glacioeustacy is the dominant process for river incision and terrace formation in river systems near a short, steep, continental shelf. Maximal glacioeustatic variations of 130 m (Bintanja et al., 2005) cause pronounced incision by the lower Miño River in the lowermost 67-km of its reach as well as a strong increase in stream power (Fig. 7.1). It controls the timing of terrace formation, the number of terraces that are formed, and the downstream gradient of the terrace surfaces. Climate change, that is the interplay in changes over time between vegetation cover, precipitation and parameters depending upon them, (such as river discharge and sediment load), led to an estimated fourfold increase in stream power (Viveen et al., 2013a, see Chapter 4). These dynamics do not affect the timing of terrace formation, nor the number of terraces, nor its downstream gradient in the lowermost 67-km reach of the Miño River (Fig. 7.1). So glacioeustatic motions have a dominant effect on terrace formation. This is the reason why along passive margins with a steep, continental shelf, river systems tend to have deeply incised river valleys and similar terrace staircases, despite different climate regimes (e.g. Martins et al., 2010; Ramos et al., 2012). It is possible that climate change does affect the middle and upper reaches of such river systems, as the effect of glacioeustacy is no longer present (Blum and Törnqvist, 2000). At various locations in the middle and upper reaches of the Miño-Sil system, local terrace staircases are found, usually where there is sufficient accommodation space, for instance in the Tertiary basins of A Rua, O Barco and the Bierzo (Martin-Gonzalez and Heredia, 2011), and where valley widening occurred because of less resistant bedrock associated with a fault (cataclastic shearing) (Perez-Alberti et al, 2013). In the upper reaches of the Miño-Sil, the effects of deglaciation events trigger stronger landscape responses because of their high intensity, whereas they are effectively smoothed out in the lower reaches. In the upper reaches for instance, alluvial terraces tend to have colluvial-torrential characteristics as well (Rodriguez-Fernandez, 1982).

A prerequisite for terrace preservation is the presence of tectonic uplift, as this moves the terraces away from the active river. Without tectonic uplift, the terraces would simply become a stack of accumulated sediments, without individual terrace scarps (Bridgland and Westaway, 2008a). There are certain limits to which extent vertical uplift is a favourable condition. In the lower Miño valley, a series of at least 3 fault-bounded, stepped peneplain surfaces is present that is assumed to be the resultant of a Mesozoic peneplain surface that was broken up in different blocks during the Alpine orogenesis (Yepes-Temiño, 2002). The 3 surfaces have general altitudes of 600-700 m, 1000-1200 m and 1500-1700 m, and mark the transition to increasingly higher uplift rates (Viveen et al., 2012a, see Chapter 2), see Fig. 7.1. The first peneplain with a calculated uplift rate of 0.08 m ka^{-1} is found in the

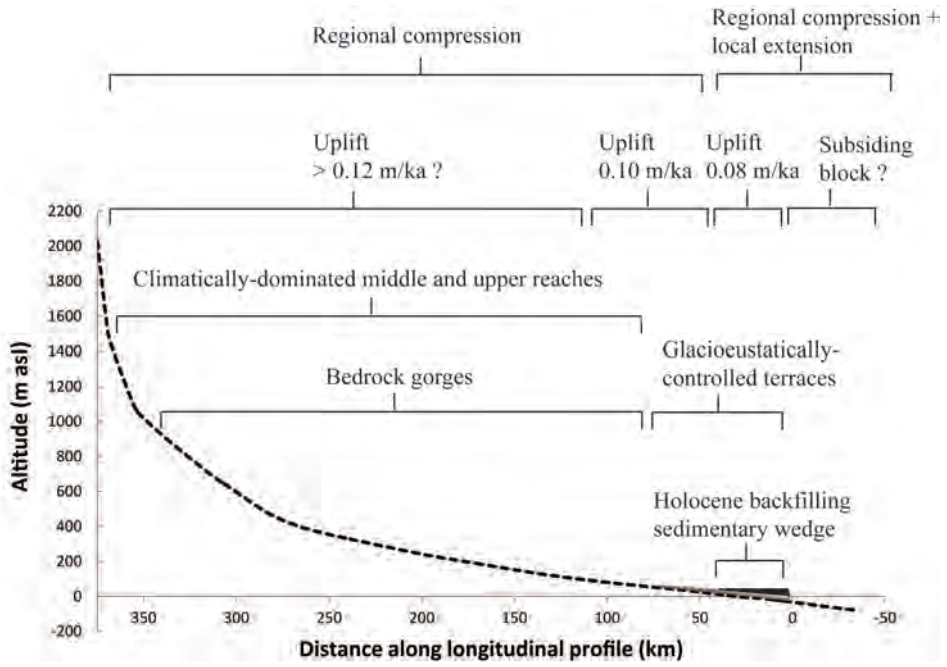

Fig. 7.1. Longitudinal profile of the Miño-Sil river system (dashed line). The Fig. shows upon which reaches of the river the different climatic, glacioeustatic, and tectonic controls act.

lowermost 40-km reach, and a second peneplain with an increased uplift rate of 0.10 m ka^{-1} is found from 40 to 110 km. The terrace staircase described by Perez-Alberti et al. (2013), just falls within the 0.10 m ka^{-1} uplift domain. These rates are considered optimal uplift rates for terrace preservation in other river systems (Veldkamp and Van den Berg, 1993; Veldkamp and Van Dijke, 2000), and perhaps therefore the most well-developed terrace staircase is found in the lower reach. Further upstream, fluvial terraces are no longer present (outside the tectonic basins), and the Miño-Sil runs through a bedrock gorge system (Fig 7.1). This change coincides with the transition to another, higher, large-scale peneplain surface (Fig. 7.1), where uplift rates probably exceed 0.12 m ka^{-1}, and terrace formation is no longer possible because vertical incision outpaces lateral valley wall erosion, preventing the river from forming fluvial terraces (Merritts et al., 1994). Cosmogenic Ray Exposure (CRE) dating of a marine terrace on the northern Iberian coast indeed suggests that uplift rates have been as high as 0.13 m ka^{-1} over the past 1 Ma (Alvarez-Marron et al., 2008). It is possible that another peneplain surface exists in the offshore part of the Miño River. Close to where the lower Miño River enters the Atlantic Ocean, a 700-m high N-S trending massif ends abruptly at the ocean. It is likely that here a N-S trending fault exists, along which block subsidence took place, which is now situated

below sea level (Fig. 7.1). Block subsidence along N-S trending faults have been observed elsewhere along the NW Iberian margin (Pinheiro et al., 1996; Muñoz et al., 2003). This further demonstrates that offshore, the stress regime is (locally) extensive, just as in the lowermost 50 km of the onshore part of the Miño River, as indicated by normal faulting and downlifting of tectonic basins (Viveen et al., 2012a, see Chapter 2). More upstream, a purely compressive regime is present (De Vicente and Vegas, 2009).

In conclusion, glacioeustacy and vertical tectonic uplift are the main controlling factors for terrace formation in settings similar as the Miño River. Also, there are a number of secondary factors that affect fluvial terrace patterns on a more local scale. Localised block movements may cause large terrace surfaces with thick stacks of sediments (tectonic basins), and cause unpaired terrace surfaces and unpaired sediment thicknesses. These movements only cause limited altitudinal differences of several tens of meters maximum (Cunha et al., 2008; Martins et al., 2009; Perez-Alberti et al., 2013; Viveen et al., 2013b, submitted, see Chapters 5 and 6) for the oldest terrace surfaces, and as such, only have a subtle influence on terrace formation. These small movements are not bound to a certain reach, but can occur anywhere along a river where active faulting occurs. Their effect will be most visible however, where well-developed terraces occur with up to a couple of meters of sediment. In the deltaic plain these effects will not be noticeable because several tens of meters of fluvio-deltaic sediment obscure the delicate difference in sediment thickness of the different blocks. Equally, in the upstream reaches where, if any at all, only strath terraces are formed, insufficient sediment may also obscure these subtle influences, especially in areas with granite bedrock, where erosive terraces may be confused with sub horizontal sheeting structures of the granite itself (Twidale and Vidal-Romani, 2005). In the lower reach of the Miño River, the tectonic basins were probably formed along normal and possibly strike-slip faulting in a locally extensive regime (Fig. 7.1), but in the middle and upper reaches, these basins are mainly compressive and the result of strike-slip, thrust, or oblique-thrust faulting (De Vicente et al., 2011; Martin-Gonzalez and Heredia, 2011). Local bedrock structure creates terrace accommodation space, especially where the bedrock is weakened by cataclastic sheering along faults.

7.6 Implications for further research

In this thesis it is demonstrated that fluvial terraces may be transient features in the landscape, with different response times to the same event that may be as full as a glacial-interglacial cycle. When they are formed during periods of sea level fall, their surfaces have a gradient that is not parallel to the current river bed (Viveen et al., 2013a, see Chapter 4). This has significant implications for long-distance terrace correlations within river basins near steep, short continental shelves, where glacioeustacy is probably the most dominant

factor for terrace formation. Such river systems are for instance found along the entire northern and western Iberian margins, western Africa and the United States. Too often terraces are correlated on basis of a limited dating set, or sedimentological characteristics (Briant et al., 2012; Stokes et al., 2012b), but this will be insufficient in the case of river systems that experience profound changes in their gradients over time, and where the same terrace may have a significantly different age along a river reach. A process-based approach whereby the influence of glacioeustatic movements on river profile development can be quantified would be needed to reliably correlate such terraces over longer distances.

Another topic that needs more attention in future terrace research is the prominence of variable uplift rates through time. Over larger time scales, for instance the entire Quaternary or even the late Cenozoic, this already happens (Bridgland and Westaway, 2008b) and it has been demonstrated that for instance during the Mid Pleistocene revolution, uplift increased, for which the cause is still under debate (Gibbard and Lewin, 2009). But on shorter time scales, for instance the middle or late Pleistocene periods, uplift rates are usually derived from incision calculations between a limited set of dated terraces, or even extrapolated on the basis of one observation (e.g. Ramos et al., 2012). In such scenarios it is insufficiently taken into account that on shorter time scales the local stress field may change, leading to variations in tectonic activity. This was demonstrated, for instance in Viveen et al., submitted, see Chapter 6, where tectonic basin activity has only been active for the past ±500 ka. Changes in uplift rates over middle to late Pleistocene timescales have been reported for the Avon and Frome Rivers in the United Kingdom, but in these cases changes in lower crustal flow regime, which in itself is suggested to be the result of climate-triggered, isostatic denudation response, was proposed to be the cause (Westaway et al., 2006).

The effect of local block movements is also a matter that needs more attention in fluvial terrace research. Terraces are still correlated on the basis of similarities in sediment thicknesses, or stratigraphy (Briant et al., 2012; Stokes et al., 2012b) and fill and strath terraces are considered to have formed under different conditions. However, we demonstrated that the difference between fill and strath terraces can have a tectonic rather than a climatic cause (Viveen et al., submitted, see Chapter 6). Other clear indications for faulting and local block tectonics are sudden bends in river channels that are not caused by meandering, asymmetrically-developed river catchments, knick points in river channels that coincide with the positions of lineaments and faults, seismic activity, uncharacteristically thick stacks of sediments in some terraces, and unpaired terraces. For some rivers in the Iberian Peninsula it has also been demonstrated that differential block movement leads to unpaired terraces (Cunha et al., 2008; Martins et al., 2009; Viveen et al., submitted, see Chapter 6), and also for northern Germany (Peters and Van Balen, 2007) and

the southern Netherlands (Veldkamp and Van den Berg, 1993). But for many tectonically active regions in Europe and overseas, terrace correlation schemes do not incorporate this effect of local block movement, even though some rivers are clearly structurally-controlled and undergo active faulting, and as such, local block movements may be expected. Examples include the Goring Gap through which the Thames flows in the UK (Bridgland and Schreve, 2009), the Massif Central region in France with its rift system (Veldkamp and Kroonenberg, 1993; Pastre, 2005; Larue, 2009), most river systems in southeast Europe, for instance in Greece (e.g. Maroukian et al., 2008), and the Moselle in Germany and France (Cordier et al., 2009). An interesting area in the Miño-Sil catchment itself is the tectonic Bierzo basin (Fig. 1.1). Here, the Cantabrian mountain belt thrusts over the northern border of the basin (De Vicente and Vegas, 2009) and the basin experienced several hundreds of meters of sedimentation with fluvial- and colluvial sediments. The Sil River formed a terrace staircase of 4 broad terraces on only one side of the river, suggesting the influence of block tilt. A preliminary assessment of fluvial terraces on the north eastern border of the basin, suggested many more terrace levels than in the basin itself. This might be due to differences in uplift (or down lift) rates between the Cantabrian Chain and the Bierzo basin.

In conclusion, this thesis has shown that regional and local tectonics have an important influence on the formation of fluvial terraces. Future research on fluvial terraces in tectonically active regions, even where tectonic activity is moderate, should therefore include a tectono-geomorphic analysis, of which ample examples are given in this thesis.

References

Abril-Hurtado, J. 1972. Hoja 298 La Guardia. Mapa geologico de España 1:50.000. I.G.M.E. Madrid, Servicio de publicaciones del Ministerio de Industria y Energia.

Abril-Hurtado, J. 1972. Hoja 299 Tomiño. Mapa geologica de España 1:50.000. I.G.M.E. Madrid, Servicio de publicaciones del Ministerio de Industria y Energia.

Adamiec, G., Aitken, M., 1998. Dose-rate conversion factors: update. Ancient TL 16, 37-50.

Alonso, A. and Pages, J.L., 2007. Stratigraphy of Late Pleistocene deposits in Northern Spain. Journal of Iberian Geology 33(2), 207-220.

Alvarez-Marron, J., Hetzel, R., Niedermann, S., Menendez, R., Marquinez, J., 2008. Origin, structure and exposure history of a wave-cut platform more than 1 Ma in age at the coast of northern Spain: a multiple cosmogenic nucleid approach. Geomorphology 93, 316-334.

Alves, M. I. C. and Pereira, D.I., 2000. A sedimentação e a gliptogenese no registro Cenozoico continental do Minho (NW Portugal). 1 Congresso sobre o Cenozoico de Portugal. Ciências da Terra (UNL), Lisboa. 14: 101-112.

Alves, M.I.C., 2004. A sedimentação fluvial Cenozoica na região do entre-Douro-e-Minho (NW de Portugal). In : Araujo, M.A., Gomes, A.A., (eds.), Geomorfologia do
noroeste da peninsula Iberica. Faculdade de letras da universidade do Porto, Porto, Portugal, pp. 93-115.

Anderson, R.S., Repka, J.L., Dick, G.S., 1996. Explicit treatment of inheritance in dating depositional surfaces using in situ 10Be and 26Al. Geology 24 (1), 47–51.

Andeweg, B., De Vicente, G., Cloetingh, S., Giner, J. and Muñoz-Martin, A., 1999. Local stress fields and intraplate deformation of Iberia: variations in spatial and temporal interplay of regional stress sources. Tectonophysics 305, 153-164.

Antoine, P., Lozouet, N.L., Chausse, C., Lautridou, J.-P., Pastre, J.-F., Auguste, P., Bahain, J.-J., Falgueres, C., Galehb, B., 2007. Pleistocene fluvial terraces from northern France (Seine, Yonne, Somme): synthesis, and new results from interglacial deposits. Quaternary Science Reviews 26, 2701-2723.

Anton, L., Muñoz-Martin, A., De Vicente, G., 2010. Alpine paleostress reconstruction and active faulting in western Iberia. Central European Journal of Geosciences 2(2), 152-164.

Arnold, M., Merchel, S., Bourlès, D.L., Braucher, R., Benedetti, L., Finkel, R.C., Aumaître, G., Gottdang, A. , Klein, M., 2010. The French accelerator mass spectrometry facility ASTER: Improved performance and developments. Nuclear Instruments and Methods in Physics Research B, 268, 1954 - 1959.

Benito, G., Sopeña, A.,Sanchez-Moya., Y, Machado, M.J., Perez-Gonzalez, A., 2003. Palaeoflood record of the Tagus River (central Spain) during the late Pleistocene and Holocene. Quaternary Science Reviews 22 (15-17), 1737-1756.

Beyer, H. L. 2004. Hawth's Analysis Tools for ArcGIS. www.spatialecology.com/htools, retrieved 8th of January 2009.

Bintanja, R., Van de Wal, R.S.W., Oerlemans, J., 2005. Modelled atmospheric temperatures and global sea levels over the past million years. Nature 437, 125-128.

Birot, P. and Solé-Sabaris, L., 1954. Recherches morphologiques dans le NW de la Peninsule Iberique. Memoires et documents C.N.R.S. 4, 7-61.

Blanco-Chao, R., Costa-Casais, M., Martinez-Cortizas, A., Perez-Alberti, A., Trenhaile, A.S., 2003. Evolution and inheritance of a rock coast: western Galicia, north western Spain. Earth Surface Processes and Landforms 28, 757-775.

Blum, M.D., Aslan, A., 2006. Signatures of climate vs. sea-level change within incised valley-fill successions: Quaternary examples from the Texas Gulf Coast. Sedimentary Geology 190, 177-211.

Blum, M.D., Törnqvist, T.E., 2000. Fluvial response to climate and sea-level change: a review and look forward. Sedimentology 47 (Suppl. 1), 2-48.

Boogaart, P.W., Van Balen, R.T., 2000. Numerical modeling of the response of alluvial rivers to Quaternary climate change. Global and Planetary Change 27 (1-4), 147-163.

Bogaart, P.W., Tucker, G.E., De Vries, J.J., 2003. Channel network morphology and sediment dynamics under alternating periglacial and temperate regimes: A numerical simulation study. Geomorphology 54 (3-4), 257-277.

Bourlès, D.L., Raisbeck, G.M., Yiou, Y., 1989. ^{10}Be and ^{9}Be in marine sediments and their potential for dating. Geochim. Cosmochim. Acta 53, 443-452.

Braucher, R. , Del Castillo, P., Siame, L., Hidy, A.J., Bourlès, D.L. 2009. Determination of both exposure time and denudation rate from an in situ-produced ^{10}Be depth profile: A mathematical proof of uniqueness. Model sensitivity and applications to natural cases. Quaternary Geochronology 4 (1), 56-67.

Braucher, R., Merchel, S., Borgomano, J., Bourlès, D., 2011. Production of cosmogenic radionuclides at great depths: A multi element approach. Earth Planet. Sci. Lett. 309, 1-9.

Briant, R.M., Bates, M.R, Marshall, G.D., Schwenninger, J.-L., Wenban-Smith, F.F., 2012. Terrace reconstruction and long profile projection: a case study from the Solent River system near Southampton, England. Proceedings of the Geologists' Association 123, 438-449.

Bridgland, D.R., 2000. River terrace systems in north-west Europe: an archive of environmental change, uplift and early human occupation. Quaternary Science Reviews 19, 1293-1303.

Bridgland, D. R., Keen, D., Westaway, R., 2007. Global correlation of Late Cenozoic fluvial deposits: a synthesis of data from IGCP 449. Quaternary Science Reviews 26(22-24), 2694-2700.

Bridgland, D.R., Schreve, D.C., 2009. Implications of new Quaternary uplift models for correlation between

the Middle and Upper Thames terrace sequences, UK. Global and Planetary Change 68 (4), 346-356.

Bridgland, D., Westaway, R., 2008a. Climatically controlled river terrace staircases: a worldwide Quaternary phenomenon. Geomorphology 98 (3-4), 285-315.

Bridgland, D.R, Westaway, R., 2008b. Preservation patterns of Late Cenozoic fluvial deposits and their implications: Results from IGCP 449. Quaternary International 189, 5-38.

Bridgland, D.R., Westaway, R., 2012. The use of fluvial archives in reconstructing landscape evolution: the value of sedimentary and morphostratigraphical evidence. Netherlands Journal of Geosciences 91 (1-2), 5-24.

Brocard, G.Y., Van der Beek, P.A., Bourlès, D.L., Siame, L.L., Mugnier, J.-L., 2003. Long-term £uvial incision rates and postglacial river relaxation time in the French Western Alps from ^{10}Be dating of alluvial terraces with assessment of inheritance, soil development and wind ablation effects. Earth and Planetary Science Letters 209, 197-214.

Brown, E.T., Edmond, J.M., Raisbeck, G.M., Yiou, F., Kurz, M.D., Brook, E.J., 1991. Examination of surface exposure ages of Antarctic moraines using in situ produced ^{10}Be and ^{26}Al. Geochimica et Cosmochimica Acta, Vol. 55, 2269-2283.

Brown, E.T., Bourlès, D.L., Colin, F., Raisbeck, G.M., Yiou, F., Desgarceaux, S., 1995. Evidence for muon-induced production of 10Be in near-surface rocks from the Congo. Geophysical Research Letters 22 (6), 703–706.

Brum Ferreira, A., 1991. Neotectonics in northern Portugal. A geomorphological approach. Z. Geomorph. N.F. Suppl. bd. 82, 73-85.

Bull, W.B., 1991. Geomorphic Responses to Climatic Change. Oxford University Press, New York, USA.

Bull, W. B., 2007. Tectonic geomorphology of mountains: a new approach to paleoseismology, Blackwell Publishing.

Burbank, D. W. and Anderson, R.S., 2001. Tectonic geomorphology, Blackwell Science.

Busschers, F.S., Kasse, C., van Balen, R.T., Vandenberghe, J., Cohen, K.M., Weerts, H.J.T., Wallinga, J., Johns, C., Cleveringa, P., Bunnik, F.P.M., 2007. Late Pleistocene evolution of the Rhine Meuse system in the southern North Sea basin: imprints of climate change, sea-level oscillation and glacio-isostacy. Quaternary Science Reviews 26, 3216-3248.

Butzer, K.W., 1967. Geomorphology and stratigraphy of the Paleolithic site of Budiño. Eiszeitalter und Gegenwart 18, 82-103.

Buylaert, J. P., Murray, A. S., Thomsen, K. J. and Jain, M., 2009. Testing the potential of an elevated temperature IRSL signal from K-feldspar. Radiation Measurements 44 (5-6), 560-565.

Cabral, J., 1995. Neotectonica em Portugal continental. Memórias do Instituto Geológico e Mineiro 31.

Candido de Medeiros, 1970. Carta geologica de Portugal, escala 1:50.000. Hoja 5A Viano do Castelo. Direcção Geral de Minas e Serviços Geologicos.

Cano-Pan, J., Aguirre-Enriquez, E., Giles-Pacheco, F., Gracia-Prieto, J., Santiago-Perez, A., Mata-Almonte, E., Gutierrez-Lopez, J.M., Diaz-Del Olmo, F., Baena-Escudero, R., Borja, F., 1997. Evolucion del Pleistoceno en la cuenca baja del Miño, sector La Guardia-Tuy. Secuencia de los primeros poblamientos humanos y registro arqueologico. Actas Cuaternario Iberico, Huelva, Spain, pp. 201-212.

Cano-Pan, J., Aguirre-Enriquez, E., Giles-Pacheco, F., Gracia-Prieto, J., Santiago-Perez, A., Mata-Almonte, E., Gutierrez-Lopez, J.M., Aguilera-Rodriquez, L., Prieto-Reina, O., 1999a. Secuencia cronoestratigrafica y poblamiento paleolitico en la cuenca media-baja del rio Miño. Sector Tuy (Pontevedra)-Cortegada (Orense). In: Palli-Buxo, L., and Roque-Pau, C. (Eds.), Avances en el estudio del Cuaternario español, Girona, Spain, pp. 231-240.

Cano-Pan, J., Fumanal, M.P., Ferrer, C., Usera, J., Blazquez, A.M., Olmo, J., 1999b. Evolution of the Southern Coast of Galicia (Spain) over Upper Quaternary. Zeitschrift Fur Geomorphologie 43, 521-540.

Carvalho, G. S., 1981. Uma metodologia para analise dos depositos do quaternario. Arqueologia 4, 3-18.

Carvalho, A.F. and Rosa, M.M.P., 1988. Localizacão do Paleovale do Rio Douro. Anais do Instituto Hidrografico 9, 77–82.

Casas-Sainz, A. M. and De Vicente, G., 2009. On the tectonic origin of the Iberian topography. Tectonophysics 474(1-2), 214-235.

Chmeleff, J., von Blanckenburg, F., Kossert, K., Jakob, J., 2010. Determination of the ^{10}Be half-life by multicollector ICP-MS and liquid scintillation counting. Nuclear Instruments and Methods in Physics Research B, 268 (2), 192-199.

Claessens, L., Veldkamp, A., Ten Broeke, E.M., Vloemans, H., 2009. A Quaternary uplift record for the Auckland region, North Island, New Zealand, based on marine and fluvial terraces. Global and Planetary Change 68 (4), 383-394.

Cloetingh, S., Burov, E., Beekman, F., Andeweg, B., Andriessen, P.A.M., Garcia-Castellanos, G., De Vicente, G., Vegas, R., 2002. Lithospheric folding in Iberia. Tectonics 21(5), 1-26.

Cloetingh, S., Gallart, J., De Vicente, G., Matenco, L., 2011. TOPO-EUROPE: From Iberia to the Carpathians and analogues. Tectonophysics 502 (1-2), 1-27.

Cloetingh, S., Ziegler, P.A., Beekman, F., Andriessen, P.A.M., Matenco, L., Bada, G., Garcia-Castellanos, D., Hardebol, N., Dezes, P., Sokoutis, D., 2005. Lithospheric memory, state of stress and rheology: neotectonic controls on Europe's intraplate continental topography. Quaternary Science Reviews 24 (3-4), 241-304.

Coelho, A., Chamine, H.I., Gomes, A., Fonseca, P.E., Rocha, F.T., 2009. Kaolin deposits along the Espinho–Albergariaa- Velha metamorphic belt (NW Portugal): structural geology and morphotectonics framework. Cadernos Lab. Xeolóxico de Laxe 34, 89-120.

Cordier, S., Frechen, M., Harmand, D., 2009. The pleistocene fluvial deposits of the Moselle and middle Rhine valleys: new correlations and compared evolutions. Quaternaire 20 (1), 35-47.

Cotilla-Rodriguez, M. O. and Cordoba-Barba, D., 2003. Caracterizacion morfotectonica de Galicia, España. Revista Geofisica 58, 5-56.

Cowton, T., Hughes, P.D., Gibbard, P.L., 2009. Palaeoglaciation of Parque Natural Lago de Sanabria, northwest Spain. Geomorphology 108, 282-291.

Cox, R. T., 1994. Analysis of drainage basin symmetry as a rapid technique to identify areas of possible Quaternary tilt-block tectonics: An example of the Mississippi embayment. Geological Society of America bulletin 106, 571-581.

Cunha, P.P., Martins, A.A., Daveau, S., Friend, P.F., 2005. Tectonic control of the Tejo river fluvial incision during the late Cenozoic, in Ródão -central Portugal (Atlantic Iberian border). Geomorphology 64, 271-298.

Cunha, P.P., Martins, A.A., Huot, S., Murray, A., Raposo, L., 2008. Dating the Tejo river lower terraces in the Rodão area (Portugal) to assess the role of tectonics and uplift. Geomorphology 102, 43-54.

D'Allesandro, L., Miccadei, E., Piacentini, T., 2008. Morphotectonic study of the lower Sangro River valley (Abruzzi, Central Italy). Geomorphology 102, 145-158.

De Moor, J.J.W., Kasse, C., Van Balen, R., Vandenberghe, J., Wallinga, J., 2008. Human and climate impact on catchment development during the Holocene - Geul River, the Netherlands. Geomorphology 98 (3-4), 316-339.

De Mulder, E.F.J., Geluk, M.C., Ritsema, I., Westerhoff, W.E., Wong, T.E. (eds.), 2003. De ondergrond van Nederland. NITG-TNO, Utrecht, 379 p.

De Vicente, G., Cloetingh, S., Muñoz-Martin, A., Olaiz, A., Stich, D., Vegas, R., Galindo-Zaldivar, J., and Fernandez-Lozano, J., 2008. Inversion of moment tensor focal mechanisms for active stresses around Microcontinent Iberia: tectonic implications. Tectonics 27, 1-22.

De Vicente, G., Vegas, R., 2009. Large-scale distributed deformation controlled topography along the western Africa-Eurasia limit: tectonic constraints. Tectonophysics 474, 124-143.

De Vicente, G., Cloetingh, S., Van Wees, J.D., Cunha, P.P., 2011. Tectonic classification of Cenozoic Iberian foreland basins. Tectonophysics 502 (1-2), 38-61.

Delmas, M., Calvet, M., Gunnell, Y., Braucher, R., Bourles, D., 2011. Palaeogeography and ^{10}Be exposure-age chronology of middle and late Pleistocene glacier systems in the northern Pyrenees: implications for reconstructing regional palaeoclimates. Palaeogeography, Palaeoclimatology, Palaeoecology 305, 109-122.

DeLong, S.B. and Arnold, L.J., 2007. Dating alluvial deposits with optically stimulated luminescence, AMS ^{14}C, and cosmogenic techniques, western Transverse Ranges, California, USA. Quaternary Geochronology 2, 129-136.

Desprat, S., 2005. Reponses climatiques marines et continentales du sud-ouest de l'europe lors des derniers interglaciaires et des entrees en glaciations. Ph.D. thesis. University of Bordeaux 1, Bordeaux, France.

Desprat, S., Sanchez-Goñi, M.F., Turon, J.-L., McManus, J.F., Loutre, M.F., Duprat, J., Malaize, B., Peyron, O., Peypouquet, J.-P., 2005. Is vegetation responsible for glacial inception during periods of muted insolation changes? Quaternary Science Reviews 24, 1361-1374.

Desprat, S., Sanchez-Goñi, M.F., Turon, J.-L., Duprat, J., Malaize, B., Peypouquet, J.-P., 2006. Climate variability of Marine Isotope Stage 7: direct land-sea-ice correlation from a multiproxy analysis of a north-western Iberian margin deep-sea core. Quaternary Science Reviews 25, 1010-1026.

Desprat, S., Sanchez-Goñi, M.F., Turon, J.-L., Duprat, J., Malaize, B., Cortijo, E., Peypouquet, J.-P., 2007. Climate variability of the last five isotopic interglacials: direct land-sea-ice correlation from the multiproxy analysis of north-western Iberian margin deep sea cores. Developments in Quaternary Science 7 (C), 375-386.

Desprat, S., Sanchez-Goñi, M.F., McManus, J.F., Duprat, J., Cortijo, E., 2009. Millennial-scale climatic variability between 340 000 and 270 000 years ago in SW Europe: evidence from a NW Iberian margin pollen sequence. Clim. Past 5, 53-72.

El Hamdouni, R., Irigaray, C., Fernandez, T., Chacon, J., Keller, E.A., 2008. Assessment of relative active tectonics, southwest border of the Sierra Nevada (southern Spain). Geomorphology 96, 150-173.

FAO, 2000. Lecture notes on the major soils of the world. World Soil Resources Reports 94. Food and Agriculture Organization of the United Nations, Rome. 334 pp.

Fernandez-Mosquera, D., Marti, K., Vidal-Romani, J.R., Weigel, A., 2000. Late Pleistocene deglaciation chronology of the NW Iberian Peninsula using cosmic-ray produced 21Ne in quartz. Nuclear Instruments and Methods in Physics Research B 172, 832-837.

Font, M., Amorese, D., Lagarde, J-L., 2010. DEM and GIS analysis of the stream gradient index to evaluate effects of tectonics: the Normandy intraplate area (NW France). Geomorphology 119, 172-180.

Garcia-De Celis, A., 1997. El relieve de la montaña occidental de Leon. Ph.D. thesis, Universidad de Valladolid, Valladolid, Spain.

Garcia-Garcia, A., Garcia-Gil, S., Vilas, F., 2005. Quaternary evolution of the Ria de Vigo, Spain. Marine Geology 220, 153-179.

Garcia-Gil, S., Vilas-Martin, F., Muñoz, A., Acosta, J., Uchupi, E., 1999. Quaternary sedimentation in the Ria de Pontevedra (Galicia), NW Spain. Journal of Coastal Research 15(4), 1083-1090.

Garcia-Castellanos, D., Verges, J., Gaspar-Escribano, J., Cloetingh, S., 2003. Interplay between tectonics, climate, and fluvial transport during the Cenozoic evolution of the Ebro Basin (NE Iberia). Journal of Geophysical Research B: Solid Earth 108 (7), 1-8.

Gardner, T., Webb, J., Pezzia, C., Amborn, T., Tunnell, R., Flanagan, S., Merritts, D., Marshall, J., Fabel, D., Cupper, M.L., 2009. Quaternary Science Reviews 28, 39-53.

Gargani, J., Stab, O., Cojan, I., Brulhet, J., 2006. Modelling the long-term fluvial erosion of the River Somme during the last million years. Terra Nova 18 (2), 118-129.

Gasparini, N.M., Bras, R.L., Whipple, K.X., 2006. Numerical modeling of non-steady-state river profile evolution using a sediment-flux-dependent incision model. Special paper of the Geological Society of America 398, 127-141.

Gibbard, P.L., Lewin, J., 2002. Climate and related controls on interglacial fluvial sedimentation in lowland Britain. Sedimentary Geology 151, 187-210.

Gibbard, P.L., Lewin, J., 2009. River incision and terrace formation in the Late Cenozoic of Europe. Tectonophysics 474, 41-55.

Guralnik, B., Matmon, A., Avni, Y., Porat, N., Fink, D., 2011. Constraining the evolution of river terraces with integrated OSL and cosmogenic nucleid data. Quaternary Geochronology 6, 22-32.

Hack, J. T., 1973. Stream-profile analysis and stream-gradient index. U.S. Geological Survey Journal of research 1, 421-429.

Hancock, G.S., Anderson, R.S., Chadwick, O.A., Finkel, R.C., 1999. Dating fluvial terraces with 10 Be and 26Al profiles: application to the Wind River, Wyoming. Geomorphology 27, 41–60.

Hancock, G.S., Anderson, R.S., 2002. Numerical modelling of fluvial strath-terrace formation in response to oscillating climate. Geological Society ofAmerica Bulletin 114 (9), 1131-1142.

Hare, P. W. and Gardner, T.W., 1985. Geomorphic indicators of vertical neotectonism along converging plate margins, Nicoya Peninsula, Costa Rica. Tectonic geomorphology: proceedings of the 15th Annual Binghamton geomorphology symposium.

Harmand, D., Cordier, S., 2012. The pleistocene terrace staircases of the present and past rivers downstream from the vosges massif (Meuse and Moselle catchments). Netherlands Journal of Geosciences 91 (1-2), 91-109.

Hayakawa, Y.S., Oguchi, T., 2006. DEM-based identification of fluvial knickzones and its application to Japanese mountain rivers. Geomorphology 78, 90-106.

Heisinger, B., Lal, D., Jull, A.J.T., Kubik, P., Ivy-Ochs, S., Knie, K., Nolte, E. 2002. Production of selected cosmogenic radionuclides by muons 2: Capture of negative muons. Earth and Planetary Sciences Letters 200, 357-369.

Hernandez-Pacheco, F., 1949. Geomorfologia de la cuenca media del Sil. Memoria de Real Academia de Ciencias exactas, fisicas y naturales 13.

Hidy, A. J., Gosse, J.C., Pederson, J.L., Mattern, J. P., Finkel, R.C., 2010. A geologically constrained Monte Carlo approach to modeling exposure ages from profiles of cosmogenic nuclides: An example from Lees Ferry, Arizona. G cube Vol 11, doi: 10.1029/2010GC003084.

Holcombe, R. J. 2003. GEOrient version 9.1. www.holcombe.net.au/software/index.html, retrieved 1st of

December 2010.

Hossain, S.M, De Corte, F., Vandenberghe, D., Van den haute, P., 2002. A comparison of methods for the annual radiation dose determination in the luminescence dating of loess sediment. Nuclear Instruments and Methods in Physics Research A 490 (3), 598-613.

Howard, J.L., Amos, D.F., Daniels, W.L., 1995. Micromorphology and dissolution of quartz sand in some exceptionally ancient soils. Sedimentary Geology 105, 51-62.

Huntley, D. J. and Baril, M. R., 1997. The K content of the K-feldspars being measured in optical dating or in thermoluminescence dating. Ancient TL 15 (1), 11-13.

Huntley, D. J., Hancock, R. G. V., 2001. The Rb contents of the K-feldspar grains being measured in optical dating. Ancient TL 19 (2), 43-46.

Instituto Tecnologico Geominero de España, 2001. Mapa Geologico de la Peninsula Iberica, Baleares y Canarias. Scale 1:1.000.000. ITGE, Madrid.

Jalut, G., Turu i Michels, V., Deboubat, J.-J., Otto, T., Ezquerra, J., Fontugne, M., Belet, J.M., Bonnet, L., De Celis, A.G., Redondo-Vega, J.M., Vidal-Romani, J.R., Santos, L., 2010. Palaeoenvironmental studies in NW Iberia (Cantabrian range): vegetation history and synthetic approach of the last deglaciation phases in the western Mediterranean. Palaeogeography, Palaeoclimatology, Palaeoecology 297 (2), 330-350.

Kasse, C., Vandenberghe, J., Van Huissteden, J., Bohncke, S.J.P., Bos, J.A.A., 2003. Sensitivity of Weichselian fluvial systems to climate change (Nochten mine, eastern Germany). Quaternary Science Reviews 22, 2141-2156.

Keller, E. A. and Pinter, N., 1999. Active tectonics: earthquakes, uplift and landscape. Upper Saddle River, New Jersey, Prentice Hall.

Kettner, A.J., Syvitski, J.P.M., 2008. HydroTrend v.3.0: A climate-driven hydrological transport model that simulates discharge and sediment load leaving a river system. Computers and Geosciences 34, 1170-1183.

Kettner, A.J., Syvitski, J.P.M., 2009. Fluvial responses to environmental perturbations in the northern Mediterranean since the Last Glacial Maximum. Quaternary Science Reviews 28, 2386-2397.

Khavari, R., Arian, M., Ghorashi, M., 2009. Neotectonics of the South Central Alborz drainage basin, in NW Tehran, N Iran. Journal of Applied Sciences 9 (23), 4115-4126.

Kiden, P., Törnqvist, T.E., 1998. Can river terrace flights be used to quantify Quaternary tectonic uplift rates? J. Quaternary Sci. 13 (6), 573-575.

Korschinek, G., Bergmaier, A., Faestermann, T., Gerstmann, U.C., Knie, K., Rugel, G.,Wallner, A., Dillmann, I., Dollinger, G., von Gostomski, Ch. L.., Kossert, K., Maiti , M., Poutivtsev, M., Remmert, A., 2010. A new value for the half-life of ^{10}Be by Heavy-Ion ElasticRecoil Detection and liquid scintillation counting. Nuclear Instruments and Methods in Physics Research B 268, 187–191.

Kueppers, U., Scheu, B., Spieler. O., Dingwell, D.B., 2005. Field-based density measurements as tool to identify pre-eruption dome structure: set-up and first results from Unzen volcano, Japan. Journal of Volcanology and Geothermal Research 141 (1-2), 65-75.

Ladekarl, U.L., Rasmussen, K.R., Christensen, S., Jensen, K.H., Hansen, B., 2005. Groundwater recharge and evapotranspiration for two natural ecosystems covered with oak and heather. Journal of Hydrology 300, 76-99.

Lal, D., 1991. Cosmic ray labeling of erosion surfaces: in situ nuclide production rates and erosion models. Earth Planet. Sci. Lett. 104, 424–439.

Lantzsch, H., Hanebuth, T.J.J., Bender, V.B., Krastel, S., 2009. Sedimentary architecture of a low-accumulation shelf since the late Pleistocene (NW Iberia). Marine Geology 259, 47-58.

Lantzsch, H., Hanebuth, T.J.J., Henrich, R., 2010. Sediment recycling and adjustment of deposition during deglacial drowning of a low-accumulation shelf (NW Iberia). Continental Shelf Research 30, 1665-1679.

Larue, J.-P., 2009. Morphodynamic evolution of the Orb River (Languedoc, France): evidence of eustatic, tectonic and climatic controls. Journal of Quaternary Science 24(3), 294-310.

Lautensach, H., 1945. Formação dos terraços interglaciarios do norte de Portugal e suas relaçoes com os problemas da epoca glaciaria. Publ. Soc. Geol. Portugal, 5-44.

Le Dortz, K., Meyer, B., Sébrier, M., Braucher, R., Bourlès, D., Benedetti, L., Fattahi, M., Nazari, H., Foroutan. 2012. Interpreting scattered in-situ produced cosmogenic nuclide depth-profile data. Quaternary Geochronology. doi: 10.1016/j.quageo.2012.02.020.

Leopold, L.B., Wolman, M.G., Miller, J.P., 1964. Fluvial Processes in Geomorphology. Freeman, San Francisco.

Lewin, J., Gibbard, P.L., 2010. Quaternary river terraces in England: forms, sediments and processes. Geomorphology 120, 293-311.

Lisiecki, L.E., Raymo, M.E., 2005. A Pliocene-Pleistocene stack of 57 globally distributed benthic $\delta^{18}O$ records. Paleoceanography 20, 1-17.

Lopez-Fernandez, C., 2008. Actividad sismica, zonacion sismotectonica y riesgo sismico en el no de la peninsula iberica. Serie Nova Terra 35, A Coruña, Instituto Universitario de Geologia Isidro Parga Pondal.

Maddy, D., 1997. Uplift-driven valley incision and river terrace formation in southern England. Journal of Quaternary science 12(6), 539-545.

Maddy, D., Bridgland, D.R., Green, C.P., 2000. Crustal uplift in Southern England: evidence from river terrace records. Geomorphology 33, 167-181.

Maddy, D., Bridgland, D., Westaway, R., 2001. Uplift-driven incision and climate-controlled river terrace development in the Thames Valley, UK. Quaternary International 79, 23-36.

Maddy, D., Demir, T., Bridgland, D.R., Veldkamp, A., Stemerdink, C., van der Schriek, T., Westaway, R. 2005. An

obliquity-controlled Early Pleistocene river terrace record from Western Turkey? Quaternary Research 63, 339-346.

Maroukian, H., Gaki-Papanastassiou, K., Karymbalis, E., Vouvalidis, K., Pavlopoulos, K., Papanastassiou, P., Albanakis, K., 2008. Morphotectonic control on drainage network evolution in the Perachora Peninsula, Greece. Geomorphology 102, 81-92.

Martin, J., Cantelli, A., Paola, C., Blum, M., Wolinsky, M., 2011. Quantative modeling of the evolution and geometry of incised valleys. Journal of Sedimentary Research 81, 64-79.

Martin-Gonzalez, F., 2009. Cenozoic tectonic activity in a Variscan basement: evidence from geomorphological markers and structural mapping (NW Iberian massif). Geomorphology 107, 210-225.

Martin-Gonzalez, F., Heredia, N., 2011. Complex tectonic and tectonostratigraphic evolution of an Alpine foreland basin: the western Duero basin and the related Tertiary depressions of the NW Iberian peninsula. Tectonophysics 502 (1-2), 75-89.

Martin-Gonzalez, F., Barbero, L., Capote, R., Heredia, N., Gallastegui, G., 2011. Interaction of two successive Alpine deformation fronts: constraints from low-temperature thermochronology and structural mapping (NW Iberian Peninsula). Int. J. Earth Sci. (Geol. Rundsch.), DOI 10.1007/s00531-011-0712-9.

Martins, A.A., Cunha, P.P., Buylaert, J.P., Huot, S., Murray, A.S., Dinis, P., Stokes, M., 2010. K-feldspar IRSL dating of a Pleistocene river terrace staircase sequence of the lower Tejo River (Portugal, western Iberia). Quaternary Geochronology 5, 176-180.

Martins, A.A., Cunha, P.P., Huot, S., Murray, A.S., Buylaert, J.P., 2009. Geomorphological correlation of the tectonically displaced Tejo River terraces (Gavião – Chamusca area, central Portugal) supported by luminescence dating. Quaternary International 199, 75-91.

Martin-Serrano, A., 1982. El Terciario de Galicia. Significado y posicion cronoestratigrafica de sus yacimientos de lignito. Tecniterrae 48, 19-41.

Martin-Serrano, A., 1989. Rasgos generales y problematica de las superficies de erosion de Galicia. Cuadernos Lab. Xeoloxico de Laxe 14, 7-18.

Martin-Serrano, A., 1994. El relieve del Macizo Hesperico: Genesis y cronologia de los principales elementos morfologicos. Cuaderno Lab. Xeoloxico de Laxe 19, 37-55.

Martin-Serrano, A. and Molina, E., 2005. El macizo Iberico. Mapa geomorfologico de España y del margen continental 1:1.000.000, Supplemental book 65-85. A. Martin-Serrano (Ed), Madrid, Instituto Geologico y Minero de España.

Martrat, B., Grimalt, J.O., Shackleton, N.J., De Abreu, L., Hutterli, M.A., Stocker, T.F., 2007. Four climate cycles of recurring deep and surface water destabilizations on the Iberian margin. Science 317 (5837), 502-507.

Matsuzaki, K.M.R., Eynaud, F., Malaizé, B., Grousset, F.E., Tisserand, A., Rossignol, L., Charlier, K., Jullien, E., 2011. Paleoceanography of the Mauritanian margin during the last two climatic cycles: from planktonic foraminifera to African climate dynamics. Marine Micropaleontology 79 (3-4), 67-79.

Mattheus, C.R., Rodriguez, A.B., 2011. Controls on late Quaternary incised-valley dimension along passive margins evaluated using empirical data. Sedimentology 58, 1113-1137.

Meijer, X.D., 2002. Modelling the drainage evolution of a river-shelf system forced by Quaternary glacio-eustacy. Basin Research 14, 361-377.

Merchel, S., Herpers, U., 1999. An update on radiochemical separation techniques for the determination of long-lived radionuclides via accelerator mass spectrometry. Radiochimica Acta 84, 215-219.

Merchel, S., Arnold, M., Aumaitre, G., Benedetti, L., Bourlès, D.L., Braucher, R., Alfimov, V., Freeman, S.P.H.T., Steier, P., Wallner, A., 2008. Towards more precise ^{10}Be and ^{36}Cl data from measurements at the 10-14 level: Influence of sample preparation. Nucl. Instrum. Meth. Phys. Res. Sect. B 266, 4921–4926.

Merritts, D.J., Vincent, K.R., Wohl, E.E., 1994. Long river profiles, tectonism, and eustacy: a guide to interpreting fluvial terraces. J. Geophys. Res. 99, 14031-14050.

Ministerio de Obras Publicas y Urbanismo (MOPU) – Centro de Estudio y Apoyo Tecnico (CEAT), 1982. Reconocimiento del terreno: Nuevo puente sobre el Rio Miño en la variante de la CN-550 de La Coruña a Vigo y Tuy. P.K. 26/30. Tramo Tuy-frontera Portuguesa Tuy (Pontevedra). Unpublished geotechnical report. Ref. 88433 / 88440-82003 AV /ij. Obra numero 2487.

Minasny, B., McBratney, A.B., Whelan, B.M., 2002. VESPER version 1.6, Australian Centre for Precision Agriculture, University of Sydney. www.usyd.edu.au/su/agric/acpa, retrieved 10th of March, 2009.

Molina-Ballesteros, E., Cantano-Martin, M., 2002. Study of weathering processes developed on old piedmont surfaces in western Spain: new contributions to the interpretation of the "Raña" profiles. Geomorphology 42, 279-292.

Moreira, A. and Simões, M., 1988. Noticia explicativa da folha 1-D Arcos de Valdevez. Carta geologica de Portugal escala 1:50.000, Serviços geologicos de Portugal.

Moreno, A., Valero-Garces, B.L., Jimenez-Sanchez, M., Dominguez-Cuesta, M.J., Pilar-Mata, M., Navas, A., Gonzalez-Samperiz, P., Stoll, H., Farias, P., Morellon, M., Corella, J.P., Rico, M., 2010. The last deglaciation in the Picos de Europa National Park (Cantabrian Mountains, northern Spain). Journal of Quaternary Science 25 (7), 1076-1091.

Moreno, A., Gonzalez-Samperiz, P., Morellon, M., Valero-Garces, B.L., Fletcher, W.J., 2012. Northern Iberian abrupt climate change dynamics during the last glacial cycle: A view from lacustrine sediments. Quaternary Science Reviews 36, 139-153.

Muñoz, A., Acosta, J., Uchupi, E., 2003. Cenozoic tectonics on the Galicia margin, northwest Spain. Geo-Marine Letters 23(1), 72-80.

Murray, A.S. and Wintle, A.G., 2000. Luminescence dating of quartz using an improved single-aliquot regenerative- dose protocol. Radiation Measurements 32, 57-73.

NASA, 2000. SRTM 90m Digital Elevation Data from the CGIAR-CSI Consortium for Spatial Information. University of Maryland, College Park, Maryland.

Naughton, F., Sanchez-Goñi, M.F., Desprat, S., Turon, J.-L., Duprat, J., Malaize, B., Joli, C., Cortijo, E., Drago, T., Freitas, M.C., 2007a. Present-day and past (last 25 000 years) marine pollen signal off western Iberia. Marine Micropaleontology 62, 91-114.

Naughton, F., Sanchez-Goñi, M.F., Drago, T., Freitas, M.C., Oliveira, A., 2007b. Holocene changes in the Douro estuary (north western Iberia). Journal of Coastal Research 233, 711-720.

Naughton, F., Sanchez-Goñi, M.F., Kageyama, M., Bard, E., Duprat, J., Cortijo, E., Desprat, S., Malaize, B., Jolv, C., Rostek, F., Turon, J.-L., 2009. Wet to dry climatic trend in north-western Iberia within Heinrich events. Earth and Planetary Science Letters 284 (3-4), 329-342.

Nonn, H., 1966. Les régions cotières de la Galice (Espagne). Etude géomorphologique. University of Strasbourg, France.

Nonn, H., 1967. Les terrasses du rio Mino inferieur. Localisation et etude sedimentologique. Revue de Geomorphologie Dynamique 17(3), 97-108.

Ohmura, A., 2011. Observed mass balance of mountain glaciers and Greenland Ice Sheet in the 20th Century and the present trends. Surv. Geophys. 32, 537-554.

Overeem, I., Veldkamp, A., Tebbens, L., Kroonenberg, S.B., 2003. Modelling Holocene stratigraphy and depocentre migration of the Volga delta due to Caspian Sea-level change. Sedimentary Geology 159 (3-4), 159-175.

Pais, J., Cunha, P.P., Pereira, D., Legoinha, P., Dias, R., Moura, D., Brum da Silveira, A., Kullberg, J.C., Gonzalez-Delgado, J.A., 2012. The Paleogene and Neogene of Western Iberia (Portugal): A Cenozoic record in the European Atlantic Domain. Springer, 158 pp.

Pannekoek, A. J., 1966. The geomorphology of the surroundings of the Ria de Arousa. Investigations in and around the Ria de Arousa, NW Spain. Leidse Geologische Mededelingen 37, 7-32.

Pannekoek A.J., 1970a. Pleistocene history of the Ria de Arosa. Leidse Geologische Mededelingen, 37, 174-176.

Pannekoek, A. J., 1970b. Additional geomorphological data on the ria area of western Galicia (Spain). Leidse Geologische Mededelingen 37, 185-194.

Pastre, J.-F., 2005. The river Allier terraces in Limagne (France). Stratigraphy and correlation with the Massif Central volcanism. Quaternaire 16 (3), 153-175.

Pederson, J.L., Anders, M.D., Rittenhour, T.M., Sharp, W.D., Gosse, J.C., Karlstrom, K.E., 2006. Using fill terraces to understand incision rates and evolution of the Colorado River in Eastern Grand Canyon, Arizona. Journal of Geophysical Research 111, F02003, doi:10.1029/2004JF000201.

Pereira, D.I. 1991. Evolução quaternaria do rio Minho na região entre s. Pedro da torre e Valença. Publicaçoes do museu e laboratorio mineralogico e geologico da universidade de Coimbra 112, 327-345.

Pereira, D.I., Alves, M.I.C., Araujo, M.A., Proença-Cunha, P., 2000. Estratigrafia e interpretação paleografica do Cenozoico continental do norte de Portugal. Ciencias da Terra (UNL) 14, 73-84.

Perez-Alberti, A., Gomes, A., Trenhaile, A., Oliveira, M., Horacio, J., 2013. Correlating river terrace remnants using an Equotip hardness tester: An example from the Miño River, northwestern Iberian Peninsula. Geomorphology, in press. http://dx.doi.org/10.1016/j.geomorph.2013.03.017.

Peters, G. and van Balen, R.T., 2007. Tectonic geomorphology of the Northern Upper Rhine graben. Global and Planetary Change 58, 310-334.

Pinheiro, L.M., Wilson, R.C.L., Pena dos Reis, R., Whitmarsh, R.B., Ribeiro, A., 1996. The western Iberian margin: a geophysical and geological overview. Proceedings of the Ocean Drilling Program, part B: scientific results 149, 3-23.

Pliego-Dones, D., Rubio-Navas, J., Abril-Hurtado, J., 1972. Hoja 261 Tuy. Mapa geologica de España 1:50.000. I.G.M.E. Madrid, Servicio de publicaciones del Ministerio de Industria y Energia.

Poręba, G.J., Fedorowicz S., 2005. Gamma spectrometry for OSL and TL dating of loess deposits at Dybawka and Tarnawce (SE Poland). Geochronometria 24, 27-32.

Posamentier, H.W., Vail, P.R., 1988. Eustatic controls on clastic deposition II –Sequence and systems tract models. In: Wilgus, C.K., Hastings, B.S., Kendall, C.G.S.C., Posamentier, H.W., Ross, C.A., Van Wagoner, J.C. (Eds.), Sea-level changes: an Integrated Approach. Eds. Special Publ. Soc. Econ. Paleont. Miner. 42, Tulsa, Oklahoma, pp. 125-154.

Ramos, A.M., Cunha, P.P., Cunha, L.S., Gomes, A., Lopes, F.C., Buylaert, J.-P., Murray, A.S., 2012. The River Mondego terraces at the Figueira da Foz coastal area (western central Portugal): geomorphological and sedimentological characterization of a terrace staircase affected by differential uplift and glacio-eustasy. Geomorphology 165-166, 107-123.

Repka J.L., Anderson, R.S., Finkel, R.C., 1997. Cosmogenic dating of fluvial terraces, Fremont River, Utah. EPSL 152, 59-73.

Ribeiro, A., 1990. Geodynamic evolution of the Iberian Massif. In: Dallmeyer, R.D., and Martinez-Garcia, E. (Eds.), Pre-Mesozoic geology of the Iberian Peninsula. Springer Verlag, Berlin, Germany, pp. 399-409.

Ribeiro, M.L., and Moreira, A., 1986. Noticia explicativa da folha 1-B Monção. Carta geologica de Portugal escala 1:50.000. Serviços geologicos de Portugal.

Rio-Barja, J., Rodriguez-Lestegas, F., 1992. Os rios Galegos, Consello da Cultura Galega, Santiago de Compostela, Spain, 303 pp.

Rodrigues, A., Magalhães, F., Dias, J.A., 1991. Evolution of the north Portuguese coast in the last 18.000 years. Quaternary International 9, 67-74.

Rodrigues, T., Voelker, A.H.L., Grimalt, J.O., Abrantes, F., Naughton, F., 2011. Iberian margin sea surface temperature during MIS 15 to 9 (580-300 ka): glacial suborbital variability versus interglacial stability. Paleoceanography 26, 1-16, PA1204, doi:10.1029/2010PA001927.

Rodriguez-Fernandez, L.R., 1982. Hoja 158 Ponferrada. Mapa geologica de España 1:50.000. I.G.M.E. Madrid, Servicio de publicaciones del Ministerio de Industria y Energia.

Rodriguez-Rodriguez, L., Jimenez-Sanchez, M., Dominguez-Cuesta, M.J., Rico, M.T., Valero-Garces, B., 2011. Last deglaciation in north western Spain: new chronological and geomorphologic evidence from the Sanabria region. Geomorphology 135, 48-65.

Rubio-Navas, J. 1981. Hoja 262 Salvatierra de Miño. Mapa geologico de España 1:50.000. I.G.M.E. Madrid, Servicio de publicaciones del Ministerio de Industria y Energia.

Salvany, J.M., 2004. Tilting neotectonics of the Guadiamar drainage basin, SW Spain. Earth Surface Processes and Landforms 29, 145-160.

Sanchez-Goñi, M.F., Loutre, M.F., Crucifix, M., Peyron, O., Santos, L., Duprat, J., Malaize, B., Turon, J.-L., Peypouquet, J.-P., 2005. Increasing vegetation and climate gradient in western Europe over the Last Glacial Inception (122-110 ka): data-model comparison. Earth and Planetary Science Letters 231, 111-130.

Sanchez-Goñi, M.F., Landais, A., Fletcher, W.J., Naughton, F., Desprat, S., Duprat, J., 2008. Contrasting impacts of Dansgaard–Oeschger events over a western European latitudinal transect modulated by orbital parameters. Quaternary Science Reviews 27, 1136-1151.

Santanach, P., 1994. Las cuencas Terciarias gallegos en la terminacion occidental de los relieves pirenaicos. Cuadernos Lab. Xeoloxico de Laxe 19, 57-71.

Santisteban, J.L., Schulte, L., 2007. Fluvial networks of the Iberian Peninsula : a chronological framework. Quaternary Science Reviews 26 (22-24), 2738-2757.

Schoorl, J.M., Veldkamp, A., 2003. Late Cenozoic landscape development and its tectonic implications for the Guadalhorce valley near Alora (Southern Spain). Geomorphology 50 (1-3), 43-57.

Schoorl, J.M., Veldkamp, A., Bouma, J., 2002. Modeling water and soil redistribution in a dynamic landscape context. Soil Science Society of America Journal, 66 (5), 1610-1619.

Schumm, S.A., 1977. The Fluvial System. Wiley, New York, USA.

Schumm, S.A., 1993. River response to baselevel change: implications for sequence stratigraphy. Journal of Geology 101, 279-294.

Sepulchre, P., Ramstein, G., Kageyama, M., Vanhaeren, M., Krinner, G., Sanchez-Goñi, M.F., d'Errico, F., 2007. H4 abrupt event and late Neanderthal presence in Iberia. Earth and Planetary Science Letters 258, 283-292.

Siame, L.L., Bourlès, D.L., Sébrier, M., Bellier, O., Castano, J.C., Arauio, M., Ferez, M., Raisbeck, G.M., Yiou, F., 1997. Cosmogenic dating ranging from 20 to 700 ka of a series of alluvial fan surfaces affected by the El Tigre fault, Argentina. Geology 25 (11), 975-978.

Siame, L.,Bellier, O., Braucher, R., Sébrier, M., Cushing, M., Bourlès, D.L., Hamelin B, Baroux E., De Voogd, B., Raisbeck, G., Yiou, F., 2004. Local erosion rates versus active tectonics: Cosmic ray exposure modelling in Provence (South-East France), EPSL 220 (3-4), 345-364.

Silva, P. G., Goy, J.L., Zazo, C., Bardaji, T., 2000. Fault-generated mountain fronts in southeast Spain: geomorphological assessment of tectonics and seismic activity. Geomorphology 50, 203-225.

Soegaard, H., Hasholt, B., Firborg, T., Nordstroem, C., 2001. Surface energy- and water balance in a high-arctic environment in NE Greenland. Theoretical and Applied Climatology 70, 35-51.

Sos-Baynat, V., 1965. Geomorfologia del valle del Louro, Porriño, Tuy, Pontevedra. Bol. Geol. Min. 76, 3-49.

Stange, K.M., Van Balen, R., Vandenberghe, J., Peña, J.L., Sancho, C., 2012. External controls on Quaternary fluvial incision and terrace formation at the Segre River, Southern Pyrenees. Tectonophysics, in press. http://dx.doi.org/10.1016/j.tecto.2012.10.033.

Stange, K.M., Van Balen, R., Carcaillet, J., Vandenberghe, J., 2013. Terrace staircase development in the Southern Pyrenees Foreland: Inferences from 10Be terrace exposure ages at the Segre River. Global and Planetary Change 101, 97-112.

Starkel, L., 2003. Climatically controlled terraces in uplifting mountain areas. Quaternary Science Reviews 22 (20), 2189-2198.

Stemerdink, C., Maddy, D., Bridgland, D.R., Veldkamp, A., 2010. The construction of a palaeodischarge time series for use in a study of fluvial system development of the middle to late Pleistocene upper Thames. Journal of Quaternary Science 25 (4), 447-460.

Stokes, M., Cunha, P.P., Martins, A.A., 2012b. Techniques for analysing Late Cenozoic river terrace sequences. Geomorphology 165-166, 1-6.

Stokes, M., Griffiths, J.S., Mather, A., 2012a. Palaeoflood estimates of Pleistocene coarse grained river terrace landforms (Río Almanzora, SE Spain). Geomorphology 149-150, 11-26.

Stone, J.O., 2000. Air pressure and cosmogenic isotope production. Journal of Geophysical Research, 105, 23753–23759.

Syvitski, J.PM., Peckham, S.D., Hilberman, R., Mulder, T., 2003. Predicting the terrestrial flux of sediment to the global ocean: A planetary perspective. Sedimentary Geology 162 (1-2), 5-24.

Talling, P.J., 1998. How and where do incised valleys form if sea level remains above the shelf edge? Geology 26 (1), 87-90.

Tebbens, L.A., 1999. Late Quaternary evolution of the Meuse fluvial system and its sediment composition: a reconstruction based on bulk sample geochemistry and forward modelling. Ph.D. thesis Landbouwuniversiteit Wageningen, Wageningen, the Netherlands, 152 pp.

Tebbens, L.A., Veldkamp, A., Van Dijke, J.J., Schoorl, J.M., 2000. Modelling longitudinal-profile development in response to late Quaternary tectonics, climate and sea-level changes: a modeling case study of the River Meuse. Global and Planetary Change 27, 187-206.

Teixeira, C., 1952. Os terraços da parte Portugesa do rio Minho Comunicações dos servicios geologicos de Portugal 33.

Thiel, C., Buylaert, J.-P., Murray, A., Terhorst, B., Hofer, L., Tsukamoto, S., Frechen, M., 2011. Luminescence dating of the Stratzing loess profile (Austria) - Testing the potential of an elevated temperature post-IR IRSL protocol. Quaternary International 234 (1-2), 23-31.

Thomsen, K.J., Murray, A.S., Jain, M., Botter-Jensen, L., 2008. Laboratory fading rates of various luminescence signals from feldspar-rich sediment extracts. Radiation Measurements 43, 1474-1486.

Törnqvist, T.E., Wortman, S.R., Mateo, Z.R.P., Milne, G.A., Swenson, J.B., 2006. Did the last sea level lowstand always lead to cross-shelf valley formation and source-to-sink sediment flux? Journal of Geophysical Research F: Earth Surface 111 (4), F04002.

Trenhaile, A.S., Perez-Alberti, A., Martinez-Cortizas, A., Costa-Casais, M., Blanco-Chao, R., 1999. Rock coast inheritance: an example from Galicia, north western Spain. Earth Surface Processes and Landforms 24, 605-621.

Tripathi, J.K., Rajamani, V., 2003. Weathering control over geomorphology of supermature Proterozoic Delhi quartzites of India. Earth Surface Processes and Landforms 28, 1379-1387.

Twidale, C. R. and Vidal-Romani, J.R., 1994. La herencia de Pangea. Cuadernos Lab. Xeoloxico de Laxe 19, 7-36.

Twidale, C.R., Vidal-Romani, J.R., 2005. Landforms and geology of granite terrains. Balkema Publishers, Leiden.

Tzedakis, P.C., Roucoux, K.H., De Abreu, L., Shackleton, N. J., 2004. The duration of forest stages in southern Europe and interglacial climate variability. Science 306, 2231-2235.

USGS, 2009. ASTER DEM, https://lpdaac.usgs.gov, retrieved 12 october 2009.

Van Balen, R.T., Busschers, F.S.A., Tucker, G.E., 2010. Modeling the response of the Rhine-Meuse fluvial system to late Pleistocene climate change. Geomorphology 114, 440-452.

Van Balen, R.T., Houtgast, R.F., Van der Wateren, F.M., Vandenberghe, J., Bogaart, P.W., 2000. Sediment budget and tectonic evolution of the Meuse catchment in the Ardennes and the Roer Valley Rift System. Global and Planetary Change 27 (1- 4), 113 – 129.

Vandenberghe, J., 1995. Timescales, climate and river development. Quaternary Science Reviews 14 (6), 631-638.

Vandenberghe, 2002. The relation between climate and river processes,landforms and deposits during the Quaternary. Quaternary International 91, 17-23.

Vandenberghe, 2003. Climate forcing of fluvial system development: an evolution of ideas. Quaternary Science Reviews 22, 2053-2060.

Vandenberghe, J., 2008. The fluvial cycle at cold–warm–cold transitions in lowland regions: A refinement of theory. Geomorphology 98, 275-284.

Vandenberghe, J., Vanacker, V., 2008. Towards a system approach in the study of river catchments. Geomorphology 98 (3-4), 173-175.

Vassallo, R., Ritz, J.-F., Carretier, S., 2011. Control of geomorphic processes on ^{10}Be concentrations in individual clasts: Complexity of the exposure history in Gobi-Altay range (Mongolia). Geomorphology 135 (1-2), 35-47.

Vegas, R., 2010. La continuación de la Cordillera Cántabro-Pirenaica en el borde atlántico de la Península Ibérica. Geogaceta 48, 179-181.

Vegas, R., De Vicente, G., Muñoz-Martin, A., Palomino, R., 2004. Los corredores de fallas de Regua-Verín y Vilariça: Zonas de transferencia de la deformación intraplaca en la
Peninsula Ibérica. Geotemas 6, 245-248.

Veldkamp, A., 1992. A 3-D model of fluvial terrace development in the Allier basin (Limagne, France). Earth surface processes and landforms 17, 487-500.

Veldkamp, A., Kroonenberg, S.B., 1993. Late Quaternary chronology of the Allier terrace sediments (Massif Central, France). Geologie en Mijnbouw 72 (2), 179-192.

Veldkamp, A. Schoorl, J.M. Wijbrans, J.R. Claessens, L., 2012. Mount Kenya volcanic activity and the Late Cenozoic landscape reorganisation in the upper Tana fluvial system. Geomorphology 145–146, 19–31.

Veldkamp, A., Tebbens, L.A., 2001. Registration of abrupt climate change within fluvial systems: insights from numerical modelling experiments. Global and Planetary Change 28, 129-144.

Veldkamp, A., Van den Berg, M.W., 1993. Three-dimensional modelling of Quaternary fluvial dynamics in a climo-tectonic dependant system. A case study of the Maas record (Maastricht, The Netherlands). Global and Planetary Change 8, 203-218.

Veldkamp, A., Van den Berg, M.W., Van Dijke, J.J., Van den Berg van Saparoea, R.M., 2002. Reconstructing Late Quaternary fluvial process controls in the upper Aller Valley (North Germany) by means of numerical modelling. Geologie en Mijnbouw/Netherlands Journal of Geosciences 81, 375-388.

Veldkamp, A., Van Dijke J.J., 1998. Modelling long-term erosion and sedimentation processes in fluvial systems: a case study for the Allier/Loire system. In: Benito, G., Baker, V.R., Gregory, K.J. (Eds.), Palaeohydrology and Environmental Change, Wiley, Chichester, UK, pp. 53-66.

Veldkamp, A., Van Dijke, J.J., 2000. Simulating internal and external controls on fluvial terrace stratigraphy: a qualitative comparison with the Maas record. Geomorphology 33, 225-236.

Veldkamp, A., Vermeulen, S.E.J.W. 1989. River terrace formation, modelling, and 3-D graphical simulation. Earth Surface Processes and Landforms 14, 641-654.

Vidal-Box, C., 1941. Contribucion al conocimiento morfologico de las cuencas de los rios Sil y Miño. Boletin de la Real Sociedad española de historia natural 39(3-4), 121-153.

Vidal Romaní, J. R., Fernández-Mosquera, D., Marti, K., Brum-Ferreira, A., 1999. Nuevos datos sobre la cronología glaciar pleistocena en el NW de la Península Ibérica. Cuadernos do Laboratorio Xeolóxico de Laxe 24, 7-30.

Vidal-Romani, J. R., Yepes-Temiño, J., Rodriguez-Martinez Conde, R., 1998. Evolución geomorfológica del macizo Hesperico Peninsular. Estudio de un sector comprendido entre las provincias de Lugo y Ourense (Galicia, NW de Espana). Cadernos Lab. Xeóloxico de Laxe 23, 165-199.

Vieira, G., 2008. Combined numerical and geomorphological reconstruction of the Serra da Estrela plateau icefield, Portugal. Geomorphology 97, 190-207.

Vieira, M., Poças, E., Pais, J., Pereira, D.I., 2011. Pliocene flora from S. Pedro da Torre deposits (Minho, NW Portugal). Geodiversitas 33 (1), 71-85.

Vis, G.-J., Kasse, C., Vandenberghe, J., 2008. Late Pleistocene and Holocene palaeogeography of the lower Tagus valley (Portugal): effects of relative sea level, valley morphology and sediment supply. Quaternary Science Reviews 27 (17-18), 1682-1709.

Viveen, W., Van Balen, R.T., Schoorl, J.M., Veldkamp, A., Temme, A.J.A.M., Vidal-Romani, J.R., 2012a. Assessment of recent tectonic activity on the NW Iberian Atlantic margin by means of geomorphic indices and field studies of the lower Miño River terraces. Tectonophysics 544-545, 13-30.

Viveen, W., Braucher, R., Bourlès, D., Schoorl, J.M., Veldkamp, A., Van Balen, R.T., Wallinga, J., Fernandez-Mosquera, D., Vidal-Romani, J.R., Sanjurjo-Sanchez, J., 2012b. A 0.65 Ma chronology and incision rate assessment of the NW Iberian Miño River terraces based on ^{10}Be and luminescence dating. Global and Planetary Change 94-95, 82-100.

Viveen, W., Schoorl, J.M., Veldkamp, A., van Balen, R.T., Desprat, S., Vidal-Romani, J.R., 2013a. Reconstructing the interacting effects of base level, climate, and tectonic uplift in the lower Miño terrace record: a gradient modelling evaluation. Geomorphology 186, 96-118.

Viveen, W., Schoorl, J.M., Veldkamp, A., Van Balen, R.T., Vidal-Romani, J.R., 2013b. Fluvial terrace map of the northwest Iberian lower Miño River. The Journal of Maps, in press.

Wallinga, J., 2002. Optically stimulated luminescence dating of fluvial deposits: A review. Boreas 31 (4), 303-322.

Wallinga, J., Bos, A.J.J., Dorenbos, P., Murray, A.S., Schokker, J., 2007. A test case for anomalous fading correction in IRSL dating. Quaternary Geochronology 2 (1-4), 216-221.

Wallinga, J., Johns, C.A., 2011. Netherlands Centre for Luminescence dating (NCL) optical dating report. Project number: NCL-2110. Delft University of Technology, Delft. 15 pp.

Ward, G.K. and Wilson, S.R., 1978. Procedures for comparing and combining radiocarbon age determinations: a critique. Archaeometry 20, 19-31.

Westaway, R., 2002. Long-term river terrace sequences: evidence for global increase in surface uplift rates in the Late Pliocene and Early Middle Pleistocene caused by flow in the lower continental crust induced by surface processes. Netherlands Journal of Geosciences 81, 305-328.

Westaway, R., Bridgland, D.R., White, M., 2006. The Quaternary uplift history of central southern England: evidence from the terraces of the Solent River system and nearby raised beaches. Quaternary Science Reviews 25, 2212-2250.

Westaway, R., Bridgland, D.R., Sinha, R., Demir, T., 2009. Fluvial sequences as evidence for landscape and climatic evolution in the Late Cenozoic: A synthesis of data from IGCP 518. Global and Planetary Change 68 (4), 237 – 253.

Whittaker, A.C., Attal., M., Cowie, P.A., Tucker, G.E., Roberts, G., 2008. Decoding temporal and spatial patterns of fault uplift using transient river long profiles. Geomorphology 100, 506-526.

Wintle, A.G., 1973. Anomalous fading of thermoluminescence in mineral samples. Nature 245, 143-144.

Wintle, A.G., Murray, A.S., 2006. A review of quartz optically stimulated luminescence characteristics and their relevance in single-aliquot regeneration dating protocols. Radiation Measurements 41 (4), 369-391.

Yepes-Temiño, J., 2002. Geomorfologia de un sector comprendido entre las provincias de Lugo y Ourense (Galicia, Macizo Hesperico). Serie Nova Terra 21, Laboratorio Xeoloxico de Laxe. O Castro, University of A Coruña.

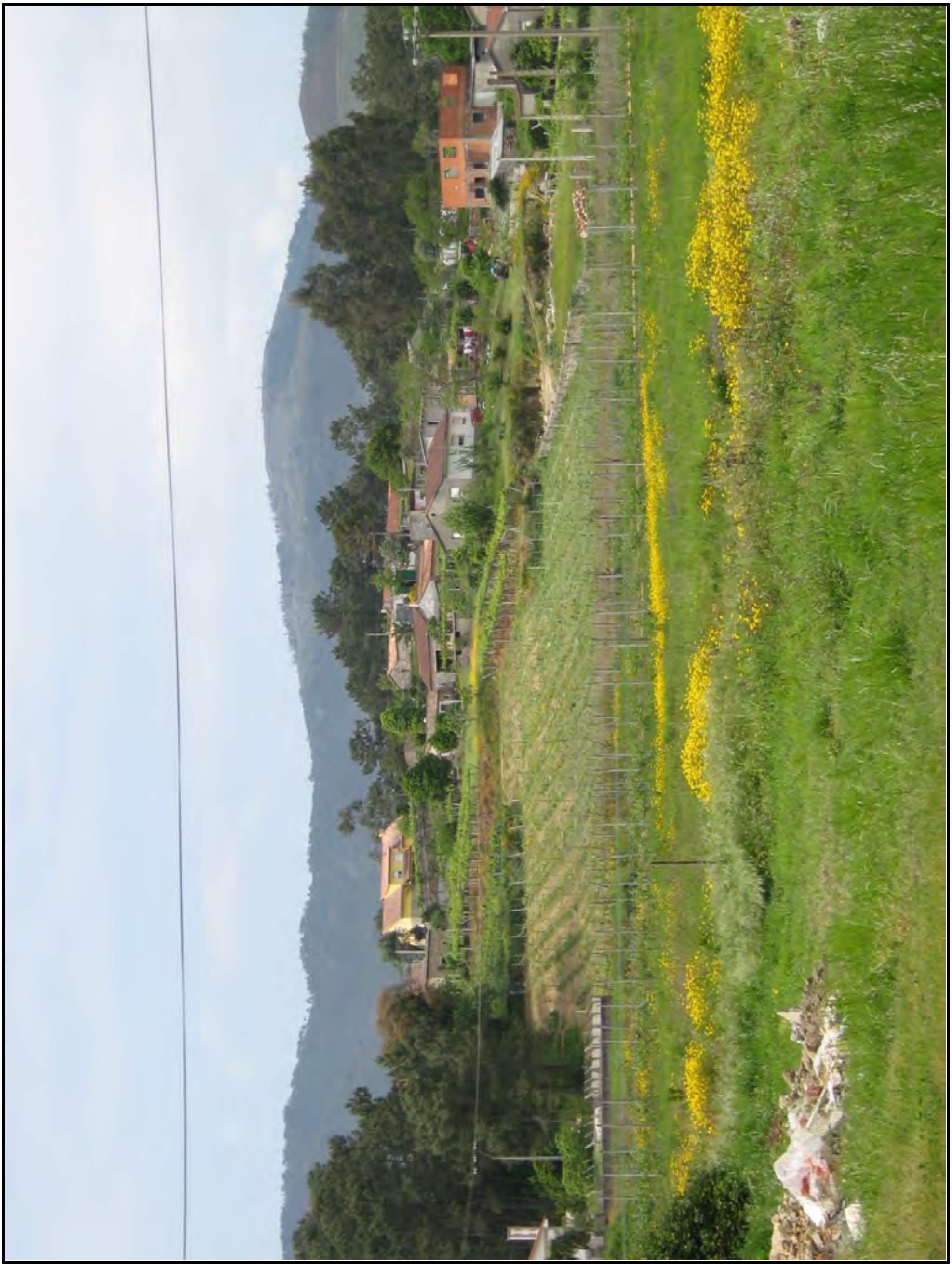

Summary

The general aim of this thesis is to untangle the interacting effects of climate, glacioeustacy, and regional, and local tectonics on fluvial terrace formation. The NW Iberian lower Miño River valley was chosen as a study site, because for this region, a very detailed, long-term, climate record is available. The lower Miño is situated near the Atlantic Ocean, which ensures that the influence of changing past sea levels was registered in the terrace record. Then, there is controversy about the presence or absence of tectonic activity, although a well-developed network of pre-existing faults and seismic activity in the region suggest that tectonic activity is present. Lastly, a completely preserved terrace sequence makes it possible to study the evolution of the area in detail. These, and more details, are found in Chapter 1.

In Chapter 2, a regional assessment of recent tectonic activity is made. Studies on faulted terrace deposits and the recognition of small, fault-bounded tectonic basins indicate the presence of neo-tectonic activity. Further evidence is gathered from a tectono-geomorphic analysis, whereby deeply incised valleys, as well as asymmetrically-developed tributary catchments, and the presence of knick points in river profiles that coincide with the presence of structural lineaments, show that the eastern part of the study area experiences tectonic deformation. It is proposed that due to the non-optimal angle between the orientation of the pre-existing faults, and the current horizontal stress orientation, these older faults are re-activated, resulting in strain transfer from one fault segment to another. This results in differential block movements leading to local extension and basin subsidence. Alternatively, strike-slip activity may have caused the tectonic basins, but for this mechanism no evidence was found.

The focus of Chapter 3 is on a local terrace staircase near the village of Vila Meã. First, the terrace staircase and associated fluvial deposits are described in detail. Then, an age model for the Vila Meã terraces is presented on basis of thermoluminescence and Cosmogenic Ray Exposure (CRE) dating. Minimum ages of up to 650 ka are calculated. On basis of these ages, and terrace surface altitudes, maximum incision rates of 0.07 to 0.09 m ka^{-1} are reconstructed. It is then discussed that these rates can be used as proxies for regional, vertical tectonic uplift. In the final part of the Chapter, new ideas are presented on the evolution of the lower Miño fluvial terraces. Based on observations made from the terrace deposits, and the proximity of a narrow, steep continental shelf, it is suggested that the fluvial terraces were formed during the initial period of sea level fall, and subsequently incised. Vertical uplift would then have occurred to preserve the terraces above the current river bed.

In Chapter 4, the focus shifts from a local terrace staircase to the regional terrace record. The entire 55-km long terrace section of the lower Miño is investigated, and 4 selected terrace transects are discussed in terms of number of terraces and sedimentology. Because there is disagreement on the exact number of terraces and their correlations, a new long-distance terrace correlation scheme is presented. The new scheme is based on studies of weathered quartzite gravels in the 4 selected transects. Observed similarities in weathering rate between the transects leads to a proposed terrace correlation gradient of 1 m km^{-1}. The often used correlation model that the terraces tread parallel to the current river bed (gradient 0 m km^{-1}) is then rejected. The second half of the Chapter focuses on a longitudinal profile modelling experiment with the FLUVER 2 model. The evolution of the entire Miño-Sil system is modelled over a time period of 450 ka. The outcomes show that a regional uplift rate of 0.08 m ka^{-1} in combination with glacioeustatic movements seem to be responsible for terrace formation in the lower Miño valley, and thus confirm the earlier hypotheses in Chapter 3. Climate-induces variations in discharge intensity or timing do not have a dominant effect on terrace formation. The outcomes furthermore indicate that the CRE ages presented in Chapter 3, appear to be very close to exact timing of terrace abandonment.

The results of the foregoing Chapters are integrated and implemented in Chapter 5, resulting in a new, detailed, fluvial terrace map of the entire 67-km reach of the lower Miño River. Both the Spanish and Portuguese part is incorporated. The map is derived from detailed mapping from a 5-m Digital Elevation Model (DEM) and over 1500 hours of fieldwork. The map shows the regional distribution of 10 terrace levels and one floodplain level, as well as 9 tectonic basins. A layer with fault elements gives a structural tectonic context to the map. Additional layers give information about more than 400 sites with mapped terrace sediment thicknesses and palaeoflow directions. Results from this mapping exercise show the highly fragmented nature of terrace and basin distribution, which is controlled by N-S, E-W and NW-SE trending faults. The map also suggests the presence of unpaired terraces along the river, which may be caused by localised differential movements of tectonic blocks.

These localised movements are the topic of Chapter 6. Here, the interactions between regional vertical uplift, local basin subsidence, and unequal uplift on both sides of the Miño River on terrace formation are investigated by means of a forward modelling exercise with the TERRACE model. The model simulations that match best with mapped terraces and fluvial sediment thicknesses are the ones that incorporate all three effects of vertical uplift, basin subsidence, and unequal uplift. This shows that terrace preservation is the complex end result of three, interacting, tectonic processes. A regional uplift rate of 0.10 m ka^{-1} gave the best results, which is slightly higher than the rate of 0.08 m ka^{-1} presented in Chapter 3. This confirms that regional uplift increases from the coast towards the east, which is in

agreement with the findings of Chapter 2. Another important result is that the interacting effect of the three aforementioned tectonic processes can lead to fill terraces one valley side, and strath terraces at the other.

In Chapter 7, all findings of the previous Chapters are combined. The separate effects of climate change, glacioeustacy, and regional and local tectonic movements on fluvial terrace formation are discussed. This shows that in many published terrace correlation schemes for tectonically active regions, the effects of multi-scale tectonics are insufficiently incorporated or considered. The same applies for the possible effects of variable uplift pulses over middle to late Quaternary timescales. This leads for instance to the separation of fill and strath terraces in a chronological context, because they are still thought to be the resultant of climate-triggered changes in discharge and sediment load of the river. But this thesis shows that they can form at the same time due to localised tectonic movements. The Chapter concludes with a number of recommendations on how to incorporate tectono-geomorphic analysis in fluvial terrace research, which will lead to a better understanding of tectonic control on fluvial terrace formation world-wide.

Samenvatting

Het doel van dit proefschrift is om de afzonderlijke effecten te bepalen die lange-termijn klimaat veranderingen, zeespiegelbewegingen, en regionale en lokale aardkorstbewegingen hebben op de ontwikkeling van rivierterrassen. Hiertoe wordt het benedenstroomse deel van het Miño riviersysteem, op de grens van Spanje en noord Portugal, onderzocht. Deze rivier kenmerkt zich door de beschikbaarheid van een zeer gedetailleerd klimaat archief, dat een duidelijk beeld geeft van de vroegere vegetatie- en klimaat geschiedenis van het gebied. Daarnaast bevindt het benedenstroomse deel van de Miño zich nabij de Atlantische Oceaan, waardoor er altijd invloeden van vroegere zeespiegelbewegingen zijn geweest. Er zijn ook verschillende denkbeelden over de dan al niet aanwezigheid van aardkorstbewegingen (tektoniek) in het gebied, ook al zijn er aanwijzingen in de vorm van een dicht netwerk van breuken, en aardbevingen, die erop duiden dat er activiteit in de aardkorst plaatsvindt. Een goed ontwikkeld en bewaard gebleven rivierterrassenstelsel tenslotte, maakt het mogelijk om de vroegere ontwikkeling van het gebied in detail te bestuderen. Deze, en meer details kunnen terug gelezen worden in Hoofdstuk 1.

In Hoofdstuk 2 wordt er gekeken naar de aanwezigheid van aardkorstbewegingen op regionale schaal. Studies aan rivierterrassen die door breuken ontzet zijn, en de beschrijving van kleine, door breuken begrensde tektonische bekkentjes laten zien dat er tot op de dag van vandaag aardkorstbewegingen plaatsvinden. Aanvullend bewijs wordt aangedragen middels een tektono-geomorfologische analyse. De aanwezigheid van diep ingesneden rivierdalen, asymmetrisch ontwikkelde riviernetwerken, en de aanwezigheid van knikpunten in rivierlopen die samenvallen met de aanwezigheid van structurele lineamenten in het landschap, wijzen erop dat het oostelijk deel van het onderzochte gebied tektonisch actief is. Er wordt voorgesteld dat een niet-optimale hoek tussen de strekkingsrichting van oudere breuken en het huidige horizontale spanningsveld leidt tot het opnieuw geactiveerd worden van oudere breuken. Dit leidt op zijn beurt weer tot het overdragen van spanning van één breuk segment naar een volgend segment. Het geheel resulteert in onafhankelijke bewegingen van kleine tektonische blokken, en lokale rek van de aardkorst, waardoor er dalende bekkentjes ontstaan. Een alternatieve verklaring zou zijn dat de aanwezigheid van horizontaal schuivende breuken de oorzaak is van de tektonische bekkentjes, maar hiervoor zijn geen aanwijzingen in het veld gevonden.

Hoofdstuk 3 richt zich op een lokale terrassensequentie nabij het dorp Vila Meã. Als eerste worden de terrassen en de bijbehorende fluviatiele afzettingen beschreven. Daarna wordt op basis van thermoluminescentie- en cosmogene nucleidendateringen minimumleeftijden tot 650 duizend jaar voor de terrassen besproken en een

leeftijdsmodel voor de terrassen aangedragen. Op basis van deze leeftijden worden rivierinsnijdingssnelheden variërend van 0.07 m per duizend jaar tot 0.09 m per duizend jaar, berekend. Vervolgens wordt bediscussieerd dat de snelheden gebruikt kunnen worden om de regionale, verticale aardkorstbewegingen te bepalen. In het laatste deel van dit Hoofdstuk worden nieuwe ideeën gepresenteerd ten opzichte van de ontwikkeling van de rivierterrassen van het benedenstroomse deel van de Miño rivier. Op basis van waarnemingen aan de terrasafzettingen, en de nabijheid van een korte, steile continentale plaatrand, wordt gesuggereerd dat de terrassen afgezet zijn tijdens de beginfase van zeespiegeldalingen, en vervolgens versneden. Verticale aardkorstbewegingen zouden er dan voor gezorgd hebben dat de terrassen in het landschap bewaard zijn gebleven.

In Hoofdstuk 4 verschuift de focus van een lokale terrassensequentie naar een regionale sequentie. Het gehele, 55 kilometer lange benedenstroomse deel van de Miño wordt onderzocht, en de terrassen en bijbehorende sedimentologie van 4 geselecteerde terrassensequenties worden besproken. Omdat er tussen wetenschappers onderling geen eensgezindheid bestaat over het exacte aantal terrassen en hun onderlinge lange-afstandscorrelaties, wordt er een nieuw correlatiemodel besproken. Dit nieuwe model is gebaseerd op studies aan de verweerde kwartsiet grinden in de 4 terrassensequenties. Overeenkomsten in de verweringsgraad van de kwartsieten tussen de 4 terrassensequenties leidt tot een correlatiemodel waarbij de terrassen een stroomafwaartse gradiënt hebben van 1 m per km afstand. Het tot dan toe geldend correlatiemodel waarbij de terrassen een gradiënt hebben die gelijk is aan de huidige rivierbedding (0 m per km), wordt dan verworpen. Het tweede deel van het hoofdstuk richt zich op een numeriek modelleerexperiment, waarbij de ontwikkeling van het lengteprofiel van de Miño over een periode van 450 duizend jaar wordt nagebootst. De resultaten laten zien dat regionale verticale deformatie van de aardkorst plaatsvindt met een snelheid van 0.08 m per duizend jaar. Dit in combinatie met glaciale-interglaciale zeespiegelbewegingen is verantwoordelijk voor de vorming van de fluviatiele terrassen in het benedenstroomse deel van de Miño rivier. Deze resultaten bevestigen de in Hoofdstuk 3 gepresenteerde hypothese over de vorming van de rivierterrassen. Klimaat gestuurde schommelingen in waterafvoer en periodisatie van waterafvoer hebben geen dominante invloed op de terrasvorming. De resultaten laten tenslotte nog zien dat de terrasouderdommen op basis van de cosmogene nucleidendateringen uit Hoofdstuk 3 zeer dicht bij de werkelijke ouderdom van de terrassen liggen.

De resultaten van de voorgaande 3 Hoofdstukken worden geïntegreerd in het volgende Hoofdstuk 5, dat resulteert in een nieuwe, zeer gedetailleerde terrassenkaart van het gehele 67 kilometer lange benedenstroomse deel van de Miño rivier. Zowel de Spaanse als de Portugese kant zijn daar, voor het eerst, in opgenomen. De kaart is gebaseerd op een gedetailleerde studie aan satellietbeelden van het landschap, alsmede meer dan 1500

uren veldwerk. De kaart laat de ruimtelijke verspreiding van 10 terrasniveaus en één huidige overstromingsvlakte, evenals 6 tektonische bekkens, zien. Een kaartlaag met breukelementen voegt een structureel geologische dimensie toe aan de kaart. Andere kaartlagen geven informatie over meer dan 400 veldwaarnemingen aan terrassedimenten (diktes van sedimentpakketten), en vroegere stroomrichtingen van de Miño rivier. De kaart laat duidelijk zien dat de terrassen gefragmenteerde clusters in het landschap vormen, die afgewisseld zijn met tektonische bekkens. De fragmentatie wordt veroorzaakt door breuken met een N-Z, O-W en NW-ZO strekking. Tevens laat de kaart zien dat terrassen op sommige plaatsen aan weerszijde van de riviervallei niet gepaard zijn, wat veroorzaakt zou kunnen worden door lokale bewegingen van tektonische blokken.

Deze bewegingen van lokale tektonische blokken zijn het onderwerp van Hoofdstuk 6. In dit Hoofdstuk wordt het samenspel tussen regionale verticale aardkorstbewegingen, relatieve daling van tektonische bekkentjes, en ongelijke verticale bewegingen aan weerszijde van de riviervallei onderzocht. Hiertoe wordt het TERRACE computermodel gebruikt. De modelresultaten die het beste overeenkomen met gekarteerde terrassensequenties en diktes van sedimentpakketten, zijn het resultaat van simulaties die alle eerder genoemde tektonische bewegingen meenemen in de berekeningen. Het laat zien dat de preservatie van terrassen het eindresultaat is van het complexe samenspel van drie tektonische processen. Regionale verticale aardkorstbewegingen met snelheden van 0.10 m per duizend jaar gaven de beste modelvoorspellingen. Dit zijn enigszins hogere snelheden dan de eerder gepresenteerde snelheden van 0.08 m per duizend jaar in Hoofdstuk 3. De verklaring kan gezocht worden in het feit de snelheid van regionale verticale aardkorstbewegingen toeneemt van de kust richting het oosten van het studiegebied, iets dat al al in Hoofdstuk 2 aan de orde is gekomen. Nog een belangrijk resultaat van de modellering is dat het samenspel tussen verschillende tektonische processen kan leiden tot terrassen met dikke sedimentpakketten aan één zijde van de riviervallei, en tot terrassen met een erosief karakter aan de andere zijde.

In het laatste Hoofdstuk 7 worden de resultaten van alle voorgaande Hoofdstukken gecombineerd. De afzonderlijke invloeden van klimaatsverandering, zeespiegelbewegingen, en regionale en lokale aardkorstbewegingen op de vorming van rivierterrassen worden onder de loep genomen. Het laat zien dat veel huidige terrassencorrelatiemodellen voor andere rivieren in tektonisch actieve gebieden, wellicht ontoereikend zijn, omdat het effect van aardkorstbewegingen op verschillende ruimtelijke schalen niet goed meegenomen is. Hetzelfde geldt voor het mogelijke effect van variabele snelheden van aardkorstbewegingen over de afgelopen miljoen jaar. Van de vorming van terrassen met dikke sedimentpakketten en die met een erosief karakter bijvoorbeeld, wordt nog steeds gedacht dat ze in verschillende tijdsperioden gevormd worden door veranderingen in water en sedimentlast van de rivier, die op hun beurt weer

klimaat gestuurd zijn. Maar de resultaten in dit proefschrift laten zien dat ze ook op hetzelfde moment door lokale aardkorstbewegingen gevormd kunnen worden. Hoofdstuk 7 eindigt met een aantal aanbevelingen over hoe tektono-geomorfologische analyses opgenomen kunnen worden in onderzoek aan rivierterrassen. Dit zal leiden tot een beter begrip van de invloed die tektonische processen op verschillende ruimtelijke schalen hebben op de vorming van rivierterrassen in tektonisch actieve gebieden over de gehele wereld.

Appendices

Appendix 1

Below the main equations that calculate sediment transport along the longitudinal profile are listed (Veldkamp and Van Dijke, 1998, 2000). Equation symbols are explained in Table 4.

Sediment mass conservation:

Eq. (A.1.) $\partial A / \partial t = -\partial L \partial x + U + B$

Sediment tranport between river flow and substrate:

Eq. (A.2.) $\partial F / \partial x = D - T$

Rate of sediment transfer from the river bed to the river flow:

Eq. (A.3.) $D = k_{det} G (\partial A / \partial x)^m$

Rate of sediment transfer from the river flow to the river bed:

Eq. (A.4.) $T = L / h$

Table A.1 Main equations used in the FLUVER2 model.

Symbol	Unit	Description
A	m	Altitude above reference level
t	s	Time
L	$m^2 s^{-1}$	Longitudinal sediment flux along the profile
x	m	Distance along longitudinal profile
U	$m s^{-1}$	Uplift rate
B	$m s^{-1}$	Lateral influx rate of sediment
D	$m s^{-1}$	Transfer rate from the substrate to sediment flow
T	$m s^{-1}$	Transfer rate from the sediment flow to the substrate
k_{det}	$m s^{-1}$	Sediment erodibility factor
G	n. r.	Force function (discharge proxy), tuning variable with value 1
m	[-]	Fluvial exponent
h	m	Height difference

Appendix 2

Descriptions of fluvial terrace exposures (road cuts, gravel mines, etc)

Sites with fluvial sediments where the underlying bedrock is visible.

Ref.	East	North	Layer 1	Layer 2	Layer 3	Layer 1 depth (m)	Layer 2 depth (m)	Layer 3 depth (m)	Sediment thickness (m)
1	541318	4659449	Saprolite			1.20	0.00	0.00	0.00
1	515169	4637056	Gravel	Gravel	Bedrock	0.70	3.00	6.00	3.00
2	519136	4646880	Sand, gravel, clay	Saprolite		6.00	6.10	0.00	6.00
3	513412	4640707	Gravel			3.00	0.00	0.00	3.00
4	520908	4642104	Bedrock			8.00	0.00	0.00	0.00
5	521002	4642193	Gravel	Bedrock		1.00	1.00	0.00	1.00
14	514555	4640749	Bedrock			0.00	0.00	0.00	0.00
15	517081	4642635	Bedrock			0.00	0.00	0.00	0.00
18	517384	4644251	Clay			1.90	0.00	0.00	1.90
19	517123	4644485	Bedrock			0.00	0.00	0.00	0.00
19	516754	4644729	Bedrock			0.00	0.00	0.00	0.00
21	517990	4645483	Fine sand	Coarse sand	Gravel	0.70	2.70	4.15	4.15
23	518344	4643501	Gravel	Saprolite		4.00	4.50	0.00	4.00
24	518717	4643341	Colluvium	Saprolite		3.00	6.00	0.00	0.00
24	518763	4643154	Saprolite			4.00	0.00	0.00	0.00
24	518642	4642675	Saprolite			2.00	0.00	0.00	0.00
25	520034	4643813	Gravel	Clay	Saprolite	5.00	6.00	7.00	6.00
26	520590	4643544	Colluvium	Saprolite		1.00	4.00	0.00	0.00
28	520186	4643825	Gravel	Saprolite		6.50	7.00	0.00	6.50
30	519879	4644352	Gravel	Saprolite		2.00	13.00	0.00	2.00
31	520131	4644250	Colluvium	Saprolite		0.75	5.50	0.00	0.00
32	520397	4644230	Gravel	Saprolite		2.80	3.50	0.00	2.80
32	520702	4644628	Saprolite			0.00	2.00	0.00	0.00
32	520223	4644787	Colluvium	Saprolite		0.50	2.00	0.00	0.00
34	517631	4643216	Gravel	Saprolite		5.70	6.50	0.00	5.70
35	519612	4646892	Colluvium	Saprolite		1.00	1.00	0.00	0.00

35	518308	4646623	Saprolite			0.00	2.00	0.00	0.00
38	519842	4647565	Gravel	Gravel	Saprolite	2.00	2.50	10.00	2.50
39	522204	4647665	Gravel	Saprolite		1.50	3.00	0.00	1.50
40	521706	4647896	Gravel	Saprolite		2.00	2.30	0.00	2.00
40	522372	4648899	Gravel	Saprolite		1.00	3.00	0.00	1.00
40	521255	4648229	Gravel	Saprolite		2.50	3.00	0.00	2.50
42	524312	4650165	Fine sand	Gravel	Saprolite	0.70	3.30	0.00	3.30
42	523517	4651165	Saprolite			2.00	0.00	0.00	0.00
42	525546	4649425	Gravel	Saprolite		2.00	2.50	0.00	2.00
43	523061	4649801	Gravel	Saprolite		2.50	4.00	0.00	2.50
46	523448	4649843	Gravel	Saprolite		1.00	1.50	0.00	1.00
47	523356	4650457	Gravel	Saprolite		2.00	6.00	0.00	2.00
48	523024	4650270	Gravel	Saprolite		3.50	5.00	0.00	3.50
49	525938	4649644	Coarse sand	Gravel	Saprolite	1.50	1.95	3.00	1.95
51	526501	4649280	Gravel	Saprolite		3.80	4.20	0.00	3.80
51	523434	4645733	Colluvium	Saprolite		1.00	2.30	0.00	0.00
52	521571	4644581	Gravel	Saprolite		4.00	5.00	0.00	4.00
52	521847	4644406	Saprolite			1.00	0.00	0.00	0.00
52	524012	4646431	Saprolite			4.00	0.00	0.00	0.00
54	523863	4647186	Gravel	Saprolite		8.50	9.00	0.00	8.50
54	524033	4647220	Gravel	Saprolite		1.50	7.50	0.00	1.50
54	523882	4647336	Gravel	Saprolite		7.30	8.00	0.00	7.30
54	524012	4647424	Gravel	Saprolite		1.20	2.00	0.00	1.20
54	524026	4647403	Gravel	Saprolite		0.30	1.60	0.00	0.30
55	524073	4647315	Gravel	Saprolite		1.00	8.00	0.00	1.00
57	524608	4646762	Gravel	Saprolite		2.00	3.00	0.00	2.00
58	524516	4646617	Gravel	Saprolite		3.30	3.35	0.00	3.30
59	524565	4645272	Saprolite			3.00	0.00	0.00	0.00
59	522255	4644901	Saprolite			3.00	0.00	0.00	0.00
59	522403	4645796	Saprolite			3.50	0.00	0.00	0.00

60	523206	4645841	Gravel	Saprolite		1.00	3.00	0.00	1.00
60	522754	4645653	Saprolite			2.50	0.00	0.00	0.00
61	521238	4645467	Coarse sand	Bedrock		1.00	4.00	0.00	1.00
62	526030	4647014	Gravel	Saprolite		3.50	10.00	0.00	3.50
63	526922	4648472	Gravel	Saprolite		2.40	2.50	0.00	2.40
64	528165	4648568	Gravel	Saprolite		3.10	3.30	0.00	3.10
65	525475	4646720	Colluvium	Saprolite		0.70	2.50	0.00	0.00
66	524437	4646335	Gravel	Saprolite		1.15	1.40	0.00	1.15
67	525724	4646302	Gravel	Bedrock		0.10	1.00	0.00	0.10
67	525197	4646698	Fine sand	Saprolite		0.50	1.00	0.00	0.50
68	525435	4646239	Gravel	Saprolite		0.45	0.70	0.00	0.45
69	526025	4644579	Saprolite			10.00	0.00	0.00	0.00
70	526724	4645715	Gravel	Saprolite		0.50	2.00	0.00	0.50
73	528163	4646164	Gravel	Saprolite		1.50	2.10	0.00	1.50
75	527360	4646799	Gravel	Saprolite		4.70	6.10	0.00	4.70
76	528643	4647919	Gravel			4.10	0.00	0.00	4.10
79	530679	4648285	Gravel	Saprolite		3.00	3.50	0.00	3.00
82	536384	4654513	Gravel	Saprolite		6.50	8.80	0.00	6.50
83	542122	4658411	Gravel	Saprolite		5.20	5.50	0.00	5.20
84	529283	4653004	Gravel	Saprolite		7.50	10.00	0.00	7.50
86	531712	4652266	Saprolite			1.00	0.00	0.00	0.00
86	531275	4652773	Saprolite			1.00	0.00	0.00	0.00
86	531150	4653848	Saprolite			1.00	0.00	0.00	0.00
88	531525	4650222	Saprolite			4.00	0.00	0.00	0.00
91	530981	4649318	Gravel	Saprolite		0.30	2.50	0.00	0.30
94	530969	4649023	Gravel	Sand, gravel, clay	Saprolite	5.10	7.00	12.00	7.00
95	530591	4653057	Saprolite			2.00	0.00	0.00	0.00
97	513718	4644739	Colluvium			0.00	0.00	0.00	0.00
98	514666	4644018	Saprolite			1.00	0.00	0.00	0.00

99	511203	4631894	Saprolite			1.00	0.00	0.00	0.00
100	511237	4631277	Saprolite			1.00	0.00	0.00	0.00
101	513366	4631720	Saprolite			1.00	0.00	0.00	0.00
102	513254	4632265	Saprolite			1.00	0.00	0.00	0.00
104	526856	4646161	Gravel	Saprolite		8.00	8.50	0.00	8.00
105	523922	4647225	Gravel	Bedrock		8.50	9.00	0.00	8.50
105	515805	4644312	Bedrock			1.00	0.00	0.00	0.00
105	515960	4642988	Bedrock			8.00	0.00	0.00	0.00
106	513832	4641106	Gravel	Saprolite		4.00	4.50	0.00	4.00
107	522275	4649050	Saprolite			2.00	0.00	0.00	0.00
110	546320	4660371	Fine sand	Gravel	Saprolite	2.00	2.10	9.00	2.10
112	541341	4659155	Gravel		Bedrock	2.00	10.00	0.00	2.00
113	539900	4659026	Gravel	Saprolite		1.00	7.00	0.00	1.00
114	540053	4659365	Gravel	Saprolite		1.60	10.00	0.00	1.60
115	540195	4659538	Gravel	Saprolite		2.00	8.00	0.00	2.00
116	540278	4659563	Gravel	Saprolite		6.00	7.00	0.00	6.00
117	540569	4660304	Gravel	Saprolite		0.50	4.00	0.00	0.50
117	540485	4660286	Saprolite			0.00	0.00	0.00	0.00
120	541063	4659945	Gravel	Saprolite		6.00	7.00	0.00	6.00
121	541298	4660538	Gravel			1.00	0.00	0.00	1.00
122	541493	4660305	Sand, gravel, clay	Saprolite		3.00	4.00	0.00	3.00
123	541121	4659895	Gravel	Saprolite		0.50	10.00	0.00	0.50
123	541404	4660076	Gravel	Saprolite		0.50	10.00	0.00	0.50
123	541458	4660170	Saprolite			10.00	0.00	0.00	0.00
124	541524	4661027	Saprolite			8.00	0.00	0.00	0.00
125	542345	4659581	Bedrock			0.00	0.00	0.00	0.00
126	542677	4659620	Gravel	Saprolite		3.00	4.50	0.00	3.00
128	543798	4660735	Colluvium			3.00	0.00	0.00	0.00
129	544495	4661205	Gravel	Saprolite		4.00	4.10	0.00	4.00

129	544614	4661278	Saprolite		0.00	0.00	0.00	0.00
131	544319	4658630	Saprolite		3.00	0.00	0.00	0.00
131	544185	4658118	Saprolite		0.00	0.00	0.00	0.00
132	544371	4657852	Gravel	Saprolite	3.00	3.50	0.00	3.00
133	544683	4657982	Gravel	Saprolite	1.00	5.00	0.00	1.00
134	545943	4657622	Gravel	Saprolite	5.00	5.10	0.00	5.00
135	546672	4657385	Gravel	Saprolite	3.00	7.00	0.00	3.00
136	541756	4658103	Gravel	Saprolite	0.01	7.00	0.00	0.01
137	542738	4658239	Clay	Saprolite	1.50	3.00	0.00	1.50
138	542750	4657814	Colluvium	Saprolite	0.50	1.30	0.00	0.00
139	542608	4657193	Saprolite		2.50	0.00	0.00	0.00
140	546460	4658705	Gravel	Bedrock	0.20	1.00	0.00	0.20
141	546038	4658818	Colluvium	Saprolite	1.00	1.50	0.00	0.00
142	545712	4659112	Gravel	Saprolite	0.10	2.00	0.00	0.10
143	545843	4658517	Gravel	Saprolite	0.10	0.70	0.00	0.10
144	544864	4658222	Saprolite		1.70	0.00	0.00	0.00
144	544830	4658006	Saprolite		0.00	0.00	0.00	0.00
144	545070	4657436	Saprolite		0.00	0.00	0.00	0.00
145	544642	4657886	Gravel	Saprolite	2.50	4.00	0.00	2.50
148	549425	4658668	Gravel	Saprolite	3.00	3.50	0.00	3.00
150	549389	4658976	Gravel	Bedrock	0.01	1.00	0.00	0.01
151	549652	4658278	Gravel	Saprolite	1.00	2.00	0.00	1.00
153	546892	4656960	Saprolite		2.00	0.00	0.00	0.00
154	547287	4656932	Saprolite		2.00	0.00	0.00	0.00
155	547253	4657258	Gravel	Saprolite	1.00	2.50	0.00	1.00
156	547061	4657381	Gravel	Saprolite	3.00	3.50	0.00	3.00
157	547567	4657345	Saprolite		2.70	0.00	0.00	0.00
158	547831	4657311	Gravel	Saprolite	1.00	3.50	0.00	1.00
159	544329	4658626	Saprolite		4.00	0.00	0.00	0.00
160	542000	4655618	Bedrock		0.00	0.00	0.00	0.00

160	541604	4655822	Gravel	Bedrock		0.20	1.00	0.00	0.20
161	541329	4656192	Gravel	Saprolite		1.90	2.00	0.00	1.90
162	541860	4656128	Saprolite			7.00	0.00	0.00	0.00
163	541228	4657341	Gravel	Saprolite		1.50	2.50	0.00	1.50
164	541079	4658215	Gravel	Saprolite		1.00	2.00	0.00	1.00
165	540121	4658487	Gravel	Saprolite		2.00	3.00	0.00	2.00
166	540494	4658557	Bedrock			10.00	0.00	0.00	0.00
167	541015	4658581	Sand, gravel, clay	Bedrock		3.70	4.00	0.00	3.70
168	541193	4658599	Gravel	Saprolite		3.00	4.00	0.00	3.00
169	541473	4658587	Sand, gravel, clay	Saprolite		1.50	3.00	0.00	1.50
170	539653	4658114	Gravel	Saprolite		2.50	3.00	0.00	2.50
171	539353	4656928	Bedrock			0.00	0.00	0.00	0.00
172	539569	4657323	Colluvium	Gravel	Bedrock	1.00	1.30	8.00	0.30
173	539838	4657645	Gravel	Saprolite		1.50	2.00	0.00	1.50
174	539865	4657490	Gravel	Saprolite		1.80	2.00	0.00	1.80
175	540484	4657002	Gravel	Saprolite		1.00	1.60	0.00	1.00
176	540484	4657277	Gravel	Saprolite		0.30	1.50	0.00	0.30
177	540497	4657083	Gravel	Saprolite		1.00	1.50	0.00	1.00
178	540096	4656145	Gravel	Saprolite		1.00	4.00	0.00	1.00
179	539616	4656193	Saprolite			3.00	0.00	0.00	0.00
180	539669	4655957	Gravel	Saprolite		0.30	1.30	0.00	0.30
182	538798	4656425	Saprolite			0.00	0.00	0.00	0.00
182	540431	4656820	Gravel	Saprolite		6.50	6.60	0.00	6.50
183	540311	4656813	Gravel	Saprolite		0.50	8.00	0.00	0.50
184	539924	4656895	Saprolite			9.00	0.00	0.00	0.00
185	538916	4656336	Gravel	Saprolite		0.20	8.00	0.00	0.20
186	538692	4656080	Gravel	Saprolite		3.50	10.00	0.00	3.50
186	538546	4655648	Gravel	Saprolite		0.70	9.00	0.00	0.70

186	538027	4655402	Bedrock			0.00	0.00	0.00	0.00
187	537934	4655656	Bedrock			15.00	0.00	0.00	0.00
188	538826	4656439	Saprolite			2.50	0.00	0.00	0.00
188	539026	4656616	Bedrock			0.00	0.00	0.00	0.00
189	536344	4655159	Gravel	Saprolite		0.50	4.00	0.00	0.50
191	535921	4654938	Gravel	Saprolite		1.10	2.00	0.00	1.10
192	535713	4655369	Gravel	Saprolite		0.50	2.00	0.00	0.50
193	536038	4655384	Gravel	Saprolite		0.60	1.50	0.00	0.60
194	536162	4655509	Gravel	Saprolite		1.00	10.00	0.00	1.00
195	536719	4655566	Bedrock			4.00	0.00	0.00	0.00
196	534455	4654703	Saprolite			1.00	0.00	0.00	0.00
196	534653	4654731	Fine sand	Saprolite		1.20	2.20	0.00	1.20
197	535173	4655440	Gravel			1.00	0.00	0.00	1.00
198	534722	4655344	Gravel			2.20	0.00	0.00	2.20
199	531784	4654851	Saprolite			2.20	0.00	0.00	0.00
200	532112	4655121	Colluvium	Saprolite		1.00	2.50	0.00	0.00
202	534157	4655214	Saprolite			3.00	0.00	0.00	0.00
203	534898	4655038	Colluvium	Saprolite		1.00	3.00	0.00	0.00
204	543766	4658856	Saprolite			2.50	0.00	0.00	0.00
205	527917	4654179	Saprolite			1.50	0.00	0.00	0.00
206	528395	4654682	Saprolite			4.00	0.00	0.00	0.00
207	528572	4654814	Gravel	Saprolite		1.60	1.70	0.00	1.60
210	527522	4653651	Colluvium	Bedrock		1.00	2.00	0.00	0.00
211	527244	4653463	Saprolite			2.00	0.00	0.00	0.00
212	526559	4653044	Saprolite			1.00	0.00	0.00	0.00
213	526323	4652951	Saprolite			3.00	0.00	0.00	0.00
214	527250	4650873	Colluvium	Gravel	Saprolite	1.00	1.10	2.10	1.00
215	526877	4650640	Saprolite			2.00	0.00	0.00	0.00
216	526665	4649588	Gravel	Saprolite		2.00	3.00	0.00	2.00
217	526980	4652652	Saprolite			1.00	0.00	0.00	0.00

218	526246	4650421	Gravel	Saprolite		4.00	4.50	0.00	4.00
219	525190	4652040	Saprolite			3.00	0.00	0.00	0.00
220	524443	4651666	Saprolite			0.00	0.00	0.00	0.00
221	527461	4652179	Gravel	Saprolite		0.50	7.00	0.00	0.50
223	525984	4651126	Gravel	Saprolite		3.20	4.00	0.00	3.20
224	525705	4651100	Saprolite			0.00	2.50	0.00	0.00
225	525756	4652018	Saprolite			2.50	0.00	0.00	0.00
227	526732	4651918	Saprolite			0.00	0.00	0.00	0.00
228	526439	4652460	Bedrock			3.00	0.00	0.00	0.00
229	527726	4651600	Gravel	Saprolite		1.40	2.70	0.00	1.40
230	527980	4651564	Colluvium	Saprolite		0.50	3.00	0.00	0.00
231	528066	4651579	Gravel	Saprolite		1.00	4.00	0.00	1.00
232	527899	4651942	Gravel	Saprolite		0.30	7.00	0.00	0.30
233	527801	4652555	Saprolite			4.00	0.00	0.00	0.00
234	527825	4653114	Saprolite			3.20	0.00	0.00	0.00
235	529000	4654787	Saprolite			6.00	0.00	0.00	0.00
236	528577	4655213	Saprolite			8.00	0.00	0.00	0.00
237	528041	4655746	Bedrock			2.50	0.00	0.00	0.00
239	529364	4657195	Bedrock			3.80	0.00	0.00	0.00
241	531996	4656829	Bedrock			3.00	0.00	0.00	0.00
242	531677	4656914	Colluvium	Saprolite		0.50	2.00	0.00	0.00
242	531849	4657297	Bedrock			1.00	0.00	0.00	0.00
253	530294	4656295	Bedrock			5.00	0.00	0.00	0.00
256	531693	4657303	Bedrock			6.00	0.00	0.00	0.00
256	531907	4657916	Bedrock			1.00	0.00	0.00	0.00
257	535132	4658196	Saprolite			3.00	0.00	0.00	0.00
260	535170	4657682	Gravel	Saprolite		0.65	1.85	0.00	0.65
261	535786	4657197	Gravel	Saprolite		0.60	2.80	0.00	0.60
262	536147	4657079	Clay	Gravel	Gravel	1.50	3.00	6.00	7.00
263	535023	4656766	Gravel	Saprolite		1.00	2.00	0.00	1.00

264	533634	4656784	Colluvium	Saprolite		1.50	2.30	0.00	0.00
265	533883	4657312	Bedrock			4.00	0.00	0.00	0.00
267	533183	4658034	Saprolite			2.80	0.00	0.00	0.00
268	533171	4657360	Gravel	Saprolite		1.00	1.50	0.00	1.00
272	536418	4656644	Colluvium	Saprolite		0.80	1.40	0.00	0.00
273	536815	4656860	Saprolite			0.60	0.00	0.00	0.00
274	536305	4656886	Gravel	Saprolite		0.60	1.30	0.00	0.60
274	536187	4657081	Gravel	Saprolite		0.10	0.50	0.00	0.10
275	536417	4657243	Gravel	Saprolite		0.10	1.10	0.00	0.10
276	536578	4657936	Bedrock			2.00	0.00	0.00	0.00
277	536919	4656438	Gravel	Saprolite		0.50	1.50	0.00	0.50
278	537264	4656795	Gravel	Saprolite		1.10	3.00	0.00	1.10
279	537944	4657090	Gravel	Saprolite		0.50	1.80	0.00	0.50
280	538491	4657949	Saprolite			1.00	0.00	0.00	0.00
281	538251	4658042	Gravel	Saprolite		0.40	1.60	0.00	0.40
282	537855	4656567	Gravel	Saprolite		0.70	2.00	0.00	0.70
283	538724	4657738	Bedrock			3.00	0.00	0.00	0.00
284	538604	4659368	Saprolite			2.30	0.00	0.00	0.00
285	538578	4659650	Saprolite			1.40	0.00	0.00	0.00
286	537708	4658120	Gravel	Saprolite		0.80	2.70	0.00	0.80
287	537426	4657717	Gravel	Saprolite		1.00	2.50	0.00	1.00
288	537267	4657413	Gravel	Saprolite		2.00	5.30	0.00	2.00
289	537688	4657834	Gravel	Saprolite		2.00	2.50	0.00	2.00
290	538069	4657563	Colluvium	Gravel	Saprolite	0.50	1.00	1.50	0.50
291	538259	4659141	Saprolite			2.00	0.00	0.00	0.00
292	545265	4660910	Gravel	Saprolite		7.00	8.00	0.00	7.00
293	545519	4661044	Gravel	Saprolite		0.50	4.00	0.00	0.50
294	545251	4661323	Gravel	Saprolite		2.50	4.00	0.00	2.50
296	545731	4661172	Gravel	Saprolite		0.50	7.00	0.00	0.50
297	546021	4661470	Saprolite			9.00	0.00	0.00	0.00

297	545943	4661056	Saprolite			0.00	0.00	0.00	0.00
298	544879	4659606	Gravel	Saprolite		7.50	7.60	0.00	7.50
300	546608	4659561	Gravel	Saprolite		2.50	10.00	0.00	2.50
302	546315	4659526	Gravel	Saprolite		1.50	7.00	0.00	1.50
303	546200	4660074	Gravel	Saprolite		3.80	4.00	0.00	3.80
304	547235	4660311	Bedrock			2.50	0.00	0.00	0.00
304	547506	4659559	Bedrock			0.00	0.00	0.00	0.00
305	547960	4658559	Colluvium	Gravel	Bedrock	1.00	1.10	3.00	1.90
306	548063	4658863	Colluvium	Gravel	Saprolite	0.50	0.60	0.80	0.20
307	548236	4659445	Bedrock			2.00	0.00	0.00	0.00
308	543040	4659796	Gravel	Saprolite		3.20	3.30	0.00	3.20
309	546369	4660083	Colluvium	Gravel	Saprolite	0.50	1.00	1.50	0.50
311	547634	4658486	Gravel	Saprolite		4.50	7.00	0.00	4.50
314	547158	4658686	Gravel	Saprolite		2.70	3.10	0.00	2.70
317	513702	4641537	Gravel	Saprolite		4.00	7.00	0.00	4.00
317	513685	4641398	Gravel			4.00	0.00	0.00	4.00
318	513060	4642076	Colluvium	Saprolite		1.80	1.90	0.00	0.00
319	513050	4642137	Colluvium	Gravel		1.00	2.30	0.00	1.30
320	513377	4642234	Gravel	Saprolite		6.30	13.00	0.00	6.30
321	512978	4642791	Gravel	Saprolite		4.00	6.00	0.00	4.00
323	512989	4642880	Gravel	Saprolite		7.00	7.10	0.00	7.00
324	513673	4642046	Colluvium	Saprolite		1.50	1.90	0.00	0.00
325	550733	4659520	Gravel	Saprolite		9.80	10.30	0.00	9.80
326	551154	4660264	Saprolite			2.50	0.00	0.00	0.00
327	550902	4659197	Gravel	Saprolite		1.90	3.20	0.00	1.90
328	550862	4658932	Gravel	Saprolite		0.60	1.00	0.00	0.60
329	513178	4641262	Gravel	Saprolite		8.00	9.00	0.00	8.00
528	534786	4657963	Gravel	Saprolite		0.50	2.30	0.00	0.50
1982	528615	4654197	Gravel	Bedrock		5.00	23.00	0.00	5.00
1982	528708	4654097	Gravel	Bedrock		5.00	24.00	0.00	5.00

1982	528801	4653996	Gravel	Bedrock		2.00	20.00	0.00	2.00
1982	528861	4653932	Fine sand	Saprolite	Bedrock	8.00	9.00	20.00	8.00
1982	528971	4653823	Fine sand	Saprolite	Bedrock	2.00	5.00	10.00	2.00
1982	528885	4653770	Fine sand	Saprolite		19.00	23.00	0.00	19.00
1982	528806	4653851	Fine sand	Bedrock		21.00	23.00	0.00	21.00
1982	528783	4653873	Fine sand	Saprolite	Bedrock	22.00	25.00	29.00	22.00
1982	528708	4653953	Gravel	Saprolite	Bedrock	6.00	16.00	30.00	6.00
1982	528628	4654038	Gravel	Saprolite	Bedrock	4.00	14.00	35.00	4.00
1982	528564	4654100	Gravel	Saprolite	Bedrock	2.00	5.00	23.00	2.00
1982	528464	4654113	Gravel	Saprolite	Bedrock	3.00	7.00	17.00	3.00
1982	528504	4654028	Gravel	Bedrock		7.00	21.00	0.00	7.00
1982	528557	4653919	Gravel	Bedrock		3.00	20.00	0.00	3.00
1982	528675	4653810	Fine sand	Bedrock		22.00	29.00	0.00	22.00
1982	528759	4653739	Fine sand	Bedrock		11.00	13.00	0.00	11.00

Sites with fluvial sediments where the underlying bedrock is not visible. Sediment thickness is a minimum value.

Ref.	East	North	Layer 1	Layer 2	Layer 3	Layer 1 depth (m)	Layer 2 depth (m)	Layer 3 depth (m)	Sediment thickness (m)
6	518779	4641104	Gravel			2.00	0.00	0.00	2.00
13	513693	4643220	Gravel			8.00	0.00	0.00	8.00
16	517765	4643822	Gravel	Reworked saprolite		0.90	1.30	0.00	1.30
17	517574	4643943	Gravel			5.50	0.00	0.00	5.50
20	517938	4644418	Gravel			4.00	0.00	0.00	4.00
20	517713	4644384	Gravel			2.00	0.00	0.00	2.00
21	517990	4645483	Fine sand	Coarse sand	Gravel	0.70	2.70	4.15	4.15
22	518215	4645264	Gravel			3.50	0.00	0.00	3.50
27	520079	4643276	Gravel			12.00	0.00	0.00	12.00
29	519130	4644192	Gravel			6.00	0.00	0.00	6.00
33	519063	4644517	Gravel			4.50	0.00	0.00	4.50
34	517814	4643319	Gravel	Sand, gravel, clay		8.00	13.00	0.00	13.00
35	519048	4646971	Clay	Coarse sand	Clay	3.20	3.40	5.00	6.00
35	519172	4646851	Gravel			5.00	0.00	0.00	5.00
36	518901	4644634	Gravel			6.00	0.00	0.00	6.00
37	518525	4644403	Gravel			2.60	0.00	0.00	2.60
41	524317	4648842	Fine sand	Gravel		0.50	2.50	0.00	2.50
44	522994	4649915	Gravel			4.00	0.00	0.00	4.00
45	523426	4650184	Gravel			7.00	0.00	0.00	7.00
45	523346	4650312	Coarse sand			7.00	0.00	0.00	7.00
50	525933	4649550	Gravel	Reworked saprolite		2.20	4.50	0.00	4.50
54	523858	4647359	Gravel			5.00	0.00	0.00	5.00
54	523928	4647391	Gravel			3.50	0.00	0.00	3.50
56	523960	4646016	Gravel			6.00	0.00	0.00	6.00

71	527866	4647587	Colluvium	Reworked saprolite	Sand, gravel, clay	0.50	1.10	2.50	2.50
72	528090	4646918	Gravel			2.35	0.00	0.00	2.35
74	530365	4646849	Gravel			2.00	0.00	0.00	2.00
77	529622	4646527	Gravel			11.00	0.00	0.00	11.00
78	529665	4646393	Gravel			7.10	0.00	0.00	7.10
80	530272	4648605	Colluvium	Gravel		1.00	2.20	0.00	1.20
81	530022	4649002	Gravel			3.00	0.00	0.00	3.00
85	530109	4651637	Gravel			2.00	0.00	0.00	2.00
86	531116	4651692	Gravel			4.50	0.00	0.00	4.50
87	531216	4651067	Gravel			1.90	0.00	0.00	1.90
88	531227	4649965	Gravel			3.50	0.00	0.00	3.50
89	530599	4650307	Gravel	Clay		2.00	2.50	0.00	2.50
90	531229	4649617	Gravel			3.10	0.00	0.00	3.10
90	531080	4649634	Gravel			6.00	0.00	0.00	6.00
93	529854	4649277	Gravel			4.00	0.00	0.00	4.00
95	530114	4650561	Gravel			3.00	0.00	0.00	3.00
96	526558	4646837	Gravel			9.00	0.00	0.00	9.00
103	531050	4659576	Gravel			10.00	0.00	0.00	10.00
108	541000	4659789	Gravel			10.00	0.00	0.00	10.00
109	541122	4660046	Gravel			8.00	0.00	0.00	8.00
111	545817	4659897	Gravel			10.00	0.00	0.00	10.00
118	540834	4659636	Gravel			5.50	0.00	0.00	5.50
119	540916	4659755	Gravel			4.00	0.00	0.00	4.00
121	541344	4660373	Gravel	Coarse sand		2.50	3.00	0.00	2.50
123	541079	4659881	Gravel			10.00	0.00	0.00	10.00
123	541274	4659988	Sand, gravel, clay			10.00	0.00	0.00	10.00
125	541838	4660253	Gravel			1.50	0.00	0.00	1.50
127	544114	4659710	Gravel			6.00	0.00	0.00	6.00

130	542924	4658704	Sand, gravel, clay			7.00	0.00	0.00	7.00
146	544474	4657917	Gravel			2.00	0.00	0.00	2.00
147	547868	4657416	Gravel			4.50	0.00	0.00	4.50
149	549237	4658960	Gravel			4.00	0.00	0.00	4.00
152	544315	4658378	Gravel			2.50	0.00	0.00	2.50
181	540186	4655424	Gravel			1.30	0.00	0.00	1.30
190	536229	4655056	Gravel			3.50	0.00	0.00	3.50
201	532515	4655491	Gravel			3.00	0.00	0.00	3.00
208	529047	4654492	Fine sand	Gravel	Reworked saprolite	1.70	4.00	4.10	4.10
209	528582	4654270	Fine sand	Gravel		1.00	3.00	0.00	3.00
217	526497	4649562	Gravel			2.00	0.00	0.00	2.00
222	526054	4651195	Gravel			3.50	0.00	0.00	3.50
222	526224	4651396	Gravel			3.50	0.00	0.00	3.50
226	526223	4651693	Gravel			2.80	0.00	0.00	2.80
238	529556	4656652	Gravel			2.20	0.00	0.00	2.20
240	532777	4656687	Gravel			2.00	0.00	0.00	2.00
243	531463	4658016	Gravel			1.60	0.00	0.00	1.60
244	531414	4658323	Coarse sand	Gravel	Clay	2.50	2.70	4.00	4.00
245	531151	4657247	Gravel			2.00	0.00	0.00	2.00
246	531047	4657484	Gravel			4.50	0.00	0.00	4.50
247	530724	4657481	Gravel			5.00	0.00	0.00	5.00
248	530537	4657729	Gravel			2.60	0.00	0.00	2.60
248	530514	4657751	Saprolite			0.00	0.00	0.00	0.00
249	531141	4658368	Gravel	Coarse sand	Sand, gravel, clay	2.50	3.80	7.50	7.50
250	531429	4658724	Gravel	Clay	Fine sand	2.50	10.00	10.10	10.10
251	531099	4659508	Fine sand	Gravel		1.50	1.51	0.00	1.51
252	530814	4659652	Coarse sand			2.30	0.00	0.00	2.30
254	529951	4656370	Clay			2.20	0.00	0.00	5.00

255	529967	4657092	Clay	Gravel		1.50	2.50	0.00	2.50
259	534723	4657958	Gravel			2.00	0.00	0.00	2.00
266	533107	4657582	Gravel			3.50	0.00	0.00	3.50
269	535592	4656473	Gravel			3.50	0.00	0.00	3.50
270	535279	4656062	Gravel			2.00	0.00	0.00	2.00
271	536278	4656739	Gravel			1.60	0.00	0.00	1.60
290	537627	4657133	Gravel			0.50	0.00	0.00	2.00
295	545077	4661214	Gravel			6.00	0.00	0.00	6.00
299	544764	4659490	Gravel			7.50	0.00	0.00	7.50
301	546234	4659594	Gravel			8.00	0.00	0.00	8.00
310	546873	4660142	Gravel			1.30	0.00	0.00	1.30
312	547333	4659042	Gravel			1.50	0.00	0.00	1.50
313	546789	4659231	Gravel	Clay		2.10	2.20	0.00	2.20
315	512853	4642916	Gravel			4.00	0.00	0.00	4.00
316	512787	4642828	Gravel			2.50	0.00	0.00	2.50
322	512836	4642873	Gravel			5.00	0.00	0.00	5.00
326	550811	4659716	Gravel			1.50	0.00	0.00	1.50
330	541851	4657587	Gravel	Sand, gravel, clay		0.70	3.00	0.00	3.00
331	545869	4660049	Gravel	Clay	Gravel	2.50	5.50	20.00	20.00
332	545728	4660302	Gravel	Clay	Gravel	2.00	5.00	20.00	20.00
333	544845	4660670	Gravel	Clay	Gravel	2.00	5.00	15.00	15.00

Appendix 3

Palaeoflow direction data

Ref.	East	North	Flow direction (degrees)
25	520034	4643813	100
27	520079	4643276	120
30	519879	4644352	130
33	519063	4644517	30
34	517814	4643319	150
37	518525	4644403	300
38	519842	4647565	240
39	522204	4647665	150
40	521706	4647896	90
40	521706	4647896	220
41	524317	4648842	190
45	523426	4650184	230
49	525938	4649644	215
50	525933	4649550	265
51	526501	4649280	200
54	523857	4647356	240
54	523877	4647340	310
55	524035	4647317	350
56	523995	4646030	250
57	524608	4646762	315
62	526006	4646987	235
66	524437	4646335	245
75	527360	4646799	240
75	527360	4646799	270
77	529622	4646527	100
77	529622	4646527	280
77	529622	4646527	190
77	529622	4646527	230
78	529665	4646393	80
78	529665	4646393	170
81	530022	4649002	220
83	542122	4658411	240
87	531216	4651067	205
88	531227	4649965	175
90	531229	4649617	202
96	526566	4646796	315
97	540830	4659751	240
113	539900	4659026	180
114	540053	4659365	225

116	540278	4659563	270
118	540834	4659636	270
119	540916	4659755	270
122	541493	4660305	280
127	544114	4659710	225
146	544474	4657917	245
147	547868	4657416	215
165	540121	4658494	260
175	540484	4657002	260
177	540497	4657083	250
197	535173	4655440	240
198	534722	4655344	280
201	532515	4655491	260
207	528572	4654814	200
223	525984	4651126	190
226	526223	4651693	212
240	532777	4656687	230
247	530724	4657481	225
251	531099	4659508	312
252	530814	4659652	0
255	529967	4657092	180
259	534723	4657958	272
261	535786	4657197	240
262	536147	4657079	235
263	535023	4656766	270
266	533107	4657582	265
269	535586	4656455	250
289	537688	4657834	25
298	544879	4659606	280
301	546234	4659594	310
303	546200	4660074	340
308	543040	4659796	275
310	546873	4660142	307
311	547634	4658486	295
313	546789	4659231	275
315	512853	4642916	155
317	513685	4641398	140
319	513050	4642137	210
320	513377	4642234	200
321	512978	4642791	150

Appendix 4

Fluvial terrace map of the lower Miño

Appendix 5

GeoPDF file of fluvial terrace map and deposits

About the author

I grew up in Asten, Noord-Brabant, the Netherlands, where I spent my childhood roaming the pine forests, first as a boy scout and later on my own. My parents had a vegetable garden outside town and I spent many, many summers weeding, sowing and harvesting the various crops and observing insects and other small living beings. An annual highlight was the first harvest of strawberries in May, which announced that summer was near. Summer was always an exciting time for any youth, and in our case especially as every year we would go to the Dutch coast for summer holidays. My sisters and I would pass the time climbing the dunes, searching for sea shells, crabs, shrimps and starfish. But most time I spent digging deep holes in the beach in search for certain strata of broken shells. I would sieve these strata in search for fossil shark and ray teeth. Over the years I collected thousands of them. We would stay at a camp site and every night me and my elder sister would listen to the sound of the sea, of the breaking of waves until we fell asleep.
My father was a diver, a frogman as they called it, in the Dutch Navy. From his long voyages abroad he brought foreign souvenirs, strange coins, and also a collection of books by Jacques Yves Cousteau. I devoured these books and became fascinated by everything to do with the sea.

These early images from childhood laid the foundation for my further life as nature and adventure became intertwined with my life. After high school (Dutch “gymnasium” or grammar school) I wanted to study marine biology, but a deficiency in chemistry-related subjects made that I enrolled in forestry at Wageningen University instead. Already in the first year of my studies I studied a number of soil and geology-related courses and decided to switch studies. I enrolled in the “Soil Science” BSc/MSc programme and choose the Geomorphology specialisation. This resulted in a BSc-thesis on Weichselian periglacial alluvial fan dynamics in the central parts of the Netherlands.

During my early years at Wageningen University I travelled a lot. When I was twenty, I spent two months alone in Kenya and Tanzania, roaming the rain forests and climbing volcanoes. I hitch hiked through the Tanzanian desert and stayed with the Masai in my small tent. I was also active in an international forestry students commission (IFSA) and organised and participated in many international meetings. I spent two months in Indonesia studying illegal logging in Java and Kalimantan, set up a forest monitoring program with the

Zambian Commonwealth forestry association branch in Zambia, and travelled all over Europe. Overall, I hitch hiked more than 20.000 km. During this time, I obtained funding from the European Union to organise two student group exchanges; one with South America and one with Spain. I spent ten days in Spain, and became fascinated by the landscape and culture of the country. Another stay in southern Spain was realised the year after, when I participated in a one-month field mapping course organised by my research group. During this time I also learned to dive. In 2006, I did a 4-month internship at the Soil Science department of the University of Santiago de Compostela, Spain, where I worked on the geochemical aspects of colluvia that were deposited under influence of anthropological influences for the past 7 ka. After my internship I spent three months in Nerja, Andalucia, Spain, working as a scuba dive guide.
After that I wrote a proposal for my MSc-thesis on alluvial river terraces in the Miño River basin. The proposal was accepted by my research group. I set up a collaboration with the Physical Geography Group at the University of Santiago de Compostela, where I stayed for another year. This resulted in an MSc-thesis on river dynamics over the past 0.8 Ma in the Miño River basin and I finally graduated at Wageningen University in 2008 with the highest grades possible for my internship and MSc-thesis.

After graduation I worked almost two years as a geomorphological engineer, first for an archaeological consultancy company and later on for Alterra, the national research institution on the environment, where I worked on geomorphological mapping of the Dutch coast and on modelling of the catchment dynamics of the German-Dutch Vecht River.

End of 2009, I began my work as a PhD researcher at the Land Dynamics Group (now Soil Geography and Landscape Group) at Wageningen University and the University of A Coruña. My MSc-thesis was well received at the time, and I was allowed to expand it into a PhD-thesis, of which the result you have in your hands. Curiously enough this thesis integrates all important aspects of my life: travelling, geomorphology, adventure and above all, the sea. The last has been of major importance in my later life, as having lived in A Coruña for the past four years, I have spent every weekend diving the Galician coast, searching for ship wrecks and observing marine life.

PE&RC PhD Training Certificate

With the educational activities listed below the PhD candidate has complied with the educational requirements set by the C.T. de Wit Graduate School for Production Ecology and Resource Conservation (PE&RC) which comprises of a minimum total of 32 ECTS (= 22 weeks of activities)

Review of literature (6 ECTS)

- Challenges in untangling climate and tectonic control on river systems (2010)

Writing of project proposal (4.5 ECTS)

- Long-term development of fluvial systems: separating the effect of climate and tectonic change (2008)

Post-graduate courses (4.5 ECTS)

- Geostatistics: PE&RC (2010)
- C + + Programming course; TU Eindhoven (2012)

Laboratory training and working visits (4.5 ECTS)

- Training preparation samples for OSL-dating; University of A Coruña (2009)

Invited review of (unpublished) journal manuscript (1 ECTS)

- Geomorphology: River incision (2013)

Competence strengthening / skills courses (2.3 ECTS)

- Career assessment; WGS (2011)
- Writing grant proposals; WGS (2012/2013)

PE&RC Annual meetings, seminars and the PE&RC weekend (1.2 ECTS)

- PE&RC Weekend (2011)
- PE&RC Day (2012)

Discussion groups / local seminars / other scientific meetings (4.5 ECTS)

- PyrTec Meeting; VU, Amsterdam (2010)
- Cosmogenic Ray Exposure dating discussion group; CEREGE, Aix-en-Provence, France (2011)
- NW Iberian climate and tectonics discussion group; Uni. Bordeaux1, France / VU Amsterdam / Uni Coruña, Spain / Uni O Porto, Portugal (2009-2013)

International symposia, workshops and conferences (9.5 ECTS)

- VII Meeting on the Iberian Quaternary: the future of the environment of the Iberian Peninsula: lessons from the recent geological past; Faro, Portugal (2009)
- Fluvial Archives Group meeting; Rodão, Portugal (2010)
- VII Symposium on the Atlantic Iberian margin; Lisbon, Portugal (2012)

Lecturing / supervision of practical's / tutorials; 21 days (3 ECTS)

- Geology and landscapes of the world (2010)
- Environmental data collection and analysis (2011)

Supervision of 3 MSc student; 50 days

- Kees Lommertzen: marine and river terraces around the Miño estuary
- Peter Kuijten: applied palynology, analyzing past climate change by means of a deep sea pollen record
- Jurriaan ten Broek: assessment of weathering processes in quartzite gravel terraces

Fluvial terrace map of the northwest Iberian lower Miño River
Scale 1:200,000

Willem Viveen (a,b), Jeroen M. Schoorl (a), Antonie Veldkamp (c), Ronald T. van Balen (d), Juan R. Vidal-Romani (b)

(a) Soil Geography and Landscape Group, Wageningen University, P.O. Box 47, NL-6700 AA, Wageningen, the Netherlands
(b) Instituto Universitario de Geologia, Edificio de Servicios Centrales de Investigacion, Campus de Elviña, University of A Coruña, 15071, A Coruña, Spain
(c) ITC Faculty of Geo-Information Science and Earth Observation, University of Twente, PO Box 217, 7500 AE Enschede, the Netherlands
(d) Faculty of Earth and Life Sciences, Vrije Universiteit, Amsterdam, De Boelenlaan 1085, 1081 HV Amsterdam, the Netherlands